CONTENTS

Page

INTENTIONALLY LEFT BLANK

TABLES

Page

INTENTIONALLY LEFT BLANK

FIGURES

Page

FIGURES (Continued)

FIGURES (Continued)

Page

INTENTIONALLY LEFT BLANK

2.3.9 Saturated Zone Flow and Transport

[NUREG-1804, Section 2.2.1.3.8.3: AC 1, AC 2, AC 3, AC 4, AC 5; Section 2.2.1.3.9.3: AC 1, AC 2, AC 3(1), (2), (4) to (6), AC 4, AC 5; Section 2.2.1.3.12.3: AC 1, AC 2, AC 3, AC 4, AC 5]

The information presented in this section addresses the requirements of proposed 10 CFR 63.114(a)(1) through (a)(5), (a)(7), and (b), for conducting a performance assessment in the area of saturated zone flow and transport. The requirement of proposed 10 CFR 63.114(a)(6) is not referenced below because degradation, deterioration, and alteration processes are addressed in Sections 2.2, 2.3.4 to 2.3.7, and 2.3.11. This section also provides information that addresses specific regulatory acceptance criteria in Sections 2.2.1.3.8, 2.2.1.3.9, and 2.2.1.3.12 of NUREG-1804.

This section presents the following pertinent information with regard to saturated zone flow and transport:

- Data from the site, surrounding region, the regional area, and applicable analogues; uncertainties and variabilities in parameter values; and alternative conceptual models used in the analyses

- Specific features, events, and processes (FEPs) included in the analyses, with technical bases for inclusion

- Technical bases for models used in the performance assessment.

The categories of information provided in this section, as well as the corresponding proposed 10 CFR Part 63 regulatory requirements and NUREG-1804 acceptance criteria, are presented in the following table. With regard to Acceptance Criterion 1(10) in NUREG-1804, Section 2.2.1.3.8.3, Acceptance Criterion 1(6) in NUREG-1804, Section 2.2.1.3.9.3, and Acceptance Criterion 1(6) of NUREG-1804, Section 2.2.1.3.12.3, no formal peer reviews were used directly to support development of the current models discussed in this Section 2.3.9. In addition, this section does not discuss the approach used for data qualification. However, scientific analyses, model development, and data qualification activities were conducted in accordance with project procedures that comply with Quality Assurance Program requirements. The project procedures governing data qualification are consistent with NUREG-1298 (Altman et al. 1988) in keeping with the three acceptance criteria. Acceptance Criterion 3(3) in NUREG-1804, Section 2.2.1.3.9.3, is not referenced in the table below because it pertains to criticality, which is excluded from the TSPA (Section 2.2.1.4.1).

While the acceptance criteria in Section 2.2.1.3.12.3 of NUREG-1804 relating to the groundwater protection standard are referenced below, they are effectively addressed by information presented in this section and Section 2.4.4 relating to acceptance criteria in Section 2.2.1.3.9.3 of NUREG-1804. Section 2.4.4 presents the total system performance assessment (TSPA) results for groundwater protection pursuant to 10 CFR 63.331. All radionuclides that reach the wells of the reasonably maximally exposed individual (RMEI) in a given year are included in the annual water demand of 3,000 acre-ft., a value specified in 10 CFR 63.332(a)(3). NUREG-1804, Section 2.2.1.3.12 discusses this approach. The effects of hypothetical wells are thus included in the TSPA analyses, consistent with FEP 1.4.07.02.0A, Wells (Table 2.3.9-1). In addition, the implicit

dilution in calculating the average concentration in the annual water demand and the representative volume of groundwater associated with the annual water demand includes FEP 2.2.07.16.0A, Dilution of radionuclides in groundwater (Table 2.3.9-1). This approach results in groundwater concentration being solely dependent on calculation of the mass of radionuclides reaching the RMEI via transport through the saturated zone. Section 2.3.9.3 addresses the acceptance criteria of Section 2.2.1.3.9.3 of NUREG-1804. Throughout Section 2.3.9, the general location of the wells where the RMEI extracts groundwater approximately 18 km from the repository is referred to as the accessible environment.

SAR Section	Information Category	Proposed 10 CFR Part 63 Reference	NUREG-1804 Reference
2.3.9	Saturated Zone Flow and Transport	63.114(a)(1) 63.114(a)(2) 63.114(a)(3) 63.114(a)(4) 63.114(a)(5) 63.114(a)(7) 63.114(b) 63.115(a)[a] 63.115(b)[a] 63.115(c)[a] 63.342(c)	Section 2.2.1.3.8.3: Acceptance Criterion 1 Acceptance Criterion 2 Acceptance Criterion 3 Acceptance Criterion 4 Acceptance Criterion 5 Section 2.2.1.3.9.3: Acceptance Criterion 1 Acceptance Criterion 2 Acceptance Criterion 3(1) Acceptance Criterion 3(2) Acceptance Criterion 3(4) Acceptance Criterion 3(5) Acceptance Criterion 3(6) Acceptance Criterion 4 Acceptance Criterion 5 Section 2.2.1.3.12.3: Acceptance Criterion 1 Acceptance Criterion 2 Acceptance Criterion 3 Acceptance Criterion 4 Acceptance Criterion 5
2.3.9.1	Summary and Overview	Not applicable	Not applicable
2.3.9.2	Saturated Zone Flow System	See details in sections below	See details in sections below
2.3.9.2.1	Conceptual Description	63.114(a)(3) 63.114(a)(4) 63.114(a)(7) 63.115(a)[a] 63.115(b)[a]	Section 2.2.1.3.8.3: Acceptance Criterion 1(1) Acceptance Criterion 1(2) Acceptance Criterion 1(3) Acceptance Criterion 1(5) Acceptance Criterion 1(6)
2.3.9.2.2	Data and Data Uncertainty	63.114(a)(1) 63.114(a)(2) 63.114(b)	Section 2.2.1.3.8.3: Acceptance Criterion 1(3) Acceptance Criterion 2 Acceptance Criterion 3

SAR Section	Information Category	Proposed 10 CFR Part 63 Reference	NUREG-1804 Reference
2.3.9.2.3	Site-Scale Saturated Zone Flow Model and Model Uncertainty	63.114(a)(1) 63.114(a)(2) 63.114(a)(3) 63.114(a)(7) 63.114(b) 63.342(c)	Section 2.2.1.3.8.3: Acceptance Criterion 1(3) Acceptance Criterion 1(4) Acceptance Criterion 1(8) Acceptance Criterion 4 Acceptance Criterion 5(3) Acceptance Criterion 5(4)
2.3.9.2.4	Model Abstraction and Confidence Building	63.114(a)(1) 63.114(a)(5) 63.114(a)(7) 63.114(b) 63.342(c)	Section 2.2.1.3.8.3: Acceptance Criterion 1(1) Acceptance Criterion 1(2) Acceptance Criterion 1(3) Acceptance Criterion 1(4) Acceptance Criterion 1(7) Acceptance Criterion 1(8) Acceptance Criterion 1(9) Acceptance Criterion 4 Acceptance Criterion 5
2.3.9.3	Saturated Zone Radionuclide Transport	See details in sections below	See details in sections below
2.3.9.3.1	Conceptual Description	63.114(a)(3) 63.114(a)(4) 63.114(a)(7) 63.115(a)[a] 63.115(b)[a]	Section 2.2.1.3.9.3: Acceptance Criterion 1(1) Acceptance Criterion 1(2) Acceptance Criterion 1(3) Acceptance Criterion 1(5) Section 2.2.1.3.12.3: Acceptance Criterion 1(1) Acceptance Criterion 1(2) Acceptance Criterion 1(3) Acceptance Criterion 1(4) Acceptance Criterion 1(5)
2.3.9.3.2	Data and Data Uncertainty	63.114(a)(1) 63.114(a)(2) 63.114(b)	Section 2.2.1.3.9.3: Acceptance Criterion 1(3) Acceptance Criterion 1(5) Acceptance Criterion 2 Acceptance Criterion 3(1) Acceptance Criterion 3(2) Acceptance Criterion 3(4) Acceptance Criterion 3(5) Acceptance Criterion 3(6) Section 2.2.1.3.12.3: Acceptance Criterion 1(4) Acceptance Criterion 1(5) Acceptance Criterion 2 Acceptance Criterion 3

SAR Section	Information Category	Proposed 10 CFR Part 63 Reference	NUREG-1804 Reference
2.3.9.3.3	Site-Scale Saturated Zone Transport Model and Model Uncertainty	63.114(a)(2) 63.114(a)(3) 63.114(a)(7) 63.114(b) 63.342(c)	Section 2.2.1.3.9.3: Acceptance Criterion 1(1) Acceptance Criterion 1(3) Acceptance Criterion 2(1) Acceptance Criterion 3(1) Acceptance Criterion 3(2) Acceptance Criterion 3(4) Acceptance Criterion 3(5) Acceptance Criterion 4 Section 2.2.1.3.12.3: Acceptance Criterion 1(1) Acceptance Criterion 1(2) Acceptance Criterion 1(3) Acceptance Criterion 1(4) Acceptance Criterion 2(1) Acceptance Criterion 3(1) Acceptance Criterion 3(2) Acceptance Criterion 3(3) Acceptance Criterion 4
2.3.9.3.4	Model Abstraction and Confidence Building	63.114(a)(2) 63.114(a)(3) 63.114(a)(7) 63.114(b) 63.115(c)[a] 63.342(c)	Section 2.2.1.3.9.3: Acceptance Criterion 1(1) Acceptance Criterion 1(2) Acceptance Criterion 1(3) Acceptance Criterion 1(4) Acceptance Criterion 3(1) Acceptance Criterion 3(2) Acceptance Criterion 3(4) Acceptance Criterion 5 Section 2.2.1.3.12.3: Acceptance Criterion 1(1) Acceptance Criterion 1(2) Acceptance Criterion 1(3) Acceptance Criterion 1(4) Acceptance Criterion 3(1) Acceptance Criterion 3(2) Acceptance Criterion 3(3) Acceptance Criterion 3(4) Acceptance Criterion 5
2.3.9.4	Conclusions	Not applicable	Not applicable

NOTE: [a]Not changed by the proposed rule.

2.3.9.1   Summary and Overview

The saturated zone below the repository is a component of the Lower Natural Barrier, which prevents or substantially reduces the rate of movement of water or radionuclides from the Yucca Mountain repository to the accessible environment (Section 2.1.2.3). The saturated zone flow and transport abstraction model, which is based upon the site-scale saturated zone flow and site-scale saturated zone transport process models, simulates the features and processes that are important to the functioning of the Lower Natural Barrier with regard to the movement of radionuclides.

Radionuclide transport in the saturated zone from beneath the repository to the accessible environment depends on the geologic material, hydrologic conditions, and geochemistry along the pathways of groundwater flow. Several processes contribute to the ability of the saturated zone component of the Lower Natural Barrier to reduce the rate of movement and concentration of radionuclides, including the diffusion of radionuclides from water flowing in fractures into the rock matrix, sorption of radionuclides onto rock or colloid surfaces, filtration of colloids by the rock, hydrodynamic dispersion, and radioactive decay.

The characteristics and processes that have been determined to be important to the capability of the saturated zone component of the Lower Natural Barrier (Section 2.1.2.3 and Table 2.1-4), and that are addressed by the saturated zone flow and transport abstraction model, include the following:

- **Fractures**—Fracture characteristics and their effects on radionuclide transport velocities and filtration of colloids are important in the fractured tuffs where the flow is primarily through the fracture network, rather than the matrix. The fracture networks appear to be well-connected over large distances, and are important to the capability of the barrier because of their role as pathways for groundwater flow and the advective transport of radionuclides. Uncertainty in fracture transport characteristics is included in the saturated zone transport analysis model report (SNL 2008a).

- **Faults**—Fault hydrologic characteristics are incorporated into the rock properties, which affect the groundwater flow path to the accessible environment. Some faults, particularly those that are inferred to act as barriers to groundwater flow, such as the Solitario Canyon fault, have an important impact on the simulated paths and rates of groundwater flow in the Yucca Mountain area (SNL 2007a). Large-scale heterogeneity is in part incorporated in the site-scale saturated zone flow model through faults (SNL 2007a, pp. 6-20). Faults affect groundwater flow patterns because they may act as preferred conduits or barriers to flow (SNL 2007a, pp. 6-21).

- **Climate Change**—Climate change alters the volumetric flow through the saturated zone by increasing precipitation, increasing the regional recharge, and causing the water table to rise (SNL 2007a, Section 6.6.4.1). The effect of this increased recharge and associated water table rise is to increase the saturated zone groundwater volumetric flow between the repository and the accessible environment. This increased flow tends to decrease the advective transport time from beneath the repository to the accessible environment for both sorbing and nonsorbing radionuclides that may be released from the unsaturated zone below the repository. This increased flow, and potential changes to the groundwater flow paths, are conservatively approximated in the saturated zone transport abstraction by increasing the specific discharge, but not explicitly including water table rise. The approximation is considered conservative because simulations using the site-scale saturated zone transport model with water table rise explicitly included indicate longer transport times in the saturated zone than simulations without water table rise (SNL 2008a, Appendix E). This increase in groundwater flow rates associated with climate change causes a significant increase in the rate of movement of radionuclides, which degrades the capability of the saturated zone feature of the Lower Natural Barrier (SNL 2007a, Section 6.6.4.1).

- **Climate Modification Increases Recharge**—The increase in recharge associated with future climate states significantly increases the groundwater flow through the tuff and alluvial water-conducting features, which reduces the contribution of these features to barrier capability (SNL 2008a; SNL 2007a, Section 6.6.4.1) by increasing the rate of transport of radionuclides.

- **Stratigraphy**—Stratigraphic heterogeneity affects likely saturated zone flow paths, based on variations in permeability among stratigraphic units. Various parameters that are significant in defining the transport of radionuclides through the saturated zone (e.g., effective diffusion, matrix porosity, and bulk density) are dependent on the stratigraphy and corresponding hydrogeologic units of the saturated zone. Many of these parameters are treated as constants within a stratigraphic unit, but vary between units (SNL 2008b, Section 6.5.2; SNL 2007a, Section 6.3.1.9). Stratigraphy is included in the performance assessment through the hydrogeologic framework model (saturated zone).

- **Rock Properties of Host Rock and Other Units**—Rock properties have a significant effect on the rate of radionuclide movement through their influence on the transport properties (notably, the flowing interval spacing, matrix diffusion coefficient, fracture porosity, sorption coefficients, matrix porosity of the volcanic units, and effective porosity of the alluvium) (SNL 2008b, Section 6.5.2). Flowing interval spacing is a parameter used to represent the distance between fractures, or sets of fractures, that transmit significant quantities of groundwater.

- **Saturated Groundwater Flow in the Geosphere**—The magnitude and direction of groundwater flow under present and future conditions in the saturated zone are estimated in the performance assessment (SNL 2007a; SNL 2008b). Advection of radionuclides by groundwater flow is one of the primary transport processes in the transport simulations (SNL 2008a, Section 6.4), and thus has a direct impact on the rate of radionuclide migration and the contribution of the saturated zone to the capability of the Lower Natural Barrier.

- **Water-Conducting Features in the SZ**—Water flow along potential flow paths from beneath the repository to the accessible environment in the saturated zone occurs within the fractured tuff units and the alluvium. The groundwater flow rates, radionuclide transport velocities, and radionuclide retardation characteristics of these different water-conducting features are significantly different. In addition to the differences in flow and transport characteristics of the different hydrogeologic units in the saturated zone, the presence of discrete flowing features in the fractured tuff units controls the advective velocities and, therefore, transport times from the base of the unsaturated zone to the alluvium. The flow in the alluvium provides a significant reduction in the movement of radionuclides to the accessible environment due to the nature of the alluvium as a porous medium. These characteristics of the saturated zone have been included in the *Saturated Zone Flow and Transport Model Abstraction* (SNL 2008b).

- **Advection and Dispersion in the SZ**—Advection is the principal transport mechanism for both dissolved and colloidal radionuclides in the saturated zone. The advective flux is dependent on the hydrogeologic characteristics of the water-conducting features in the

saturated zone, as well as the groundwater flow rates through these features. Dispersive processes tend to spread transient radionuclide pulses that may be released to the saturated zone (e.g., following the water table rise associated with climate changes, which could mobilize a pulse of radionuclide mass from the unsaturated zone above the present-day water table). These processes have been included in *Saturated Zone Flow and Transport Model Abstraction* (SNL 2008b).

- **Matrix Diffusion in the SZ**—Matrix diffusion, like advection and dispersion, is an important component of the saturated zone feature (SNL 2008a, Sections 4.1.2.10 and 6.4.2.4). The process of matrix diffusion enhances the barrier capability of the fractured tuff units in the saturated zone by effectively slowing the migration of radionuclides to the accessible environment. After diffusion into the matrix, radionuclides effectively stop moving until they diffuse out of the matrix at some later time. In addition, matrix diffusion provides access to the sorptive capacity of the tuff matrix, further slowing the migration of sorbing radionuclides.

- **Sorption in the SZ**—Radioelements released from the repository have varying retardation characteristics. Several radioelements, including those that contribute the most significant fraction of the inventory (for example, strontium, cesium, plutonium, radium, and americium), are moderately to highly sorbed in the saturated zone. The sorption behavior of these radioelements helps to prevent or substantially reduce the rate of movement of these radioelements from beneath the repository to the accessible environment. Other radioelements, such as neptunium and uranium, are slightly sorbed (SNL 2008a, Table C-14). For any radioelement with multiple radioisotopes (such as ^{241}Am, and ^{243}Am), the chemical properties of sorption are assumed to be the same for all radioisotopes. Sorption effects are included in the site-scale saturated zone transport model (SNL 2008a, Section 4.1.2.4).

Conceptual and Numerical Models—Several distinct conceptual and numerical models comprise the saturated zone flow and transport abstraction model for the TSPA. Figure 2.3.9-1 depicts the flow of information passed between and among the component models. The Death Valley regional groundwater flow system model simulates the regional water balance, and provides estimates of groundwater volumetric flow rates at the boundaries of the site-scale saturated zone flow model. The site-scale saturated zone flow model provides the three-dimensional groundwater flow field from beneath the repository to the accessible environment. The site-scale saturated zone flow model forms the basis of the site-scale saturated zone transport model, which adds the simulation of radionuclide transport. The site-scale saturated zone transport model is the basis for two abstraction models that feed directly into the TSPA analyses: (1) the saturated zone flow and transport abstraction model; and (2) the saturated zone one-dimensional transport model. The results of these abstraction models incorporate both the conceptual model and parameter uncertainty. The uncertainty is represented through a series of Monte Carlo simulations used to evaluate the impact of the range of values for each parameter.

The site-scale saturated zone flow model is a three-dimensional, steady-state, groundwater flow model based on observations and data from in situ field tests, regional-scale groundwater flow modeling, and expert elicitation (Section 2.3.9.2.3.1). This information was used to define flow processes and to derive model input parameters. The model incorporates recharge and volumetric

flow rates at the lateral boundaries from the Death Valley regional groundwater flow system model. The water table is located approximately 300 m below the repository at Yucca Mountain. Groundwater flows southeasterly from beneath the repository, then turns southerly and eventually southwesterly as it enters the Amargosa Desert. In the volcanic rocks underlying Yucca Mountain, flow is predominantly in fractures. To the south and southeast of Yucca Mountain, groundwater flow occurs primarily in the porous alluvial deposits that comprise the valley-fill aquifer that replaces or overlies the volcanic rocks (Section 2.3.9.2.1). The parameters that most affect regional saturated zone flow include the hydraulic gradient, hydraulic conductivity, and the rates of recharge and discharge.

The site-scale saturated zone flow model has been calibrated to water-level observations and boundary volumetric flow rates by adjusting the hydraulic parameters—primarily, the permeability values of the hydrogeologic units (Section 2.3.9.2.3.2). The results of the site-scale saturated zone flow model have also been validated with observed data on water-level elevation, permeability and specific discharge data, and flow paths interpreted from geochemistry and isotope data (Section 2.3.9.2.4.2). Uncertainty associated with the site-scale saturated zone flow model and model parameters has been incorporated (Sections 2.3.9.2.2 and 2.3.9.2.3). The product of the site-scale saturated zone flow model is used by the saturated zone flow and transport abstraction model to simulate a range of possible flow paths, including the fraction of the flow path length in alluvium, and flow rates from beneath the repository to the accessible environment. The effects of future climate change are also included by scaling up the specific discharge (Section 2.3.9.3.4.1.1).

The site-scale saturated zone transport model uses the same three-dimensional model domain, flow parameters, and flow boundary conditions as the site-scale saturated zone flow model. In addition, it incorporates the chemical and physical processes that affect the movement of radionuclides (dispersion, advection, matrix diffusion, sorption, and colloid-facilitated transport). A combination of field tests, laboratory experiments, expert elicitation, and natural analogue studies were also used to develop conceptual models and model parameters. Probabilistic parameter distributions were used to incorporate variability and uncertainty in processes and properties. The radionuclide transport simulations in fractured and porous media are accomplished using a particle-tracking algorithm. The parameters that primarily affect saturated zone transport include flow path length in fractured tuff and alluvium, specific discharge, flowing interval spacing and flowing interval porosity of fractured tuff, effective porosity of the alluvium, effective matrix diffusion coefficient, sorption coefficients, colloid retardation factor, and dispersivity. The flowing interval porosity for fractured rock units in the saturated zone is defined as the volume of the pore space through which large amounts of groundwater flow occur relative to the total volume of the rock.

The site-scale saturated zone transport model is implemented in the TSPA through the saturated zone flow and transport abstraction model and the saturated zone one-dimensional transport model (Figure 2.3.9-1). The saturated zone flow and transport abstraction model provides radionuclide breakthrough curves at the accessible environment (Section 2.3.9.3.4) for most radionuclides. The model considers a range of spatial locations and times of radionuclide releases from the unsaturated zone to provide transport times through the saturated zone. The saturated zone one-dimensional transport model provides the transport simulation capability for radionuclide daughter products resulting from decay and ingrowth during transport. These radionuclides are included because the regulations require explicit analysis of certain radionuclides and sources of radioactivity that are not captured in the saturated zone flow and transport abstraction model (Section 2.3.9.3.4.2.1). The

saturated zone one-dimensional transport model relies on a simplified representation of groundwater flow paths and flow rates that is based upon the full three-dimensional model.

The saturated zone flow and transport abstraction model provides the TSPA with a set of radionuclide unit mass breakthrough curves at the accessible environment, and the methodology for coupling these results into the TSPA simulations of radionuclide releases to the biosphere. The breakthrough curves are generated using multiple realizations of uncertain parameters in the site-scale saturated zone transport model. The convolution integral method is used to quantify radionuclide releases to the biosphere as a function of the transient radionuclide mass flux at the water table beneath the repository in the TSPA (SNL 2008b, Section 6.5.1.1). The saturated zone one-dimensional transport model is incorporated into the TSPA model and simulates transport of radioactive decay and ingrowth products. Climate change is incorporated into the transport abstraction models (Section 2.3.9.3.4.1.1) using a linear increase in the specific discharge. The timing of climate changes is consistent with the other models in the TSPA simulations (Section 2.3.1.2.3.1).

Analysis of the performance of the saturated zone component of the Lower Natural Barrier at Yucca Mountain (Section 2.3.9.3.4.1.1) indicates that the saturated zone contributes to the prevention or substantial reduction of the rate of movement of water or radionuclides from beneath the Yucca Mountain repository to the accessible environment. For the glacial-transition climate state, the median transport times in the saturated zone from the unsaturated zone below the repository to the accessible environment generally exceed 10,000 years for strongly sorbing radionuclides, and generally range from about 500 to more than 10,000 years for moderately sorbing radionuclides. In contrast, the simulated median transport times for nonsorbing species range from about 10 years to several thousand years in the uncertainty analysis. For plutonium and americium that is irreversibly attached to colloids, the median transport times vary from about 100 years to more than 100,000 years. These results also represent the post-10,000-year case because, in the saturated zone flow and transport abstraction model, the groundwater specific discharge multiplier is the same for the glacial-transition and post-10,000-year cases. The glacial-transition climatic state is appropriate for use in the post-10,000-year simulations of saturated zone flow and transport, because the hydrologic conditions for this state are consistent with proposed regulations (10 CFR 63.342). The proposed regulation in 10 CFR 63.342 specifies that the constant value for climate change in the post-10,000-year period is based on a distribution of deep percolation ranging from 13 to 64 mm/yr. The range of simulated average glacial-transition infiltration from the MASSIF (Mass Accounting System for Soil Infiltration and Flow) model (16.0 mm/yr at the 10th percentile to 46.2 mm/yr at the 90th percentile) approximately covers the range of deep percolation specified in proposed 10 CFR 63.342. (SNL 2008b, Table 6-1[a]). Therefore, the glacial-transition climate, as defined in the MASSIF infiltration model (SNL 2008c) and in the saturated zone flow and transport abstraction model, is the appropriate constant representation of climate change for use in the post-10,000-year simulations of radionuclide transport.

Components of the Saturated Zone Flow and Transport Model Abstraction—Figure 2.3.9-1 schematically represents all the components that, together, are used to create the saturated zone flow and transport abstraction model. The two most important process models that feed the abstraction model are the site-scale saturated zone flow model and the site-scale saturated zone transport model. The site-scale saturated zone flow model is a three-dimensional simulation model of the groundwater system. Data for the site-scale saturated zone flow model come from several analyses,

including the water level data analysis, the recharge and lateral flow boundary condition analysis, and saturated zone in situ testing. Other models also provide information—including (1) the site-scale unsaturated zone flow model, which provides the recharge component to the water table immediately surrounding the repository; (2) the Death Valley regional groundwater flow system model, which provides both recharge and boundary flow values; and (3) the hydrogeologic framework model, which provides the three-dimensional spatial pattern of hydrogeologic units in the study area. The site-scale saturated zone flow model is used by both the site-scale saturated zone transport model and the saturated zone flow and transport abstraction model. Using the three-dimensional groundwater flow field, the site-scale saturated zone transport model simulates radionuclide transport using properties specific to each radionuclide and hydrogeologic unit.

Role of the Saturated Zone Flow and Transport Model Abstractions in the TSPA—The TSPA model integrates the essential components of the conceptual and process models used to simulate repository behavior. Figure 2.3.9-2 provides a schematic representation of the TSPA model. The saturated zone flow and transport models described in this section are used to calculate the transport of radionuclides from their introduction at the water table below the repository to the accessible environment. The flow of information between the component models that constitute the saturated zone flow and transport model is shown in Figure 2.3.9-1, and the inputs to and outputs from the saturated zone flow and transport abstraction model are shown schematically in Figure 2.3.9-2. The TSPA uses two models to represent saturated zone flow and transport: (1) a three-dimensional saturated zone flow and transport abstraction model that calculates flow fields and transport of individual radionuclides important to dose; and (2) a one-dimensional saturated zone transport model that calculates the transport of daughter radionuclides. The saturated zone flow and transport abstraction model (Section 2.3.9.3.4.1.1) produces radionuclide mass breakthrough curves at the accessible environment that are direct feeds to the TSPA.

The same methods for the abstraction of flow and transport in the saturated zone were used for the four repository scenario classes considered in the TSPA (Section 2.4.2.1). For the nominal scenario class, the saturated zone flow and transport abstraction model considers radionuclides derived from degradation of waste packages that are transported through the unsaturated zone. In the igneous scenario class, the model considers radionuclides from disrupted waste packages that are subsequently transported through the unsaturated zone. In the seismic scenario class, a low-probability seismic event disrupts the repository, and leads to exposure of radioactive waste to water and transport through the unsaturated zone. Saturated zone flow and transport in the igneous and seismic scenario classes is modeled in the same way as in the nominal scenario class, because the igneous and seismic effects on saturated zone flow and transport are shown to be negligible (Table 2.2-5). In the early failure scenario class, flow and transport in the saturated zone is the same as in the nominal scenario class.

Summary of Features, Events, and Processes (FEPs) Evaluated in the Saturated Zone Flow and Transport Models and Analyses—The complete list of FEPs relevant to the saturated zone, both included and excluded, is presented in Table 2.2-5. The approach for the evaluation and incorporation of each FEP included in the models and analyses in this section is summarized in Table 2.3.9-1. The physical features incorporated in the models include the stratigraphy and rock properties of the hydrogeologic units at the site, the distribution and characteristics of fractures and faults, the location of extraction wells, chemical characteristics of the groundwater, and undetected features of the saturated zone. The processes important to evaluation of saturated zone

flow and radionuclide transport include saturated groundwater flow, advection, dispersion, matrix diffusion, sorption, chemical complexation, and climate change.

2.3.9.2   Saturated Zone Flow System
[NUREG-1804, Section 2.2.1.3.8.3: AC 1(1) to (9), AC 2, AC 3, AC 4, AC 5]

The Yucca Mountain saturated zone flow system lies within the Death Valley regional groundwater flow system. The Death Valley regional groundwater flow system is situated within the southern Great Basin, which is a subprovince of the Basin and Range physiographic province. The site-scale saturated zone flow model boundary is depicted in the context of the Death Valley regional groundwater flow system model shown in Figure 2.3.9-3. The locations of monitoring boreholes and wells used to characterize the site-scale saturated zone flow system are shown in Figure 2.3.9-4. The boreholes and wells include those drilled and tested by the DOE in support of the Yucca Mountain Project, those drilled and tested by Nye County as part of the Nye County Early Warning Drilling Program (BSC 2004a, Figure 1-2; SNL 2007a, Tables 6-8 and 7-1), and other public and private wells located in Crater Flat and Amargosa Valley. Hydrogeologic, geochemical, and isotopic data have been collected from boreholes that penetrate the saturated zone, as well as from nonintrusive field investigations such as geophysical surveys. These data from field and laboratory investigations were incorporated into the modeling to develop an understanding of the site-scale groundwater flow system, and to simulate groundwater flow and radionuclide transport from the water table beneath the repository to the accessible environment. In these site-scale studies, the results of characterization and modeling of the Death Valley regional groundwater flow system (Belcher 2004) provided input to the site-scale saturated zone flow model in the form of recharge and discharge boundary conditions (locations where water enters or leaves the model domain).

2.3.9.2.1   Conceptual Description
[NUREG-1804, Section 2.2.1.3.8.3: AC 1(1) to (3), (5), (6)]

Hydrology in the Death Valley regional groundwater flow system reflects both the arid climatic conditions and the complex geology of Basin and Range flow systems. Groundwater flow is dominated by interbasinal flow and may be conceptualized as having a series of relatively shallow and localized flow paths that are superimposed on deeper regional flow paths. A significant amount of the regional groundwater flow is through a thick Paleozoic carbonate rock sequence. Groundwater flows through zones of high transmissivity that result from individual permeable rock units and such regional structural processes as faulting and fracturing (Belcher 2004).

In the vicinity of Yucca Mountain, groundwater flows from recharge areas in the vicinity of Yucca Mountain (Section 2.3.1), through the Tertiary volcanic rocks into the valley-fill aquifer, and south toward the Amargosa Desert. The rock units include fractured volcanic rocks (primarily aquifers), porous volcanic units (confining units), alluvium, and fractured carbonate rocks. The modeling approach simulates flow through all the rock units present (SNL 2007a).

Within the site-scale saturated zone flow model, recharge occurs from infiltration of precipitation and infiltration of flood flows from Fortymile Wash and its tributaries. Groundwater outflow from the site-scale saturated zone flow model domain is primarily across the southern boundary of the model, toward Amargosa Valley (Belcher 2004; SNL 2007a, Section 6.3).

The water table under most of the repository is in the Tertiary age Crater Flat Group (SNL 2007a, Figure 6-11). This stratigraphic unit is also referred to in hydrostratigraphic terms as the lower volcanic aquifer (SNL 2007a, Section A6.3.10). It is composed of three volcanic tuffs: the Tram, Bullfrog, and Prow Pass tuffs. After reaching the water table, flow continues away from the immediate vicinity of the repository site in the Crater Flat Group. Permeability of volcanic rocks in the Crater Flat Group is small where the rocks are not fractured. Consequently, most flow of the groundwater in these rocks occurs in fractures (SNL 2007a, Section 7.2.2.1.4). The groundwater leaves the volcanic rocks and enters the porous alluvium prior to reaching the accessible environment.

If the specific discharge in volcanic rocks and alluvium were the same, the velocity of flow must be slower in the alluvium because the effective porosity of the alluvium is larger than the fracture porosity of the volcanic rocks (SNL 2008a, Table 4-2). Specific discharge is the volumetric groundwater flow rate per unit cross-sectional area in the aquifer. Although the average specific discharge is lower in the volcanics than in the alluvium along the flow paths from Yucca Mountain (SNL 2007a, Section 8.3.1), the contrast in flow porosity in the two media is much greater than the difference in specific discharge. Consequently, flow velocities are greater in volcanic rocks than in alluvium. The exact location of the volcanic rock–alluvium contact is uncertain and is treated stochastically in the saturated zone transport abstraction model using an alluvium uncertainty zone (Figure 2.3.9-5) (SNL 2008b, Section 6.5.2.2[a]). This zone allows the distance of travel through alluvium to vary as a result of uncertainty in the specific location of the volcanic rock–alluvium contact.

Beneath the volcanic rocks and alluvium lies a regionally extensive carbonate aquifer (SNL 2007a, Section 6.3.1). The carbonate rocks are relatively permeable and laterally continuous. They are sometimes referred to by their hydrostratigraphic name: the regional Paleozoic carbonate aquifer. An upward gradient of hydraulic head from the carbonate rocks to the overlying volcanic tuffs and/or alluvium is observed in boreholes located near Yucca Mountain, and is also simulated by the site-scale saturated zone flow model (SNL 2007a, Section 6.3.1.5, Section 6.3.1.6, and Table 6-8). In addition, an upward gradient is observed in borehole UE-25 p#1 and in Nye County well NC-EWDP-2DB, which are boreholes that penetrate the Paleozoic carbonate aquifer in the immediate vicinity of Yucca Mountain (SNL 2007a, Section 6.3.1.5). This upward gradient is potentially important to the performance of the repository because it would restrict groundwater flow and radionuclide transport pathways to the volcanic rocks and alluvial aquifers, thereby precluding transport in the deeper regional Paleozoic carbonate aquifer for the groundwater flow regime under present-day climatic conditions. On the basis of simulations of the Death Valley regional groundwater flow system under past and future climate scenarios, it is expected that the upward gradient of hydraulic head will persist during future wetter climates (D'Agnese et al. 1999, p. 36).

2.3.9.2.2   Data and Data Uncertainty
[NUREG-1804, Section 2.2.1.3.8.3: AC 1(3), AC 2, AC 3]

Characterization of the saturated zone flow system includes hydrogeologic properties, potentiometric surface, groundwater recharge, discharge and volumetric flow rates at the boundary segments, a hydrogeologic framework, and geochemistry. These flow system elements and their associated data and data uncertainty are discussed below. In cases where site-specific data are

limited, an expert elicitation provided additional guidance for selecting parameters and defining parameter uncertainty.

2.3.9.2.2.1   Hydrogeologic Properties

The permeability of rock units in the vicinity of Yucca Mountain has been determined by single- and cross-hole hydraulic testing. These data are used in the development and evaluation of the site-scale saturated zone flow model (Figure 2.3.9-6) (SNL 2007a, Section 7.2.2.6 and Figure 7-4).

Hydrogeologic Characteristics of the Tuff Derived from Testing—Testing of the tuff units was conducted at numerous locations, with extensive cross-hole testing conducted at the C-Wells Complex. The C-Wells Complex (Figure 2.3.9-7) comprises three boreholes that are open to groundwater from near the top of the Calico Hills Volcanic Unit to the middle portion of the Tram Tuff of the Crater Flat Group. The complex has been used to test the hydraulic and transport characteristics of the volcanic tuff units along the likely transport path of groundwater from Yucca Mountain. The stratigraphy, lithology, matrix porosity, fracture density, and the major flowing intervals from open-hole surveys at the C-Wells Complex are described in *Saturated Zone In-Situ Testing* (SNL 2007b, Section 6.2, Figure 6.1-2).

A large-scale, long-term pump test was performed at the C-Wells Complex in 1996-1997, in conjunction with a series of cross-hole tracer tests. Pumping of the lower Bullfrog Tuff at approximately 150 gallons per minute was sustained at a nearly uninterrupted level for over a year, which resulted in observed drawdowns in some boreholes located several kilometers away from the C-Wells Complex (SNL 2007b, Figure C-38). However, drawdown was not observed in all wells monitored (SNL 2007b, Sections C4.7). This variability in observed drawdowns indicates heterogeneity and horizontal anisotropy in the volcanic aquifer in the Crater Flat Group (SNL 2007b, Sections C4.6 and C6.).

In early 2006, well NC-EWDP-24PB (24PB) was drilled by the Nye County Early Warning Drilling Program at a location just outside the western NTS boundary, about 3 km west of NC-EWDP-22S and about 1 km west of the simulated flow paths in the saturated zone from beneath the repository. The water table in this well is at the base of the alluvium or the top of the underlying bedrock, which is the Bullfrog member of the Crater Flat Tuff. Two methods were employed to estimate ambient volumetic groundwater crossflow as a function of depth in 24PB (Freifeld et al. 2006, Section 3.2, Figures 10 and 18): flowing fluid electrical conductivity logging and distributed thermal perturbation sensor logging. The flowing fluid electrical conductivity method involved replacement of wellbore water with deionized water, pumping of the well at a low rate, and measuring profiles of electrical conductivity within the well as a function of time (Freifeld et al. 2006, Section 3.1). The electrical conductivity of the wellbore water increased as higher-conductivity groundwater from fractures entered the wellbore and mixed with the lower-conductivity deionized water. A computer program was used to estimate the locations and magnitudes of groundwater flow rates into and out of the wellbore from the flowing fluid electrical conductivity logs. The thermal logging method involved emplacement of an electrical heating element and distributed temperature sensor, along with a piezometer tube, all of which were grouted into the borehole. A uniform heat source was provided by the heating element, and the resulting temperature profiles were recorded as a function of time (Freifeld et al. 2006, Section 4). Advective lateral transport of heat by flowing groundwater resulted in less of an increase in temperature in those zones with flowing groundwater. In summary,

both logging methods identified a relatively high crossflow zone in the Bullfrog tuff at a depth of ~230 m below land surface, or ~100 m below the water table in 24PB (Freifeld et al. 2006, Section 3.2, Figures 10 and 18). Although a relatively wide range of flow rates could be deduced from the different logs, the overall conclusion was that there was an ambient volumetric crossflow "on the order of a few liters per minute" over an interval of fractured rock about 30 m long (Freifeld et al. 2006, Section 5). For comparison, the simulated volumetric flow rate through the grid cells at the same depth and at the location of well 24PB in the calibrated site-scale saturated zone flow model is about 0.9 L/min. The simulated volumetric flow rate, however, is for the entire width of the model cell (250 m), whereas the estimated cross flow rate from the well testing is for a width about twice the borehole diameter (0.34 m) (SNL 2008b, Section 6.9.2[a]). Because estimates of ambient volumetric crossflow had not previously been attempted in fractured volcanic rocks near Yucca Mountain, it is not known how representative these crossflow estimates are or how laterally extensive the deduced flow rates might be. To convert the crossflow estimates to specific discharge requires an assumption of cross-sectional area and porosity. Such an estimate would be considered a local value, with applicability over a relatively small region surrounding the well.

The implication of the relatively high deduced crossflow in well 24PB is that the degree of channelization of groundwater flow at some locations in the fractured volcanic tuffs may be significantly greater than what was deduced from estimates of flow porosity from crosshole tracer testing at the C-Wells Complex (Section 2.3.9.3.2.1). However, these high deduced flow rates are consistent with flowing interval spacing at the higher end of the distribution of values used in saturated zone transport modeling (Section 2.3.9.3.2.1) if estimates of groundwater specific discharge based on the calibrated site-scale saturated zone flow model are assumed.

An additional issue related to the results of testing at 24PB is how to appropriately scale the measurement for the modeling. The local scale measurements of groundwater flow in fractured media are generally not applicable directly at the larger model scale. It is possible that the inferred flow rate in the fracture zone tested in 24PB is representative of other flowing fractures in the volcanic units. As noted later in Section 2.3.9.3.2.1, the median flowing interval spacing is about 26 m. When the relatively high crossflow in 24PB is distributed across the flowing interval spacing, which is an appropriate way to scale the local measurement up to the model scale, the scaled up value is smaller (SNL 2008b, Section 6.9.2[a]). It is appropriate to distribute the crossflow across the flowing interval spacing because the flow through the low-permeability rock matrix between the flowing intervals is insignificantly small. Thus, the relatively large value at 24PB does not necessarily mean that flow in the entire flow system is relatively large.

Site-Scale Permeability Horizontal Anisotropy—Groundwater primarily flows in fractures within the volcanic units downgradient of Yucca Mountain. In addition, fractures and faults occur in preferred orientations. Therefore, it is probable that anisotropy of horizontal permeability exists along the potential pathway of radionuclide migration in the saturated zone (SNL 2007b, Section 6.2.6). Performance of the repository could be affected by horizontal anisotropy if the permeability tensor is oriented in a north–south direction, because the groundwater flow could be diverted to the south, causing any transported solutes to remain in the fractured volcanic rock for longer distances before moving into the valley-fill alluvial aquifer (Section 2.3.9.2.3.6). More southerly-oriented flow directions would, therefore, reduce the length of the transport path through the alluvium to the accessible environment. A reduction in the length of the flow path in the alluvium would decrease the amount of radionuclide retardation that could occur for

radionuclides with greater sorption capacity in the alluvium than in fractured volcanic rock matrix. The conceptual model of the saturated zone incorporates horizontal anisotropy in the volcanic tuff aquifer because flow in the volcanic tuff aquifer generally occurs in a fracture network that is preferentially oriented in a north–northeast direction. Major faults near Yucca Mountain that have been mapped at the surface and have been included in the site-scale hydrogeologic framework model (via a smoothed fault offset of hydrogeologic units) also have a similar preferential orientation (Figure 2.3.9-8) (SNL 2007c, Figure 6-2; BSC 2004b, Figure 6-2). In addition, north to north–northeast-striking structural features are oriented perpendicular to the direction of least principal horizontal compressive stress, thus promoting flow in that direction and suggesting a tendency toward dilation and higher permeability along fractures (Ferrill et al. 1999, pp. 5 to 6).

Evaluation of the long-term pumping tests at the C-Wells Complex supports the conclusion that large-scale horizontal anisotropy of aquifer permeability exists in the saturated zone. Results of this hydrologic evaluation (SNL 2007b, Sections 6.2.4 and 6.2.6) are consistent with the structural analysis of potential anisotropy, and indicate anisotropy that is oriented in a north–northeast to south–southwest direction when the response in borehole USW H-4 is not considered. Alternatively, the response in borehole USW H-4 indicates the possibility of a more complex system in which the effect of the Antler Wash Fault is superimposed on this uniform anisotropy, resulting in a bidirectional northwest and north–northeast anisotropy (SNL 2007b, Appendix C6.2). Estimates of horizontal anisotropy ratios (permeability in the north-south direction/permeability in the east-west direction) range from 3.3 to 17, with directions tending to be oriented more north-south than east-west (only one of six direction estimates deviated more than 35° from north-south) (SNL 2007b, Table 6.2-4).

Hydrogeologic Characteristics of the Alluvium Derived from Nye County Testing—Hydraulic testing of the alluvium has been performed at the Alluvial Testing Complex and at Site 22 (Figure 2.3.9-7). A summary of the lithology in the boreholes at the Alluvial Testing Complex and at Site 22 can be found in *Saturated Zone In-Situ Testing* (SNL 2007b, Section 6.4, Figures 6.1-9 and 6.1-10). The Alluvial Testing Complex is composed of one pumping well (NC-EWDP-19D), one piezometer (NC-EWDP-19P), and two injection wells (IM1 and IM2). Single-hole and cross-hole hydraulic tests and single-hole tracer tests have been conducted at the Alluvial Testing Complex. The cross-hole hydraulic tests at Site 22 involved simultaneous pumping of all four combined intervals in NC-EWDP-22S, as well as isolated interval pumping of each of the four individual well screens in 22S, while using NC-EWDP-22PA and NC-EWDP-22PB as observation wells. These tests provided hydraulic conductivity and storativity estimates in each of the intervals, as well as valuable insights into the vertical hydraulic communication between the test intervals.

Single-well hydraulic testing of the saturated alluvium in borehole NC-EWDP-19D was conducted between July and November 2000. During this testing, a single-well test of the four combined intervals of the alluvial aquifer to a depth of 247.5 m below land surface at NC-EWDP-19D resulted in a permeability measurement of 2.7×10^{-13} m^2 (SNL 2007a, Section 7.2.2.3.1 and Table 7-4). A cross-hole hydraulic test was also conducted at the Alluvial Testing Complex in January 2002. During this test, borehole NC-EWDP-19D was pumped in the open-alluvium section, while water-level measurements were made in the two adjacent boreholes. The intrinsic permeability measured in this test for the tested interval is 2.7×10^{-12} m^2 (equivalent hydraulic conductivity of 2.3 m/day for water at a temperature of 20°C) (SNL 2007a, Section 7.2.2.3.2; SNL 2007b, Section 6.4.5).

Results from the injection–pumpback tracer tests at NC-EWDP-19D1 show that the migration of the tracer during the intervening time between injection and pumpback is controlled by the natural groundwater flow rate (Figure 2.3.9-9). The designation 19D1 is used to represent the uppermost completion interval of borehole NC-EWDP-19D. For assumed values in the typical effective porosity range of 5% to 30%, the specific discharge was estimated to be between 1.2 and 9.4 m/yr (SNL 2007b, Table 6.5-5) for the valley fill material in the vicinity of the Alluvial Testing Complex (Table 2.3.9-2). The injection-pumpback tracer tests at NC-EWDP-22S, and the cross hole tracer test with NC-EWDP-22PA, with assumed values in the typical effective porosity range of 5% to 30%, produced a specific discharge range of 0.46 to 5.4 m/yr (Table 2.3.9-3). The specific discharge values were used to develop the parameter distributions in the flow and transport model abstraction (Section 2.3.9.3.4).

2.3.9.2.2.2 Hydrogeologic Framework

The site-scale hydrogeologic framework model, called HFM2006, is a representation of the hydrogeologic units and major structural features within the saturated zone flow system, encompassed by the domain of the site-scale saturated zone flow model (SNL 2007c). The Death Valley regional groundwater flow system hydrogeologic framework model, which was used in the development of HFM2006 (SNL 2007c), is described by Belcher (2004, Chapter E). The site-scale saturated zone flow model uses HFM2006 (which is smaller in areal extent than the Death Valley regional hydrogeologic framework model, but uses the same hydrostratigraphic units), which is described in *Hydrogeologic Framework Model for the Saturated Zone Site-Scale Flow and Transport Model* (SNL 2007c). By providing a simplified three-dimensional interpretation of the hydrostratigraphy and structure within the site-scale saturated zone flow model domain, the site-scale hydrogeologic framework model provides the fundamental geometric framework for constructing the site-scale saturated zone flow model (SNL 2007a, Section 6.4.3), which simulates groundwater flow directions and flow rates of water from beneath the repository to the southern end of the controlled area boundary. The spatial distribution of hydrogeologic units represented by HFM2006 is used to provide the spatial distribution of hydraulic properties used by the site-scale saturated zone flow model to simulate groundwater flow.

The geologic setting, geologic history, stratigraphy, and structure of Yucca Mountain are summarized by Luckey et al. (1996) and *Yucca Mountain Site Description* (BSC 2004c, Sections 2 and 3). Yucca Mountain consists of a group of north–south-trending block-faulted ridges composed of volcanic rocks of Tertiary age that may be several kilometers thick. Crater Flat, the basin to the west of Yucca Mountain, contains a thick sequence (about 2,000 m) of Tertiary volcanic rocks, Tertiary and Quaternary alluvium, and small Quaternary basaltic lava flows. The Solitario Canyon Fault separates Crater Flat from Yucca Mountain. West of Crater Flat is Bare Mountain, which is composed of Paleozoic carbonates and Precambrian meta-sedimentary rocks. Fortymile Wash, a prominent topographic feature and an inferred structural trough, delimits the eastern extent of Yucca Mountain. East of Fortymile Wash are the Calico Hills, an assemblage of altered Tertiary volcanic rocks and Paleozoic sedimentary rocks. Yucca Mountain terminates to the south in the Amargosa Desert, which contains near-surface deposits of interbedded Quaternary and Tertiary alluvial, paludal (marsh or swamp origin), and tuffaceous sediments.

To represent the geologic heterogeneity introduced by stratigraphy in a groundwater model, geologic units were simplified into hydrogeologic units on the basis of similar hydrogeologic

properties (Belcher 2004, Tables E-3 and E-4). The rocks and surficial deposits in the vicinity of Yucca Mountain were classified into 23 hydrogeologic units (of the 27 units in the Death Valley regional hydrogeologic framework model, 23 are present within the Yucca Mountain Model Domain) (SNL 2007c, Section 6.1 and Tables 6-2 and 6-3). Stratigraphic information is thus included in the site-scale saturated zone flow model, consistent with FEP 2.2.03.01.0A, Stratigraphy (Table 2.3.9-1).

The basic conceptual model used to construct the site-scale hydrogeologic framework model acknowledges that the hydrogeologic units at Yucca Mountain form a series of volcanic aquifers and confining units above the regional carbonate aquifer. Many of the formations have eroded significantly since deposition. The volcanic rocks generally thin toward the south away from their eruptive source areas in the vicinity of Timber Mountain. Downgradient, the undifferentiated valley-fill and the valley-fill aquifer to the south and southeast replace or overlie the volcanic aquifers. Structural features define the eastern, western, and portions of the southern boundaries of Yucca Mountain. The Tertiary volcanic rocks at Yucca Mountain consist of pyroclastic flow and fallout deposits, lava flows, and volcanic breccias of the Miocene age. The tuffs at Yucca Mountain are primarily nonwelded to densely welded, vitric to devitrified pyroclastic-flow deposits that are separated by nonwelded, vitric fallout deposits. These deposits are laterally continuous and fairly homogeneous throughout the Yucca Mountain area. (Luckey et al. 1996, pp. 7 to 13; BSC 2004c, Section 3).

The site-scale hydrogeologic framework model was constructed using stratigraphic and structural data from boreholes, and existing framework models that were constructed using data from boreholes, surface geologic maps, inferred geologic cross sections, and geophysical surveys (seismic, magnetic, and gravity) (SNL 2007c, Section 6.3.1 and Appendix B). The boundaries of HFM2006 coincide with the boundaries of the site-scale saturated zone flow model (Figure 2.3.9-3). HFM2006 is constructed with a horizontal grid spacing of 125 m (SNL 2007c, Section 6.3.2). The top of unit elevations from HFM2006 are interpolated onto the 250 m grid used by the site-scale saturated zone flow model for groundwater simulations. In general, the distribution of the data used to construct the site-scale hydrogeologic framework model is uneven, and the properties of the formations from which the unit surfaces are derived are highly variable. Typically, there is a higher degree of certainty in the shallower units, and in locations closer to the repository, because of more data points and better characterization of faults. In the vicinity of the Yucca Mountain repository, HFM2006 utilizes the geologic framework model (BSC 2004b) to provide the elevation of five of the hydrogeologic units (SNL 2007c, Section 4.1.3). Uncertainty in relatively less complex areas of the geologic framework model with some geologic constraints has been described as plus or minus 23.8 m at a distance of about 1,000 m from a known data point (BSC 2004b, Section 6.6.3 and Table 6-4). It is reasonable to conclude that the uncertainty in the top of unit elevation of a hydrogeologic unit will be larger than about 25 m as the distance from known locations, such as wells, increases.

As long as the horizontal spatial ambiguity in the location of hydrogeologic contacts is less than 125 m (one-half the site-scale saturated zone flow model gridblock dimension), there is essentially no impact on site-scale saturated zone flow model-specific discharge or volumetric flow calculations (SNL 2007a, Section 6.7.3). As noted above, 125 m is the gridblock dimension of HFM2006, so an error in the horizontal location of a contact by up to one HFM2006 gridblock will have no impact on the site-scale saturated zone flow model. However, away from the repository

(e.g., near the location of the accessible environment), the uncertainty in the location of the contact between the alluvium and the volcanic aquifers has been estimated to range over a horizontal distance of about 1 to 2 km (Figure 2.3.9-5 and SNL 2008b, Section 6.5.2.2[a]). Although uncertainty exists in the location of the contact, the location is constrained by the geology observed in wells located south and southeast of Yucca Mountain and by surface outcrops of volcanic rocks. The remaining uncertainty has been incorporated into the saturated zone flow and transport abstraction model and the one-dimensional saturated zone transport model used to simulate radionuclide decay (SNL 2008b, Section 6.5.2.2[a]), as described in Section 2.3.9.3.4.

In the site-scale saturated zone flow model (SNL 2007a), flow under the repository area is primarily in the most permeable units through the Bullfrog Tuff and Prow Pass Tuff and migrates into alluvial units near the boundary of the accessible environment. Errors in the vertical location of a hydrogeologic contact may impact the site-scale saturated zone flow model because the vertical spacing of the flow model varies from 10 to 50 m along the primary flow path from beneath the repository. For a 10-m-thick cell in the flow model, an error in the vertical location of a contact in HFM2006 may lead to an incorrect parameter value in that cell. The site-scale saturated zone flow model was used to perform an assessment of the change in specific discharge that would occur for an assumed error in the vertical location of a contact of from 10 to 50 m. A study of the impacts of hydrogeologic contact location uncertainty on the simulation of groundwater flow (SNL 2007a, Section 6.7.3) reveals the following:

1. Sensitivity to uncertainty in the hydrogeologic contact surfaces in the horizontal directions is much less than in the vertical direction due to the averaging effect of site-scale saturated zone flow model 250-m gridblock spacing. As long as the uncertainty in the horizontal contact location is less than one HFM2006 grid cell of dimension 125 m, there is essentially no impact to flow.

2. The change in specific discharge due to an assumed 50-m uncertainty in the vertical hydrogeologic surface (which is two times the uncertainty of 23.8 m noted above) can produce up to a 13% change in the local specific discharge near the repository, and in the alluvial flow regions where the vertical thickness of the flowing zone in the aquifer is 400-m thick.

3. In the transition zone of the flow system (south of UTM Northing 4,065,000 m) where the thickness of the flow zone is 25-m thick, an assumed 10-m uncertainty in the vertical hydrogeologic surface can produce up to a 40% change in the local specific discharge (SNL 2007a, Section 6.7.3). The assumed 10-m uncertainty is approximately 3 times the uncertainty in the measured elevation of the unit contacts (SNL 2007c, Section 6.4.3).

The range of uncertainty in specific discharge in the saturated zone flow and transport abstraction model (nearly two orders of magnitude) (SNL 2008b, Section 6.5.2.1[a]) is significantly greater than the changes in specific discharge due to uncertainty in the hydrogeologic contacts described above (SNL 2007a, Section 6.7.3). Uncertainty in the site-scale hydrogeologic framework model is addressed during development of the site-scale saturated zone flow model (Section 2.3.9.2.3.4).

The site-scale hydrogeologic framework model provides an internally consistent representation of the spatial distribution of block-averaged hydrologic properties within the site-scale saturated zone flow model domain. This representation is based on the underlying stratigraphic and structural framework. However, the significance of the site-scale hydrogeologic framework model is that it enables the computational grid of the site-scale saturated zone flow model to be populated with an initial set of hydrologic property values that are refined through calibration. The calibrated property sets are used to generate groundwater flow fields that are used in the simulation of radionuclide migration in the saturated zone from beneath the repository to the accessible environment.

2.3.9.2.2.3   Groundwater Recharge, Discharge, and Volumetric Flow Rates at the Boundaries of the Site-Scale Saturated Zone Flow Model

The site-scale saturated zone flow model uses estimates of recharge at the upper boundary (water table), and of horizontal flow at the lateral boundaries of the model domain, which are derived from several sources for present-day conditions. Increased groundwater flow rates associated with future climatic conditions are simulated in the saturated zone flow and transport abstraction model (Section 2.3.9.3.4.1.1). The recharge flow rates for the upper boundary of the flow model were taken from three sources: (1) the Death Valley regional groundwater flow system model; (2) the 2004 version of the site-scale unsaturated zone flow model; and (3) measured stream losses along Fortymile Wash. Estimated volumetric groundwater flow rates along the lateral boundaries of the site-scale saturated zone flow model domain were extracted from the Death Valley regional groundwater flow system model (Section 2.3.9.2.1) (Belcher 2004, pp. 118 and 132). These estimates of underflow at the lateral boundaries of the site-scale saturated zone flow model were used as calibration targets in the calibration process (Section 2.3.9.2.3.2).

Groundwater recharge in the Death Valley region is principally from water that directly infiltrates the soil horizon due to rainfall and snowmelt, and which is not lost from the soil horizon due to evaporation or transpiration (collectively, referred to as evapotranspiration). Net infiltration in the region is controlled by variability in precipitation and other factors, including elevation, slope, soil or rock type, vegetation, and the timing of precipitation. Net infiltration does not necessarily equal recharge because of possible losses or redistribution of water in the unsaturated zone.

The recharge distribution derived from the Death Valley regional groundwater flow system model were determined as part of the model calibration of that model (Belcher 2004, Table F-16). Specifically, the initial recharge estimates were categorized into zones with an adjustable multiplier that was varied as part of the calibration. The Death Valley regional groundwater flow system model was calibrated against water level observations, groundwater discharge observations, and boundary flow observations (Belcher 2004, pp. 279 to 283). These flow observations, particularly the discharge observations, provide a strong constraint on the total recharge that can occur in the Death Valley regional groundwater flow system. Based on these observations, it is concluded that the uncertainty in the total recharge is on the order of a factor of 2 or 3. The uncertainty in the recharge at any one location in the Death Valley regional groundwater flow system model would be expected to be larger than the uncertainty on the total value. Thus, the uncertainty in the recharge applied to the site-scale saturated zone flow model can be expected to be greater than or equal to a factor of 2 or 3.

For the portion of the area directly below the site-scale unsaturated zone flow model, the simulated present-day recharge is taken directly from the output at the entire bottom boundary of the 2004 version of the site-scale unsaturated zone flow model domain (BSC 2004d; SNL 2007a, Section 6.3.1.7). An updated version of the site-scale unsaturated zone flow model has been developed (Section 2.3.2) and is utilized in other components of the TSPA model. The infiltration model that was used for the upper boundary condition of the 2004 version of the site-scale unsaturated zone flow model also differs from the MASSIF infiltration model (Section 2.3.1) used in the current site-scale unsaturated zone flow model.

The impact of using an older version of the site-scale unsaturated zone flow model is small, because the site-scale unsaturated zone component of recharge is 9% of the total recharge (SNL 2007a, Section 6.4.3.9) in the site-scale saturated zone flow model, and total recharge is as much as 19% of the total inflow of groundwater in the upper part of the site-scale saturated zone flow model. The total flow in the site-scale saturated zone flow model includes the portions of flow in the alluvium, volcanics, and the carbonate aquifers. The flow paths from beneath the repository do not enter the carbonate aquifer, so the impact of the carbonate aquifer has been accounted for in this recharge assessment. The value of 19% is based on the total flow in the model after subtracting the contribution to the site-scale saturated zone flow model from the deepest layer (layer 16) of the Death Valley regional groundwater flow system model (SNL 2007a, Section 6.4.3.9). Layer 16 is about 2,600-m thick, and represents about 57% of the total flow system thickness. This deepest layer also contains a large portion of the lower carbonate aquifer.

A recent update to the analysis of infiltration in the region immediately surrounding Yucca Mountain using the MASSIF model (SNL 2008c; SAR Section 2.3.1) was used to supply an updated upper flow boundary condition to the site-scale unsaturated zone flow model, which yielded a weighted flow through its footprint of 8.4 kg/s (about 7.1 mm/yr) under present-day climatic conditions (SNL 2007d, Table 6.2-7, SAR Section 2.3.2; SNL 2008b, Tables 6-1[a] and 6-2[a]; SNL 2007a, Section 6.4.3.9). While this is a 49% increase over the previous net infiltration through the unsaturated zone footprint (5.6 kg/s), it remains only 13% of the infiltration budget and correspondingly only about 1% of the entire flow budget through the lateral boundaries (SNL 2007a, Section 6.4.3.9).

Focused recharge along Fortymile Wash was estimated (BSC 2004d, Section 6.2.3) on the basis of stream flow loss along four reaches of Fortymile Wash, as described by Savard (1998). The magnitude of groundwater recharge from ephemeral flow along Fortymile Wash decreases from Fortymile Canyon southward to the distributary channels south of Highway 95 (BSC 2004d, Table 6-3, Figure 6-6).

The combined recharge map developed for the site-scale saturated zone flow model area is shown in Figure 2.3.9-10. These data are assigned to nodes in the flow model at a 250-m spacing (SNL 2007a, Sections 6.4.3.2 and 6.4.3.9). The majority of the recharge entering the system in the area of the site-scale saturated zone flow model occurs in the northern part of the model domain (SNL 2007a, Figure 6-14). An estimated total recharge of 61.3 kg/s enters the saturated zone system. Of this total, about 5.6 kg/s recharge occurs in the area of the site-scale unsaturated zone flow model, and about 2.0 kg/s recharge occurs from focused recharge along Fortymile Wash (SNL 2007a, Section 6.4.3.9). The remainder, 53.7 kg/s, is obtained from the Death Valley regional groundwater flow system model. As noted earlier, the site-scale saturated zone flow model uses the

recharge beneath the site-scale unsaturated zone model area from an older version of the site-scale unsaturated zone flow model that does not include the impact of the recent revisions to the infiltration estimates. The impact of the revised infiltration estimates on the saturated zone flow system is expected to be small. The portion of the total flow in the site-scale saturated zone flow model that is obtained from the site-scale unsaturated zone flow model is between 1% and 2% of the total groundwater flow. A four-fold increase in the recharge from the site-scale unsaturated zone flow model, corresponding approximately to the ratio of the 90th percentile infiltration simulated by the MASSIF model (SNL 2008c) to the 5.6 kg/s from the previous net infiltration through the unsaturated zone footprint, translates into an increase of only 4% to 8% of the total flow. The impact of differences between versions of the site-scale unsaturated zone flow model to the flow system in the immediate vicinity beneath the repository is expected to be larger than elsewhere in the site-scale saturated zone flow model domain, but decreases with distance from the repository. Considering that specific discharge uncertainty in the saturated zone flow and transport abstraction model is nearly two orders of magnitude (Sections 2.3.9.2.3.6 and 2.3.9.3.4.1), the impact of the small percent change in recharge is already taken into account in the simulations.

The estimates of combined recharge (magnitude and spatial pattern) are appropriate for the purpose of calibrating the site-scale saturated zone flow model. Although the estimates of recharge for the three different components of the recharge analysis were derived by different methods, the results are sufficiently consistent for the purposes of defining a combined recharge in the site-scale saturated zone flow model. Therefore, residual uncertainties in the recharge will have a relatively small impact on the overall calibrated model results for the current climate state (the treatment of future climates is presented in Section 2.3.9.3.4.1.1). Recharge uncertainty is included as part of the uncertainty in specific discharge (Table 2.3.9-4).

The bulk inflow and outflow occurs along the lateral boundaries of the site-scale saturated zone flow model (SNL 2007a, Section 6.4.3.9). Present-day average volumetric flow rates along the lateral boundaries of the site-scale saturated zone flow model domain were extracted from the Death Valley regional groundwater flow system model (Section 2.3.9.2.1) (Belcher 2004. pp. 118 and 132). Groundwater flows into and across the model boundaries, and ultimately discharges to the south of the site model. Inflow generally occurs along the eastern boundary and, to a lesser extent, the northern and western boundaries, and discharge is generally along the southern boundary (SNL 2007a, Section 6.4.3.9). The segments of the model boundary and the corresponding volumetric flow rates across those segments are presented in Table 2.3.9-5. Inflow from the north is generally the result of regional recharge that occurs at Timber Mountain, Pahute Mesa, and Rainer Mesa. Inflow from the east is generally the result of regional underflow in the Paleozoic carbonate aquifers that were recharged in the Specter Range. Significant differences between target and site-scale saturated zone flow model results along the east boundary are evident in Section 2.3.9.2.3.3. A key factor that affects the match between the target and model results include the horizontal and vertical resolution and the permeability distribution. The horizontal resolution of the site-scale saturated zone flow model is 36 times finer than the regional model (250-m versus 1,500-m gridblock size). The vertical resolution of the site-scale saturated zone flow model is about four times finer than the regional model (67 versus 16 layers). The increased resolution at the site scale means that, compared to the regional-scale, volumetric/mass flow rates calculated by the site-scale saturated zone flow model may depend more strongly on a few units. Flow distribution in the regional model is also impacted by the use of hydraulic conductivity classes. In the Death Valley regional groundwater flow system model, permeabilities (actually hydraulic conductivities) associated with

specific units are not defined. Rather, the hydraulic conductivities are grouped into classes, which are assigned to a particular gridblock based on the percentages of the rock types contained in the gridblock. Thus, although the Death Valley regional groundwater flow system model was based on the same complex hydrogeologic framework model used for the site-scale saturated zone flow model, the regional model used only four hydraulic conductivity classes. Because of these fundamental differences, it is not possible to reproduce the distribution of volumetric/mass flow rates corresponding to the sides of the site-scale flow model, when examined on a unit-by-unit basis. Integrated along the entire boundary, the two models have similar flow values. The underflow at the site-scale saturated zone flow model lateral boundaries does not affect the flow paths where radionuclides could travel to the accessible environment. Outflow to the south is the result of carbonate underflow and flow in the alluvial aquifers that ultimately discharge at Ash Meadows or into wells in Amargosa Valley. The groundwater flow system in the carbonate aquifer is generally separate from the flow system in the overlying tuff aquifer downgradient of Yucca Mountain, as indicated by the large and sustained upward vertical hydraulic gradient between the systems. The separation of these flow systems tends to insulate simulated groundwater flow in the volcanic units downgradient of Yucca Mountain from uncertainties in the underflow to the carbonate aquifer at the lateral boundaries of the site-scale saturated zone flow model.

The site-scale saturated zone flow model is calibrated to observed water levels and to volumetric flow rates at the boundary segments obtained from the Death Valley regional groundwater flow system model (SNL 2007a, Section 6.5.2.2). Calibration of the site-scale saturated zone flow model to the Death Valley regional groundwater flow system model volumetric flow rates is useful because the regional model is based on a regional mass balance, incorporates groundwater divides, and is itself calibrated to measured spring flow and other estimated discharges (Belcher 2004). A degree of uncertainty is inherent in the regional model outputs used to identify lateral boundary conditions for the site-scale saturated zone flow model. This uncertainty in the lateral boundary flows was not explicitly included in the simulations. Rather, these uncertainties are addressed by using volumetric flow rates from the regional model as targets during site-scale saturated zone flow model calibration. Although the target values were fixed and not considered explicitly uncertain, the model was not forced to match the target values exactly. Thus, uncertainty in the boundary flows was indirectly included in the calibration. Additionally, a key result of the groundwater model—the specific discharge estimate—is sensitive to the specified values of boundary volumetric flows (SNL 2007a, Sections 6.7.1 and 6.7.2). This is as expected because to match observed hydraulic heads, the permeability values determined from calibration would adjust in proportion to the change in boundary flow to maintain the hydraulic gradient. The result, via Darcy's Law, is that groundwater specific discharge would also change proportionally.

2.3.9.2.2.4   Water Level Data and Potentiometric Surface

Water level measurements began in 1981 in the network of monitoring boreholes (BSC 2004a, Table A-4). The network of monitoring boreholes has evolved as additional wells were installed as part of the ongoing Nye County Early Warning Drilling Program (SNL 2007a, Tables 6-8 and 7-1). The locations of monitoring boreholes used to characterize the groundwater flow system in the vicinity of Yucca Mountain are shown in Figure 2.3.9-4.

The water-level data from boreholes throughout and adjacent to the site-scale flow model domain were compiled and evaluated for use during the development of the potentiometric surface map.

Water-level data collected as early as 1952 (BSC 2004a, Table A-4) were compiled from project data sources, and the U.S. Geological Survey National Water Information System, and used as appropriate to construct the potentiometric surface that supported the development of the site-scale saturated zone flow model. Additionally, some new water level data from recent measurements in existing wells, and from new wells drilled by Nye County, were also incorporated (SNL 2007a, Appendices D and E). The potentiometric surface map is representative of contemporary conditions (early 1990s). The water level data compiled for the Death Valley regional groundwater flow system model (Belcher 2004, Chapter C) was developed to represent predevelopment and transient conditions during the period before 1913 to 1998, and this model was used to provide volumetric flow rates at the boundary that served as calibration targets for the site-scale saturated zone flow model (SNL 2007a, Section 6.3.1.6). Consequently, the water-level data available for each borehole location from the 1980s and 1990s were averaged to provide a mean water level at each location that is representative of water levels during the early 1990s (BSC 2004a, Figure 6-3). The water levels in the wells within the site-scale saturated zone flow model domain do not show significant temporal variation (BSC 2004a, Section 6.5). When developing the potentiometric surface, water-level altitudes representing the uppermost aquifer system—typically the volcanic or alluvial system—were used. Water-level altitudes in some boreholes represent composite heads from multiple hydrogeologic units and fracture zones. Generally, water levels in the uppermost saturated zone appear to represent a laterally continuous, well-connected aquifer system. However, it is possible that the uppermost observed water represents a perched or semiconfined interval at some locations, or that a more transmissive unit deeper in the borehole controls the potentiometric surface (BSC 2004a, Section 6.4).

The analysis of water level data was subsequently updated, which led to the development of the most recent map of the potentiometric surface (Figure 2.3.9-11). Four distinct hydraulic gradient areas in the vicinity of Yucca Mountain can be identified in Figure 2.3.9-11: a large hydraulic gradient between water-level elevations of 1,030 and 750 m at the northern end of Yucca Mountain, a moderate hydraulic gradient west of the crest of Yucca Mountain, a small hydraulic gradient extending from Solitario Canyon to Fortymile Wash, and a moderate to large hydraulic gradient area southwest of Yucca Mountain, along U.S. Highway 95, near southern Crater Flat (BSC 2004a, Section 6.4; SNL 2007a, Figure 6-4). This map combined the data set used to develop previous potentiometric surface maps with additional water-level data obtained from the expanded Nye County Early Warning Drilling Program (SNL 2007a, Appendix D) and data from borehole USW WT-24 (BSC 2004a, Section 6.4). USW WT-24 was drilled in an effort to understand the cause of the high gradient area, and to determine if the water levels in USW G-2 and UE-25 WT#6 represented perched conditions or the regional water-table elevation. Drilling, testing, and monitoring of borehole USW WT-24 indicated the existence of perched conditions and a regional water-table elevation of 840 m. In addition, the potentiometric surface map also treats water levels from boreholes USW G-2, UE-25 WT#6, and NC-EWDP-7S as representative of perched conditions.

The potentiometric surface map presented in Figure 2.3.9-11 was developed from the average water levels that incorporate potential discrepancies and uncertainties in these data and their interpretation. Hence, the accuracy of the map of the potentiometric surface varies spatially. In the repository area, the potentiometric surface elevation values have an uncertainty of 1 m (BSC 2004a, Section 6.5); however, in other areas within the model domain, the uncertainty in the potentiometric surface is greater because of reduced density of data. There is additional uncertainty in the

potentiometric surface from water-level measurements in wells with long screen intervals. Areas where perched-water zones may exist, water-level drawdown associated with pumping in the Amargosa Valley, and the effect of faults on water level altitudes all add to the uncertainty in the potentiometric surface constructed using these data (BSC 2004a, Section 6.5; SNL 2007a, Appendix E). The uncertainty in the potentiometric surface was considered in assigning weights to water-level observations used in the site-scale flow model calibration process (SNL 2007a, Section 6.5.1.2). In areas of small uncertainty, such as the repository area, the calibration was expected to match observed water levels better than in areas where the uncertainty in the potentiometric surface was greater. Larger uncertainties, such as removal of the low permeability in the region of the large hydraulic gradient area to the north of Yucca Mountain, are evaluated using an alternative conceptual model (Section 2.3.9.2.3.4).

A number of explanations have been provided for the presence of the large hydraulic gradient at the north end of Yucca Mountain (Czarnecki and Waddell 1984, p. 19; Ervin et al. 1994, pp. 8 to 11), including presence of (1) faults that contain nontransmissive fault gouge; (2) faults that juxtapose transmissive tuff against nontransmissive tuff; (3) a less fractured lithologic unit; (4) a change in the direction of the regional stress field and a resultant change in the intensity, interconnectedness, and orientation of open fractures on either side of the area with the large hydraulic gradient; and (5) a disconnected, perched, or semiperched water body (i.e., one in which the high water-level altitudes are caused by local hydraulic conditions and are not part of the regional saturated zone flow system). The cause of the large hydraulic gradient is not known (SNL 2007a, Section 6.6.3). However, as long as the gradient is simulated, the unknown cause does not introduce significant uncertainty in the site-scale saturated zone flow model, considering that the large hydraulic gradient is located north of the repository and not along the path of radionuclide transport from beneath the repository to the accessible environment. The water level observations and the simulated water levels from the site-scale saturated zone flow model are evaluated in the underground facility design to address the issue of potential intersection of the water table with the repository under future wetter climatic conditions (Section 1.3.2.4.6.1).

The area with moderate hydraulic gradient west of the crest of Yucca Mountain is likely to be the result of the Solitario Canyon Fault and its splays functioning to restrict flow from west to east (BSC 2004a, Section 6.4; Luckey et al. 1996, p. 25). The moderate hydraulic head area southwest of Yucca Mountain also appears to be related to a fault that is approximately parallel to U.S. Highway 95. The small hydraulic gradient occupies most of the repository area and the downgradient area eastward to Fortymile Wash. Over a distance of 6 km, the hydraulic head declines only about 2.5 m between the crest of Yucca Mountain and Fortymile Wash. The small gradient could indicate highly transmissive rocks, little groundwater flow in this area, or a combination of both (Luckey et al. 1996, p. 27).

In addition, upward vertical hydraulic gradients have been observed in individual boreholes with isolated test intervals (Table 2.3.9-6). Depending on the location of the borehole, small vertical water level differences may not be indicative of vertical flow but, instead, may be caused by horizontal heterogeneity or uncertainties inherent in measuring deep water levels. However, large vertical water level differences—such as those between the regional Paleozoic carbonate aquifer and the overlying volcanic or alluvial aquifers as observed at UE-25 p#1 and NC-EWDP-2D/2DB—are generally representative of more extensive flow field differences (BSC 2004a, Section 6.3.2). At UE-25 p#1, water levels in the Paleozoic carbonate rocks are about

20 m higher than those in the overlying volcanic rocks. Water levels measured within the carbonate aquifer at NC-EWDP-2DB are about 7 m higher than levels measured in overlying volcanic rocks (BSC 2004a, Section 6.3.2, Table 6-4). Section 2.3.9.2.3.3 presents a comparison of the modeled hydraulic head versus the observed hydraulic head.

The hydraulic gradient data were used in the evaluation of the site-scale saturated zone flow model. The generally upward gradients effectively limit the downward potential for migration of water within the tuffs or between the tuffs and the underlying regional Paleozoic carbonate aquifer, and maintain flow paths originating from beneath the repository in the volcanic system. Although locally downward hydraulic gradients are observed, these may be attributed, in most cases, to the presence of local recharge conditions and low permeability confining units, or perched conditions (BSC 2004a, Sections 6.3.2, 6.4, and 7.1.1). It should be noted that water-level differences of a few tenths of a meter could reflect measurement uncertainties, and inferences regarding the direction of the hydraulic gradient from these differences are questionable (BSC 2004a, Section 6.3.2).

2.3.9.2.2.5   Geochemistry

Hydrochemical data and chemical data on rock types in the saturated zone flow system are used to corroborate groundwater flow patterns and flow rates, and to provide input to determine the sorption coefficient distributions (SNL 2007a, Appendices A and B). The flow pattern and flow rate data are used in the validation discussion that is presented in Section 2.3.9.3.4.1.3.

Groundwater in the volcanic units at Yucca Mountain is mostly sodium-bicarbonate water with low total dissolved solids (SNL 2007a, Appendix A). Variations in major ion chemistry of this relatively dilute groundwater from the volcanic aquifer are not large with regard to factors affecting radionuclide transport, but small differences in chemical composition are useful indicators of groundwater flow pathways, mixing of groundwaters, and potential water-rock interactions. Groundwater from the alluvium further to the south along the inferred flow path from Yucca Mountain is also dilute sodium-bicarbonate water, with chemical characteristics suggesting some mixing with recharge from the Fortymile Wash channel (SNL 2007a, Appendices A and B).

In the saturated zone, there are two distinct water types in the ambient system. One is typified by water from well UE-25 J-13 (J-13), located on the east side of Fortymile Wash (Figure 2.3.9-4). The other is from well UE-25 p#1, located near the southern entrance to the Exploratory Studies Facility. Well J-13 is pumped from volcanic units (Topopah Spring Tuff), whereas UE-25 p#1 water is pumped from the carbonate aquifer. The J-13 and UE-25 p#1 waters were used in sorption experiments as end-member compositions intended to bracket the impact of water composition on sorption coefficients. Although simulated flow paths from beneath the repository do not enter the carbonate aquifer, the uncertain extent to which groundwater chemistry along the flow paths from beneath the repository is influenced by upflow from the carbonate aquifer is bracketed by consideration of this water composition. As shown in Table 2.3.9-7, for most constituents, these two water compositions approximately bracket the compositions of other wells both in the volcanic rocks and alluvium along the potential flow paths to the accessible environment (SNL 2008a, Appendix A).

There are two rock types in the saturated zone that dominate the geology and potentially influence the chemistry along potential flow paths in volcanic rocks to the accessible environment: devitrified

tuff and zeolitic tuff. Devitrified tuff is composed primarily of silica (quartz and cristobalite) and alkali feldspar. It may also contain minor to trace amounts of mica, hematite, calcite, tridymite, kaolinite, and hornblende and minor amounts (less than 25%) of smectite, zeolite, or both (SNL 2008a, Appendix A). Zeolitic tuff has a similar mineralogic composition, but with a higher percentage of zeolite minerals.

2.3.9.2.2.6   Expert Elicitation

In cases where site-specific data were limited, an expert elicitation conducted in a manner consistent with NUREG-1563 (Kotra et al. 1996) provided additional guidance for selecting parameters and defining parameter uncertainty. The objectives of the expert elicitation were to quantify uncertainties associated with certain key issues in the TSPA, and to provide perspectives on modeling and data collection activities that could help characterize and reduce uncertainties. With respect to the saturated zone, an expert elicitation was conducted in 1997 by a panel of five experts in the field of saturated zone hydrology to address 16 technical issues (CRWMS M&O 1998, Table 3-1) related to saturated zone groundwater flow and radionuclide transport.

The key issues associated with groundwater flow included the conceptual models of groundwater flow upgradient, beneath, and downgradient of the repository, the magnitude and direction of advective flow rate (specific discharge), applicability of the C-Wells data (including hydraulic conductivity and anisotropy) at the model scale, estimates of recharge and discharge, the use of geochemical data to characterize the flow system dispersivity, and the impacts of climate change and water table rise. Many of the recommendations of the elicitation panel were implemented in subsequent work conducted at Yucca Mountain. For two parameters related to saturated zone flow and transport—the vertical anisotropy and the dispersivity—parameter values or ranges of values were taken from the elicitation for use in saturated zone flow and transport modeling. In addition, the impacts of uncertainty in these parameters were examined during sensitivity analyses. The elicitation results for vertical anisotropy were used for developing the parameter value presented below (Section 2.3.9.2.3.2). The elicitation results for dispersivity values were used in the development of the dispersivity parameter distributions (Section 2.3.9.3.3.4). The elicitation results for specific discharge were used as one source of information for developing the uncertainty distribution for this parameter (Section 2.3.9.2.3.6).

2.3.9.2.3   Site-Scale Saturated Zone Flow Model and Model Uncertainty
[NUREG-1804, Section 2.2.1.3.8.3: AC 1(3), (4), (8), AC 4, AC 5(3), (4)]

A numerical site-scale saturated zone flow model was developed that simulates groundwater flow in the area of the repository to provide the basis for the analysis of radionuclide transport from the water table, beneath the repository, to the accessible environment. The steady-state model is calibrated to represent current groundwater flow conditions in the Yucca Mountain area. The site-scale saturated zone flow model provides the flow fields necessary to generate radionuclide breakthrough curves. Table 2.3.9-8 summarizes the key hydrologic features for the site-scale saturated zone flow model and the alternative flow models that are discussed below.

2.3.9.2.3.1 Site-Scale Saturated Zone Flow Model Development

The conceptual model of groundwater flow provides the basis for selecting a modeling approach. Observations at Yucca Mountain indicate that, in the fractured volcanic rock, the flow is primarily through the fracture network instead of the matrix and that, at the scales of interest (hundreds of meters to kilometers), the fracture networks appear to be well-connected over large distances. The approach to simulate flow is supported by the following observations:

- At Yucca Mountain, studies of the density and spacing of flowing intervals generally indicate that flow in the volcanic rocks occurs through fracture zones (SNL 2007a, Section 6.3.2).

- Part of the flow system is in an alluvial unit, and results of pumping and tracer tests at the Alluvial Testing Complex and Nye County Site 22 indicate that the alluvium is a porous medium (SNL 2007b, Sections 6.4.4, 6.5.5, and 7.1).

- The drawdown response to pumping at wells surrounding the C-Wells Complex in multiwell pump tests indicates a well-connected fracture network in the volcanic rock aquifer in the region impacted by C-Wells testing (SNL 2007a, Section 6.3.2).

- Geochemical studies (SNL 2007a, Section 6.3.2) independently confirm a south–southeasterly trace of the particle flow path.

Two methods were considered to simulate groundwater flow in fractured rock: discrete fracture and equivalent continuous medium approaches (de Marsily 1986, p. 65). The discrete fracture models suffer a number of limitations in site-scale flow studies, as described in Section 2.3.2. The continuum approaches mathematically represent the fractures and matrix media with a set of effective parameters for each medium.

Based on the above observations and numerical considerations, a continuum approach was adopted to simulate groundwater flow through the fractured rock and alluvial materials in the saturated zone. Several continuum approaches are available, including single continuum, dual porosity, and dual permeability–dual porosity. The single continuum approach is the porous media approach. The dual porosity approach simulates the flow of water in the fractures, but allows for interaction with the water in the matrix porosity. In this case, the matrix acts as a large storage reservoir for water. This method is useful for simulating transient flow in fractured media, where the permeability of the matrix is much less than in the fractures. The dual permeability–dual porosity approach can be used when the permeability of the matrix is similar to that of the fractures, and significant flow occurs in both fracture and matrix. In most cases of dual permeability–dual porosity in saturated flow, a single continuum approach would work as well. From a flow perspective, steady-state flow in fractured media could be successfully simulated with a single continuum approach. A single continuum approach was used for the site-scale saturated zone flow model (SNL 2007a, Section 6.3.2). However, as discussed in Section 2.3.9.3.3.1, considerations of transport processes, primarily matrix diffusion, require the implementation of a dual porosity effective continuum approach. The dual porosity effective continuum approach includes flow through fractures, consistent with FEP 1.2.02.01.0A, Fractures (Table 2.3.9-1) (SNL 2008a, Section 6.3).

Groundwater flow in the Yucca Mountain area is simulated using the site-scale saturated zone flow model (SNL 2007a, Section 6.4.2) implemented with the FEHM code (Zyvoloski et al. 1997). The process of saturated groundwater flow is thus included in the site-scale saturated zone flow model, consistent with FEP 2.2.07.12.0A, Saturated groundwater flow in the geosphere (Table 2.3.9-1). The model domain was defined to be coincident with the grid cell corners of selected cells of the Death Valley regional groundwater flow system model, and covers a 45 km long by 30 km wide area of approximately 1,350 km^2. The model domain extends to a depth of approximately 4,000 m below mean sea level, and includes the equivalent part of the regional Paleozoic carbonate aquifer as the Death Valley regional groundwater flow system model (SNL 2007a, Section 6.3). The model domain was made sufficiently large to (1) minimize the effects of boundary conditions on the calibrated permeability values and simulated flow paths at Yucca Mountain; (2) to assess groundwater flow and contaminant transport to the accessible environment downgradient from the repository area; and (3) to include wells in the Amargosa Desert at the southern end of the modeled area (SNL 2007a, Section 6.3). Although domestic wells are located within the southern boundary of the site-scale saturated zone flow model, the impact of pumpage is not directly simulated. Instead, the water levels from the domestic wells are used as calibration targets, as well as the flow of groundwater across the boundaries of the model, as obtained from the Death Valley regional groundwater flow system model. The regional model explicitly includes the pumpage from the domestic wells and, thus, the boundary flows implicitly include the effects of the pumpage. By simulating the water table elevation defined by the domestic wells and the boundary flows from the Death Valley regional groundwater flow system model (SNL 2007a, Section 6.3.1.6), the effect of the domestic wells is adequately accounted for in the site-scale saturated zone flow model. The steady state simulations of the site-scale saturated zone flow model assume that the domestic water usage will cause no future impacts to the water table elevation.

A structured computational grid using orthogonal hexahedral elements was developed for the site-scale saturated zone flow model (SNL 2007a, Section 6.4.3.2 and Figure 6-7). A horizontal grid spacing of 250 m was selected to provide better accuracy than the grid spacing of 500 m, which was demonstrated to provide appropriate horizontal resolution for the model (Bower et al. 2000; SNL 2007a, Section 6.4.3.2). Although uniform horizontal spacing was adopted, a nonuniform vertical spacing was established to provide the resolution necessary to accurately represent critical flow and transport pathways in the saturated zone. A 10-m grid spacing was adopted for portions of the site-scale saturated zone flow model near the water table, which varies in elevation from about 730 m below the repository to about 707 m at the boundary of the accessible environment. A progressively coarser grid was adopted for cells above an elevation of 760 m, and for deeper portions of the aquifer from an elevation of 580 m to the bottom of the model domain (SNL 2007a, Section 6.4.3.2 and Table 6-4).

To represent discrete features and regions having distinct hydrologic properties within the site-scale saturated zone flow model domain, a set of 10 hydrogeologic features—based on components of the site-scale hydrogeologic framework model (see Table 2.3.9-8) (SNL 2007a, Section 6.4.3.7)—were identified and incorporated into the site-scale saturated zone flow model in addition to an eleventh thermally altered zone to the north to represent the high hydraulic gradient region. The thermally altered zone to the north of Yucca Mountain is a simplified representation of reduced permeability in the volcanic units that approximates the higher water levels observed in this area. The features primarily represent faults, fault zones, and areas of mineralogic alteration. These features are distinct from the subhorizontal geologic formations, which form zones with distinct

geometry and material properties. Each of these features includes multiple geologic formations and represents zones of differing permeability within the individual formations: enhanced permeability, reduced permeability, or anisotropic permeability (SNL 2007a, Section 6.5). Some of these features function as zones of increased groundwater flow in the saturated zone, and thus include FEP 2.2.07.13.0A, Water-conducting features in the saturated zone (Table 2.3.9-1), in the site-scale saturated zone flow model. Major faults are conceptualized as zones of enhanced permeability parallel to the fault plane and reduced permeability perpendicular to the fault in most cases. However, in the case of the Fortymile Wash fault zone, the fault is not a barrier to groundwater flow, based on its location as a focus of apparent convergent groundwater flow. The faults are represented with gridblocks that are nominally 250 m by 250 m in the horizontal directions because the model cannot resolve features smaller that the 250-m grid cell size. Fault zone properties are volume-averaged because fault zones are typically much less than 250 m in width. While the precise flow regime within the fault may not be simulated in detail when using volume-averaged representations of faults, overall flow through the system, particularly at the model boundaries, is not significantly affected by the volume-averaged approach (SNL 2007a, Section 6.7.7). Specific discharge values obtained by volume averaging are appropriate values for the size of the model cell.

For example, consider a fault zone 25 m wide in a 250 m wide cell. The bulk of the flow will be through the fault and the local specific discharge value in the fault will be approximately 10 times larger than the volume averaged value. The volume averaged value is the appropriate value for the model, because it preserves the correct volumetric flow rate from one cell to the next. For transport, however, parameter values may need to be adjusted to account for the fault zone. For example, if the porosity is reduced by a factor of 10, then the velocity of transport through the cell will more closely represent the fault flow than the volume averaged flow. The effects of faults on groundwater flow are thus included in the site-scale saturated zone flow model, consistent with FEP 1.2.02.02.0A, Faults (Table 2.3.9-1).

In the site-scale saturated zone flow model, fixed-head boundary conditions (water levels specified around the boundary of the model) were established around the periphery of the computational grid based on the water levels identified from the map of the potentiometric surface developed for the site-scale saturated zone flow model area (Section 2.3.9.2.2.4). The constant head specified for each node along the boundary was applied uniformly through each layer of the model. This approach created a zero vertical hydraulic gradient at the boundary of the model. In spite of such simplified constant-head boundary conditions, vertical gradients develop internally in the model domain in response to geohydrologic conditions, and the calibrated model is capable of representing the upward vertical gradients observed between the regional Paleozoic carbonate aquifer and overlying volcanic aquifers. A no-flow boundary was assigned to the bottom layer. Although flow conditions in the deeper portions of the model domain are not well established, the depth of the bottom boundary is such that this boundary condition does not exert significant influence on flow at shallower levels where groundwater flow and radionuclide transport is of greater interest to the TSPA. At the top of the site-scale saturated zone flow model, a specified-flow boundary condition was established to represent recharge to the system (SNL 2007a, Section 6.4).

Representative hydrologic properties were assigned to each node in the computational grid. For flow modeling, these properties include permeability, porosity, and viscosity (SNL 2007a, Section 6.4.3.10). During model calibration, permeability values were obtained for each node. Because the viscosity of groundwater depends on temperature, the nodal values for viscosity were

assigned based on the expected temperature distribution in the subsurface using an average value for the local geothermal gradient, thus approximating the impacts of temperature variation. The effects of variations in natural temperature on viscosity are thus included in the site-scale saturated zone flow model, consistent with FEP 2.2.10.03.0A, Natural geothermal effects on flow in the saturated zone (Table 2.3.9-1). Using a variable viscosity allows the calibration of intrinsic permeability to be made, instead of hydraulic conductivity. The former is a rock property, whereas the latter is both a rock and fluid property. This approach, in turn, allows for more accurate flow calculations at the boundaries of the model (SNL 2007a, Section 6.4.3.10).

2.3.9.2.3.2 Site-Scale Saturated Zone Flow Model Calibration

Calibration is the process by which values of important model parameters are estimated and optimized to produce the best fit between model output and observed data. Calibration is generally accomplished by adjusting model input parameters (e.g., permeabilities) to minimize the difference between observed and simulated conditions (in this case, comparing simulated and observed head values and lateral boundary volumetric/mass flow rates). Model calibration may be performed manually or through automated optimization procedures. Automated optimization procedures generally employ a carefully prescribed mathematical process that selects the optimal set of parameters based on minimizing an objective function describing the difference between observed and simulated conditions. Consequently, an automated optimization procedure was used to calibrate the site-scale saturated zone flow model. However, manual adjustments to the calibration were also performed (SNL 2007a, Section 6.5.1) to ensure that the flow direction southeast of the repository (in the low-gradient, anisotropic region) matched the direction indicated from the range and distribution of head values in this area, and that simulated particle pathlines fall within the bounds indicated by the geochemical analysis (SNL 2007a, Appendices A and B). Discussed below are the criteria used to guide calibration, along with optimization procedures used during calibration, model outputs for which the difference between simulated and observed values were minimized during calibration (calibration targets or observations), and those parameters that were optimized during calibration.

The site-scale saturated zone flow model was calibrated with the commercial parameter estimation code, PEST. PEST is a Levenberg-Marquardt-based optimization algorithm used to simultaneously minimize the difference between simulated and observed water levels and boundary flows. These combined differences are usually referred to as an objective function. The Levenberg-Marquardt package is a well-established algorithm (Press et al. 1992, pp. 678 to 683); it is robust, and widely applicable. In this case, the "function" is the sum of squared weighted differences between a set of observations (the heads in 161 wells in the Yucca Mountain region plus lateral boundary volumetric/mass flow rates from the Death Valley regional groundwater flow model) and the solution to the partial differential equation that describes saturated flow. PEST seeks the minimum of the sum of squared weighted differences function with respect to the various parameters. As discussed, those parameters optimized during calibration are the intrinsic permeability or permeability multiplier of each of the various hydrogeologic units, faults, and features. The following steps are taken to estimate optimized permeabilities:

1. An initial estimate for each unknown parameter is specified at the beginning of the fitting process.

2. FEHM computes the resulting heads for the initial estimate of parameters.

3. The results are returned to the PEST code.

4. Through a series of FEHM simulations with perturbations in the parameters, the PEST Levenberg-Marquardt package computes the derivative of the sum-of-squares difference function with respect to each of the parameters.

5. The Levenberg-Marquardt package then determines the amount to change each parameter's current value to improve the fit to the data. It does this through a mathematical process that combines gradient information and second derivative (approximated) information.

6. This process is repeated until the fit to data is within a prescribed tolerance, or until no further improvement is possible.

The site-scale saturated zone flow model was calibrated to achieve a minimum difference between observed water levels and simulated water levels, and also between volumetric/mass flow rates along specific boundary segments simulated by the Death Valley regional groundwater flow system model and site-scale saturated zone flow model. For calibration targets, 161 water level and head measurements were used. This was the complete set of wells available at the time of calibration. The water level measurements (BSC 2004a, Table A-1; SNL 2007a, Appendix E) represent either water table levels or deeper head measurements. The deeper measurements represent average values over "open" or "packed-off" intervals, and the coordinates of the observations represent midpoints of the open interval, midpoint of the bottom of the open interval and the average water level, or the depth of the node at the water table, whichever is smallest. The calibration targets represent steady-state values and, where pumping is taking place, as in the Amargosa Valley, current water levels are used. When comparing simulated water levels to target water levels, the model represents water levels at the target locations by assigning the target head value to the nearest FEHM node. Refer to Appendix A of *Water-Level Data Analysis for the Saturated Zone Site-Scale Flow and Transport Model* (BSC 2004a) for a complete description of water levels, well locations, and measurement depths.

During the calibration process, emphasis was placed on minimizing the difference between observed and simulated water levels at selected target locations, based on probable flow pathways as identified using geochemical analyses (SNL 2007a, Appendices A and B). This was accomplished by multiplying the squared differences at that location by a weighting factor. A weighting factor of 1 (i.e., standard importance) was applied to most calibration targets (SNL 2007a, Section 6.5.1.2). However, a preferential weighting factor ($\Sigma = 20$) was applied to 22 calibration targets in the low-gradient region to the south and east of Yucca Mountain (SNL 2007a, Section 6.5.1.2). These calibration targets were given high weighting because they are in the likely groundwater pathway leaving the repository site, based on the geochemical analyses, and because small changes in head in this area could produce a large effect on the flow direction. Six calibration targets are north of Yucca Mountain in the high head region. These are either assigned a low weighting (0.1, which implies little importance) if they were thought to represent perched conditions, or a weight of 10 to help ensure that no unphysical "mounding" of water occurs. Four additional water levels that are assumed to represent perched conditions are assigned weights of 0.1.

The assumption that perched water levels were measured in several wells (BSC 2004a, Sections 5.1 and 6.4) means those measurements do not represent the true water table surface and it is appropriate to use a low weight for those values. Three wells (USW WT-7, USW WT-10, and both completions of USW H-6) in the moderately high head area just west of the Solitario Canyon Fault are assigned weights of 20 (the combined weight of the two H-6 completions is 20) because their accuracy ensures proper representation of this fault as a hydraulic barrier. Because Crater Flat tuffs are important to estimated flow paths, those wells completed in these units (and not already assigned a high weight for being in the flow path) are given a weight of 5.

Two wells—USW UZ-14 and USW H-5—were deweighted because of anomalously high heads. The high potentiometric heads in these two boreholes is attributed to the presence of a splay of the Solitario Canyon Fault penetrated by the boreholes (Ervin et al. 1994, pp. 9 to 10). This splay is believed to be an extension of the hydrologic barrier to west-to-east groundwater flow from Crater Flat (related to the Solitario Canyon Fault). The high heads in USW H-5 (about 775 m) are related to heads in Crater Flat (ranging from 775 to 780 m), and this borehole defines part of the moderate hydraulic gradient along the western edge of Yucca Mountain. Borehole USW UZ-14 is in a transition zone between the large and moderate hydraulic areas, and the high potentiometric level (about 779 m) is related to either of these areas. Rousseau et al. (1999, p. 172) hypothesized that perched water in USW UZ-14 could be caused by a nearby projected growth fault that impedes percolation of water from the surface. The high heads in USW UZ-14 also could be caused by the low permeability rocks in the upper part of the saturated zone at that borehole. These hypotheses, in combination with the lack of a corresponding feature or process used to specify faults, supports the deweighting of USW UZ-14 and USW H-5. Wells showing an upward gradient are assigned a weight of 10 because it is important to reproduce this phenomenon (SNL 2007a, Section 6.5.1.2). If multiple calibration targets (head measurements) are available from a single well, the sum of weights from each well sum to the specified value (i.e., four measurements from USW H-1 each have weights of 7, 1, 1, and 1). The weighting of measurements was performed to ensure a close match to observations in and around the Yucca Mountain repository and in the downgradient flow direction. Other weighting distributions were examined, but none were deemed acceptable because they led to flow paths that did not match the observed water level information as well as the weighting described here. These other flow paths include those that are more easterly or more southerly than in the base case model. Uncertainty in flow paths is incorporated in the site-scale flow and transport abstraction model through uncertainty in the horizontal anisotropy parameter, which produces a range of flow directions (SNL 2008b, Figure 6-1[a]).

The model formulation and the FEHM code require a specified permeability at each node. Sets of nodes are grouped into specific permeability zones, based on similar permeability characteristics, as identified in HFM2006 (SNL 2007c). A single permeability value is assigned to each zone. These zonal values of permeability are the parameters that are optimized during model calibration. Permeability zones correspond to hydrogeologic units identified in the HFM2006 conceptual model, or to specific hydrogeologic features (Table 2.3.9-8). All of the nodes within a specific hydrogeologic unit were assigned a calibrated permeability unless a node was included in one of the permeability zones established for specific hydrogeologic features or faults. The zone sizes were fixed based on data from HFM2006. Uncertainty associated with geologic contacts is discussed in Section 2.3.9.2.2.2.

The vertical anisotropy in permeability is assigned a value of 10:1 (horizontal to vertical) in the volcanic and valley-fill units. Lower permeability in the vertical direction than in the horizontal direction typically occurs in stratified media, and the ratio of 10:1 is in the generally accepted range (CRWMS M&O 1998, Table 3-2). For a site-specific example, the relatively high vertical gradient observed in well UE-25 p#1 indicates that vertical permeability is lower than horizontal permeability (minimal hydraulic connectivity). Ten wells exhibited vertical gradients corresponding to head differences of greater than 1.0 m (BSC 2004a, Table 6-4).

Specific hydrogeologic features thought to potentially impact groundwater flow are classified as distinct permeability zones. The permeability variable or permeability multiplication factor used for a specific feature was assigned to all of the nodes within that feature. The hydrogeologic features for which special permeability zones were established are primarily faults, fault zones, and areas of potential chemical or mineralogical alteration. As previously discussed, these features are distinct from the subhorizontal hydrogeologic units identified in HFM2006. Each of the identified hydrogeologic features includes multiple geologic formations, and represents a zone of altered permeability within individual formations. Twenty-three permeability zones were established based on the geologic units within the site-scale saturated zone model domain from HFM2006 for model calibration (SNL 2007a, Table 6-2). Additional (usually low) permeability zones, reflecting the altered northern region, were added to the model to help establish known system characteristics (like the large hydraulic gradient). These were established by dividing existing (base) geologic units into altered northern regions with permeabilities defined by multipliers. These permeability multipliers are calibration parameters that modify the permeability values assigned to geologic units in the altered northern regions. Eight additional permeability zones representing faults and the Lower Fortymile Wash alluvium were established because they were identified as important structural features (e.g., the Solitario Canyon Fault), or they were necessary for some conceptual feature, such as the large hydraulic gradient north of Yucca Mountain.

In addition to the PEST optimization described above, several manual adjustments were made to improve the model in ways that were not possible during the PEST run. Specifically, during calibration, only water levels (and lateral volumetric/mass flows) were considered in the objective function and hence head gradients or important head differences between wells were not explicitly considered. Manual adjustments were made to the values of permeability for some hydrogeologic units and features (SNL 2007a, Section 6.5.1.3) to ensure that the flow direction southeast of the repository (in the small-gradient, anisotropic region) matched the direction inferred from the range and distribution of head values in this area and the geochemical pathline analysis (SNL 2007a, Appendices A and B). These adjustments modified the direction of particle paths emanating from beneath the repository (to match the direction inferred from differences in the measured water levels) while maintaining good calibration (low objective function and low weighted root-mean-square residual for heads). The specific discharge was adjusted by changing the permeability of several units without adversely affecting the simulated heads or gradient in the low hydraulic gradient area near Yucca Mountain (SNL 2007a, Section 6.5.1.3 and Table 6-10). A zone was defined near Yucca Mountain with a quadrilateral identified as the anisotropy zone shown on Figure 2.3.9-12. This zone of enhanced permeability was composed only of Crater Flat Tuffs within the quadrilateral, and was incorporated into the model between Solitario Canyon and Fortymile Wash Faults because of the somewhat anomalous water levels noted in wells USW H-5, G-1, and UZ-14. Specifically, these wells are located east of the Solitario Canyon Fault, yet they showed heads closer to those wells west of Solitario Canyon Fault (USW H-6, WT-7, and WT-14) than those

in the low-gradient area southeast of the repository (e.g., the C-Wells). This indicates that some noncharacterized feature or process is impacting the water levels just to the east of Solitario Canyon Fault, and the newly defined zone allows the model to better represent these data. The quadrilateral is defined to encompass the low-gradient area southeast of the repository without including wells USW H-5, G-1, and UZ-14. The anisotropic zone was defined based on responses of USW H-4, ONC-1, UE-25 WT#14, and UE-25 WT#3 to pumping at the C-holes from May 1996 to November 1997 (SNL 2007b, Section 6.2.6), and includes the area with similar alignment of faults that potentially contribute to horizontal anisotropy in the tuff units (SNL 2007a, Table 6-7 and Figure 6-3). The permeability of the Bullfrog Tuff within the quadrilateral identified as the anisotropy zone (Figure 2.3.9-12) was adjusted during hand calibration to ensure that the small hydraulic gradient region observed southeast of the repository is simulated accurately by the model. Additionally, the hydraulic conductivity of the Bullfrog tuff unit was adjusted to better match observations. The size and shape of the quadrilateral zone were determined based on the small hydraulic gradient region that is bounded on the west by the Solitario Canyon fault, on the north by the steep hydraulic gradient of the thermally altered region, on the east by the Fortymile Wash Fault, and on the south by the transition of small hydraulic gradient to moderate hydraulic gradient in the vicinity of Well UE-25 J-12.

2.3.9.2.3.3 Calibration Results

The site-scale saturated zone flow model calibration results consist of water levels and volumetric flow rates at the boundary. These results are discussed below.

Simulated and Observed Water-Level Elevations—The distribution of residuals (the differences between measured and modeled heads), along with the potentiometric (left) and simulated water-level (right) surfaces, is provided in Figure 2.3.9-13. The actual water levels (not the interpolated potentiometric surface) in each well are used for comparison.

As can be seen in Figure 2.3.9-13, the largest head residuals (~100 m) are in the northern part of the model in the altered northern region and in the vicinity of the moderate hydraulic gradient. These residuals are largely the result of the low weighting factor (of 0.1), and the possibility that they reflect perched conditions (SNL 2007a, Sections 6.5.2.1 and 6.7.7). In the figure, a negative residual means that the calibrated value was lower than the target data.

The next highest head residuals border the Crater Flat and Solitario Canyon Faults. These residuals (~25 m) are most likely the result of 250-m gridblocks not being able to resolve the 780-m to 730-m drop in head in the short distance just east of the above-mentioned features. It is more difficult to match water levels in steep gradient regions than in small gradient regions. The change in water level over the distance of a 250 m grid cell would be approximately 0.3 m, which is equivalent to the average horizontal hydraulic gradient between the area beneath the repository and the boundary of the accessible environment. In the steep gradient region, the water level change over the distance of a cell is about 19 m. The model produces an average water level over the area of a cell. A well located in a cell is unlikely to have a measured water level that is exactly the same as the average value for the cell. In a small gradient area, the difference between the cell average value and the measured value in a well will be small, but in a steep gradient area, the difference can be much larger. Thus, it is not unusual to have greater hydraulic head residuals in a steep gradient region. There may be additional complicating factors, such as varied hydrologic characteristics in the Solitario Canyon

Fault along its north-south transect. The fault is modeled as a barrier to groundwater flow with only one calibration parameter. This may not be adequate to represent the local behavior of such a long feature. For example, well USW G-1, about 1,000 m from the Solitario Canyon fault, shows an 8-m difference between measured and simulated heads. The measured head for this well (754 m), located on the eastside of the fault, is closer to measured head values on the west side of the fault. Because the majority of wells on the east side have heads of approximately 745 m, the simulated head for USW G-1 has a calibrated result close to that value. Overall results indicate that the model adequately represents the current water table near Yucca Mountain. The calibrated site-scale saturated zone flow model has a weighted root-mean-square residual of 0.82 m when considering only differences between observed and simulated heads (lateral volumetric flow calibration targets were not included) (SNL 2007a, Table 6-8). Without weighting, the root-mean-square residual is 24.39 m, but this result is biased by the expected larger residuals in the steep gradient regions. Compared to the overall head drop of approximately 500 m in the model domain, the 24.39-m average residual corresponds to a 5% difference. The weighted root-mean-square residual in water levels is 0.82 m (SNL 2007a, Section 6.5.2.1).

The simulated water levels in the carbonate aquifer at well UE-25 p#1 are about 12 m lower than measured. The upward vertical gradient between the carbonate and the volcanic rocks is still maintained, although the magnitude of the gradient is smaller than indicated by measured water levels. Using Nye County water-level data, the model was able to simulate an upward head difference of about 0.5 m between the carbonate and the overlying units at wells NC-EWDP-2D and NC-EWDP-2DB (SNL 2007a, Table 6-8). In both cases, the model simulated the correct direction of the vertical gradient, but the magnitude of the simulated gradient was less than measured values. Transport results with the flow model adequately simulate the effects of the upward vertical gradient on flow paths from beneath the repository, regardless of the underestimation of the magnitude of the vertical gradient. Under the present-day climate conditions, flow paths simulated by the site-scale groundwater flow model do not enter the carbonate units; this is entirely consistent with the observed hydraulic gradient between the carbonate and volcanic rocks. For future wetter and cooler climates expected during the 10,000 years after closure, and for the period after 10,000 years, the flow and transport abstraction model uses a scaling factor to increase groundwater-specific discharge to account for the effect of water table rise (Section 2.3.9.2.4.1). Simulations with the Death Valley regional flow system model under wetter glacial climatic conditions indicate that the groundwater flow paths from below Yucca Mountain do not significantly change, and that the upward hydraulic gradient is maintained (D'Agnese et al. 1999).

Comparing Volumetric/Mass Flow Rates from the Regional-Scale Model with Volumetric/Mass Flow Rates from the Calibrated Site-Scale Model—The site-scale saturated zone flow model corresponds to only a small part of the Death Valley regional groundwater flow system model, which is used to supply target lateral volumetric/mass flow rates. The Death Valley regional groundwater flow system model simulates a closed system and uses data from spring discharges to calibrate the water flow through the system (Belcher 2004). Thus, the regional model provides a good estimate of volumetric/mass flow rates expected through the site-scale saturated zone model domain, which is recognized to be part of the much larger Death Valley regional flow system.

With fixed-head boundary conditions, the flow through a boundary is a function of the permeabilities on that boundary (SNL 2007a, Section 6.3.1.6). Flow targets were derived from the

values simulated by the Death Valley regional groundwater flow system model (SNL 2007a, Appendix C). A comparison of the calibration target volumetric/mass flow rates and volumetric/mass flow rates derived from the calibrated site-scale saturated zone flow model is provided in Table 2.3.9-5. The western boundary, for instance, has a total flow of 120.3 kg/s (3.8×10^6 m³/yr) across it for the target flow values, and 101.0 kg/s (3.2×10^6 m³/yr) across it in the calibrated model (SNL 2007a, Section 6.5.2.2). The simulated southern volumetric/mass flow rate (527.1 kg/s), which is simply a sum of the other boundary volumetric/mass flow rates plus the recharge, is about 23% smaller than the target value. In addition, the sum of all target boundary volumetric/mass flow rates (64.9 kg/s) is nearly equal to the sum of all volumetric/mass flow rates through the calibrated flow model (64.1 kg/s).

Factors that affect the boundary flow match between the regional- and site-scale models include the horizontal and vertical resolution and the permeability distribution. The horizontal resolution of the site-scale saturated zone flow model is 36 times finer than the regional model (250-m versus 1,500-m gridblock size). The vertical resolution of the site-scale saturated zone flow model is about four times finer than the regional model (67 versus 16 layers). The increased resolution at the site scale means that, compared to the regional-scale model, volumetric/mass flow rates calculated by the site-scale saturated zone flow model may depend more strongly on a few units. Flow distribution in the regional model is also impacted by the use of hydraulic conductivity classes. In the regional model, permeabilities (actually hydraulic conductivities) associated with specific units are not defined. Rather, the permeabilities are grouped into classes, which are assigned to a particular grid block based on the percentages of the rock types contained in the gridblock. Thus, although the Death Valley regional groundwater flow system model was based on the same complex hydrogeologic framework model as HFM 2006 used in the site-scale saturated zone flow model, the Death Valley regional groundwater flow system model used hierarchical zonation of hydraulic conductivity classes (Belcher 2004, Chapter F).

It is not possible to reproduce the distribution of volumetric/mass flow rates corresponding to the sides of the site-scale saturated zone flow model, when examined on a unit-by-unit basis, because of these fundamental differences. There are significant differences between the target flow rates and the simulated flow rates for East3 and East4 boundary zones; however, these differences partially offset one another. These differences indicate inconsistencies between the Death Valley regional flow system model and the site-scale saturated zone flow model at the scale of these individual boundary zones. Given the location of these boundary zones in a direction approximately perpendicular to inferred flow paths from beneath the repository, which are at a distance of greater than 10 km, and the fact that the differences between target flow rates and simulated flow rates partially offset one another, this discrepancy has a negligible impact on simulated flow paths or rates. Also, the simulated flow paths and rates are corroborated by other lines of evidence (Section 2.3.9.2.4.2). In addition, the simulated flow rate for the north boundary is less than the target flow rate. This difference is the result of a trade-off in the calibration process between matching the high head observations in the northern part of the site-scale saturated zone flow model and matching the estimated target flow rate on the north boundary. Nevertheless, the difference in the total flow across the southern boundary between the site-scale saturated zone flow model and the Death Valley regional flow system model is considered acceptable within the uncertainty in the recharge and boundary flow rates, as presented in Section 2.3.9.2.2.3. Mass balance error for all runs with the site-scale saturated zone flow model was essentially zero (SNL 2007a, Section 6.5.2.4).

Simulated Flow Paths—The particle-tracking capability of FEHM illustrates flow paths simulated by the calibrated site-scale saturated zone flow model. One hundred particles were distributed randomly over the area beneath the repository, and were allowed to migrate subject to advection only (nondispersive) until they reached the site-scale saturated zone flow model boundary (Figure 2.3.9-14). The pathways generally leave the area beneath the repository and travel in a south-southeasterly direction to the southern part of the postclosure controlled area. From the southern part of the postclosure controlled area to the end of the model, the flow paths trend to the south-southwest and generally follow Fortymile Wash. Some of the pathways follow fault zones along Fortymile Wash (SNL 2007a, Figure 6-12). The hydrogeologic units through which the flow below the repository passes consist of the Crater Flat Group (Bullfrog, Tram, and Prow Pass), with most of the flow in the Bullfrog unit, the upper volcanic aquifer, the upper volcanic confining unit, the valley fill unit, and the undifferentiated valley-fill unit (SNL 2007a, Section 6.5.2.3). Figure 2.3.9-14 includes a vertical cross section of the path lines. Evident in the figure is the shallow depth of the path lines along most of the pathways in the vicinity of the southern end of the postclosure controlled area boundary, which is consistent with data supporting an upward head gradient. The fluid pathways compare favorably with those inferred from geochemical data (Figure 2.3.9-15) (SNL 2007a, Figure 7-5).

Specific Discharge—Using the calibrated site-scale saturated zone flow model, specific discharge was estimated as the average over 100 particles. These particles were randomly distributed below the repository and tracked until they traveled across a line located about 5 km south of the southern tip of the repository. The sole purpose of the plane is to provide a location to make comparisons between simulation results and other information at a distance intermediate between the repository and the postclosure controlled area boundary. Path length divided by travel time (using a porosity of 1) yields the specific discharge for a particle, and the average across 100 particles was 0.36 m/yr (1.08 ft/yr) for the calibrated model (SNL 2007a, Section 6.5.2.4). End members of the 100-particle plume had specific discharges of 0.11 and 0.66 m/yr (SNL 2007a, Section 6.5.2.4). This range of specific discharge represents the uncertainty in the model due to the spatial distribution of hydrogeologic units and unit properties. The impact of other sources of uncertainty on the specific discharge are addressed in Section 2.3.9.2.3.6. For comparison, the expert elicitation panel (CRWMS M&O 1998, Figure 3-2e) estimated the aggregate uncertainty in specific discharge to have a range of values from less than 0.01 m/yr to about 10 m/yr, with a median value of 0.6 m/yr (2.0 ft/yr) for the 5-km (3-mile) distance. Thus, the specific discharge simulated by the calibrated site-scale saturated zone flow model falls within the range of values determined by the expert elicitation panel. Uncertainty in specific discharge is incorporated in the saturated zone flow and transport abstraction model with the groundwater specific discharge multiplier, which incorporates a range of flow values (Section 2.3.9.3.3.4). In the alluvium, the simulated specific discharge values of 11.7 and 21.0 m/yr in grid cells corresponding to wells NC-EWDP-19 and NC-EWDP-22 are larger than the observed range of 0.5 to 12 m/yr (SNL 2007a, Section 7.2.3 and Table G-10) (Tables 2.3.9-2 and 2.3.9-3).

The simulated specific discharge can also be compared with the measurements in Well NC-EWDP-24PB (Freifeld et al. 2006). The experiments in well 24PB were conducted primarily in the Crater Flat Tuff unit. Relatively high volumetric flow rates were observed in several intervals in the well. Using the observations from fluid electrical conductivity logging and distributed thermal perturbation sensor measurements, the ambient velocity in the flowing intervals ranged from 0.5 to 31 km/yr (Freifeld et al. 2006, Section 3.3.3 and Table 4). Converting to specific

discharge by multiplying values of velocity by the porosity of 0.01 (as assumed by Freifeld et al. (2006)) and converting from km to m, the range of specific discharge values is 5 to 310 m/yr. These values appear to be much larger that the simulated values, but these measured values must be assessed with respect to scale. The measured values were obtained using an assumption of a 30-m-long and 0.34-m-wide interval for the well. Thus, the scale of the measurement is very small, particularly in the lateral direction. To be comparable to the model simulations, these values must be scaled up to the simulation scale. One way to scale the values is to assign the measured flow to a single flowing interval. The median flowing interval spacing (see parameter FISVO in Table 2.3.9-4) is 25.8 m. Over a single model grid cell of dimension 250 m, there are approximately 10 flowing intervals. The volume averaged specific discharge across one flowing interval of 25.8 m wide ranges from 0.07 to 4.1 m/yr (obtained by dividing the measured specific discharge of 5 to 310 m/yr by the ratio of the flowing interval spacing of 25.8 m divided by the measurement width of 0.34 m). Scaled up to the model scale, the specific discharge values from the 24PB test are in the same range as the simulated values and the range of uncertainty considered in those simulated values (Section 2.3.9.2.3.6).

2.3.9.2.3.4   Site-Scale Saturated Zone Model Uncertainty and Sensitivity Analyses

The site scale saturated zone flow model propagates information to the performance assessment calculations, which are used to evaluate potential risks to groundwater users downgradient from the repository area. The results of these performance assessment calculations depend upon the specific discharge of groundwater leaving the area beneath the repository, as well as on the flow paths and the distribution of flow among the various hydrostratigraphic units that may act as conduits or barriers to flow. This section presents analyses of the alternative conceptual models as a method of assessing uncertainty, their representation in the numerical model, and a discussion about possible impacts on the model outputs (specific discharge and flow paths).

The calibrated site-scale saturated zone flow model described in detail in *Saturated Zone Site-Scale Flow Model* (SNL 2007a, Section 6.5) provides the basis for the evaluation of alternative conceptual models. That is, the same numerical grid and HFM2006 were used for the alternative conceptual models. Various parameterization schemes were used to define the alternative conceptual models (e.g., change in potentiometric surface). The following alternative conceptual models were evaluated:

- Removal of vertical anisotropy: this alternative conceptual model relates to removal of vertical anisotropy in permeability.

- Removal of horizontal anisotropy: this alternative conceptual model relates to removal of horizontal anisotropy in the volcanic units downgradient from Yucca Mountain.

- Removal of the altered northern region: this alternative conceptual model relates to removal of the permeability multipliers that reduce the permeability in the northern region, which help the model match the observed high head.

- Increase in permeability in the vertical direction for the Solitario Canyon Fault.

- Water table rise: this alternative conceptual model relates to future water table rise. The impact of the higher water table is assessed with the site-scale saturated zone transport model.

Removal of Vertical Anisotropy—Anisotropy occurs when hydraulic properties have different values in the three principal directions: vertical, horizontal (along the direction of maximum permeability), and horizontal along the direction of minimum permeability. The ratio of horizontal to vertical permeability, 10:1, is in the generally accepted range provided by the expert elicitation panel (CRWMS M&O 1998, Table 3-2). The removal of vertical anisotropy (i.e., 1:1) produces a 28% increase in specific discharge across the 5 km boundary from 0.36 to 0.46 m/yr (SNL 2007a, Section 6.6.1). Weighted root-mean-square error increases significantly (89%) from 0.82 to 1.55 m, and nonweighted root-mean-square error increases 20% from 24.39 to 29.21 m. Differences in volumetric flow through the model boundaries changed by no more than 8% (SNL 2007a, Section 6.6.1). Without vertical anisotropy, particles travel deeper in the system (from 353 m elevation for the anisotropic case to −175 m without vertical anisotropy) (SNL 2007a, Figure 6-18). Overall, 10:1 vertical anisotropy yields better flow calibration because removal of vertical anisotropy degrades the accuracy and representativeness of the model results. A vertical anisotropy of 10:1 was used in the site-scale saturated zone flow model.

Removal of Horizontal Anisotropy—Anisotropy in the volcanic units near Yucca Mountain was investigated using an alternative conceptual model with variable horizontal anisotropy ratios (north-south to east-west permeability changes). The area to which the anisotropy ratio was applied is bounded by the quadrilateral shown in Figure 2.3.9-12. This effect was investigated by rerunning the calibrated model with a 1:1 horizontal permeability ratio in this region and checking the sensitivity of the modeled output (water levels and flow paths). A detailed description of the development of the horizontal anisotropy distribution used in this model is found in *Saturated Zone In-Situ Testing* (SNL 2007b, Section 6.2.6 and Appendix C6). Modeling the Yucca Mountain volcanic zones as isotropic yielded insignificant changes to the weighted root-mean-square error for head residuals (0.82 m) (SNL 2007a, Section 6.6.2). Specific discharge across the 5 km boundary decreases by 31%, from 0.36 to 0.25 m/yr. Associated pathlines, as expected, have a more easterly trend immediately downstream from beneath the repository, as compared to the calibrated model. In addition, pathlines go somewhat deeper: to 319 from 353 m for the horizontally isotropic case. A range of horizontal anisotropy, including isotropic conditions, is incorporated in the TSPA analysis because of its impact on specific discharge results.

Removal of Large Hydraulic Gradient and Change to the Solitario Canyon Fault Anisotropy—A large hydraulic gradient just north of Yucca Mountain has been inferred from hydraulic head measurements. The saturated zone flow model implements the large hydraulic gradient with a conceptual model that characterizes the northern region by alteration due to the Claim Canyon Caldera north of Yucca Mountain, and divides hydrogeologic units into distinct northern and southern zones. Although the genesis of the large hydraulic gradient has yet to be fully explained, logic dictates that—so long as the large hydraulic gradient in this region is faithfully represented (regardless of its conceptualization)—effects on flow paths are minimal because the region is upgradient from the zone of interest (and away from zones that are weighted heavily during calibration). However, removal of the large hydraulic gradient from the conceptual

model yielded an increase in specific discharge across the 5 km boundary to 4.79 m/yr (an increase by nearly a factor of 15), because the zone of reduced permeability was eliminated from the altered northern region (permeability multipliers set to one, but no recalibration performed), and the overall flow of water through the northern model boundary was significantly increased. The weighted root-mean-square error was increased by nearly a factor of 8 to 6.20 m. Clearly, removal of the large hydraulic gradient from the conceptual model yields a model that does not match observations; hence, its existence (not its conceptualization) is critical to an accurate model (SNL 2007a, Section 6.6.3). Therefore, this alternative conceptual model is not utilized in the TSPA analysis.

Changing the vertical anisotropy in the Solitario Canyon Fault from a factor of 10 to 1,000 yielded a 3% increase in specific discharge across the 5 km boundary to 0.37 m/yr. Weighted head residuals, however, actually decreased 2% to 0.80 m (non weighted residuals increased by 1% to 24.67 m). This indicates that different conceptualizations for anisotropy of the Solitario Canyon Fault do not impact water levels, but can impact specific discharge to some degree (SNL 2007a, Section 6.6.3). Therefore, this alternative conceptual model is not utilized in the TSPA analysis.

Alternative Implementation of Water Table Rise into the Saturated Zone Flow and Transport Models—In addition to modeling saturated zone flow under present conditions, it is also necessary to consider conditions as the climate changes in the future. A higher water table is expected in the Yucca Mountain region for future wetter climatic conditions. The effects of climate change on radionuclide transport simulations in the saturated zone are incorporated into the TSPA analyses by scaling the simulated saturated zone breakthrough curves by a factor representative of the future climate state (SNL 2008d, Section 6.3.10.2). The scaling factor used in this approach is the ratio of average saturated zone groundwater flow under the future climatic conditions to the flow under present conditions. This approach approximates the impacts of future, wetter climatic conditions in which the saturated zone groundwater flow will be greater. However, this approach implicitly models the same flow path for radionuclide transport through the saturated zone under wetter climatic conditions of the future. In reality, a significant rise in the water table due to climatic changes may result in different flow paths through the saturated zone system, including the potential for encountering different hydrogeologic units by radionuclides during transport. As noted in the site-scale saturated zone transport model, the Calico Hills volcanic-rock hydrostratigraphic unit overlying the present water table under much of the repository has lower permeability and, thus, travel times under a higher water table scenario will be longer than using the present-day water table (SNL 2008a, Table 6.6-1a and Appendix E).

Estimating Water Table Rise from Climate Change—Rise in the water table during wetter glacial transition conditions at Yucca Mountain is a function of greater recharge to the saturated zone and changes to the amount and spatial distribution of lateral flow from the Death Valley regional groundwater flow system. Simulations of groundwater flow under wetter climatic conditions with the saturated zone regional scale flow model (D'Agnese et al. 1999) indicate that groundwater flow paths from below Yucca Mountain do not significantly change under glacial climatic conditions. These simulations also show that groundwater surface discharge from the saturated zone for the wetter glacial climatic conditions would not occur along the flow path from Yucca Mountain at any location closer than the postclosure controlled area boundary of the accessible environment, which is approximately 18 km south of the repository (SNL 2007a, Section 6.6.4.2.1). Thus, although the analysis of the water table rise discussed in this section is

for glacial-transition climatic conditions, the water table rise analysis is a reasonable approximation of changes expected in the saturated zone for time periods beyond 10,000 years in the future (Section 2.3.9.1). Accordingly, the conclusions are applicable to TSPA analyses that extend to peak simulated dose during the time of geologic stability.

The estimated elevation of the water table under wetter, glacial-transition conditions within the domain of the site-scale saturated zone flow model was calculated using simple linear increases in the elevation of the water table. The site-scale saturated zone flow model cannot explicitly simulate water table rise because the saturated zone is represented as a confined system; so this simplified approach was used to estimate water table rise. At the discharge locations along Highway 95, paleospring deposits indicate that the water table rise will be limited to about 30 m because discharge to the land surface will occur and prevent further rise at that location (SNL 2007a, Section 6.6.4.1). Further south, the water table rise is expected to be somewhat smaller; generally, about 20 m. To the north at the location of the repository, a recent multidisciplinary workshop identified the median water table rise beneath the repository for future climates to be 50 m (SNL 2007a, Section 6.6.4.1). To increase flow under a wetter future climate scenario, the water table gradient must increase (based on Darcy's Law). This means that the amount of water table rise at Yucca Mountain must be larger than at the discharge area along Highway 95. To approximate that increase in the water table gradient, a linear increase in the water table rise from 20 m at the southern end of the model area, to about 50 m under the repository, to as much as 100 m north of the repository, was incorporated. This estimated linear increase in water level was calculated with a 20-m rise at locations with a present-day water table elevation of 700 m, which is a 50-m rise at locations with a present-day water table elevation of 740 m, and a 100-m rise at locations with a present-day water table elevation of 1,000 m (SNL 2007a, Sections 6.6.4.1 and 6.6.4.2.1). The estimated higher water table for glacial-transition climatic conditions at other locations was calculated by linear interpolation or extrapolation. In addition, the rise in the water table was limited by the topographic surface.

This approach results in a water table rise of approximately 50 m in the area beneath the repository. The approach also approximately preserves the direction of the horizontal hydraulic gradient at the water table, which is consistent with the results of the saturated zone regional-scale flow model with regard to the simulated flow paths from beneath the repository under wetter climatic conditions (D'Agnese et al. 1999). The approach to assess water table rise in the saturated zone model differs from the approach used in the site-scale unsaturated zone transport (Section 2.3.8), where a fixed value of 120 m is used for the rise in the glacial transition case. The usage in Section 2.3.8 is conservative because it reduces the radionuclide transport time through the unsaturated zone.

The estimated elevation of the water table under wetter, glacial-transition climatic conditions, as calculated with the approach described above, was shown (SNL 2007a, Section 6.6.4.2.1) to produce groundwater flow directions that are similar to the groundwater flow directions for the present water table (Figure 2.3.9-13), with the exception of the area in Fortymile Canyon in the northern part of the model domain. The deflection of the water table contour in Fortymile Canyon corresponds to an area in which the water table rise has been limited by the topographic surface. There is little information upon which to base estimates of the water table configuration under future climatic conditions in the area to the north of Yucca Mountain in the site-scale saturated zone flow model domain. Regardless, the approach used to estimate water table rise to the north of the

repository has an insignificant impact on the simulated flow system downgradient of Yucca Mountain in the site-scale saturated zone flow model.

The higher water was shown to be consistent with the location of paleospring deposits located along U.S. Highway 95 and at the southern end of the Crater Flat. This shows consistency between the estimated higher water table and the geologic features associated with Pleistocene spring discharge. The specific paleospring locations are probably controlled by structural features too small to be resolved with this model. Another site of calculated spring flow under a higher water table case is the northern end of Fortymile Canyon. Paleospring deposits are not observed in Fortymile Canyon, but it is reasonable to postulate that such deposits would not be preserved in this geomorphic location because the canyon is narrow and flood flows would have eroded paleospring deposits. It is also reasonable to expect that the water table would rise to the extent that upper Fortymile Wash would become a perennial gaining stream in Fortymile Canyon under wetter climatic conditions, because the present depth to water in that area is small (depth to water at well UE-29a#2 is only 27.7 m (BSC 2004a, Table A-1)). The areas of simulated shallow groundwater near and on the southern boundary of the model domain do not correspond to specifically identified paleodischarge locations, but paleospring deposits could have been buried by aggradation of alluvium in these locations.

Analyses of the impacts of climate change and water table rise on groundwater flow in the area near Yucca Mountain were conducted using an independently developed site-scale flow model described by Winterle (2003; 2005). These modeling studies included increased values of specified head at the flow model boundaries, increased recharge, and potential discharge of groundwater from springs activated by the higher water table. It was concluded that neither the increase in the water table elevation nor the discharge of groundwater from springs significantly affected the flow paths from beneath Yucca Mountain. Comparison of the predicted locations of shallow groundwater under glacial-transition climatic conditions from the *Saturated Zone Site-Scale Flow Model* (SNL 2007a, Figure 6-21) with the simulated locations of potential discharge locations (Winterle 2005, Figure 3) indicates similar results. Both approaches indicate similar patterns of potential discharge at the southern end of Crater Flat and in two areas near the southern boundary of the site-scale saturated zone flow model domain. The results from the water table rise analysis (SNL 2007a, Section 6.6.4.2.1) differ from the results of Winterle (2005, Figure 3) in that potential discharge in Fortymile Canyon is predicted in the approach used in the site-scale saturated zone flow model, and is not predicted by the modeling of Winterle (2005). The predicted potential discharge in Fortymile Canyon occurs to the north of Yucca Mountain and would not be a location for the potential release of radionuclides from the repository. The specific discharge for the flow path from beneath the repository to a distance of about 5 km was 1.26 m/yr after the water table rise (SNL 2007a, Section 6.6.4.2.2).

In summary, a reasonable estimate of the water table elevation under wetter, glacial-transition conditions was developed for the site-scale saturated zone flow model domain. The estimated rise in the water table is consistent with the conclusion that the general direction of flow paths from beneath the repository would not change for wetter climatic conditions: although differences in hydrogeologic units occurring at the water table below the repository would have an impact on local flow paths, the overall impact is an increase in travel time from the repository to the accessible environment (SNL 2008a, Table 6.6-1a and Appendix E). In addition, the pattern of the estimated

rise in the water table is generally consistent with the locations of paleospring deposits within the domain.

Model Uncertainty—Uncertainty in flow modeling arises from a number of sources including, but not limited to, the conceptual model of the processes affecting groundwater flow, water-level measurements and simplifications of the model geometry, boundary conditions, hydrogeologic unit extent and depth, and the values of permeability assigned to hydrogeologic units (SNL 2007a, Section 6.7). These sources of uncertainty are discussed in the following subsections.

Model uncertainty arises in a calibrated model simulation due to the necessary simplifications made during model development (e.g., using HFM2006, applying constant boundary conditions, representing a heterogeneous geologic unit with a homogenized geologic unit, single porosity model of a dual porosity medium, etc.). Model uncertainty represents the differences between real world conditions and their simulated equivalents arising from the inability of model parameters to precisely represent the innate complexity of the real world. Solution space uncertainty, which is a form of epistemic uncertainty, is contained in a model parameter that arises from the fact that its estimation through calibration is based on data that is uncertain because of measurement errors and spatial variability (including that induced by the simplification process required when constructing a hydrologic model). One of the key outputs of the site-scale saturated zone flow model is the specific discharge across the flow field. An assessment was performed to examine the impact of uncertainty on the simulated specific discharge values (SNL 2007a, Section 6.7.1).

2.3.9.2.3.5   Uncertainty in Specific Discharge

Uncertainty in the specific discharge value simulated by the site-scale saturated zone flow model comes from a variety of sources. These include uncertainty in the underlying HFM2006, the impact of fault flow and perched water, scaling, and the flow path uncertainty.

Effect of Hydrogeologic Contact Uncertainty on Specific Discharge—The hydrogeologic framework model conceptual model for the site-scale saturated zone flow model was created from a variety of field data, and exists in electronic form as Earthvision surfaces (SNL 2007c). There is uncertainty in the spatial positions of these surfaces that is primarily due to the nature of subsurface investigations where direct observations come from a number of boreholes. These surfaces were used to generate the finite element mesh such that each node is assigned those hydrogeologic properties found at that location. There is interest in how uncertainties in the representation of hydrogeologic-unit horizontal locations affect specific discharge calculations. Due to the coarseness of the finite element mesh, some horizontal uncertainty in the hydrogeologic framework model can be accommodated. As long as the horizontal spatial ambiguity in the location of hydrogeologic contacts is less than 125 m (one half the gridblock dimension), there is essentially zero impact on model specific discharge or flow calculations (SNL 2007a, Section 6.7.3).

The vertical dimension deserves special consideration because flow leaving the repository area is confined to a few of the most permeable units. From the site-scale saturated zone flow model, it is known that the fluid leaves the repository area through the Crater Flat Tuffs and migrates to alluvial units. The flow paths in areal and vertical views are reproduced in Figure 2.3.9-14. Note that the vertical thickness of the flowing zone varies between 25 and 400 m, and the elevation changes from 400 to 700 m above sea level. The spacing in this part of the finite element mesh

varies from 10 to 50 m (SNL 2007a, Table 6-4). Consider, for example, that the uncertainty in the vertical location of a geologic contact is 50 m in the portion of the model where the flow path is 400 m thick. Changing a single element's hydrogeologic designation, either to or from one unit to another, could not result in a change to the average local specific discharge by more than a factor of 50/400 (13%). This is well within the overall specific discharge uncertainty range (Section 2.3.9.2.3.6). The vertically thin flow path in the vicinity of the southern boundary of the postclosure controlled area (Figure 2.3.9-14) is primarily the result of the spatial arrangement of the hydrostratigraphic units. Here the fluid flow is vertically constrained by the hydrostratigraphy to about 25 m. If the bottom contact of the local hydrogeologic unit were to change by 10 m (the thickness of a single layer), this could result in a change to the average specific discharge in that area of up to 40% (SNL 2007a, Section 6.7.3). Integrated specific discharge calculations will be affected to a lesser degree. A study of the impacts of hydrogeologic contact location uncertainty reveals the following:

- Sensitivity to uncertainty in the hydrogeologic contact surfaces in the horizontal directions is much less than in the vertical direction due to the averaging effect of 250 m gridblock spacing

- The change in specific discharge due to the 50 m uncertainty in the vertical hydrogeologic surface can produce up to a 13% change in the local specific discharge near the repository and in the alluvial flow regions

- 10 m uncertainty in the vertical hydrogeologic surface can produce up to a 40% change in the local specific discharge in the transitional zone along the flow path in the vicinity of the southern boundary of the postclosure controlled area.

Because of the averaging effect across elements in the integrated specific discharge calculations (0 to 18 km), a 50% regional change in a relatively small portion of the 0 to 18 km compliance boundary affects model results only moderately. The range of uncertainty considered for specific discharge in the saturated zone flow and transport abstractions model is significantly greater than the uncertainty in the hydrogeologic framework model (SNL 2007c, Section 6.4.3).

Fault-Dominated Flow Impact on Specific Discharge Estimates—The analyses and corresponding assignment of an uncertainty range for the groundwater specific discharge assume that the porous continuum approach is appropriate for the fractured volcanic tuffs. A remaining uncertainty is whether or not the continuum approach can be employed at the scale of the model. An alternative interpretation is one in which most of the flow from Yucca Mountain moves through faults rather than through the unfaulted rock. Important faults are included in the model to capture their impact on flow and transport. Furthermore, the adoption of a range of parameter values that includes larger specific discharge values, smaller effective porosities, and larger flowing interval spacing introduces realizations that replicate the behavior of a fault dominated flow and transport system by providing a few realizations with very rapid travel times (Section 2.3.9.3.4.1 and Figure 2.3.9-16). Therefore, the suite of performance assessment transport simulations currently used encompasses the range of behavior that would be obtained with a fault-based flow and transport model (SNL 2007a, Section 6.7.5).

Effect of Perched Water on Flow Paths and Specific Discharge—Perched water was not explicitly modeled in the site-scale saturated zone flow model, because the weights applied to these observations were insignificant (0.1). It is noted that the conceptualization of the large hydraulic gradient through introduction of the altered northern region yielded water levels in wells UE-25 WT#6 and USW G-2 (suspected to be perched) that were much lower than the reported water levels. Modeled water levels are about 150 m lower than the data in this area to the north of Yucca Mountain (SNL 2007a, Table 6-8); but this is consistent with the perched water level interpretation in that area (BSC 2004a, Section 5). The area of suspected perched water is near the steepest hydraulic gradient in the model (see Wells USW G-2 and UE-25 WT #6 on Figure 2.3.9-13), and these hydraulic gradients occur over only a few model elements. Because the large hydraulic gradient is upgradient of the repository, it only minimally affects particle flow paths and transport times, as long as nonperched water levels at well USW WT #24 are honored by the model. Therefore, uncertainty due to perched water on flow paths and specific discharge is not propagated forward into the saturated zone flow and transport abstraction model (SNL 2007a, Section 6.7.6).

Scaling Issues—For most parameters, the spatial scale over which the measurement was taken (generally up to a few hundred meters and often times only a few meters) is often much smaller than the scale to which it is applied in a model (often kilometers). As a result, measured values may need to be adjusted when applied at the model scale (Neuman 1990; Harter and Hopmans 2004). Although there are many approaches that address the effects of scaling on model results, none has been widely accepted as an industry standard. Flow modeling is generally not very sensitive to scaling issues in both space and time. First, time scales are relatively unimportant because hydrogeologic properties change little over the time frame of interest (see excluded FEPs, such as 2.2.06.01.0A, Seismic activity changes porosity and permeability of rock, and 2.2.10.04.0A, Thermo-mechanical stresses alter characteristics of fractures near repository, in Table 2.2-5). While water level data and infiltration rates may change over long time periods, any flow model can easily account for these changes given appropriate boundary conditions. Second, while hydrogeologic properties measured through borehole pumping tests may not be appropriate to apply at distances far from the sample site (distance scaling), the site-scale saturated zone flow model that is described here does not use these measured properties directly. Instead, they are used to aid and validate calibration. Comparisons between measured and calibrated values for permeability are provided in Figure 2.3.9-6.

Flow Path Uncertainty—There are several metrics that could be used to evaluate uncertainty in specific discharge. However, to be consistent with specific discharge calculations, the flow path lengths from release below the repository to the 5 km and postclosure controlled area boundaries are examined. It should be noted that the random distribution of initial particle positions below the repository can significantly impact particle flow path length, if for no other reason than particles are distributed over a 5 km distance in the north south direction. The nominal distance to a boundary, such as the 5 km boundary, is based on the approximate center of the repository. From beneath the southern end of the repository, the distance to the nominal 5 km boundary is actually closer to 3 km or less. Flow paths are notably affected by the N-S:E-W horizontal anisotropy applied to the volcanic units in the anisotropic zone (Figure 2.3.9-5). The average flow path length across the 5 km boundary for 5:1 N-S:E-W horizontal anisotropy is 6.0 km (range of 3.1 to 8.6 km). The flow path length from beneath the repository to the postclosure controlled area boundary ranges from 19.4 to 25.4 km, with an average of 22.9 km. Average path lengths across

the 5 km boundary for 20:1 and 0.05:1 N-S:E-W anisotropies are 9.6 and 6.2 km, respectively. Correspondingly, the average flow path lengths are 29.7 and 22.8 km across the postclosure controlled area boundary. For the isotropic case, average flow path lengths are 6.0 and 23.2 km across the 5 km and postclosure controlled area boundaries, respectively (SNL 2007a, Section 6.7.9).

2.3.9.2.3.6   Parameter Uncertainty

Uncertainty exists in the groundwater flow rates in the saturated zone along the potential flow paths from beneath the repository to the boundary of the accessible environment. Uncertainty in groundwater flow rates and flow paths is explicitly incorporated into the saturated zone flow and transport abstraction model and the one-dimensional saturated zone transport model (Section 2.3.9.2.4.1) through two key parameters: the groundwater specific discharge multiplier, and the horizontal anisotropy in permeability, as described below. Table 2.3.9-4 summarizes the values and uncertainty distributions for all parameters used in the saturated zone flow and transport abstraction model simulations (SNL 2008b).

Groundwater Specific Discharge Multiplier—The uncertainty in groundwater specific discharge was quantified as a distribution of specific discharge in the volcanic aquifer near Yucca Mountain in the saturated zone flow and transport expert elicitation (CRWMS M&O 1998, p. 3-43). Conclusions regarding the uncertainty in specific discharge by the expert panel were primarily based on single-well and multiwell hydraulic testing at the C-Wells Complex in the volcanic units near Yucca Mountain. The aggregate uncertainty distribution of specific discharge in the saturated zone from the expert elicitation had a median value of about 0.6 m/yr, with a range of values from less than 0.01 m/yr to about 10 m/yr (SNL 2008b, Section 6.5.2.1).

The measurements in well NC-EWDP-24PB provide useful data with which to assess the range of values for specific discharge. As explained at the end of Section 2.3.9.2.3.3, the specific discharge values derived from measurements in well 24PB range from 5 to 310 m/yr, which are much larger than the previous estimates or other measurements in the alluvium (see the paragraph below). The scale of the measurements was very small in the lateral direction, and must be scaled up to be comparable to model scale parameters. An approximate scaling presented at the end of Section 2.3.9.2.3.3 yielded scaled-up values from well 24PB in the range of 0.07 to 4.1 m/yr.

Additional data from the testing conducted by Nye County in the alluvium south of Yucca Mountain on the specific discharge in the alluvium indicate significantly less uncertainty in the specific discharge relative to the assessment by the expert elicitation panel. The range of estimated specific discharge at the Alluvial Testing Complex spans a factor of about 7.8 (1.2 to 9.4 m/yr) and at the Well NC-EWDP-22 complex, spans a factor of about 11.7 (0.46 to 5.4 m/yr) (SNL 2007b, Tables 6.5-5 and 6.5-6). This indicates a range of estimated values of specific discharge that is about a factor of 20, which is considerably less than the degree of uncertainty from the saturated zone expert panel, which spans more than 3 orders of magnitude (CRWMS M&O 1998, p. 3-43). A great deal of additional information has been gathered since the time of the saturated zone expert elicitation. As more data became available, the range of uncertainty in the specific discharge was reduced. Estimates of specific discharge from the Alluvial Testing Complex and the NC-EWDP-22 complex are appropriate for quantitative use in the assessment of uncertainty in specific discharge because these estimates were made in the porous medium of the alluvium, in which questions of

scaling and representativeness are relatively minor. Estimates of specific discharge from well NC-EWDP-24PB are not appropriate for quantitative use in the assessment of uncertainty in specific discharge, because these estimates were made in the fractured volcanic units, in which uncertainties of scaling and representativeness are very large.

The probability distribution representing the uncertainty in the specific discharge multiplier (Figure 2.3.9-17) is determined from two sources of information: (1) the saturated zone expert elicitation (CRWMS M&O 1998); and (2) estimates of groundwater-specific discharge from the tracer testing at the alluvial testing complex (SNL 2007b).

A statistical analysis of these data was performed using Bayesian updating (Gelman et al. 2004), in which the results of the saturated zone expert elicitation were used as prior information and the estimated values of specific discharge from tracer testing at the alluvial testing complex were used as new information (SNL 2008b, Section 6.5.2.1[a]). The resulting normal distribution for uncertainty in the specific discharge multiplier was approximated using a discrete cumulative distribution function, as shown in Figure 2.3.9-17. Uncertainty in the specific discharge spans almost two orders of magnitude, with 80% of probability between 0.4 and 2.5 times being the best estimate from the calibration of the site-scale saturated zone flow model.

Horizontal Anisotropy in Permeability—A detailed description of the analysis and derivation of the distribution of anisotropy ratio in the saturated zone near the C-Wells Complex is provided in *Saturated Zone In-Situ Testing* (SNL 2007b, Section 6.2.6). Data from the long-term pumping test conducted from 1996 to 1997 were used to evaluate the anisotropy in the vicinity of the C-Wells Complex. Transmissivity and storativity were calculated from drawdown data in response to pumping at UE-25 c#3 for four observation wells: USW H-4, UE-25 ONC#1, UE-25 WT#3, and UE-25 WT#14. Analysis of the probable direction of horizontal anisotropy shows that the direction of maximum transmissivity is likely oriented more north-south than east-west. The flow model can apply anisotropy only along the directions of the mesh-lines, which are oriented north–south and east–west. The anisotropy applied in the saturated zone flow and transport abstraction model grid is within approximately 35° of the inferred principal direction of anisotropy in 5 of 6 estimates discussed in the site-scale saturated zone insitu testing analysis report (SNL 2007b, Section 6.2.6). The impacts of uncertainty in horizontal anisotropy in permeability on the simulated flow paths in the saturated zone from beneath the repository are illustrated in Figure 2.3.9-5. The more easterly simulated flow paths corresponding to values of north-south/east-west horizontal anisotropy of less than one are relatively unlikely, with a probability of occurrence of 0.10 (Table 2.3.9-4, parameter HAVO). In particular, the flow paths shown with the green lines in Figure 2.3.9-5, corresponding to a value of 0.05 for the parameter HAVO, are associated with the lower bounding value for this parameter. Flow paths intermediate between the green lines and the purple lines in Figure 2.3.9-5 have a cumulative probability of only 0.0042. Consequently, the more easterly simulated flow paths near the eastern boundary of the postclosure controlled area shown in Figure 2.3.9-5 have a low probability of occurrence relative to the simulated flow paths with values of horizontal anisotropy of greater than one.

2.3.9.2.4   Model Abstraction and Confidence Building
[NUREG-1804, Section 2.2.1.3.8.3: AC 1(1) to (4), (7) to (9), AC 4, AC 5]

The primary output from the site-scale saturated zone flow model is the flow field, which contains the flow paths and specific discharge. The flow field information is passed to the site-scale saturated zone transport model, the transport abstraction models (the saturated zone flow and transport abstraction model and the saturated zone one-dimensional transport model), and the TSPA. The output from the site-scale saturated zone flow model is used with effective porosity distributions in the site-scale saturated zone transport model and the abstraction models to provide the advective component of radionuclide transport. The abstraction feeds from the site-scale saturated zone flow model to the TSPA are accomplished through two abstraction models: the saturated zone flow and transport abstraction model and the saturated zone one-dimensional transport model. Confidence in the site-scale saturated zone flow model output is established mainly through comparison of observations and direct and indirect flow process indicators to model simulations.

2.3.9.2.4.1   Model Abstraction

The abstraction of saturated zone flow and transport is accomplished using two models (Figure 2.3.9-1): (1) a three-dimensional saturated zone flow and transport abstraction model (Section 2.3.9.3.4.1) that simulates radionuclide breakthrough curves at the boundary of the postclosure controlled area for 12 radionuclide groups; and (2) a saturated zone one-dimensional transport model which is a GoldSim-based model incorporated directly into the TSPA that simulates the ingrowth of daughter products along one-dimensional pipe segments that approximate the three-dimensional pathlines (Section 2.3.9.3.4.2). The saturated zone flow and transport abstraction model uses the same model domain, boundary conditions, grid and parameter values as the site-scale saturated zone flow model and the site-scale saturated zone transport model. Consequently, there is no simplification of the groundwater flow field in the saturated zone flow and transport abstraction model relative to the site-scale saturated zone flow model. The saturated zone one-dimensional transport model used a simplified representation of the flow field, based on three one-dimensional flow segments. Site-scale saturated zone transport is discussed further in Section 2.3.9.3.

Uncertainty in the groundwater specific discharge is incorporated into the saturated zone flow and transport abstraction model using the specific discharge multiplier parameter (SNL 2008b, Sections 6.5.2.1[a] and 6.5.3.1). This multiplication factor is applied to all values of permeability and the values of specified volumetric flow rates at the boundaries in the site-scale saturated zone flow model to account for uncertainty in simulated specific discharge in the saturated zone flow and transport abstraction model simulations (SNL 2008b, Section 6.5.2.1). A separate steady-state groundwater flow field is simulated for each realization of the system.

The flow paths from the water table beneath the repository to the accessible environment directly affect breakthrough curves and associated radionuclide transport times. Flow path uncertainty directly affects the length of flow due to the transition from volcanic tuffs to alluvium (SNL 2008b, Section 6.5.1.2[a]). Uncertainty in flow paths is affected by permeability and horizontal anisotropy of the volcanic tuffs. Large-scale anisotropy and heterogeneity are implemented in the site-scale flow model through direct incorporation of known hydraulic features, faults, and fractures (SNL

2007a, Sections 6.3.1.9 and 6.3.2). Both sources of uncertainty have been incorporated into the saturated zone flow and transport abstraction model that is presented in Section 2.3.9.3.4.2.

The saturated zone one-dimensional transport model represents a significant simplification of the three-dimensional groundwater flow system compared to the site-scale saturated zone flow model, and is used to model radioactive decay and ingrowth. The saturated zone one-dimensional transport model is divided into three sets of pipe segments to accurately capture the three-dimensional characteristics of the saturated zone flow and transport system in this one-dimensional model. The lengths and groundwater flow rates of these pipe segments are determined from the site-scale saturated zone transport model (SNL 2008b, Section 6.5.1.2[a]).

Estimates of groundwater-specific discharge in the saturated zone one-dimensional transport model were made in the following way. The site-scale saturated zone flow model was used to estimate the specific discharge for a nominal fluid path leaving the area beneath the repository and traveling in each of three segments of approximately 0 to 5 km (Segment 1), 5 to 13 km (Segment 2), and 13 to 18 km (Segment 3). The pathways leave the area beneath the repository and generally travel south–southeasterly to the accessible environment (Figure 2.3.9-14) (SNL 2007a, Section 6.5.2.3). The average specific discharge in each pipe segment of the saturated zone one-dimensional transport model was estimated using 1,000 particles in a three-dimensional simulation using the site-scale saturated zone flow model. The specific discharge was calculated using the median transport time for these particles. These simulations were conducted using the range of uncertainty in the horizontal anisotropy of 0.05 to 20 (SNL 2008b, Section 6.5.1.2[a], Table 6-5[a]).

Specific discharge values range from 0.354 to 0.555 m/yr for flow segment 1 (nominally from 0 to 5 km) across the full range of anisotropy values (SNL 2008b, Table 6-5[a]). For segment 3 (nominally from 13 to 18 km), the range of specific discharge is 0.769 to 5.98 m/yr. The first two segments reflect flow in the tuff aquifers, and the last segment reflects flow in the alluvial aquifer. The expert elicitation panel for saturated zone flow and transport (CRWMS M&O 1998, Figure 3-2e) estimated a median value of the specific discharge of 0.6 m/yr for the first (0 to 5 km) segment (SNL 2008b, Section 6.5.2.1). Thus, the specific discharge values simulated by the site-scale saturated zone flow model are about 10 to 40% smaller than the median value estimated by the saturated zone expert elicitation (CRWMS M&O 1998) for the first segment. The median specific discharge modeled for the alluvium portion of the flow path, which is in segment 3 (between 0.769 and 5.98 m/yr), is within the range of estimated specific discharges from the tracer-injection-pumpback tests conducted in the alluvial aquifer at the Alluvial Testing Complex and the NC-EWDP-22 complex (0.46 to 9.4 m/yr) (SNL 2007b, Tables 6.5-5 and 6.5-6). The model range of 0.408 to 0.544 m/yr for segment 2 is similar to segment 1 (SNL 2008b, Table 6-5[a]) and within the range of the upscaled specific discharge values obtained from testing in the Crater Flat Tuff at well 24PB (Section 2.3.9.2.3.3).

The flow path length of each pipe segment in the saturated zone one-dimensional transport model varies as a function of the western boundary of the alluvial uncertainty zone, the horizontal anisotropy, and the source region from which the radionuclide source originates beneath the repository (SNL 2008b, Table 6-6[a]). The first pipe segment is 5 km in length for all cases (SNL 2008b, Section 6.5.1.2). The second pipe segment represents that portion of the flow path from the 5-km distance to the contact between the volcanic units and the alluvium in the saturated zone at approximately 13 km from the repository, and ranges in length 7.3 to 16.4 km depending on the

parameters noted above. The longer values of the flow path length in the second pipe segment correspond to values of the horizontal anisotropy ratio (parameter HAVO) of less than one, which have a low probability of occurrence (SNL 2008b, Table 6-8). The third pipe segment represents ranges in length from 6.5 to 8.2 km and the portion of the flow path from the contact between the volcanic units and the alluvium out to the accessible environment. The lengths of the second and third pipe segments were estimated from the particle tracking results of the three-dimensional saturated zone flow and transport abstraction model. The total path length to the postclosure controlled area boundary in the three-dimensional model ranges from 19.4 to 29.7 km (SNL 2007a, Section 6.7.9).

Water Table Rise and Climate Change—Based on forecast climate changes in the future, a higher water table is expected in the Yucca Mountain region for future, wetter climatic conditions. A higher water table impacts radionuclide transport in the unsaturated zone by shortening the transport distance between the repository and the water table. The approach used to evaluate radionuclide transport in the unsaturated zone for future climate states is discussed in Section 2.3.8.

Several independent lines of evidence are available for estimating the magnitude of rise in the water table beneath the repository at Yucca Mountain under previous glacial-transition climatic conditions (Forester et al. 1999, pp. 56 and 57). Mineralogic alteration (zeolitization and tridymite distribution) in the unsaturated zone at Yucca Mountain shows no evidence that the water table has risen more than 60 m above its present position in the geologic past (Levy 1991, p. 477). Analyses of $^{87}Sr/^{86}Sr$ ratios in calcite veins of the unsaturated and saturated zones at Yucca Mountain indicated previous water table positions of 85 m higher than present (Marshall et al. 1993, p. 1,948). However, interpretation of strontium isotopic data may be complicated by zoning (variation of isotope ratios within calcite crystals). The results of the mineralogical and geochemical studies showing maximum water table rise of up to 85 m beneath Yucca Mountain reflected the evolution of past climates of up to 1 million years, which included the effects of glacial climates (SNL 2007a, Section 6.6.4.1). The maximum water table rise under monsoon and glacial-transition climates is, therefore, expected to be smaller because the monsoon and glacial-transition climates are warmer and dryer than the glacial climate (Sharpe 2003, Section 7).

Wells at paleospring discharge locations near the southern end of Crater Flat and south of Yucca Mountain revealed shallower-than-expected groundwater (Paces and Whelan 2001; BSC 2004a, Table A-1), with depths of only 17 to 30 m to the water table. These findings indicate that the water table rise during the Pleistocene at these paleospring locations could not have been more than about 30 m because spring discharge from the volcanic aquifer through the alluvium begins when the water table reaches the land surface (SNL 2007a, Section 6.6.4.1). Therefore, the rise in the water table under future climate states with higher infiltration would not be the same at all locations. A smaller rise is expected south of the location of the spring deposits and a larger rise is expected to the north of the spring deposits.

Groundwater flow modeling of the response to a doubling of the mean annual precipitation indicated a maximum increase of 130 m of the water table in the vicinity of Yucca Mountain (Czarnecki 1985). This water table rise is considered to be an overestimate because the analysis of Czarnecki (1985) was limited to two dimensions and did not simulate vertical flow. More recent groundwater modeling of the Death Valley regional groundwater flow system was conducted for a

glacial-transition climate. The past climate simulations (D'Agnese et al. 1999) represent glacial-transition climate conditions that are expected to occur at Yucca Mountain (Section 2.3.9.1). Under the past glacial-transition climate scenario (D'Agnese et al. 1999), simulated recharge in the Death Valley regional groundwater flow system increased by a factor of six and the simulated potentiometric surface levels beneath Yucca Mountain increased from 60 to 150 m above present levels (D'Agnese et al. 1999, p. 2). The recharge increase is an average over the entire model area and includes regions of high elevation that would be expected to experience larger increases in recharge than in the vicinity of Yucca Mountain. D'Agnese et al. (1999, p. 36) highlight numerous limitations of the simulations, (1) accuracy of the version Death Valley regional groundwater flow system model used in the past climate analysis; (2) the coarse (50 km) resolution of the global-scale climate models used to provide annual average precipitation distributions; and (3) simplifications regarding the inputs and outputs from surface water and evapotranspiration. Therefore, the regional scale simulations of climate change should be considered only to describe potential relative effects on the regional groundwater flow system (D'Agnese et al. 1999, p. 39).

The geochemical and mineralogical data indicate a water table rise of no more than 85 m while the numerical simulations range from 130 to 150 m maximum rise. There were several reasons—such as the coarse vertical discretization—why the model results may overestimate the appropriate value. As a result, a value of 120 m was chosen because it is between the measurements and the model results. A water table rise of 120 m beneath Yucca Mountain was imposed in the unsaturated zone radionuclide transport model for monsoon and glacial-transition climatic conditions, and was continued for the post-10,000-year period (Section 2.3.8). This effectively decreases the length of the flow path of radionuclides in the unsaturated zone by 120 m. The 120-m rise in the water table is conservatively modeled in the TSPA to occur immediately at the end of the present-day climate. In reality, there could be a significant period of adjustment in the saturated zone flow system in response to increased recharge caused by climate change. In addition, empirical evidence for past water table elevations suggests a 120-m rise is conservative (SNL 2008e, Section 6.4.8).

Analyses using the site-scale saturated zone flow model indicate that a rise in the water table will cause flow paths from below the repository to the accessible environment to move in less permeable hydrogeologic units that are currently in the unsaturated zone immediately above the saturated zone. Accordingly, with the higher water table, radionuclides entering the saturated zone from the unsaturated zone will first enter the lower permeability units, and this will result in longer radionuclide transport time than simulated by the site-scale saturated zone transport model (SNL 2007a, Section 6.6.4.2.2; SNL 2008a, Appendix E). The saturated zone flow and transport abstraction model did not include the effect of water table rise with regard to changes in flow pathways on saturated zone flow. The effects of increased groundwater flow rates were incorporated into the calculation of radionuclide breakthrough curves using the convolution integral with a scaling factor for groundwater specific discharge that represents the future climate state (Section 2.3.9.3.4.1.1). Therefore, the TSPA is conservative with regard to the impact of water table rise on transport times of radionuclides in the saturated zone.

2.3.9.2.4.2   Confidence Building

The results of the site-scale saturated zone flow model were compared to direct and indirect indicators of groundwater flow processes (SNL 2007a, Section 7). The site-scale saturated zone flow model is shown to be consistent with observed water levels (including data excluded from the

calibration), hydraulic properties, and hydraulic gradients. The model-simulated flow paths are corroborated with the flow path analysis of the hydrochemical data (SNL 2007a, Appendices A and B).

Simulated and Observed Water-Level Elevations—Examination of differences between simulated and observed water levels (residuals) at the Nye County Early Warning Drilling Program wells that were not part of model calibration and for non-Nye County wells used to validate the hydraulic gradient (Table 2.3.9-9) indicates that uncertainty associated with the simulated water levels depends on the location of the borehole within the site-scale model domain. Residuals are generally larger in the western and southern portion of the Nye County Early Warning Drilling Program area. The water level residual is large near the Solitario Fault and south of the Highway 95 fault (Figures 2.3.9-12 and 2.3.9-13) (SNL 2007a, Section 7.2.1). An additional comparison was made at well location SD-6, where the water level residual was less than 4 m (SNL 2007a, Section 7.2.1).

Examination of the residuals reported in Table 2.3.9-9 indicates that the residuals in simulated water levels depend on their location within the site-scale saturated zone model domain. Figure 2.3.9-13 shows that NC-EWDP-32P (located about 3 km southwest of NC-EWDP-2D), with the largest residual of 9.9 m, is located in an area of steep water-level changes, along the U.S. Highway 95 fault, and the model is not able to fully replicate the steep head gradients observed in this area. Wells NC-EWDP-22PC and 24PB, located north of U.S. Highway 95 near Fortymile Wash, show small residuals of −0.4 and −1.3 m, respectively. Similar residuals were observed using the water-level data available during model calibration. NC-EWDP-33P, located just south of U.S. Highway 95 and west of Fortymile Wash, shows reasonable agreement with a residual of −4.8 m. Finally, NC-EWDP-13P, located on the eastern edge of Crater Flat near Windy Wash fault in a region of high water levels, also shows a reasonable residual of −4.4 m. Overall, the observed residuals tend to improve for wells located further to the north and east in the vicinity of Fortymile Wash, where wells are in the simulated flow path from beneath the repository. Thus, these additional water-level data confirm the site-scale saturated zone flow model's capability to simulate water levels accurately in this portion of the flow path from beneath the repository (SNL 2007a, Section 7.2.1).

Gradients—To further validate the site-scale saturated zone flow model, a comparison of the hydraulic gradients along the flow path from beneath the repository between field data and the model simulations has been performed. These gradients have a direct impact on the calculation of specific discharge along the flow path from beneath the repository, and can be used to determine whether the model meets the validation criterion.

The simulated and observed hydraulic gradient among a series of seven wells, extending from the immediate area beneath the repository to NC-EWDP-32P, are presented in Table 2.3.9-10. Only two of the last three wells actually involve water level data not used during calibration. Consequently, only the comparison of simulated and observed hydraulic gradients computed from the segment formed by these wells were used to meet the requirement of postdevelopment model validation (SNL 2007a, Section 7.1.2).

As Table 2.3.9-10 indicates, the observed and simulated gradients along the flow path are in good agreement, except towards the southern end of the flow path. This behavior is not surprising because all locations (Figure 2.3.9-13), except at the southern end, were included during model calibration.

The wells used in gradient calculations were selected because they were on (or close to) the simulated flow path, and they traverse the Solitario Canyon Fault. The difference in observed and simulated water levels between wells USW H-6 and USW-25 WT-2 are the result of the manner in which the model accounts for the effect of the splay of the Solitario Canyon fault, which lies in the general area of these wells. However, while the model does not accurately simulate the precise location for the drop in head across the fault, largely because of the 250-m gridblocks, the overall hydraulic gradient simulated between USW H-6 and USW-25 WT-2 agrees reasonably well with the measured value (within 14%) (SNL 2007a, Section 7.1.2). For the segments between USW-25 WT-2 and NC-EWDP-22PC/24PB, where the simulated hydraulic gradients differs from the observed gradients by 50% to 152%, in absolute terms the difference between the observed and simulated hydraulic gradients is very close to zero (SNL 2007a, Section 7.1.2). The underprediction of the gradient is consistent with the overprediction of the specific discharge, and indicates that the hydraulic conductivity or permeability of the shallow hydrogeologic units in that area are too high. The water table is very flat in that area, and the accuracy of land surface altitude is 0.1 m (BSC 2004a); thus, even small absolute differences may look relatively large as a percentage. The relatively large difference (58%) for the segment between the new wells (NC-EWDP-22PC/24PB to NC-EWDP 19P/2D) is due to the steep water level change near the U.S. Highway 95 fault, which is not precisely reproduced in the model (SNL 2007a, Section 7.1.2). At this location the underpredicted gradient is consistent with the overprediction of the specific discharge noted earlier.

Measured and Calibrated Permeabilities—The logarithms of permeabilities estimated during calibration of the model are compared to the logarithms of permeability estimated from pump-test data near Yucca Mountain (and elsewhere at the NTS) in Figure 2.3.9-6. Where they could be estimated, the 95% confidence limits for the mean logarithm of the permeability data are shown. For the Calico Hills Volcanic Unit, the Prow Pass, Bullfrog, Tram tuffs, and the middle volcanic aquifer, permeabilities are shown for both the single and cross hole tests at the C-Wells Complex.

Comparison between measured values of permeability and values from the calibrated site-scale flow model is complicated by several factors (SNL 2007a, Section 7.2.2). Estimated values of permeability are affected by the scale of the measurement, as indicated by differences in the results from single- and multi-well testing in fractured volcanic units. In addition, there are uncertainties in measured values of permeability associated with proximity to structural features, depth of the test interval, wellbore storage and skin effects, and conversion from transmissivity to permeability. The values of permeability, as estimated by calibration of the site-scale saturated zone flow model, are generally representative of much larger volumes than interrogated by well testing.

Calibrated effective permeabilities for the lower clastic aquitard are higher than those presented in Figure 2.3.9-6 (SNL 2007a, Section 7.2.2.5.1). However, the calibrated values are among the lowest in the model, and are consistent with the current understanding of the geology, and therefore do not significantly affect the predicted flow paths or flow rates. The Lower Carbonate Aquifer (SNL 2007a, Section 7.2.2.4.1) permeabilities, based on transmissivity measurements, are among the lowest in the model domain. The calibrated effective permeability for the Lower Carbonate Aquifer was lower than the 95% uncertainty interval. Despite this lower calibrated effective permeability, the Lower Carbonate Aquifer remained the primary water-bearing unit in the model. Flow in the carbonate aquifer is a major component of the saturated zone water balance and, because of the higher hydraulic head in the carbonate aquifer, it prevents radionuclides from going deep into the flow system and entering the carbonate.

Overall, the calibrated effective permeabilities show trends that are consistent with permeability data from Yucca Mountain and nearby Nevada Test Site. The calibrated effective permeability of the three Crater Flat tuffs and Calico Hills Formation are all within the values measured in the field. The relatively high permeability estimated for the Tram tuff from the cross hole tests may be at least partially attributable to local conditions at the site of these tests. A breccia zone is present in the Tram tuff, at boreholes UE-25 c#2 and UE-25 c#3 (Geldon et al. 1997, Figure 3), which may have contributed to a local enhancement in the permeability of the Tram tuff.

Calibrated effective permeabilities for units corresponding to the Lava Flow Aquifer and the valley fill aquifer are within the range of measured permeabilities. The calibrated effective permeability values for some of the units classified under the category of valley fill aquifer are older, deeper units or confining units that were not subjected to pump tests and thus fall below the range of test results, as shown in Figure 2.3.9-6. The calibrated effective permeabilities of units corresponding to the Welded Tuff Aquifer are more than an order of magnitude lower than field estimates, but no confidence intervals are available (SNL 2007a, Section 7.2.2.4).

Specific Discharge—Although the calibrated permeabilities of any geologic unit or feature in the site-scale saturated zone flow model may indirectly influence the simulated specific discharge, those geologic units along the flow path from beneath the repository to the compliance boundary directly determine the simulated specific discharge. Particle tracking using the site-scale saturated zone flow model (SNL 2007a, Section 6.5.2.4) indicates that fluid particles migrating from beneath the repository generally enter the saturated zone in the Crater Flat units (Prow Pass Tuff and Bullfrog Tuff) (SNL 2007a, Figure 6-22). Because of the high permeabilities of these units, and the low hydraulic gradient, the particles remain in those units until reaching their southern ends (SNL 2007a, Section 7.2.3). At this point, flow generally enters the alluvial portion of the flow system after briefly transitioning through the Paintbrush Volcanic Aquifer (SNL 2007a, Section 7.2.3). The alluvial deposits at the southern end of the flow path are represented in the site-scale saturated zone flow model by the Lower Fortymile Wash alluvium (SNL 2007a, Section 7.2.3). Thus, those calibrated permeabilities that most directly control the specific discharge simulated by the site-scale saturated zone flow model are those for the Crater Flat units and the Lower Fortymile Wash alluvium (SNL 2007a, Section 7.2.3).

Observations or prior estimates of specific discharge are available for two locations along the simulated flow paths. The first location is about 5 km downgradient from the repository and the second location is near the postclosure controlled area boundary. The pathlines near the repository are influenced by groundwater flow in the Crater Flat units. Tracer testing was performed at the C-Wells Complex (UE-25 c#3, for example), but no specific discharge estimates were obtained from that test. However, the C-Wells fall within the 5-km region for which estimates of specific discharge were proposed by the saturated zone expert elicitation. The groundwater pathlines to the postclosure controlled area boundary shown in Figure 2.3.9-14, and the radionuclide transport along the pathlines discussed throughout other documents (SNL 2008a), are strongly influenced by groundwater flow in alluvium. Estimates of specific discharge in the saturated zone were recently obtained from field testing at the well cluster NC-EWDP-22 and the Alluvial Testing Complex (SNL 2007b, Section 6.5.5). The Well 22 cluster and the Alluvial Testing Complex are located near the postclosure controlled area boundary. The technique used to estimate specific discharge at locations within the site-scale saturated zone flow model, corresponding to the locations where measurements are available (NC-EWDP-22S, NC-EWDP-19D, and NC-EWDP-24PB), was to

isolate a cubic volume within 1,000 m of the well location, extended to 10 m above and below the entire open interval, and to calculate the average specific discharge across all flowing nodes.

The simulated average specific discharge across the 5-km boundary ranges from 0.35 to 0.38 m/yr for differing values of horizontal anisotropy in permeability ranging from 20 to 0.05 (0.36 m/yr for the expected horizontal anisotropy values of 5:1 N-S/E-W with end members of the 100 particle distribution ranging from 0.11 to 0.66 m/yr) (SNL 2007a, Section 7.2.3). These values fall near the middle of the range of specific discharge values of 0.01 to 10 m/yr derived by the expert elicitation panel (CRWMS M&O 1998, Figure 3-2e, aggregate curve). Although there were no specific discharge measurements from the C-Wells tests, the average modeled specific discharge at nodes surrounding the C-Wells was 1.75 m/yr (SNL 2007a, Section 7.2.3). The simulated specific discharge near the repository location varies from location to location.

The data from the Alluvial Testing Complex and well 22S cluster field testing yielded specific discharge estimates ranging from 1.2 to 9.4 m/yr and 0.46 to 5.4 m/yr, respectively (SNL 2007b, Tables 6.5-5 and 6.5-6). The model predicted specific discharge at NC-EWDP-22S and 19P are 21.0 and 11.7 m/yr, respectively (SNL 2007a, Section 7.2.3). This relatively high value corresponds to the high effective permeability assigned to the Lower Fortymile Wash Alluvium.

The location of well NC-EWDP-24PB is about 4 km north of the Alluvial Testing Complex, and this well was used to test the Crater Flat Tuff unit. The values of specific discharge obtained from the measurements at 24PB ranged from 5 to 310 m/yr (Section 2.3.9.2.3.3). As noted in Section 2.3.9.2.3.3, the measured values are at a small scale compared with the scale of the model. When scaled up using the median flowing interval spacing, the resulting upscaled specific discharge estimates from the measurements at well 24PB range from 0.07 to 4.1 m/yr (Section 2.3.9.2.3.3).

The specific discharge from beneath the repository to the postclosure controlled area boundary was 0.55 m/yr (average across all flow path lengths divided by travel time) (SNL 2007a, Section 7.2.3). As indicated in Table 2.3.9-4, the range of specific discharge is from 1/8.93 to 8.93 times the nominal value, which are expressed as the logarithm of the of the specific discharge multiplier values in the table (−0.951 to 0.951). The measured values fall within the range of uncertainty for the specific discharge.

Upward Hydraulic Gradient—An upward hydraulic gradient between the lower regional Paleozoic carbonate aquifer and the overlying volcanic rocks has been observed in the vicinity of Yucca Mountain. Principal evidence for this upward gradient is provided by data from boreholes drilled into the upper part of the regional Paleozoic carbonate aquifer (UE-25 p#1 and NC-EWDP-2DB). Hydraulic head measurements in borehole UE-25 p#1 indicate that the head in the regional Paleozoic carbonate aquifer is about 752 m, which is about 21 m higher than the head measured in this borehole in the overlying volcanic rocks (BSC 2004a, Table 6-4). The head in the regional Paleozoic carbonate aquifer at this borehole was estimated as part of the model calibration process. The upward vertical gradient was reproduced in the calibrated model, although the head difference was only about 6 m (SNL 2007a, Table 6-8 and Figure 6-13). This upward gradient is potentially important to the performance of the repository because it would restrict groundwater flow and radionuclide transport pathways to the volcanic rocks and alluvial aquifers, thereby precluding transport in the deeper regional Paleozoic carbonate aquifer for the groundwater flow regime under present-day climatic conditions. On the basis of simulations of the

Death Valley regional groundwater flow system under past and future climate scenarios, it is expected that the upward gradient of hydraulic head will persist during future wetter climates (D'Agnese et al. 1999, pp. 27 and 30).

Corroboration of Flow Paths Using Hydrochemical Data—To provide further validation of the site-scale saturated zone flow model, flow paths (Figure 2.3.9-15) simulated by the calibrated model were compared with flow paths estimated on the basis of groundwater chemical and isotopic data (Figure 2.3.9-18). Flow paths simulated by the site-scale flow model were generated using the particle-tracking capability of the FEHM code by placing particles at different locations beneath the repository and running the model to trace the paths of these particles across a range of horizontal anisotropies (SNL 2007a, Appendices A and B).

Conservative geochemical constituents (i.e., those that show the least effects of interactions with water and rocks) were used to delineate flow paths because their concentrations primarily reflect inputs and processes that operate in recharge areas. The assessments examined major ion chemistry, isotopes such as $\delta^{34}S$, δD, and $\delta^{18}O$, and radioisotopes, including ^{14}C and uranium series ratios. Where a lack of downgradient continuity in chemical and isotopic compositions was observed, the possibility of groundwater mixing was evaluated and quantified with inverse geochemical mixing and reaction models (SNL 2007a, Appendices A and B).

Areal distribution maps of groundwater geochemical constituents and isotopes were used to obtain initial estimates of groundwater flow paths (SNL 2007a, Appendices A and B). Water type locations and the corresponding observation points used to evaluate geochemical signatures are shown in Figure 2.3.9-18. Table 2.3.9-11 summarizes the basis for the flow paths illustrated in Figure 2.3.9-18. Flow paths were interpreted based on a number of approaches: (1) examination of areal distribution plots for spatial trends; (2) examination of plots between chemical or isotopic variables that indicate relationships (e.g., mixing) between groundwater from the different geographic areas (identified in Figure 2.3.9-18); and (3) inverse geochemical models used to estimate the mixing fractions of various upgradient groundwaters present in a downgradient groundwater, recognizing that groundwater composition can be a result of mixing and water–rock interactions (SNL 2007a, Appendices A and B). The first two approaches focus on patterns and relationships displayed among relatively nonreactive species (e.g., chloride, sulfate, δD). The potential groundwater sources and mixing relationships suggested by the first two approaches were examined quantitatively by inverse mixing and reaction models that also considered the evolution of more reactive species through water–rock interaction. The first approach is essentially two-dimensional, but the second and third approaches incorporate the effects of three-dimensional mixing with local recharge or with groundwater upwelled from the deep regional Paleozoic carbonate aquifer (SNL 2007a, Appendices A and B).

The groundwater flow paths and mixing zones, identified based on the geochemical signatures, are consistent with the regional flow directions and the recharge–discharge relationships discussed in Section 2.3.9.2.1. For example, the relatively shallow southerly flow through tuff and alluvium from recharge in the Rainer Mesa area along the Fortymile Canyon and under Fortymile Wash discharges into the wells in Amargosa Valley or at natural discharge areas, such as Franklin Lake Playa. This evidence indicates a general southerly flow of regional groundwater in the vicinity of Yucca Mountain and a mixing of different groundwater types in the alluvial aquifer underlying the Amargosa Valley (SNL 2007a, Appendices A and B). The groundwater flow directions, inferred

from the geochemistry, are consistent with the flow directions calculated with the site-scale saturated zone flow model.

Despite the sometimes large distances between boreholes, differences in groundwater chemical and isotopic compositions are often large enough that groundwater flow paths over distances of tens of kilometers can be identified with some confidence (Figure 2.3.9-18). In contrast, despite the closer borehole spacing, the compositions of groundwaters in the immediate vicinity of Yucca Mountain are often too similar to allow detailed flow paths from beneath the repository to be identified with certainty. However, possible flow directions from beneath the repository area are constrained by flow paths 6, 7, and 2 (Figure 2.3.9-18) to be predominantly south or southeastward from the repository area. Geochemical inverse models (SNL 2007a, Appendices A and B) applied to water chemistry from borehole NC-EWDP-19D indicated that groundwater at this borehole could have originated from the area of borehole UE-25 WT#3 at the mouth of Dune Wash (as depicted by flow path 7), or as a result of the mixing of groundwater flowing from the vicinity of borehole USW WT-10 and local Yucca Mountain recharge (indicated schematically by small eastward-pointing arrows on flow path 6) (Figure 2.3.9-18). An origin for NC-EWDP-19D groundwater from the Solitario Canyon area would imply that groundwater from beneath the repository area should be forced to flow southeastward toward Fortymile Wash. Conversely, an origin for borehole NC-EWDP-19D groundwater from the Dune Wash area near borehole UE-25 WT#3 implies that groundwater from the area beneath the repository flows along a more southerly trajectory (SNL 2007a, Appendices A and B). The southeastern and southern flow paths are consistent with the site-scale saturated zone flow model, given the uncertainty in horizontal anisotropy (SNL 2007a, Section 6.6.2). The range of flow paths from the geochemical analyses and the flow modeling are similar.

Comparison of the flow paths indicates that most of the particles travel between flow paths 2 and 6 (Figure 2.3.9-18), and roughly follow the trajectory of flow path 2 through the alluvium along the west side of Fortymile Wash. These particle trajectories fall within the constraints provided by the groundwater geochemical and isotopic data (SNL 2002, Appendices A and B).

Summary of Confidence Building—The site-scale saturated zone flow model (1) was validated against observed hydraulic heads not previously used in model development and calibration; (2) was corroborated with hydraulic parameters derived from hydraulic testing at the C-Wells Complex, the Nye County Testing in alluvium south of Yucca Mountain, and other well locations; and (3) generated groundwater flow paths that are consistent with those independently derived from hydrochemistry and isotope analyses. Accordingly, the validated model provides an analysis tool that facilitates understanding of groundwater flow from beneath the repository to the accessible environment, and provides three-dimensional groundwater flow fields (including flow direction and groundwater flow rates) for performing the saturated zone radionuclide transport calculations described below.

2.3.9.3　Saturated Zone Radionuclide Transport
[NUREG-1804, Section 2.2.1.3.9.3: AC 1(1) to (5), AC 2, AC 3(1), (2), (4) to (6), AC 4, AC 5; Section 2.2.1.3.12.3: AC 1(1) to (5), AC 2, AC 3, AC 4, AC 5]

Radionuclides released from the unsaturated zone will enter the saturated zone as species dissolved in water or sorbed onto colloids, and will transport in the saturated zone under the influence of a

number of chemical and physical processes that determine how rapidly and in what concentration the radionuclides arrive at the accessible environment. Released radionuclides are expected to travel along the groundwater flow paths described in Sections 2.3.9.2.1 and 2.3.9.2.3.3, and Figure 2.3.9-14. The transport of radionuclides as dissolved species in the saturated zone will be affected by the processes of advection, matrix diffusion, dispersion, radioactive decay, ingrowth, and sorption. In addition, the transport of radionuclides sorbed onto colloids is affected by the rate of colloid filtration, the rate at which radionuclides desorb from colloids, and the steady-state colloid concentrations (SNL 2008a, Section 6.3). Several FEPs related to radionuclide transport are thus included in the site-scale saturated zone transport model, including FEPs 2.2.07.15.0A, Advection and dispersion in the saturated zone; 2.2.07.17.0A, Diffusion in the saturated zone;, 2.2.08.08.0A, Matrix diffusion in the saturated zone; 2.2.08.09.0A, Sorption in the saturated zone; 2.2.08.10.0A, Colloidal transport in the saturated zone; and 3.1.01.01.0A, Radioactive decay and ingrowth (Table 2.3.9-1).

The parameters associated with the processes that affect radionuclide transport include specific discharge, flowing interval porosity in the fractured volcanic rocks and effective flow porosity in the alluvium, effective matrix diffusion coefficient, radionuclide sorption coefficients, colloid retardation factors, dispersivity (longitudinal, horizontal transverse, and vertical transverse), and radioactive decay constants. The relevant physical rock properties of hydrogeologic units in the saturated zone are included in the site-scale saturated zone transport model, consistent with FEP 2.2.03.02.0A, Rock properties of host rock and other units (Table 2.3.9-1). The site-scale saturated zone transport model uses the flow field generated by the site-scale saturated zone flow model (Section 2.3.9.2) to implement the key radionuclide transport processes discussed in this section. The saturated zone flow and transport abstraction model extends the transport model to incorporate a time-varying radionuclide source from the unsaturated zone and parameter uncertainty to generate radionuclide breakthrough curves at the accessible environment that are utilized in the TSPA.

2.3.9.3.1   Conceptual Description
[NUREG-1804, Section 2.2.1.3.9.3: AC 1(1) to (3), (5); Section 2.2.1.3.12.3: AC 1(1) to (5)]

In the event that radionuclides are released, flowing groundwater in the saturated zone transports the radionuclides either in solution (dissolved) or in suspension, bound to very small particles known as colloids. Colloids can be small enough to travel with flowing water through fractures in volcanic rocks, through pores in the unfractured portion of volcanic rocks, and through pores in alluvium (BSC 2004e, Sections 6.3, 6.4, and 6.5). Under the present-day climate scenario, radionuclides released from water contacting breached waste packages in the repository must migrate a distance of approximately 300 m through the unsaturated zone to the water table, then migrate downgradient in the saturated zone to reach the accessible environment. Under the wetter glacial transition conditions, the travel distance through the unsaturated zone may be as much as 120 m less due to a higher water table under the glacial transition climate. As discussed in Section 2.3.9.2, groundwater in the saturated zone generally moves southeast from beneath the repository before flowing south and transitioning from the volcanic rocks into the thick valley-fill alluvial deposits of the Amargosa Desert near the accessible environment (SNL 2007a, Section 6.5.2.3).

The base-case conceptual model for saturated zone transport begins at the water table beneath the repository footprint and ends at the accessible environment downstream from the repository. As

illustrated in Figure 2.3.9-19, the flow path from beneath the repository to the accessible environment begins in the volcanic rocks and ends in the alluvium. The accessible environment corresponds to the location labeled Amargosa Valley on Figure 2.3.9-19, and is located approximately 18 km downgradient from the repository.

The processes relevant to the transport of radionuclides in the saturated zone component of the Lower Natural Barrier are presented conceptually in Figure 2.3.9-19. Table 2.3.9-1 describes the approach for evaluating and incorporating the FEPs included in saturated zone transport modeling. Advection, matrix diffusion, dispersion, colloid-facilitated transport, and sorption processes occur at different scales within the saturated zone. Radioactive decay and ingrowth are not scale-dependent processes but rather are unique functions for each radionuclide. The effect and importance of these processes differ in the fractured tuff units and the porous alluvium (SNL 2008a, Section 6.7). In fractured tuffs, advective transport occurs predominantly within fractures; therefore, the fracture porosity (referred to as flowing interval porosity) is important for describing the advective velocity. Major flowing fracture zones (referred to as flowing intervals) are generally spaced on the order of meters to tens of meters apart, while fractures themselves within any zone may be more closely spaced and have submillimeter apertures. In the alluvium, advective transport occurs through the pore space between particles. Because the effective porosity of the alluvium is considerably greater than the fractured volcanic rock flowing interval porosity, the transport velocity in the alluvium, which is inversely related to effective porosity, is greatly reduced in comparison to that of the tuff (Section 2.3.9.2.1). Consequently, the transport processes in the saturated zone are discussed individually with respect to volcanic rock and alluvium. The combined effect of all of the transport processes is ultimately expressed in terms of expected radionuclide arrival time profiles (i.e., breakthrough curves) (SNL 2008a, Section 6.8).

Diffusion of dissolved radionuclides into regions of slowly moving groundwater is an important process affecting radionuclide transport through the saturated zone. Dissolved radionuclides will diffuse from water flowing in the fractures into the nearly stagnant water in the volcanic rock matrix (Figure 2.3.9-19), as well as from flowing water in pores between rock grains in the alluvium into pore spaces within the rock grains or into relatively stagnant water between the rock grains (e.g., within clay lenses). Based on the results of single-well tracer testing at the Alluvial Testing Complex, radionuclides transported through the alluvium are conservatively assumed not to undergo diffusion into either the grains of the alluvium material or into near-stagnant regions between the grains (SNL 2008a, Table 6.6-1a). Thus, the matrix diffusion process is assumed to be not applicable to the alluvium (SNL 2007b, Appendix G, Section G5.4.1). This assumption is reflected in the uncertainty distribution of effective porosity in the alluvium with a mean of 0.18, which is significantly less than the estimated total porosity in the alluvium of 0.30 (SNL 2008b; Section 6.5.1.1 and SAR Table 2.3.9-4). However, average linear flow velocities in the alluvium will be much smaller than in the volcanic rock because a similar volumetric flow rate will occur within a much larger effective porosity. There is also a large amount of surface area onto which sorption can occur in the alluvium. Consequently, the alluvium constitutes an important region of the flow system in that it slows radionuclide transport in the saturated zone.

Flow occurs predominantly in fractures in the volcanic rock units, but radionuclides can diffuse out of the fractures and into the volcanic rock matrix, which can act as a large reservoir of near-stagnant water with a large surface area onto which radionuclide sorption can occur. Both diffusion into the matrix and sorption in the matrix can significantly delay the transport of radionuclides through the

fractured volcanic rocks relative to the rate of groundwater flow through fractures. The radionuclides will eventually diffuse back into faster moving groundwater, but the net effect is the overall reduction of the rate of transport.

Hydrodynamic dispersion of radionuclides in the saturated zone is caused by heterogeneities in aquifer characteristics, which result in variations in average linear velocities (magnitude and direction). The net effect of these variations is to spread radionuclides over ever larger volumes as time and distances increase. Longitudinal dispersion causes some radionuclides to migrate either faster or slower than the average velocity along the groundwater flow trajectory. Transverse dispersion (both horizontal and vertical) causes solute plumes to widen both horizontally and vertically over time and distance. Longitudinal and transverse dispersions result in reduced concentrations within a solute plume relative to concentrations that would be present in the absence of dispersion.

Ultimately, the radionuclide mass breakthrough curves from the saturated zone flow and transport abstraction model are used in the TSPA to calculate radionuclide concentrations at the accessible environment. These radionuclide breakthrough curves reflect the aggregate effects of the transport processes in the saturated zone along the flow paths from beneath the repository to the accessible environment.

2.3.9.3.2   Data and Data Uncertainty
[NUREG-1804, Section 2.2.1.3.9.3: AC 1(3), (5), AC 2, AC 3(1), (2), (4) to (6); Section 2.2.1.3.12.3: AC 1(4), (5), AC 2, AC 3]

This section describes saturated zone transport data and data uncertainty, including descriptions of how the data are used, interpreted, and appropriately synthesized into the parameters used to generate the radionuclide breakthrough curves at the accessible environment. Data from field, laboratory, and natural analogue sources were utilized to define relevant parameters and conceptual models necessary to develop the abstraction of concentrations of radionuclides in groundwater as a function of time and distance from the source. For example, stochastic scaling procedures were used to obtain uncertainty distributions for sorption coefficients on the scale of the 250-m gridblocks used in the site-scale saturated zone transport model. The quality and quantity of data are sufficient for those parameter groups (Table 2.3.9-4) considered important for developing the saturated zone flow and transport abstraction model (SNL 2008b, Sections 6.2 to 6.5 and 6.5[a]).

2.3.9.3.2.1   Advection, Matrix Diffusion, and Dispersion Processes and Parameters

The testing performed to characterize advection, matrix diffusion, and dispersion processes is presented in this section. The testing and resulting parameters for the volcanic rocks are presented first, followed by the testing and resulting parameters for the alluvial aquifer.

The processes of advection, matrix diffusion, and dispersion are characterized by a number of parameters. Advection is most commonly described by the groundwater velocity. Three parameters are typically combined to determine the velocity: hydraulic conductivity, hydraulic gradient, and effective porosity. Specific discharge is the volumetric groundwater flow rate per unit cross-sectional area. The effective porosity in fractured rocks is termed the flowing interval porosity. The process of matrix diffusion into the rock matrix requires knowledge of four

parameters: flowing interval spacing, sorption coefficient, matrix porosity, and effective diffusion coefficient for the radionuclide being analyzed. Finally, dispersion coefficients, often separated into longitudinal dispersion coefficients and transverse dispersion coefficients, are needed to describe the dispersion process. Data and discussion of colloid facilitated transport is presented in Section 2.3.9.3.2.3.

Testing Relevant to Advection, Diffusion, and Dispersion Processes for Fractured Volcanic Rocks—The transport characteristics of the fractured rock aquifers in the vicinity of Yucca Mountain generally have been inferred from hydraulic and tracer testing at the C-Wells Complex (Figure 2.3.9-7) (SNL 2007b, Section 6.2 and 6.3). Data from the hydraulic and tracer tests have been supplemented by analyses of ^{14}C concentrations in groundwater to confirm the description of advective transport over larger scales relevant to performance of the repository (SNL 2007a, Appendices A and B).

Results from hydraulic and tracer testing at the C-Wells Complex were used to identify and confirm the conceptualization of flow and transport in the fractured tuff. These results were also used to derive values for transport modeling parameters relevant to advection (which includes specific discharge and flowing interval porosity), dispersion, matrix diffusion, and sorption (Section 2.3.9.3.3). These tests confirm the dual-porosity conceptualization of radionuclide transport in the volcanic tuffs of the saturated zone in which transport primarily takes place by advection in the fractures, coupled with diffusion into the matrix of the fractured rock mass.

A series of cross-hole tracer tests were performed in the Prow Pass, Bullfrog, and Tram units at the C-Wells Complex (Figure 2.3.9-20), using suites of reactive and nonreactive tracers to determine parameters needed to model advection, diffusion, dispersion, and sorption. In this paragraph, reference to specific wells at the C-Well Complex are abbreviated to the last 3 characters. For example, well UE-25c#1 is identified as c#1. Tracer tests at the C-Wells Complex were conducted in the following order (SNL 2007b, Table 6.3-1):

- Injection of iodide into the combined Bullfrog–Tram interval in well c#2 while pumping the same interval in well c#3 (February to April 1996)

- Injection of pentafluorobenzoic acid into the lower Bullfrog interval in well c#2 while pumping the same interval in well c#3 (May to October 1996)

- Injection of iodide into the lower Bullfrog interval in well c#1 while pumping the same interval in well c#3 (June to October 1996)

- Injection of lithium bromide, pentafluorobenzoic acid, and carboxylate-modified latex microspheres into the lower Bullfrog interval in well c#2 while pumping the same interval in well c#3 (October 1996 to September 1997)

- Injection of 3-carbamoyl-2-pyridone into the lower Bullfrog interval in well c#1 while pumping the same interval in well c#3 (January to November 1997)

- Injection of 2,6-difluorobenzoic acid into the lower Bullfrog interval in well c#2 while pumping the same interval in well c#3 (January to November 1997)

- Injection of iodide and 2,4,5-trifluorobenzoic acid into the Prow Pass interval in well c#3 while pumping the same interval in well c#2 (July 1998 to January 1999)

- Injection of 2,3,4,5-tetrafluorobenzoic acid into the Prow Pass interval in well c#1 while pumping the same interval in well c#2 (July 1998 to January 1999)

- Injection of lithium bromide, pentafluorobenzoic acid, and carboxylate-modified latex microspheres into the Prow Pass interval in well c#3 while pumping the same interval in well c#2 (September 1998 to January 1999).

Injection of conservative tracers preceded multiple tracer injections in the Bullfrog and Prow Pass intervals to optimize the multiple tracer tests. The Bullfrog interval was chosen for testing because it had the highest hydraulic conductivity at the C-Wells. The Prow Pass interval was chosen for testing because it represented a much lower hydraulic conductivity interval in the fractured tuffs, thus providing diversity between the tests.

The interpretations and resulting parameters from testing at the C-Wells Complex and the Alluvial Testing Complex are presented below.

Flowing Interval Spacing—Flowing interval spacing is a parameter used to represent the distance between fractures, or sets of fractures, that transmit water. Flowing interval spacing is used in the characterization of matrix diffusion. The smaller the flowing interval spacing, the greater the number of fractures and the more rapidly diffusion occurs into the matrix. Hydrologic evidence at Yucca Mountain supports the conceptual model of fluid flow within fractures in the moderately to densely welded volcanic tuffs of the saturated zone. For example, the bulk hydraulic conductivities measured in the field are dominated by fracture flow, and tend to be several orders of magnitude higher than the hydraulic conductivities of intact, primarily unfractured volcanic tuff core samples measured in the laboratory. This implies that flow occurs primarily through the fracture system, not through the matrix between fractures. Fractures are generally found within the moderately to densely welded volcanic tuffs (SNL 2008a, Section 6.3) because the units are more brittle than the nonwelded tuffs. Also, there is a positive correlation between fractures identified using acoustic televiewer or borehole television tools and zones of high transmissivity and flow (Erickson and Waddell 1985, Figure 3). However, not all fractures transmit water. The flow of groundwater through fractures, consistent with FEP 1.2.02.01.0A, Fractures (Table 2.3.9-1), is included in radionuclide transport simulations with the flowing interval spacing parameter.

Fluid electrical conductivity and thermal logging data were collected in the Crater Flat Tuff unit in well NC-EWDP-24P, located about 4-km north of the Alluvial Testing Complex. A potential implication of the high flow rates inferred in one zone in this well is that groundwater flow can be highly channelized in the fractured tuff units of the saturated zone. The degree of groundwater channelization is represented by the flowing interval spacing parameter, with large values of flowing interval spacing corresponding to a high degree of flow channelization (SNL 2008b, Section 6.5.2.4).

Flowing interval spacing is estimated as the midpoint distance between fracture zones that transmit fluid in the saturated zone, as identified through borehole flowmeter surveys during single-well hydraulic testing (BSC 2004f, Section 1). Flowing interval spacing is distinct from fracture spacing.

Although typically used in the literature, fracture spacing was not used because field data such as fluid logging and fracture mapping conducted in the C-Wells Complex and in other wells within the saturated volcanics identify flowing intervals (Figure 2.3.9-20) that contain fluid-conducting fractures, but the data do not distinguish how many (or which) fractures comprise the flowing interval (SNL 2008b, Section 6.5.2.4). The flow logging data also indicate that numerous fractures between flowing intervals do not transmit groundwater. The uncertainty distribution for flowing interval spacings in the fractured volcanic rocks, based on analyses in numerous boreholes (BSC 2004f), is indicated in Figure 2.3.9-21 (SNL 2008b, Section 6.5.2.3[a]). The median flowing interval spacing is approximately 26 m, with 90% certainty that the intervals are spaced at less than 46 m (SNL 2008b, Table 6-7[a]).

Flowing Interval Porosity in the Fractured Tuffs—The flowing interval porosity for fractured rock units in the saturated zone is defined as the volume of the pore space through which large amounts of groundwater flow occur relative to the total volume of the rock. In the calculation of groundwater velocity, the specific discharge is divided by the effective porosity, which in this case is the flowing interval porosity. The advantage to this definition of flowing interval porosity is that cross-hole tracer test data can be used to characterize the parameter. The flowing interval porosity may also include the matrix porosity of small matrix blocks within fracture zones. The estimated flowing interval porosity values from conservative tracer tests at the C-Wells Complex are summarized in Table 2.3.9-12. Table 2.3.9-13 summarizes flowing interval porosity values derived from two multiple tracer tests at the C-Wells: one in the Prow Pass Tuff, the other in the lower Bullfrog Tuff.

Differences in the estimates of flowing interval porosity for the Prow Pass test interval in Tables 2.3.9-12 and 2.3.9-13 can be attributed primarily to differences in the assumptions used in the interpretative analyses to obtain the estimates. The flowing interval porosity estimates for the Prow Pass Tuff are smaller in Table 2.3.9-12 than in Table 2.3.9-13, because a relatively long tracer residence time was assumed for the injection borehole in the interpretation of the conservative tracer tests, which resulted in smaller residence times attributed to the aquifer (SNL 2007b, Appendix D, Sections D1., D4.8.5, and D5.2). For the multiple tracer test in the Prow Pass Tuff, a relatively short injection borehole residence time was assumed, based on the volume of the packed-off interval and the injection–recirculation rate used in the test. By assuming a smaller residence time in the injection borehole, a longer residence time is attributed to the aquifer, resulting in a larger estimate of flow porosity.

The range of flowing interval porosity estimates for the Bullfrog Tuff in Table 2.3.9-13 is wider compared to Table 2.3.9-12, because two separate tracer peaks were observed and analyzed in the multiple tracer test, whereas only one peak occurred in the initial, nonsorbing tracer tests. The additional peak in the multiple tracer test was attributed to a fraction of the tracer mass entering flow pathways in the upper portion of the Bullfrog Tuff test interval that were not accessed in the conservative tracer tests. For the multiple tracer test interpretation, flow in the injection borehole was apportioned into the upper and lower portions of the test interval in a manner consistent with borehole flow survey information. However, in the conservative tracer tests, flow was assumed to be evenly distributed over the transmissive interval thickness, which results in larger flowing interval porosity estimates (SNL 2007b, Appendix D, Sections D1.1.1 and D1.1.2).

The alternative interpretive approaches for the Prow Pass and Bullfrog tracer tests at the C-Wells Complex yield a relatively wide range of flowing interval porosity estimates in both test intervals. Although largely attributable to differences in interpretive assumptions, this wide range of estimates is retained in Table 2.3.9-4 because it reflects the large uncertainties resulting from a lack of specific knowledge of flow pathways in the aquifer (SNL 2007b, Section 6.3). However, in both cases, data corroborate the concept that flow primarily occurs through fractures (SNL 2007b, Section D5.3).

Figure 2.3.9-22 illustrates the range of likely flowing interval porosities derived from C-Wells tests and other site-specific observations from wells USW H-1, USW H-3, USW H-4, USW G-4, and UE-25 p#1 (BSC 2004f, Table 4-1). This information was used to define the uncertainty in flowing interval porosity utilized in the saturated zone flow and transport abstraction model. The uncertainty distribution (Figure 2.3.9-22) is discretized in increments of 1 order of magnitude, with all of the C-Wells estimates in the range of 0.003 to 0.1. 75% of the values in the uncertainty distribution fall between 0.0001 and 0.01 (SNL 2008b, Figure 6-13), and are consistent with the judgment that the flowing interval porosity estimates from the C-Wells tests may have been biased toward larger values by flow heterogeneity in the fractured tuff and the simplifying assumption of radial flow in some test analyses (SNL 2007b, Section 6.3.5 and Appendix D). The lower end of the uncertainty range reflects flowing interval porosities of fractured rock from core at Yucca Mountain and Pahute Mesa on the Nevada Test Site (SNL 2008b, Section 6.5.2.5). The observations from well NC-EWDP-24PB that yielded large specific discharge values over small cross sectional areas are consistent with the concept of the flowing interval porosity presented here. Discrete flow zones in some hydrostratigraphic units can be described as channeling, but that terminology is not used to describe the phenomenon in the fractured volcanics. The conceptual model of the flowing interval accounts for flow that occurs in intervals of open fractures or fracture zones. The flow of groundwater through fractures, consistent with FEP 1.2.02.01.0A, Fractures (Table 2.3.9-1), is included in radionuclide transport simulations with the flowing interval porosity parameter. The conceptual model that flow in fractured volcanic units is primarily through a relatively small number of widely spaced flowing intervals is demonstrated by the 24PB test. The scaled up specific discharge values from 24PB were in the same range as other observations when the median flowing interval spacing was used to scale the values. The range of flowing interval porosity thus includes values that will represent the observations from well 24PB.

Matrix Diffusion—Matrix diffusion is a process in which diffusing particles move in a manner similar to Brownian motion through both mobile and immobile fluids. Diffusion into stagnant water in the matrix results in a delay in the arrival of a molecule at a downgradient location relative to a molecule that remains in flowing groundwater in fractures (SNL 2008a, Section 6.4.2.4). Diffusion is a Fickian process by which species move from high to low concentration regions. The magnitude of matrix diffusion depends on the free water molecular diffusion coefficient for individual constituents and the characteristics of the flow path through which the diffusing species passes. The species diffusion coefficient in the volcanic rock matrix is less than the free water diffusive coefficient because of the increased tortuosity of the matrix relative to free water. Matrix diffusion in the volcanic rock matrix is parameterized by the effective diffusion coefficient to distinguish it from the free water diffusion coefficient. The matrix diffusion process is applied to fractured volcanic rocks only. Alluvium is modeled as a porous medium without matrix diffusion.

Laboratory experiments and field tests have demonstrated that matrix diffusion occurs in fractured volcanic rocks near Yucca Mountain. Such experiments provide a basis for quantifying the effect of matrix diffusion on radionuclide migration through the fractured volcanic rocks of the saturated zone. An empirical relationship relating matrix diffusion coefficients to matrix porosity and permeability has been developed from laboratory measurements of diffusion coefficients in samples of intact volcanic rock matrix, and from corresponding matrix porosity and permeability measurements (SNL 2007b, Appendix D, Section D4.2; Reimus, Haga et al. 2002; Reimus, Ware et al. 2002). Diffusing species in these experiments were ^{99}Tc (as TcO_4^-), ^{14}C (as HCO_3^-), tritiated water, bromide ion, and iodide ion. Rock samples were taken from the vicinity of Yucca Mountain and Pahute Mesa at the Nevada Test Site. Matrix permeability was found to account for most of the variability in effective matrix diffusion coefficients (Reimus, Haga et al. 2002). In the field, the observed tracer breakthrough curves in multiple tracer tests at the C-Wells can only be explained and interpreted using transport models that account for matrix diffusion (Figure 2.3.9-23) (SNL 2007b, Appendix D, Section D4.2). These interpretations yield estimates of matrix diffusion coefficients that are more uncertain than laboratory measurements, but they are effectively obtained at much larger and more relevant scales for the TSPA than in the laboratory. The cumulative distribution of the matrix diffusion coefficient applicable to Yucca Mountain volcanic rocks is illustrated in Figure 2.3.9-24 (SNL 2008b, Section 6.5.2.6). The cumulative distribution demonstrates a consistency across both laboratory and field scales.

Dispersion—Dispersion is the mixing of a solute in flowing groundwater. Dispersion is caused primarily by groundwater velocity variations due to aquifer heterogeneities at scales ranging from individual pore spaces to the thickness of individual strata and the length of structural features, such as faults. The spreading and dilution of radionuclides that results from these heterogeneities is important to transport in the saturated zone. Although heterogeneities at the scale of kilometers are represented explicitly in the site-scale saturated zone transport model, dispersion at smaller scales is characterized using an anisotropic dispersion coefficient tensor consisting of a three-dimensional set of dispersivity values: longitudinal, horizontal transverse, and vertical transverse (SNL 2008a, Section 6.4.2). Because the radionuclide source term at the water table will be relatively unchanging over a long period of time, longitudinal dispersivity will be important only at the leading edge of the advancing plume, while transverse dispersivity (horizontal and vertical transverse) is the strongest control on plume spreading and possible dilution for the repository (CRWMS M&O 1998, p. LG-12).

Temporal changes in the groundwater flow field may significantly increase the apparent dispersivity displayed by a contaminant plume, particularly with regard to transverse dispersion. However, observations of water levels in wells at Yucca Mountain have shown neither large nor consistent variations (Luckey et al. 1996, pp. 29 to 32), indicating that the flow field is at steady-state. Any small transients that do occur will probably not lead to significantly greater transverse dispersion than is incorporated in the site-scale saturated zone transport model. The thick unsaturated zone in the area of Yucca Mountain likely dampens the response of the saturated zone flow system to temporal variations in infiltration on timescales of less than centuries.

Field transport studies addressing dispersion have been conducted at length scales ranging from meters to kilometers. Figure 2.3.9-25 shows estimated longitudinal dispersivity as a function of length scale. Dispersivity increases as a function of observation scale, which is attributed mainly to mixing as more and larger heterogeneities are encountered by flow at larger scales (Gelhar et al.

1992, pp. 1971 and 1972). Dispersivity values determined for the C-Wells multiple tracer experiment (SNL 2007b, Appendix E, Section E4.1) illustrate a trend toward larger dispersion coefficients for transport over longer distances, and the longitudinal dispersivity estimates are consistent with values observed for similar length scales elsewhere (Figure 2.3.9-25) (SNL 2007b, Appendix E, Section E4.1). The scale of interest for the site-scale saturated zone transport model is on the order of 10 to 30 km. The dispersivity distribution (LDISP) in Table 2.3.9-4 is taken directly from the saturated zone expert elicitation (CRWMS M&O 1998), and was informed by data such as those presented in Figure 2.3.9-25.

Testing Related to Advection, Diffusion, and Dispersion Processes for Alluvium—Laboratory-scale and field-scale tracer testing has been conducted in the alluvium. To determine whether a single- or dual-porosity model best conceptualizes transport in the alluvium, three single-well injection-withdrawal tracer tests were conducted in borehole NC-EWDP-19D, and two single-well injection-withdrawal tracer tests, with two cross-hole tracer tests, were conducted at Nye County Site 22S. In each of the single well tracer tests, two nonsorbing solute tracers with different diffusion coefficients (a halide and a fluorinated benzoic acid) were dissolved in the same solution and simultaneously injected into the borehole, followed by a much larger volume of tracer-free groundwater (called chase water), and then pumped back after being allowed to remain in the aquifer for different time periods (SNL 2007b, Section 6.5.2). Two cross-hole tracer tests were conducted at Nye County Site 22, from January to October 2005. The first test involved the injection of several tracers into the second interval from the surface in two different wells (22PA and 22PC), while the same interval was continuously pumped in 22S (SNL 2007b, Figures 6.1-8 and 6.1-10). The two injection wells were located in approximately orthogonal directions to each other relative to 22S (22PA is north, and 22PC is east), so flow and transport anisotropy could be evaluated. The second cross-hole tracer test was conducted in the same configuration as the first test, but only two tracers—iodide ion and perrhenate ion—and one injection interval (the second interval from the surface in 22PA) were used.

There was virtually no difference in the normalized responses of the halide and fluorinated benzoic acid in the tests at the Alluvial Testing Complex. The similarity of the responses for the tracers with different diffusion coefficients indicates that the diffusion between flowing and stagnant water was negligible over the time scales of the experiments. At well 22S, for the test with a 30-day rest period, the different responses of the two tracers suggests that diffusion may be occurring. However, there is also a significant difference between the responses of the same tracer (iodide) in the two tests with different rest periods. These differences cannot be accounted for by diffusion alone (particularly the shorter time to peak concentration in the longer-rest-period test), so tracer drift in the ambient flow field also influenced the single-well tracer responses at this location (SNL 2007b, Section 6.5.3).

The tracer responses for the cross-hole tests at well location 22S also showed a different response for the two tracers, suggesting some diffusion (SNL 2007b, Section 6.5.4). Although there was no apparent diffusion between flowing and stagnant water in the single-well tracer tests at the Alluvial Testing Complex, the single-well and cross-hole tracer test results and interpretations at Site 22 collectively indicate dual-porosity transport behavior in the alluvium at this location. However, the diffusion time and length scales are relatively short compared to those of the fractured volcanics, and an important conclusion is that, over the time and distance scales of importance for performance assessment calculations, the tracer test interpretations suggest that the alluvium will behave as a single-porosity transport system with an effective porosity equal to the sum of the flowing and

stagnant porosities deduced from the tracer tests. The short diffusion time and distance scales are more consistent with a diffusion-into-grains (or blocks) conceptual model than a diffusion-into-layers conceptual model. However, longer diffusion time scales cannot be ruled out in the alluvium because of the short time and distance scales of the tracer tests relative to performance assessment time scales. It is possible that the tests were strongly influenced by diffusion into blocks within flow pathways, but the flow pathways were large enough in thickness or diameter (i.e., channels) that longer-time-scale diffusion into stagnant water surrounding the pathways was not observed (SNL 2007b, Section 6.5.5). As a result of these observations, diffusion was not considered for the alluvium in the site-scale saturated zone transport model, and the alluvium is represented using a porous continuum conceptual model (SNL 2007b, Section 6.5.5).

Effective Flow Porosity of the Alluvium—The advective velocity of groundwater is typically determined as the specific discharge divided by effective porosity. Effective porosity is that fraction of the porous medium through which groundwater flow occurs. The potential channelization of groundwater flow through higher permeability strata or facies within the alluvium may significantly reduce the effective porosity relative to the total porosity of the medium. Ranges of effective flow porosities for alluvial materials have been presented (SNL 2008b, Section 6.5.2.3), and to supplement this information various methods were used to estimate effective flow porosity based on testing at the Alluvial Testing Complex and at Well 22S. A value of 10% was determined for effective porosity from borehole NC-EWDP-19D, based on the single-well tracer test results (SNL 2007b, Appendix G, Section 4.2.4). Based on the cross hole testing at Well Cluster 22S, the effective flow porosity values ranged from 3.6% to 18.7% (SNL 2007b, Table 6.5-8). Total porosities ranging from about 20% to 30% were estimated for borehole NC-EWDP-19D, based on a borehole gravimeter survey (SNL 2007b, Appendix F, Section F4). A total porosity estimate of about 40% was obtained using the storage coefficient from a cross-hole hydraulic test at the Alluvial Testing Complex, and the barometric efficiency of the formation (SNL 2007b, Appendix F). These total porosity estimates were considered when establishing upper bounds for the uncertainty distribution of effective flow porosities in the alluvium.

Alluvium Specific Discharge—Groundwater advection is directly proportional to specific discharge. Specific discharge was discussed previously in Sections 2.3.9.2.3.6 and 2.3.9.2.4.2.

Alluvium Dispersivity—Longitudinal and transverse dispersion occurs due to heterogeneity in permeability within the alluvium. An estimate of longitudinal dispersivity in the alluvium (5 m) was obtained from the interpretation of the single-well tracer tests at NC-EWDP-19D that was used to calculate flow porosity. From the cross-hole tests at the Well 22S complex, longitudinal dispersivity values ranged from 1.6 to 10 m (SNL 2007b, Table 6.5-8). Longitudinal dispersivity estimates were also obtained from several column tracer experiments conducted using groundwater and alluvium from borehole NC-EWDP-19D. Dispersivity values from these experiments ranged from 1.8 to 5.4 cm (SNL 2007b, Appendix H, Section H2), which is consistent with the scale of the column experiments. Longitudinal dispersivity estimates from the single well tracer tests at the Alluvial Testing Complex are scale-dependent (Figure 2.3.9-25) and thus exhibit a large uncertainty. As presented in Figure 2.3.9-25, the range of uncertainty in longitudinal dispersivity at any particular scale is between one and two orders of magnitude. Uncertainty in dispersivity is incorporated in the saturated zone flow and transport abstraction model (Section 2.3.9.3.3.4).

2.3.9.3.2.2   Radionuclide Sorption Parameters and Mineral Precipitation Effects

Sorption reactions are chemical reactions that involve the attachment of dissolved chemical constituents onto solid surfaces. Although these reactions can be complex, they typically are represented in transport calculations by a constant sorption distribution coefficient, K_d. The sorptive properties of the tuff and alluvial aquifers have been studied in laboratory and, to a lesser degree, in field tracer tests (SNL 2007b, Sections 6.3.6 and 6.5.6, Appendices E and H).

The sorption process, as represented by sorption distribution coefficients, contributes to the capability of the saturated zone as a component of the Lower Natural Barrier for many radionuclides. The primary controls on sorption behavior include (1) the characteristics of mineral surfaces in the rock units through which water flows in the saturated zone; (2) the chemistry of the groundwater in the saturated zone; and (3) the sorption characteristics of each element. Sorption behavior can also have a nonlinear dependence on radionuclide concentrations in the water, but sorption experiments have been carried out for a range of radionuclide concentration (SNL 2008a, Section A2). Variations in groundwater chemistry may influence complexation of radionuclides with other aqueous species, which can, in turn, impact the sorption of radionuclides onto the aquifer materials. In particular, the solution and sorption behavior of uranium, neptunium, and plutonium is sensitive to bicarbonate and carbonate concentrations in groundwater. To evaluate the functional dependence of the sorption coefficient on aqueous chemistry and pH, surface complexation models were developed for key radionuclides (SNL 2008a, Appendix A). The equilibrium surface complexation model used in this analysis is based on the PHREEQC V2.3 software code. The modeling results show that the sorption and desorption laboratory data generally bracket the theoretical model for sorption coefficients. The influence of expected variations in these variables was incorporated into the uncertainty distributions developed for sorption coefficients (SNL 2008a, Appendix A). The impacts of water chemistry and complexation are thus included in the assessment of uncertainty in sorption coefficients and radionuclide transport simulations, consistent with FEPs 2.2.08.01.0A, Chemical characteristics of groundwater in the SZ, and 2.2.08.06.0A, Complexation in the SZ (Table 2.3.9-1). The sorption process in fractured volcanic rocks is the same in the saturated zone and the unsaturated zone in the Lower Natural Barrier (SNL 2008a, Section 6.3; SNL 2008e, Section 4.1.2). However, given the larger scale and the lower density of data and difference in groundwater chemistry in the saturated zone relative to the unsaturated zone, values of sorption coefficients have different uncertainties in the saturated zone and the unsaturated zone. Consequently, values of sorption coefficients are not correlated in the saturated zone and the unsaturated zone (SNL 2007e, Appendix B2).

The sorption-coefficient data on which the distributions are based were obtained in laboratory experiments in which representative rock samples from Yucca Mountain were placed in contact with groundwaters (or simulated groundwaters) representative of the site that were spiked with one or more of the elements of interest. Sorption experiments were carried out as a function of rock type, time, element concentration, atmospheric composition, grain size, and temperature. In some cases, the solids remaining from sorption experiments were placed in contact with unspiked groundwater in desorption experiments to verify that reversible sorption is occurring as modeled. All available site-specific data on sorption were considered in the development of uncertainty distributions in sorption coefficients (SNL 2008a, Appendices A and C). In addition, data from outside the Yucca Mountain project were used in the equilibrium chemical modeling that assessed the impacts of potential variations in groundwater chemistry.

In addition to sorption processes, radionuclide migration can be affected by mineral precipitation reactions caused by changes in geochemical conditions along the groundwater flow path. Redox (reduction-oxidation) potential is a measure of the oxidizing or reducing condition of the geochemical system. Redox conditions could be an important control on mineral precipitation reactions in the saturated zone for several redox-sensitive radioelements (e.g., technetium) (SNL 2008a, Appendix F), if reducing conditions exist in the saturated zone. Enhanced sorption under reducing conditions of redox-sensitive species, such as plutonium, neptunium, technetium, and uranium, could also slow the migration of those radionuclides in the saturated zone (SNL 2008a, Appendix F).

Reducing conditions have been observed in the groundwater of several boreholes in the vicinity of Yucca Mountain (SNL 2008a, Appendix F). A possible explanation for reducing groundwater in the volcanic units to the east and south of the repository is interaction between oxidizing groundwater and pyrite in the Tram Tuff. In addition, there is a range of redox conditions measured in alluvial groundwater pumped from Nye County Early Warning Drilling Program boreholes. For example, groundwater in the central portion of the expected flow path (e.g., at boreholes NC-EWDP-19D and NC-EWDP-22S) generally has oxidizing conditions, while groundwater to the east (e.g., NC-EWDP-5SB) and west (e.g., NC-EWDP-1D and NC-EWDP-3S) has reducing characteristics (SNL 2008a, Appendix F).

Although reducing conditions have been observed (SNL 2008a, Appendix F), sufficient data are not available to confidently identify flow paths with reducing conditions in the saturated zone. Because oxidizing conditions yield more rapid transport behavior for redox-sensitive radionuclides, the possible precipitation reactions and enhanced sorption as a result of reducing conditions have not been considered in the TSPA. The impact of including the reducing conditions on the transport of radionuclides in the saturated zone is presented as part of the confidence building in the TSPA (SNL 2008d, Appendix C6.7).

Radionuclide Sorption on Fractured Tuff—Sorption of radionuclides may potentially occur on the surfaces of fractures and within the rock matrix of the fractured tuff. However, fracture sorption processes were not explicitly considered in the site-scale saturated zone transport model, because of the high degree of uncertainty in the sorptive mineral distribution on fractures and, hence, radionuclide fracture sorption characteristics. Also, field testing of lithium ion, a reactive tracer, at the C-Wells Complex indicated that while it was necessary to invoke matrix sorption to explain the lithium breakthrough curves, it was not necessary to invoke fracture-surface sorption to explain the responses (SNL 2007b, Section 6.3.4). Transport rates are conservatively overestimated because some sorption will occur on fracture surfaces in volcanic rocks, but sorption is not included in the model because interpretation of the C-Wells data demonstrated that sorption onto fracture surfaces is much less important than sorption onto the matrix following matrix diffusion.

The results of one of the multiple-well injection-withdrawal tests at the C-Wells Complex are shown in Figure 2.3.9-26. The response of lithium relative to the conservative tracers is consistent with its diffusion into the matrix followed by sorption onto the matrix (SNL 2007b, Section 6.3.4). Interpretation of these test results was accomplished using a one-dimensional semianalytical dual-porosity model with the sorption coefficient of the matrix as an adjustable parameter (SNL 2007b, Appendix D, Section D4.6.1). The sorption parameters yielding good fits of the model to the

field observations (Figure 2.3.9-26) tended to be somewhat higher than the laboratory sorption test parameters (SNL 2007b, Appendix D, Section D4.8.4). Thus, in addition to supporting a dual-porosity conceptual transport model in the fractured tuffs, the lithium results suggest that laboratory-derived sorption parameters can be used to predict field-scale reactive transport behavior of radionuclides.

Additional support for using laboratory-derived sorption parameters was provided by laboratory and field measurements of sorption parameters for surrogate reactive tracers in the Topopah Spring welded and Calico Hills nonwelded hydrogeologic units at Busted Butte (Turin et al. 2002). The work performed at Busted Butte, although designed to support the modeling of flow and transport in the unsaturated zone, also provides valuable information for saturated zone studies because the Busted Butte experiment was conducted in the Calico Hills Formation, which is located below the water table at some locations downgradient of Yucca Mountain. To ensure that mineralogic composition was not altered, the fine particles produced during sample crushing were retained during the Busted Butte sorption studies. The sorption behavior of the surrogate tracers observed in the field test was consistent with their laboratory sorption behavior. Furthermore, the surrogate tracers had a range of sorption parameters that was consistent with the range of sorption parameters measured for radioelements (neptunium, plutonium, and americium) onto the same rocks. Thus, the field test results suggest that laboratory-derived sorption parameters can be used to predict field-scale transport behavior of sorbing radionuclides having a wide range of sorption characteristics.

Many laboratory batch sorption experiments have been conducted to determine K_d values for several radioelements in fractured tuffs, and these K_d values have been used to develop radionuclide-specific K_d distributions (Section 2.3.8.3.1). Examples of sorption data that were used to develop K_d distributions (Table 2.3.9-14) are presented in Figures 2.3.9-27 through 2.3.9-32 for neptunium, plutonium, and uranium. These sorption data represent different types of experiments (i.e., sorption versus desorption), different water chemistries (derived from well UE-25 J#13 and borehole UE-25 p#1), different times when the experiment was performed (i.e., old tests performed prior to 1990 and new tests performed after 1990), and different experiment durations (SNL 2008a, Appendix A).

In addition to batch sorption experiments, laboratory column transport experiments have been conducted to determine sorption characteristics of radionuclides under flowing conditions in both crushed and fractured tuff columns. If sorption reactions are slow (i.e., slow adsorption kinetics), then the equilibrium conditions determined by the batch experiments may not occur in nature. The laboratory column experiments are designed to examine the kinetics of the sorption reaction. Early breakthroughs of a fraction of the sorbing radionuclide mass in column experiments (e.g., plutonium breakthroughs coincident with tritiated water) have sometimes been observed, but have been shown to be consistent with slow adsorption kinetics. The trends in these experiments suggest that the use of the local equilibrium approach with K_d distributions derived from laboratory batch experiments yields conservative radionuclide transport times in transport simulations (SNL 2008a, Appendix G). Radionuclide sorption experiments have demonstrated that sorption kinetics are relatively unimportant for plutonium, and that the assumption of local equilibrium can be used when evaluating radionuclide transport. Because sorption kinetics are faster for other radioelements than for plutonium, the equilibrium assumption is also valid for other radioelements (SNL 2008a, Appendix A).

Radionuclide Sorption in the Alluvium—The migration behavior of sorbing radionuclides in the saturated alluvium south of Yucca Mountain has been studied in a series of laboratory-scale tests including batch sorption, batch desorption, and flow-through column experiments. The alluvium used in the experiments consists primarily of materials of volcanic origin similar to those found at Yucca Mountain (with some enrichment of clays and zeolites relative to common volcanic rocks, plus secondary mineral coatings on the detritus) (SNL 2008a, Appendix G).

Experiments conducted using alluvial materials have focused on the transport characteristics of ^{129}I, ^{99}Tc, ^{237}Np, and ^{233}U. The first two radionuclides were determined to be nonsorbing, while the second two were moderately sorbed onto the alluvium. The goal of these experiments was to determine the sorption coefficients of the radionuclides onto alluvial materials under conditions similar to natural system transport (SNL 2008a, Appendix G).

The alluvium samples used in the experiments were obtained at various depths from boreholes NC-EWDP-19IM1A, NC-EWDP-10SA, and NC-EWDP-22SA. Although the dominant minerals in the alluvium are quartz, k-feldspar, and plagioclase, considerable amounts of sorbing minerals like smectite (ranging from 3% to 8%) and clinoptilolite (ranging from 4% to 14%) were identified in the alluvium samples. The results of all three experiments (Figure 2.3.9-33) show that sorption of ^{233}U onto alluvium is fast and that, after one day of contact, the amount of ^{233}U adsorbed onto the alluvium changed little with time. The higher K_d value associated with alluvium material from well NC-EWDP-22SA may be due to the higher smectite and clinoptilolite content in the sample from this depth interval (522 to 525 ft below ground surface) (SNL 2008a, Appendix G). The experimentally determined K_d values of ^{237}Np and ^{233}U onto the alluvium samples using groundwater from NC-EWDP-19D1, Zone 1, and NC-EWDP-10S are shown in Figure 2.3.9-34. These results suggest that sorption coefficients in the alluvium range from about 3 to 13 mL/g for ^{237}Np and from about 3 to 9 mL/g for ^{233}U.

Batch sorption tests were also conducted to determine whether ^{233}U sorption behavior differs in groundwater from different zones in the same borehole (e.g., NC-EWDP-19D, Zones 1 and 4). K_d values of ^{233}U measured in Zone 4 water were less than those measured in Zone 1 water (Figure 2.3.9-35). The major differences between these two waters were the lower concentration of divalent cations and the slightly higher pH in Zone 4 relative to Zone 1. These differences may result in greater complexation of ^{233}U to carbonate in Zone 4 water, as well as more sorption competition with divalent cations in Zone 4 water, both of which yield less sorption in the Zone 4 water (SNL 2008a, Appendix G).

Laboratory column transport experiments have also been conducted to determine sorption characteristics of radionuclides under flowing conditions in the alluvium. In column transport experiments using groundwater from boreholes NC-EWDP-19D (Zones 1 and 4) and NC-EWDP-10SA, ^{99}Tc and ^{129}I exhibited no retardation relative to tritiated water, which is consistent with the absence of sorption of these radionuclides in batch experiments (Figure 2.3.9-36). In some column experiments, particularly those involving ^{237}Np (Figure 2.3.9-37), a fraction of the radionuclide mass exited the columns at the same time as tritiated water, similar to the tuff column experiments. These observations are consistent with slow sorption kinetics of ^{237}Np as an explanation for the unretarded transport of a portion of the ^{237}Np (SNL 2008a, Appendix G, Section G4).

Figure 2.3.9-37 shows the breakthrough curves of ^{237}Np and tritiated water as a function of flow rate in three columns packed with the same alluvium material. The results imply that the effective K_d values for a portion of the ^{237}Np mass in the higher flow rate experiments are significantly less than the K_d values obtained from batch sorption experiments using the same alluvium. However, the neptunium fractional mass recoveries are always significantly less than 1.0, indicating that a substantial portion of the neptunium sorbs strongly in the columns. These results differ from what was observed for plutonium in crushed tuff column experiments in that (1) the neptunium is always retarded relative to tritiated water, regardless of the flow rate; (2) its retardation increases with decreasing flow rate through the columns; and (3) it continually elutes from the columns once it appears in the effluent (i.e., long tailing behavior) (SNL 2008a, Section G4.1). Whereas the plutonium responses were consistent with slow sorption kinetics with little desorption, the ^{237}Np behavior is consistent with rapid sorption onto a distribution of sorption sites in the columns that have a wide distribution of effective K_d values. The flow rate dependence of the neptunium breakthrough curves is consistent with a range of desorption rates for different types of sorption sites. As the flow rate decreases, a greater proportion of the neptunium mass in the columns becomes attached to sites with slow desorption rates. Similar long-tailed breakthrough curves with relatively low mass recoveries were obtained for ^{233}U in column transport experiments (SNL 2008a, Appendix G, Section G4.2).

In summary, the column data indicate that, while a small fraction of radionuclide mass may arrive earlier than would be predicted using batch K_d values, this fraction decreases as flow rates decrease, and the K_d values obtained from batch sorption experiments still reflect the behavior of the majority of the radionuclide mass in the experiments. The data also indicate that the early arriving mass fraction may disappear altogether at low flow rates, such as those expected in the saturated zone, and that much of the radionuclide mass could experience much larger effective K_d values than measured in batch experiments (SNL 2008a, Appendix G). Cross-hole tracer tests at the 22S well complex also yielded sorption values for the tracer lithium that were compared with laboratory determined distribution coefficient values. The conclusion from this comparison is that the laboratory K_d values would probably result in underestimation of field-scale sorption/retardation in the alluvium if used in large-scale predictive transport models (SNL 2007b, Section 6.5.5). Final K_d distributions used in the TSPA, which were developed from the results of the batch experiments (Table 2.3.9-14), are therefore considered conservative.

2.3.9.3.2.3   Colloid-Facilitated Transport

Radionuclides can undergo colloid-facilitated transport in both the volcanic rocks and the alluvium. Radionuclide-bearing colloids transported to the saturated zone may include (1) natural colloids, typically clay or silica; (2) waste-form colloids resulting from degradation of spent nuclear fuel or glass; and (3) iron oxyhydroxide colloids resulting from degradation of the waste package. These colloids are grouped into two types—those formed from hydrolysis of dissolved radionuclides (often called true colloids), and colloidal particles of other materials with attached radionuclides (called pseudocolloids), as described in Section 2.3.7.11.1. The transport of true colloids is not included in the conceptual model of radionuclide transport in the saturated zone because these colloids would not be stable under prevailing geochemical conditions, or they would be strongly sorbed onto iron oxyhydroxide colloids (SNL 2007f, Sections 6.3.1 and 6.3.11). The transport of pseudocolloids in groundwater, and the mechanisms of sorption of radionuclides onto these colloid particles, are included in the site-scale saturated zone transport model. Movement of colloids in the

volcanic rocks is assumed to occur within fractures only (SNL 2008a, Section 6.3). Matrix diffusion of colloids will be much less than for solutes because of the much smaller diffusion coefficients of colloids and the relatively large size of the colloids compared to matrix pores. Colloid attachment onto and detachment from both fracture surfaces and alluvium surfaces are modeled with first-order rate expressions, which means colloid attachment and detachment is modeled in the same manner as sorption (BSC 2004e, Section 6.4).

Most sorbing radionuclides sorb onto colloids reversibly (i.e., they have measurable desorption rates and can be entirely desorbed from colloids) (Figure 2.3.9-38). However, plutonium and americium can sorb either reversibly or irreversibly onto colloids. Irreversibly sorbed plutonium and americium are either embedded within waste form colloids (e.g., smectite colloids formed by degradation of high level waste glass), or are so strongly sorbed onto colloids formed in the waste package environment (e.g., iron oxyhydroxide colloids formed by corrosion of waste packages) that there is no possibility of desorption over typical transport time scales (thousands of years) through the saturated zone. In general, the majority of the plutonium and americium sorbed onto colloids that form in the waste-package environment is assumed to be irreversibly sorbed—typically 90 to 99% (SNL 2007f, Section 6.3.12.2).

The transport of radionuclides that are reversibly sorbed onto colloids is governed by equilibrium partitioning of the radionuclides between the solution phase, the immobile rock matrix, and mobile colloids. Transport times through the saturated zone are slow enough that equilibrium sorption is expected even for slow radionuclide sorption and desorption rates. Transport of radionuclides that are reversibly sorbed onto colloids is modeled using the K_c model, which represents the equilibrium partitioning of radionuclides between the aqueous phase and the colloidal phase with effective distribution coefficient, K_c (SNL 2008a, Section 6.4.2.6.2). Colloid-facilitated transport of reversibly sorbed radionuclides depends on colloid transport parameters, mobile colloid mass concentrations, and radionuclide distribution coefficients onto both colloids and the immobile rock matrix. High colloid concentrations and large radionuclide distribution coefficients onto colloids (relative to the rock matrix) favor colloid-facilitated radionuclide transport at rates that can significantly exceed transport rates in the absence of colloids (SNL 2007f, Section 6.5.3).

Irreversibly sorbed plutonium and americium are transported by groundwater in a manner identical to the colloids onto which they are sorbed. Several field observations suggest that a small percentage of colloids transport with essentially no retardation in groundwater (Kersting et al. 1999, p. 56; Penrose et al. 1990, p. 233), whereas the majority undergo either reversible or irreversible filtration (i.e., attachment and detachment), which can be described by a retardation factor. The value of the colloid retardation factor is dependent on several factors, such as colloid size, colloid type, and geochemical conditions (e.g., pH, Eh, and ionic strength). These factors are folded into the retardation factor distribution that has been developed from field and experimental data collected under varying geochemical conditions with different colloid types and sizes. Attachment rate constants, k_{att}, and detachment rate constants, k_{det}, of colloids onto and from the rock matrix have been measured, and separate retardation factor uncertainty distributions have been developed for the fractured volcanic rocks and the alluvium (BSC 2004e, Sections 6.4 to 6.8).

2.3.9.3.2.3.1   Test Results for Radionuclide Sorption onto Colloids

Aqueous chemical conditions play an important role in the process of radionuclide sorption onto colloids (SNL 2007f, Section 6.3.12). The behavior of the mineral surface is primarily controlled by pH and ionic strength (particularly concentrations of sodium, calcium, and potassium). The behavior of the sorbate is primarily controlled by its oxidation state, pH, and the partial pressure of carbon dioxide ($p CO_2$). For minerals in which the sorption mechanism is primarily by ion exchange (e.g., clay minerals), ionic strength impacts sorption of cesium on clay minerals (especially at their edges), because cations compete with radionuclides for exchange sites. Ionic strength is less important for actinides, although some anions and cations contributing to ionic strength affect sorption by forming complexes with the actinides (SNL 2007f, Section 6.3.12.1).

Laboratory batch sorption experiments were conducted to evaluate (1) sorption kinetics of ^{239}Pu, ^{243}Am, ^{237}Np, and ^{238}U onto colloids of hematite, montmorillonite clay, and silica in groundwater; (2) adsorption of these four actinides onto colloids as affected by ionic strength of the solutions and water temperature; (3) ^{239}Pu and ^{243}Am adsorption onto colloids as a function of colloid concentrations; and (4) desorption of the four actinides from actinide-loaded colloids as a function of time. These four actinides were chosen for the experiments because their transport is governed by solubility and speciation in groundwater, their tendency to be sorbed onto minerals, colloids, and other matrices, and their propensity to form mobile species, such as dissolved cations, anions, and colloids. Experiments were conducted using natural groundwater collected from Well UE-25 J-13 or a synthetic sodium-bicarbonate solution that has approximately the same bicarbonate concentration as J-13 well water but without the minor cations and anions (Lu et al. 2000, pp. 7 to 10). The latter solution was used to investigate the potential effect of the minor cations and anions on radionuclide sorption. The results of the experiments indicate that very little ^{237}Np and ^{238}U were adsorbed by colloids. These two actinides may be transported primarily as dissolved species. On the other hand, strong adsorption and slow desorption of ^{239}Pu and ^{243}Am by colloids in groundwater may facilitate transport of those radionuclides to the accessible environment (Lu et al. 2000, p. 45).

The uncertainty in the values of sorption coefficients for radionuclides onto colloids was assessed using a variety of information sources (e.g., SNL 2007f, Sections 6.3.12 and 7.1.5, Tables 6-14, 6-15, 7-6, and 7-7; EPA 1999; Stenhouse 1995; Lu et al. 1998; Lu et al. 2000; Honeyman and Ranville 2002, Chapter 7, p. 140). Developed K_d intervals and probabilities (SNL 2007f, Section 6.3.12.1) are intended to cover the entire ranges of K_d values and emphasize the higher ends of the ranges, but deemphasize the highest intervals. These distributions are used (1) because the ranges are based on data for both colloids and larger minerals, and it is believed that K_d values for colloids will be higher than for larger minerals due to their higher specific surface area; and (2) because of the mechanisms of radionuclide interaction with colloid surfaces that actually prevail, the selected K_d values tend to predict less sorption than the actual retention of actinide metals by iron oxyhydroxide colloids (SNL 2007f, Section 6.3.12.1). These result in a conservative assessment of radionuclide retardation via sorption onto colloids.

2.3.9.3.2.3.2   Test Results for Colloid Concentration in Groundwater

Radionuclides that are reversibly sorbed onto colloids will transport both on colloids and in the aqueous phase, and their transport characteristics are a combination of the transport characteristics of both the solute and colloids. Transport of radionuclides reversibly sorbed onto colloids is a

function of three parameters: (1) the concentration of colloids in the groundwater; (2) the sorption coefficient for the radionuclide onto colloids; and (3) the sorption coefficient for the radionuclide onto the immobile mineral surfaces in the system.

In order for radionuclide-bearing colloids to affect transport in the saturated zone, the concentration of colloids in suspension must be stable over the time frame of transport and must carry significant amounts of radionuclides. Several types of colloids and their stability as a function of ionic strength and pH are considered (SNL 2007f, Section 6.3.2). For the saturated zone at Yucca Mountain, colloids are generally stable for ambient, relatively dilute chemical conditions. Measurements of groundwater colloid concentrations at Yucca Mountain, supplemented by data from Idaho National Laboratory (12% of the total number of samples), were used to assess the range of possible colloid concentrations present in the saturated zone for colloid-facilitated transport of reversibly sorbed radionuclides. Inclusion of the Idaho data was deemed appropriate because the area's arid climate and fractured volcanic rocks are similar to Yucca Mountain (SNL 2007f, Section 6.3.11 and Appendix I).

Studies of groundwater colloids in the Yucca Mountain region (e.g., Kingston and Whitbeck 1991; Degueldre et al. 2000) suggest that when groundwater conditions favor colloid stability, there may be a wide range of colloid concentrations observed for a narrow range of groundwater chemistry. Review of such Yucca Mountain region colloid data revealed that the largest proportion of groundwater colloid samples had colloid concentration populations between 0.001 and 0.1 mg/L (SNL 2007f, Section 6.3.11). Honeyman and Ranville (2002, p. 137) point out that, although subsurface systems identified as potential locations for radioactive waste disposal exhibit relatively low colloid concentrations (less than 10 mg/L), concentrations exceeding 100 mg/L are not uncommonly reported (SNL 2007f, Section 7.1.4). Consequently, the uncertainty distribution for colloid concentrations in the saturated zone has been conservatively set to include an upper limit of 200 mg/L (SNL 2007f, Section 6.3.11 and Table 6-13). Colloid concentrations as high as this limit are not expected at Yucca Mountain; more likely, they are orders of magnitude less, given that most groundwater samples fall within the range of 0.001 to 0.1 mg/L, as cited above.

2.3.9.3.2.3.3   Test Results for Colloid Transport in Fractured Volcanic Rock

Colloid filtration rate constants and retardation factors were determined for fractured volcanic rocks in several laboratory and field experiments. The field experiments used fluorescent carboxylate-modified latex microspheres as tracers in cross-hole tracer tests. Laboratory-scale colloid transport experiments in fractured rock columns were conducted using silica, montmorillonite, and clinoptilolite colloids in addition to the carboxylate-modified latex microspheres. Colloid attachment and detachment rate constants were derived from colloid responses in these tests. Specifically, colloid breakthrough data were modeled with solutions of the advective-dispersion equation with reversible first-order reaction to account for colloid attachment and detachment. Attachment and detachment rate constants were varied until simulated breakthrough closely matched the measured test data. For each experiment, the colloid retardation factors were then calculated as one plus the ratio of the best-fit attachment to detachment rate constants. Figure 2.3.9-39 presents the resulting distribution of retardation factors (BSC 2004e, Section 6.4.3).

Attachment rate constants derived from colloid tests tend to decrease with the time taken to reach peak nonsorbing solute concentrations (Figure 2.3.9-40). This result occurs because a small fraction of colloids tends to break through at about the same time as nonsorbing solutes in tracer tests, regardless of the overall time scale of the test. This early appearance of colloids forces attachment rate constants to decrease with time when the colloid responses are fitted using a single rate constant to account for filtration (BSC 2004e, Section 6.4.2).

To investigate the suitability of carboxylate-modified latex microspheres as surrogates for inorganic colloids in field tracer tests in fractured media, a study was conducted in laboratory-scale fractures in which 100-nm diameter silica colloid transport was compared directly with 330-nm diameter carboxylate-modified latex microsphere transport. The microspheres transported nearly identically to or conservatively (i.e., with less filtration) relative to the silica colloids at all flow rates investigated (Anghel 2001, Chapter 6). This result suggests that colloid filtration and retardation parameters derived from carboxylate-modified latex microsphere responses in field tracer tests should be conservative with respect to natural colloid transport in fractured volcanic rocks (BSC 2004e, Section 6.4.1).

2.3.9.3.2.3.4 Test Results for Colloid Transport in Alluvial Material

Colloid filtration rate constants and retardation factors were determined for alluvium in a number of laboratory and field experiments. These experiments were conducted using silica and natural colloids in addition to carboxylate-modified latex microspheres. Colloid attachment and detachment rate constants in the alluvium were derived through analysis of laboratory and field experiment data. Even though different sizes and types of colloids were used in the various tests, there is an apparent trend of decreasing attachment rate constant with residence time. This is similar to the trend observed in the fractured volcanic rocks (BSC 2004e, Section 6.5.2). In addition, field colloid transport data from the Netherlands (Schijven et al. 1999, p. 1,107, Table 3) were used to obtain field-scale estimates of colloid attachment and detachment rates to supplement site-specific, field scale data for the alluvium. The combination of the colloid selection, groundwater chemistry, and alluvium characteristics at the Schijven study site suggest that those field scale colloid filtration and detachment rate constants can be applied to Yucca Mountain alluvium (BSC 2004e, p. 6-13). The colloid retardation factors were derived from colloid attachment and detachment rate constants evaluated from the results of the field and laboratory tests (Figure 2.3.9-41) (BSC 2004e, Section 6.5).

Two field tracer experiments provide information regarding the migration of colloids in alluvium. A single well test at the Alluvial Testing Complex, and a cross-hole test at the 22S complex, were conducted using microspheres tracers (SNL 2007b, Sections G4.6 and G5.1). In both tests, detachment rate constants were estimated. For the cross-hole test, a filtration rate constant was determined as well.

For the test at the Alluvial Testing Complex, the detachment-rate constant (0.0012/hr) can be considered high (upper bound) because change in concentration with time slowly decreased as the test proceeded, and the fractional recovery of solutes increased faster than the microsphere recovery (which means that the estimate of the number of spheres remaining on the surfaces actually increased with time—a physical impossibility).

The microsphere filtration and detachment rate constants deduced from the first cross-hole tracer test at Site 22 (Table 2.3.9-15) have been used as estimates of filtration and detachment rate constants for natural colloids that could facilitate the transport of radionuclides strongly adsorbed to colloids. *Saturated Zone Colloid Transport* (BSC 2004e, Section 6.8) summarizes laboratory experiments, in which it is shown that carboxylate-modified latex microspheres transported with similar attenuation through saturated alluvium as natural colloids that were collected from well 19D, suggesting that microsphere filtration and detachment rate constants may be reasonably used for predicting natural colloid transport in saturated alluvium.

Perhaps of greater importance than the microsphere filtration and detachment rate constants derived from the field tests is the fact that the microsphere responses qualitatively indicate that colloid detachment from grains in the porous medium is a process that clearly occurs in saturated alluvium. These qualitative results suggest that it is not sufficient to consider only colloid filtration when assessing colloid facilitated radionuclide transport, but that colloid detachment and its dependence on other variables must also be considered and could possibly dominate the transport behavior of colloids. Colloid detachment, in general, can be accounted for in models with simple first-order kinetics expressions.

2.3.9.3.2.3.5   Estimates of Fractions of Colloids Transporting with No Retardation

Several field observations have indicated that a small percentage of colloids may transport without retardation while the majority of the colloids undergo either reversible (which includes detachment) or irreversible filtration. The longer the combined transport time through the unsaturated and saturated zones (i.e., the Lower Natural Barrier), the smaller the fraction of colloids that travels without retardation. Fractions of unretarded colloids range from 0.011 for one year of transport time to 2.56×10^{-4} for 10,000 years of transport time through the Lower Natural Barrier (BSC 2004e, Section 6.6). The portion of the total colloids that travel unretarded (or unfiltered) decreases with time. For short periods of time on the order of one year, the reaction times are such that about 1% of the colloids travel unfiltered or unretarded (BSC 2004e, Table 6-4). As the time increases, more of those unfiltered colloids will react, and over time only a very small portion will appear to act unfiltered.

The cumulative distribution of filtration rate constants for the volcanic rocks and alluvium are combined into a single distribution to obtain a conservative estimate of the mass fraction that moves without retardation through the entire saturated zone (BSC 2004e, Section 6.6). The fraction of colloids that travel without retardation is taken to be the cumulative probability of observed filtration rate constants that are less than the reciprocal of the transport time through the system.

The fraction of colloids that transports without retardation is specified as 1.68×10^{-3} for TSPA simulations, which is the fraction of colloids that travels without retardation over a 100-year transport time through the unsaturated and saturated zones (BSC 2004e, Table 6-4). Longer transport times lead to even smaller unretarded colloid fractions. This 100-year transport time is derived from the median transport times from 200 Monte Carlo realizations that are shown in Figure 2.3.9-16. Out of 200 realizations, the median transport time among all realizations for glacial-transition climatic conditions is 230 years (SNL 2008b, Section 6.6.2[a]), which corresponds to an interpolated value for the fraction of unretarded colloids equal to approximately

1.2×10^{-3} (BSC 2004e, Table 6-4). Using the fraction of unretarded colloids at 100 years ensures that the TSPA yields conservative results for radionuclide breakthrough due to colloid transport.

2.3.9.3.3 Site-Scale Saturated Zone Transport Model and Model Uncertainty
[NUREG-1804, Section 2.2.1.3.9.3: AC 1(1), (3), AC 2(1), AC 3(1), (2), (4), (5), AC 4; Section 2.2.1.3.12.3: AC 1(1) to (4), AC 2(1), AC 3(1) to (3), AC 4]

The site-scale saturated zone transport model simulates transport of radionuclides in the saturated zone for use in the saturated zone flow and transport abstraction model. The data used to develop relevant transport parameters (e.g., sorption coefficients), submodel processes (e.g., advection, matrix diffusion, and sorption), and site-scale model processes for the site-scale saturated zone transport model (e.g., flow paths and transport times) are based on laboratory testing, field tests, an expert elicitation panel, and analogue systems described in the literature. The principal output of the site-scale saturated zone transport model is the radionuclide arrival time at the accessible environment.

2.3.9.3.3.1 Site-Scale Saturated Zone Transport Model Development

The mathematical basis and associated numerical approaches of the site-scale saturated zone transport model are designed to incorporate the important saturated zone radionuclide transport processes in an efficient numerical code to compute breakthrough curves and transport times for use in TSPA simulations (SNL 2008a). An effective continuum modeling approach is used to simulate flow throughout the aquifer system, as explained in Section 2.3.9.2.3. The transport simulation also uses an effective continuum approach based on dual porosity to maintain consistency with the flow model. The matrix diffusion process that occurs during transport in fractured media was a key factor in choosing a dual porosity continuum model. The effective continuum governing equations can be implemented in several ways, including numerical formulation of the advective–dispersion equations or a random walk, particle-tracking method (de Marsily 1986, Section 12.5). As noted by de Marsily (1986, Section 12.5), both methods have limitations. Direct solutions of the advective-dispersion equations using either finite-difference or finite-element methods often lead to numerical dispersion where the solution technique adds an artificial numerical dispersion to the real phenomenon of dispersion. To avoid such a numerical artifact, the random walk method was chosen (Arnold et al. 2003). This method represents the mass of solutes as the sum of many particles. The path of each particle is determined by the groundwater flow model. Dispersion is modeled by randomly displacing the particle in a direction and distance that is governed by the dispersion coefficient. This random walk method better represents the dispersion process, but requires a large number of particles to yield accurate and smooth representations of concentration (de Marsily 1986, Section 12.5). Through validation and verification, the random walk, particle-tracking method has been shown to appropriately simulate transport in porous media (LANL 2003a, Section 2.23; LANL 2003b, Table 1). The dispersion coefficient consists of the hydrodynamic dispersion component and the molecular diffusion component, with the effects of molecular diffusion being significant only at very low groundwater flow velocities (SNL 2008a, Section 6.4.2.1). For the site-scale saturated zone transport simulations, a particle-tracking approach is used to compute solute trajectories and transport times and is combined with a random-walk model to incorporate dispersion. A semi-analytical method is used to simulate retardation due to diffusion and sorption and colloid-facilitated transport in the random-walk model (SNL 2008a, Section 6.4.2).

Model Implementation—The site-scale saturated zone transport model is based on the calibrated *Saturated Zone Site-Scale Flow Model* (SNL 2007a, Section 6.5.2). The dependence of the flow field on various material and fluid properties, such as permeability and viscosity, is discussed in the site-scale saturated zone flow model report (SNL 2007a, Section 6.5.1.3). Using the steady-state flow field supplied by the flow model, the transport model incorporates the transport processes of advection, matrix diffusion, dispersion, sorption, and colloid-facilitated transport (SNL 2008b, Sections 4 and 6) to compute the radionuclide transport times to the accessible environment. Radioactive decay and ingrowth are simulated as part of the saturated zone one-dimensional transport abstraction model. Input parameters to the transport model are effective porosity in alluvium, flowing interval spacing, flowing interval porosity, matrix diffusion coefficient, matrix porosity, sorption coefficients in volcanic rocks and alluvium, bulk density of volcanic matrix and alluvium, colloid retardation factor in volcanic units and alluvium, sorption coefficients onto colloids, groundwater concentration of colloids, longitudinal dispersivity, horizontal transverse dispersivity, vertical transverse dispersivity, and radioactive decay constants.

The site-scale saturated zone transport model is used as the basis for the saturated zone flow and transport abstraction model documented in *Saturated Zone Flow and Transport Model Abstraction* (SNL 2008b), which is used for generating a set of radionuclide breakthrough curves at the accessible environment for use in TSPA simulations. The outputs from the site-scale saturated zone transport model are transport times, flow paths, and radionuclide breakthrough curves at the accessible environment (SNL 2008a, Section 6.1).

2.3.9.3.3.2   Description of the Uncertainty Incorporated into the Model

Uncertainty in the model results comes from several sources, including uncertainty in the conceptual model and parameter uncertainty derived from the relevant source data (epistemic uncertainty) or to scaling of the measurements. Conceptual model uncertainty is evaluated by developing alternative conceptual models and evaluating the impact of the alternative model on transport predictions.

Epistemic parameter uncertainty is associated with lack of data, inexact measurement, or alternative interpretations of data. This form of uncertainty is explicitly addressed in the model through the use of appropriate probability distributions for uncertain model parameters. Uncertainty ranges for the various radionuclide transport parameters were propagated in the TSPA analyses (SNL 2008b, Sections 8.2.2, 8.2.2[a], and 8.2.2[b]).

There are also uncertainties in the radionuclide model simulation associated with scaling parameter values from the scale of measurements to the scale of the model. Data used to derive parameter values for the site-scale saturated zone transport model are from laboratory or field experiments conducted on spatial and temporal scales smaller than those in the site-scale saturated zone transport model. Most of the measurements were done on sample sizes of less than 1 m, with the exception of the C-Wells field tests, which were conducted on the scale of tens of meters, and the single-well tracer testing at the Alluvial Testing Complex, which integrated the alluvium at the scale of a few meters. These scales are several orders of magnitude smaller than the site scale. The measured parameter values reflect the rock properties on the scale of the measurement. Large grid spacing (250 m by 250 m) is used in the site-scale saturated zone transport model because computational limitations exist in the numerical model. This leads to averaging of properties in the model

calculations, thereby reducing the sensitivity of the output results to the stochastic variations in the parameter values. The distribution of the K_d values was upscaled from a 4-m to a 500-m scale in the absence of spatial correlations (SNL 2008a, Appendix C). The calculations were performed using the previous grid size of 500 m, not the current size of 250 m. However, the impact of the correlation length (a surrogate for the grid cell size) was shown to be small (SNL 2008a, Table C-12). Thus, the results obtained for the 500 m spacing are valid for the 250-m spacing used in the saturated zone transport model. These calculations demonstrated that the resulting 500-m-scale K_d distribution for uranium is actually narrower, with a standard deviation of 0.6 mL/g (and a mean of 6.6 mL/g), than the two 4-m-scale K_d distributions for devitrified and zeolitic rock types with standard deviations of 0.6 and 3.6 mL/g (SNL 2008a, Tables C-11 and C-4). However, geologic formations are inherently inhomogeneous and include fractures, faults, and other heterogeneities on many scales (SNL 2008a, Section 8.3). Extrapolation of data from a small scale to the site scale is difficult because different correlations exist at different scales. The scaling of parameter values and, in particular, permeability has been subject of extensive research (Renard and de Marsily 1997). The process often requires the quantification of the parameters describing the covariance or variogram (spatial variability) of the small scale spatially random parameter values. Then "change of support" adjustments (to account for the larger scale of the model parameter) are made to move from one scale to another (Renard and de Marsily 1997; Vanmarcke 1983). If the underlying probability distribution is symmetric, then upscaling usually does not change the mean value, but will typically reduce (and in some cases greatly reduce) the variability. A typical outcome of upscaling is the reduction of the uncertainty in the upscaled value when compared with the uncertainty in the underlying measurements. Thus, there is uncertainty in the parameter values used in the site-scale saturated zone transport model. There are usually not enough data to quantify a covariance or variogram; therefore, the process to assign uncertainty to model input parameters incorporates some degree of professional judgment to define the distribution of input parameter values (SNL 2008b, Sections 6.5.2, 6.5.2[a], and 8.2.2).

Several types of uncertainty have been evaluated with regard to modeling radionuclide transport in the saturated zone. Conceptual model uncertainty has been addressed either by choosing the more conservative alternative conceptual model or by using a range of uncertainty in parameter values that captures the effects of the alternative conceptual models. Epistemic uncertainty and uncertainty about the scaling of measured parameters have been addressed by using uncertainty distributions of model parameters (SNL 2008b, Section 6.5.2, 6.5.2[a], and 6.5.2[b]).

2.3.9.3.3.3   Consideration of Alternative Conceptual Models

The transport times, flow paths, and breakthrough curves predicted by the site-scale saturated zone transport model have varying degrees of uncertainty that were evaluated through comparison with alternative conceptual models (SNL 2008a, Section 6.6). Two classes of alternative conceptual models were examined. One class consists of the alternative conceptual models that were excluded from further consideration because they led to transport times greater than those calculated by the site-scale saturated zone transport model. The key components of each of these alternative conceptual models and the basis for the disposition are presented in *Site-Scale Saturated Zone Transport* (SNL 2008a, Table 6.6-1a). The other class consists of alternative conceptual models that are implicitly included in the saturated zone flow and transport abstraction model through the range of uncertainty in parameter values. The key components of each of these retained alternative conceptual models, the disposition of each alternative conceptual model, and the basis for the

disposition are presented in *Site-Scale Saturated Zone Transport* (SNL 2008a, Table 6.6-1b). The alternative conceptual models considered are discussed below (SNL 2008a, Section 6.6).

Uncertainty in the site-scale saturated zone transport model was evaluated with regard to testing at well NC-EWDP-24PB. The estimated volumetric groundwater flow rates from the testing in well 24PB are significantly higher within the high-flow zone than those simulated by the calibrated site-scale saturated zone flow model at the location of 24PB. The saturated zone flow and transport abstraction model was modified to evaluate the impact of including a high-permeability zone at the location of well 24PB on radionuclide transport simulations (SNL 2008b, Section 6.9[a]). The modifications to the saturated zone flow and transport abstraction model included reasonable assumptions about the potential orientation and dimensions of the zone in which high flow rates were inferred, and were adjusted to approximately match the estimated magnitude (6 L/min) of the flow rates at 24PB. The high-permeability zone was assumed to be oriented in a north–south direction, to have a length of 6,000 m, and to be centered on the model node closest to the location of well 24PB. The north–south orientation is consistent with the approximate strike of major faults in this area to the south of Yucca Mountain (SNL 2007a, Figure 6-3). A length of at least 6,000 m was required in the saturated zone flow and transport abstraction model to focus sufficient groundwater flow into the high-permeability zone to approximately match the inferred volumetric flow rate at well 24PB. The sensitivity of the radionuclide transport simulations to the presence of the assumed high-permeability zone was evaluated by comparing the transport simulation results using median values for uncertain parameters, both with and without the high-permeability zone. Simulated transport times in the high-permeability zone model were shorter because simulated flow paths are pulled to the west and into the higher flow of the high-permeability zone, and because transport distances through the alluvium were somewhat shorter along the altered flow paths. Simulated transport results indicate that the simulated breakthrough curve for the model with the high-permeability zone at well 24PB falls within the envelope of realizations from the saturated zone flow and transport abstraction model utilized in the TSPA model (SNL 2008b, Figure 6-18[a]). The existence of a high-flow zone at well 24PB, using reasonable assumptions about the orientation and dimensions of the zone, is captured within the range of uncertainty represented by the saturated zone flow and transport abstraction model, as shown in Figure 2.3.9-42.

2.3.9.3.3.3.1   Fluid Flow in Matrix Blocks

The conceptual model of saturated zone radionuclide transport in fractured volcanic rocks conservatively assumes that flow occurs in fractures only, with diffusion into the matrix (SNL 2008a, Section 6.3). This conceptual model includes no flow in the matrix. Including fluid flow in matrix blocks of the fractured volcanic rocks would result in transport times greater than those calculated by the site-scale saturated zone transport model. Even a small amount of fluid flow into the matrix blocks of the fractured volcanic rock would constitute an enhancement of matrix diffusion and essentially increase the flow porosity available to radionuclides in the groundwater and increase access to sorption in the matrix for sorbing radionuclides, thereby increasing the transport times through the saturated zone. Given the very low permeability of the matrix relative to the fractures in the volcanic units, the additional groundwater flow through the matrix would be negligible (SNL 2008a, Section 6.3). Accordingly, fluid flow in matrix blocks of the volcanic rock was conservatively not included in the site-scale saturated zone transport model (SNL 2008a, Section 6.6).

2.3.9.3.3.3.2   Irreversible Sorption onto Volcanic Rocks and Alluvium

Irreversible sorption reactions would result in the permanent removal of radionuclide mass from the water phase of the groundwater flow system. Thus, the process of irreversible sorption onto the volcanic rocks and alluvium would lead to an infinitely long transport time for some fraction of the radionuclides introduced into the saturated zone. Reversible sorption as implemented by the linear equilibrium sorption relationship used in the site-scale saturated zone transport model conservatively does not involve any permanent retention of radionuclides within the aquifer (SNL 2008a, Section 6.6).

2.3.9.3.3.3.3   Sorption Reactions that are not Instantaneous

The linear equilibrium sorption relationship used in the site-scale saturated zone transport model assumes instantaneous transfer between the dissolved phase and the sorbed phase (SNL 2008a, Section 6.3). Among the radionuclides identified in the waste inventory (Section 2.3.7.4.1.2), plutonium has the slowest reaction kinetics (SNL 2008a, Section 6.6, Table 6.6-1b). Therefore, in localized areas, flow rates may be fast enough for kinetic limitations to impact plutonium transport and potentially invalidate the instantaneous assumption of the linear equilibrium sorption relationship. However, calculations (SNL 2008a, Appendix D) show that, even with a conservative transport time through volcanic rocks in the saturated zone of a hypothetically assumed small value of 10 years, relative to the first neptunium breakthrough of about 100 years (SNL 2008b, Figure 6-11[a]), the value of the Damköhler number (Da) for reaction rates of plutonium is 175, exceeding the threshold value of 100, above which the local equilibrium approach is found applicable (Valocchi 1985, p. 813, Figure 2). Therefore, kinetic effects of sorption reactions do not need to be incorporated into the site-scale saturated zone transport model on this basis. Nevertheless, the possibility of the sorption reaction rate being slow relative to the flow rate is addressed by conservatively biasing the sorption-coefficient distributions downward for radionuclides that have slow sorption kinetics (SNL 2008a, Appendices A and C). Therefore, the distribution of sorption-coefficient values is conservatively biased to values smaller than the sorption measurements.

2.3.9.3.3.3.4   Water Table Rise

Wetter monsoon and glacial-transition conditions are forecast to occur at Yucca Mountain during the 10,000 years after repository closure (BSC 2004g, Section 7.1). After 10,000 years, a variety of climates, ranging from interglacial to full glacial, are expected to occur (Sharpe 2003, Section 6.5.3). These changes in the climate relative to present conditions would affect groundwater flow in the saturated zone by increasing the amount of recharge to the regional groundwater flow system. These regional and local increases in recharge will increase the groundwater flow through the saturated zone system and lead to a rise in the water table beneath Yucca Mountain. The rise in the water table would be accompanied by the release of radionuclides in the unsaturated zone between the present-day water table and the higher water table into the saturated zone (Section 2.3.8.5). The effect of increased flow on the saturated zone breakthrough curves was modeled using a scaling factor representing future climate states (SNL 2008b, Section 6.5). The scaling factor used for the period up to 10,000 years after repository closure was the ratio of average saturated zone groundwater flow rate under the future climatic conditions to the flow rate under present conditions, using the same flow path for radionuclide transport through the saturated zone

under the future climatic conditions. For the time period beyond 10,000 years, the scaling factor used was the ratio of saturated zone groundwater flux under the glacial-transition climate (existing at the end of the 10,000-year period after repository closure). The results of particle-tracking simulations incorporating the effect of water table rise on saturated zone flow paths indicate that the model with the higher water table elevations results in longer simulated transport times for both nonsorbing species (e.g., technetium, iodine, and carbon) and moderately sorbing species (e.g., neptunium), because transport would occur in lower permeability confining units (SNL 2008a, Appendix E; SNL 2007a, Section 6.6.4.2.2). In addition, flow path lengths through the alluvium are predicted to be longer for the water-table-rise model (SNL 2008a, Appendix E). Accordingly, the approach of increasing flow rates without raising the water table to simulate future climate scenarios is conservative. The effects of water table rise with climate change are thus implicitly and conservatively included in the saturated zone radionuclide transport simulations, consistent with FEP 1.3.07.02.0A, Water table rise affects SZ (Table 2.3.9-1).

2.3.9.3.3.3.5 Locally Varying Sorption Parameters

Sorption in the site-scale saturated zone transport model is modeled using linear transport equations with transport parameters treated as effective stochastic variables that are constant values in individual hydrostratigraphic units. This approach is consistent with the level of available data. The alternative conceptual model allows for varying the sorption parameters at a smaller scale than is currently in the site-scale saturated zone transport model. Transport parameters such as the K_d coefficients depend on the type and concentration of the species, rock mineralogy, and groundwater pH and Eh. In the saturated zone flow and transport abstraction model, broad distributions have been developed for effective K_ds. Sorption coefficients for the zeolitic tuff were based on samples that contain more than 50% zeolite. Surface areas used for surface complexation modeling analyses are based on silica surface areas, with the exception of the zeolitic tuff, where the surface area is larger by a factor of 10. There are indications that reducing conditions exist in the saturated zone to the east and south of the repository, which may be related to the presence of pyrite in the Tram Tuff. Eh conditions of less than approximately +150 mV could result in significantly enhanced sorption of important radionuclides, such as ^{99}Tc and ^{237}Np. Possible reducing conditions in the groundwater system have been included as part of the confidence building activities in support of the TSPA (Section 2.4) in the performance margin analysis. Given the current level of data availability, water pH data are being treated implicitly as spatially uniform along the transport path, as reflected in the uniform values of sorption coefficients applied to the volcanics and alluvium for each realization in the saturated zone flow and transport abstraction model (SNL 2008b, Table 6-8), and the assumption of oxidizing conditions results in a more conservative approach (SNL 2008a, Section 6.3, Appendices A and C).

To evaluate the effect of scale on the K_d distributions, calculations were performed to capture the effect of spatial variability of rock types and variability in water chemistries on effective K_d values. The effect of variability in water chemistry was captured in the input K_d uncertainty distributions that were used for effective K_d calculations. It was concluded that effective K_d distributions calculated for a single 250-m by 250-m gridblock were narrower than the input K_d distributions (SNL 2008a, Section C1.4). As a result, there is less variability in the sorption processes as represented in the saturated zone flow and transport abstraction model than would occur with smaller gridblocks.

2.3.9.3.3.3.6　Channeling in Alluvium

The effective continuum approach used in the saturated zone flow and transport modeling uses effective values averaged over the gridblock sizes on the order of 250 by 250 m for parameters of interest, such as porosity. The alternative conceptual model includes high permeability channels in the alluvium. These channels would reduce the area through which water flows and could be represented by smaller effective porosity. The effective porosity used in the TSPA (SNL 2008b, Section 6.5.2.3) is represented by an uncertainty distribution that includes values that are lower than the total porosity of the alluvium. Thus, the TSPA allows for the possibility that all flow is concentrated within a fraction of the alluvium. The impacts of this alternative conceptual model are included in the range of uncertainty in the effective porosity of alluvium for the TSPA.

2.3.9.3.3.3.7　Diffusion into Low-Permeability Zones in the Alluvium

The site-scale saturated zone transport model does not allow matrix diffusion to occur in the alluvium (SNL 2008a, Table 6.6-1a and Section 6.4.2.6.2). Diffusion into low-permeability zones in the alluvium was not observed to occur in the relatively small-scale, single-well tracer tests conducted at the Alluvial Testing Complex (SNL 2007b, Section 6.5.3, Appendix G, Figures G-18 to G-20). However, at the 22S testing complex, some matrix diffusion effects were observed. The alternative conceptual model would allow matrix diffusion to occur in the alluvium. On a larger scale, such diffusion would result in longer radionuclide transport times through the alluvium and is therefore excluded from further consideration on this basis (SNL 2008a, Table 6.6-1a).

2.3.9.3.3.3.8　Alternative Site-Scale Saturated Zone Flow Model

The alternative site-scale saturated zone flow model (SNL 2007a, Section 6.6) included the removal of the vertical anisotropy, the removal of the horizontal anisotropy, removal of the thermally altered zone (Figure 2.3.9-12), and an increase in the permeability in the z-direction for the Solitario Canyon Fault. In all cases, the alternative model results do not match either the known observations or the calibrated case. None of these four alternatives are passed to the saturated zone transport model for simulation, because the alternative case is already captured in the uncertainty of the model. The fifth alternative flow model case—the impact of water table rise—has already been addressed in Section 2.3.9.2.3.4.

2.3.9.3.3.3.9　Minimal Matrix Diffusion

An alternative conceptual model to the site-scale saturated zone transport model considers the possibility that diffusion of radionuclides into the pore space of the matrix in the fractured volcanic rocks is extremely limited due to highly channelized groundwater flow, fracture coatings, and other factors. A sensitivity analysis using the site-scale saturated zone transport model was conducted to show that the minimal matrix diffusion alternative conceptual model is included within the range of parameter uncertainties considered. Results from this sensitivity analysis indicate that the breakthrough curve using the 95th percentile value from the uncertainty distribution of flowing interval spacing is near the bounding case of no matrix diffusion. Similarly, low values of effective diffusion coefficient and flowing interval porosity yield breakthrough curves tending toward the no-matrix-diffusion case. This sensitivity analysis demonstrates that the minimal matrix diffusion

alternative conceptual model is captured within the range of uncertainty used in the model for the TSPA (SNL 2008b, Section 6.4, Figure 6-3).

2.3.9.3.3.4   Data/Parameter Uncertainty

The saturated zone transport simulations examined parameter uncertainty through sensitivity analyses. The bounds of the sensitivity analyses were determined from the parameter distributions presented in this section. Parameter uncertainties are quantified through uncertainty distributions that numerically represent knowledge about a particular parameter on a scale of the model domain. Uncertainty distributions incorporate uncertainties associated with field or laboratory data, use of parameters in the model, and theoretical considerations. Geologic uncertainty is incorporated with regard to the location of the contact between the volcanic rocks and alluvium in the saturated zone (SNL 2008b, Section 6.5.2.2[a]). In some cases, such parameters, as the radioactive decay constant are assigned constant values because radionuclide transport is relatively insensitive to the parameter, or the uncertainty is relatively small. Constant parameters are defined to vary from one hydrogeologic unit to another; yet, for a given hydrogeologic unit, the parameter remains constant for all realizations (SNL 2008b, Tables 6-8 and 6-9).

Parameters used in the site-scale saturated zone transport model related to the process of advection are groundwater specific discharge, flowing interval porosity, alluvium effective porosity, and horizontal anisotropy. Groundwater specific discharge and horizontal anisotropy are discussed in Section 2.3.9.2.3.6. Parameters used in the site-scale saturated zone transport model related to matrix diffusion are flowing interval spacing, effective diffusion coefficient, and matrix porosity. Parameters used in the models related to dispersion are longitudinal dispersivity, horizontal transverse dispersivity, and vertical transverse dispersivity. Parameters related to sorption are the sorption coefficients for various radioelements for tuff and alluvium, and include the bulk density of these media. Parameters used in the models related to colloid-facilitated transport include the colloid retardation factor, fast fraction of colloids, groundwater concentration of colloids, and sorption coefficients onto colloids. Table 2.3.9-4 summarizes the values and uncertainty distributions for all parameters used in the saturated zone transport simulations. The relevant physical rock properties of hydrogeologic units in the saturated zone, and corresponding uncertainties, are thus included in the saturated zone flow and transport abstraction model, consistent with FEP 2.2.03.02.0A, Rock properties of host rock and other units (Table 2.3.9-1).

Specific Discharge—The groundwater specific discharge multiplier is described in Section 2.3.9.2.3.6. Radionuclide transport times in the saturated zone are most sensitive to groundwater specific discharge (Section 2.4.2.3.3). This is because increasing the specific discharge not only increases the advective velocity, but it also reduces the time available for matrix diffusion to occur. In assessing the sensitivity of radionuclide breakthrough to the specific discharge, permeabilities of the various units were increased or decreased (along with the specific discharge) to maintain the same water levels in the site-scale saturated zone flow model.

Flowing Interval Porosity—Uncertainty in the flowing interval porosity is assessed using in situ testing at the C-Wells (Section 2.3.9.3.2.1), gas tracer tests in the unsaturated zone (BSC 2004h, Section 6.1.3.2), and core data on fracture spacing and aperture (DOE 1997). The resulting uncertainty distribution (Figure 2.3.9-22) is discretized in increments of one order of magnitude, with all of the C-Wells estimates in the range of 0.003 to 0.1 (SNL 2008b, Section 6.5.2.5); 75%

of the values fall between 0.0001 and 0.01, which reflects that flow porosity estimates from the C-Wells tests may have been biased toward higher values by flow heterogeneity in the fractured tuff and the simplifying assumption of radial flow in some test analyses (SNL 2007b, Section 6.3.5 and Appendix D). The lower end of the uncertainty range reflects some information on flowing interval flow porosities of fractured rock masses in the region near Yucca Mountain. The uncertainty in flowing interval spacing is included in the saturated zone flow and transport abstraction model presented in Section 2.3.9.3.4.

Alluvium Effective Porosity—Uncertainty in the effective porosity of the alluvium is assessed based on data from the region near Yucca Mountain and the results of saturated zone expert elicitation (SNL 2008b, Section 6.5.2.3). This assessment is augmented by the single-well pumping test and injection-withdrawal tracer test at the Alluvial Testing Complex (Section 2.3.9.3.2.1). Figure 2.3.9-43 illustrates possible distributions of alluvium effective flow porosities, and Figure 2.3.9-44 is the effective porosity distribution used in the saturated zone flow and transport abstraction model and the one-dimensional transport abstraction model (SNL 2008b, Section 6.5.2.3). The actual distribution (Figure 2.3.9-44) is truncated at an upper value of 0.3 in part because 0.29 was the largest value of total porosity estimated by borehole gravimetry in NC-EWDP-19D1 (SNL 2008b, Sections 6.5.2.3 and 6.5.2.14). This total porosity estimate was considered more reliable than the estimate of 0.40 obtained from hydraulic testing and barometric efficiency (SNL 2007b, Appendix F).

Alluvial Uncertainty Zone—Geological uncertainty in the location of the contact between fractured volcanic units and the alluvium in the saturated zone is included in the saturated zone flow and transport abstraction model and the saturated zone one-dimensional transport model with the alluvial uncertainty zone (Figure 2.3.9-5). This uncertainty is represented by a quadrilateral area in which the boundary between volcanic units and alluvium is randomly varied among realizations (SNL 2008b, Section 6.5.2.2[a]). The extent of the alluvial uncertainty zone is determined by lithologic data from wells NC-EWDP-10S and NC-EWDP-24P, the location of bedrock outcrops, and the distribution of units in the hydrogeologic framework model.

Flowing Interval Spacing—There is uncertainty regarding the flowing interval spacing due to the variability in apparent spacing and limitations in flow meter surveys. A stochastic analysis of the flow meter data was corrected for fracture dip and yielded (BSC 2004f) the uncertainty distribution for the flowing interval spacing used in the model simulations (Figure 2.3.9-21). The uncertainty distribution has a median value of about 20 m, with a lower bound of about 1.25 m and an upper bound of about 400 m (SNL 2008b, Section 6.5.2.4).

Effective Diffusion Coefficients—The variability in the effective diffusion coefficient in saturated media is caused by (1) the variability in the individual constituent's size (atom, ion, or molecule) and charge; (2) fluid temperature; and (3) unique properties of porous media's lithology at a microscopic scale. The contribution of these uncertainties and variabilities in the value of the effective diffusion coefficient is evaluated to determine the uncertainty distribution for this parameter (SNL 2008b, Section 6.5.2.6). Laboratory data (Section 2.3.9.3.2.1) and data from external sources were used in the development of the uncertainty distribution for the effective diffusion coefficient. The resulting uncertainty distribution is a discrete distribution with a median value of about 5×10^{-11} m^2/s (SNL 2008b, Section 6.5.2.6).

Volcanic Rock Matrix Porosity—Matrix porosity is treated as a constant parameter for fractured volcanic rocks that are along the flow paths from beneath the repository to the accessible environment. "Constant" in this sense means that matrix porosity will vary from one unit to another, but for a particular unit, the porosity is constant across all realizations. The matrix porosity also remains constant for each hydrogeologic unit. The values of matrix porosity vary from 0.15 to 0.25 among the volcanic rocks along the flow path (SNL 2008b, Section 6.5.2.18).

Dispersivity—Uncertainty in longitudinal, horizontal transverse, and vertical transverse dispersivity parameters was adapted from the saturated zone expert elicitation. The expert elicitation panel provided statistical distributions and parameter bounding values for longitudinal horizontal transverse and vertical transverse dispersivity (CRWMS M&O 1998, pp. 3-21, LG-12, and LG-14) and mathematical relationships between longitudinal dispersivity and horizontal transverse and vertical transverse dispersivity. The geometric mean of the lognormal uncertainty distribution used in the transport simulations for longitudinal dispersivity is 100 m (SNL 2008b, Section 6.5.2.9). The values of dispersivity that are input to the three-dimensional saturated zone flow and transport abstraction model are scaled down by one order of magnitude relative to the values sampled from the uncertainty distribution given in Table 2.3.9-4 to compensate for the dispersion imparted by the spatial distribution of hydrogeologic units of contrasting permeability (SNL 2008b, Section 6.5.2.9). For the saturated zone one-dimensional transport model, the uncertainty distribution for longitudinal dispersivity is taken from Table 2.3.9-4 but is truncated at two standard deviations above the geometric mean (SNL 2008b, Section 6.5.2.1[b]).

Sorption Coefficients in Volcanic Rocks and Alluvium—The conceptual model of linear equilibrium sorption for many radionuclides has been verified at the laboratory scale and the site-scale (Section 2.3.9.3.2.2). There are differences in the sorptive characteristics of the volcanic rock matrix and the alluvium. In addition, a considerable amount of radionuclide-specific sorption data exists from laboratory experiments using samples obtained from the Yucca Mountain site. These data are combined with information on the variability and uncertainty in hydrochemical and mineralogical composition to assess the uncertainty in sorption coefficients.

A detailed discussion of the uncertainty distributions for sorption coefficients used in the site-scale saturated zone transport model, the saturated zone flow and transport abstraction model, and the one-dimensional saturated zone transport model is provided in Section 2.3.9.3.2.2 (SNL 2008a, Appendix A, Table A-4). Table 2.3.9-4 summarizes the values and uncertainty distributions for sorption coefficients used in the site-scale saturated zone transport simulations. The probability distributions include expected variations in water chemistry, radionuclide concentrations, sorption behavior of the individual radionuclides, and rock surface properties within the major volcanic rock types and alluvium.

Bulk Density in Volcanic Rocks and Alluvium—The bulk density of the volcanic rock matrix and the alluvium is used to calculate retardation associated with sorption of radionuclides in these media. Bulk density is treated as a constant parameter for hydrogeologic units other than alluvium. "Constant" in this sense means that bulk density varies from one unit to another; however, for a particular unit, the bulk density remains constant for all realizations. The bulk density also remains spatially constant for each unit. Values of average bulk density vary from about 1.8 to 2.2 g/cm^3 among the volcanic rocks (SNL 2008b, Section 6.5.2.19). Borehole gravimeter data are

used as the basis for the uncertainty in bulk density in the alluvium, resulting in a normal distribution of uncertainty with a mean value of about 1.9 g/cm^3 (SNL 2008b, Section 6.5.2.7).

Colloid Retardation Factor in Volcanic Rocks and Alluvium—Assessments of the uncertainty in the colloid retardation factor parameter in the fractured volcanic rocks and the alluvium have been conducted (BSC 2004e, Sections 6.4, 6.5, and 6.6). The laboratory and field transport data used to derive the probability distributions were obtained at scales smaller than the scales of interest for TSPA modeling. Also, the retardation factors derived from many of the transport tests were based on fitting the low colloid concentrations in the tails of breakthrough curves. These tails were sometimes only slightly above detection or quantification limits, resulting in uncertainty in retardation factors.

The uncertainties associated with the colloid retardation factor parameter are addressed by assigning lower bounds for colloid retardation factors to cumulative distributions in the volcanic rocks and alluvium so that significant retardation of colloids always occurs for any portion of the colloid mass that is not part of the unretarded fraction (BSC 2004e, Section 6.4.3). This approach is realistic because, as retardation factors approach one, no retardation occurs, and the possibility of no retardation of colloids is incorporated through the fraction of colloids without retardation as discussed in Section 2.3.9.3.2.3.5.

Two sets of laboratory alluvium colloid transport experiments yielded different results for both carboxylate-modified latex microsphere and inorganic colloid transport in alluvium (BSC 2004e, Section 6.8.2.2). These disparate results, though possibly explained by the presence of air bubbles in one set of experiments, impart uncertainty to colloid transport in alluvium. This uncertainty is addressed by including both sets of experimental results in the overall data set used to develop cumulative distributions for colloid-filtration-rate constants and retardation factors for irreversible colloids in alluvium, resulting in the distributions shown in Figure 2.3.9-41. The resulting uncertainty distributions vary over about two orders of magnitude for colloid retardation in the volcanic units, and over almost three orders of magnitude for retardation factors in the alluvium (SNL 2008b, Section 6.5.2.11).

Concentration of Colloids—Uncertainty exists in the concentration of colloids in groundwater of the saturated zone. The uncertainty distribution in the concentration of colloids spans more than five orders of magnitude (SNL 2007f, Table 6-13). The concentration of colloids is treated as an uncertain parameter in the saturated zone flow and transport abstraction model to conservatively account for the large uncertainty (Table 2.3.9-4). The uncertainty distribution was developed (SNL 2007f, Table 6-13) based on data from 79 groundwater samples collected in the vicinity of Yucca Mountain and 11 samples collected from the Idaho National Laboratory. Inclusion of the Idaho National Laboratory groundwater colloid data was deemed appropriate for inclusion in the data analysis among the groundwater data from the Yucca Mountain area because the climate in Idaho Falls is similarly arid and the field sampling and analytical techniques used at both locations were similar (SNL 2008e, Section 4.1.2).

Sorption Coefficients onto Colloids—The sorptive characteristics of colloids for different radionuclides play an important role in the colloid-facilitated transport of reversibly attached radionuclides. As listed in Table 2.3.9-4, uncertainty distributions for sorption coefficients onto colloids for three classes of radioelements—(1) plutonium; (2) americium; and (3) cesium—

encompass wide ranges based on variability of experimental measurements, which are summarized in the derived distributions of sorption coefficients (SNL 2007f, Table 6-9; SNL 2008b, Section 6.5.2.12 and 6.5.2.4[a]). These wide ranges of values are retained in the modeling to ensure the uncertainty in sorptive characteristics of colloids is addressed.

2.3.9.3.4 Model Abstraction and Confidence Building
[NUREG-1804, Section 2.2.1.3.9.3: AC 1(1) to (4), AC 3(1), (2), (4), AC 5; Section 2.2.1.3.12.3: AC 1(1) to (4), AC 3(1) to (4), AC 5]

The results of the site-scale saturated zone transport model are abstracted through the saturated zone flow and transport abstraction model and the saturated zone one-dimensional transport model. The main output from the saturated zone flow and transport abstraction model to the TSPA is the radionuclide breakthrough curves at the accessible environment. The saturated zone one-dimensional transport model is incorporated directly into the TSPA model. The general approach to modeling radionuclide migration and the assessment of uncertainty in the saturated zone is described by Arnold et al. (2003) and *Saturated Zone Flow and Transport Model Abstraction* (SNL 2008b). The objective of abstraction is to quantify the arrival of radionuclides at the accessible environment, located as specified in 10 CFR 63.302, for use in the TSPA model (SNL 2008b, Section 6.1). The abstraction of radionuclide transport in the saturated zone is linked to the biosphere component of the TSPA through the concentrations of radionuclides in groundwater. These concentrations are calculated by dividing the radionuclide mass reaching the boundary of the accessible environment per year by the representative volume of groundwater and annual water demand of 3,000 acre-ft (SNL 2008b, Section 6.3.3)

The convolution integral method is used to determine the radionuclide mass flux at the accessible environment as a function of the transient radionuclide mass flux at the water table beneath the repository. It combines information about the response of the saturated zone to the input of one unit per year of radionuclide mass, as simulated by the saturated zone flow and transport abstraction model, with the radionuclide source history from the unsaturated zone to calculate transient system behavior. The most important assumptions of the convolution method are linear system behavior and steady-state flow conditions in the saturated zone. The output is the time-varying radionuclide mass release at the accessible environment (SNL 2008b, Section 6.5).

Because the saturated zone flow and transport abstraction model is not capable of simulating ingrowth by radioactive decay, the saturated zone one-dimensional transport model is used to generate breakthrough curves for radionuclide daughter products by simulating radioactive decay and ingrowth. The saturated zone one-dimensional transport model provides simulation results for several radionuclide chains that are not simulated in the three-dimensional saturated zone flow and transport abstraction model. The objective of the saturated zone one-dimensional transport model is to provide a simplified yet accurate representation of transport for the radionuclide decay chain daughter products (Section 2.3.9.3.4.2.1) within the TSPA (SNL 2008b, Section 6).

Confidence in the site-scale saturated zone transport model output is developed through comparison of observations and direct and indirect transport process indicators to model predictions (SNL 2008a, Section 7). The saturated zone flow and transport abstraction model and the saturated zone one-dimensional transport model are validated by comparison to the underlying process model (i.e., the site-scale saturated zone transport model) (SNL 2008b, Sections 7[a] and 7[b]).

2.3.9.3.4.1   The Saturated Zone Transport Abstraction Model

2.3.9.3.4.1.1   Methods and Results

The site-scale saturated zone flow model (SNL 2007a) and the site-scale saturated zone transport model (SNL 2008a) form the basis for the saturated zone flow and transport abstraction model. The site-scale saturated zone flow model includes the implementation of the hydrogeologic framework model, the numerical grid, and the boundary conditions for the steady-state groundwater flow model and provides the groundwater flow field required for the site-scale saturated zone transport model and site-scale flow and transport abstraction model simulations. The site-scale saturated zone transport model simulates the transport of radionuclides using a particle tracking technique. The saturated zone flow and transport abstraction model begins with the site-scale saturated zone transport model and adds the capability to perform probabilistic uncertainty analysis using multiple Monte Carlo realizations to simulate unit radionuclide breakthrough curves. The resulting radionuclide breakthrough curves are used within the TSPA to generate radionuclide mass flux in groundwater at the accessible environment (Figure 2.3.9-2), shown as the "Saturated Zone Transport" model component.

The saturated zone flow and transport abstraction model provides of the results of radionuclide transport simulations using stochastically sampled vectors of the uncertain parameters and the methodology of coupling these results to the radionuclide mass output from the unsaturated zone. The radionuclide transport simulations were conducted prior to the TSPA simulations, and the results were stored in a library of radionuclide breakthrough curves for later access by the TSPA model (SNL 2008b).

The site-scale saturated zone flow model, the site-scale saturated zone transport model, and the saturated zone flow and transport abstraction model share a common model domain, hydrogeologic framework, numerical grid, and boundary conditions (SNL 2008b, Section 6.5). Table 2.3.9-4 lists the parameters used in the saturated flow and transport abstraction model and the saturated zone one-dimensional transport model to simulate radionuclide transport in the saturated zone. Uncertainty distributions for two parameters, specific discharge and dispersivity, used information from expert elicitation in accordance with NUREG-1563 (Kotra et al. 1996). The uncertainty distribution for specific discharge also incorporates estimates from tracer testing at the Alluvial Testing Complex (SNL 2007b, Section 6.5).

Radionuclides included in the saturated zone flow and transport abstraction model are separated into 12 groupings, based on the reactivity of the radionuclide with the volcanic rock and alluvium, and on the mode of transport (Table 2.3.9-16) (SNL 2008b, Section 6.5.3[a]). Combining radionuclides into these groups was done for computational efficiency. The simulated breakthrough curves for one group represents all radionuclides in that group. The 12 groups of radionuclides are divided among three modes of radionuclide transport: (1) solute transport; (2) colloid-facilitated transport of radionuclides reversibly attached onto colloids; and (3) colloid-facilitated transport of radionuclides irreversibly attached onto colloids. For example, the nonsorbing isotopes of carbon, technetium, iodine, and chlorine are grouped together because their migration is identical. Similarly, the isotopes of americium, thorium, and protactinium reversibly attached onto colloids are grouped together because of their similar sorption characteristics. The isotopes of plutonium and americium may be transported reversibly and irreversibly attached onto colloids (SNL 2008b,

Section 6.5.3[a]). Radioactive decay is applied separately for each radionuclide within the groups as part of the convolution integral method described below.

Transport of the 12 groups of radionuclides was simulated in the saturated zone flow and transport abstraction model using a particle tracking method. This method, as implemented in the FEHM software code, simulates advection along groundwater streamlines, random-walk dispersion, retardation due to sorption, and matrix diffusion. Each simulation uses 500 particles, which results in a continuous, generally smooth cumulative mass breakthrough curve at the boundary of the accessible environment. The time-step size that determines output intervals varies from 10 to 1,000 years, depending on the radionuclide. Internally, the simulation uses local flow conditions to determine time steps for dispersion and matrix diffusion calculations. This internal time step is controlled in such a way that the particles take approximately 20 internal time steps to traverse each cell in the site-scale saturated zone transport model and saturated zone flow and transport abstraction model (SNL 2008b, Section 6.5).

Variations in radionuclide transport pathways and transport times in the saturated zone from various locations beneath the repository were considered by defining four radionuclide source regions at the water table (SNL 2008b, Figure 6-27). For each TSPA realization, a radionuclide point source was defined within each of the four regions to simulate radionuclide transport in the saturated zone flow and transport abstraction model. A point source of radionuclides in the saturated zone is appropriate for representing a single waste package, or for highly focused groundwater flow along a fault or single fracture in the unsaturated zone. While a more diffuse source of radionuclides at the water table may be more representative for later times when multiple waste package releases might occur, use of four point sources in the saturated zone is an approach that tends to minimize the variability in transport distances, and transport times from the individual source in the saturated zone to the accessible environment, because processes that would disperse the radionuclides at the source have not been included (SNL 2008b, Section 6.3.3). Minimizing the variability in transport times (effective dispersion) in the breakthrough curves tends to maximize the peak radionuclide mass release rate from the saturated zone resulting from potential pulses of mass release from the unsaturated zone.

Unit radionuclide breakthrough curves from the saturated zone flow and transport abstraction model for 200 Monte Carlo realizations of flow and transport were generated in the following manner. A steady-state groundwater flow field was produced for each of the 200 realizations prior to transport simulations. Variations in the groundwater-specific discharge were included by scaling the values of recharge and all values of permeability in the site-scale saturated zone flow model. Variations in horizontal anisotropy in permeability were included by scaling the values of north–south and east–west permeability within the zone of volcanic rocks influenced by anisotropy (SNL 2008b, Section 6.5.2.10). Radionuclide transport simulations with the saturated zone flow and transport abstraction model were performed using the estimated groundwater flow rates for glacial-transition climatic conditions. A total of 9,600 individual simulations (200 realizations × 12 radionuclide groups × 4 source regions) of saturated zone transport were conducted (SNL 2008b, Sections 6.5.2.13 and 6.5.3[a] and Table 6-9[a]).

In the TSPA, the convolution integral method used in the saturated zone transport abstraction model provides an approximation of the transient radionuclide mass flux at a specific location downgradient in the saturated zone in response to the transient radionuclide mass flux from the

unsaturated zone. The fundamental concepts of the convolution integral method, as applied to solute transport in groundwater, are presented by Jury et al. (1986), where the method is called the transfer function model. This coupling method makes full use of detailed saturated zone flow and transport simulations for a given realization of the system, without requiring complete numerical simulation of the saturated zone for the duration of each TSPA realization. The two input functions to the convolution integral method are (1) a unit radionuclide mass breakthrough curve in response to a step-function mass flux source as simulated by the saturated zone flow and transport abstraction model; and (2) the radionuclide mass flux history for simulated transport in the unsaturated zone. The output function is the radionuclide mass flux history downgradient in the saturated zone (SNL 2008b, Section 6.3.3). In the TSPA model, the convolution integral method is applied independently to each of the four point sources from the unsaturated zone, and the total radionuclide mass release from the saturated zone is calculated as the sum from the four sources (SNL 2008d, Sections 6.1.4.10 and 6.3.10).

Radioactive decay is also applied to radionuclide mass flux calculated with the convolution integral computer code SZ_Convolute in the TSPA analyses. The convolution integral method consists of numerical integration that accounts for the contributions to the outlet radionuclide mass flux from a series of time intervals. Because the transport time for each contribution to radionuclide mass flux is known, the loss of radionuclide mass (and consequent decrease in mass flux) during transport is calculated by first-order decay for that time interval, based on the half life for each radionuclide.

The effects of climate change on radionuclide transport in the saturated zone were incorporated into the convolution integral analysis in the TSPA by assuming instantaneous change from one steady-state flow condition to another steady-state condition in the saturated zone through the use of a scaling factor for groundwater specific discharge that represents the future climate state (Section 2.3.9.3.3.3.4). Three climate states are defined in the TSPA for the postclosure period. For the TSPA analyses, present-day climatic conditions are modeled from the time of repository closure to 600 years in the future, monsoonal conditions are imposed from 600 to 2,000 years in the future, and glacial-transition climatic conditions occur from 2,000 to 10,000 years following repository closure (SNL 2008d, Section ES6.1). The monsoonal climatic state is wetter than present-day conditions, and the glacial-transition state is both wetter and cooler than present-day conditions. Note that the glacial-transition climate state is approximately equivalent to the long-term average climate state. Changes in climate state affect the elevation of the water table and the magnitude of groundwater flow through the saturated zone system (D'Agnese et al. 1999, pp. 27 to 36). For monsoonal and glacial-transition climatic conditions, radionuclide mass is passed to the saturated zone from the unsaturated zone assuming a 120-m rise in the water table, relative to present conditions. The higher water table associated with climate change is not explicitly simulated in the saturated zone flow and transport abstraction model. However, sensitivity analyses indicate that the simplified approach of scaling the groundwater flow is conservative, and underestimates the radionuclide transport times in comparison to explicitly including the rise in the water table (Section 2.3.9.3.3.3.4) (SNL 2008a, Appendix E). The effect of changes in groundwater flow is incorporated into the convolution method by using a scaling factor that is the ratio of the average saturated zone groundwater flow under the future climate conditions to the flow under present conditions. This scaling factor is used to adjust the timing of radionuclide mass breakthrough curves proportionally to the change in saturated zone specific discharge. The scaling factor for radionuclide transport in the saturated zone for the monsoon climate is 1.9, and the scaling factor for glacial-transition climate is 3.9. For the post-10,000-year case, the same scaling factor for the

glacial-transition climate of 3.9 is applied throughout the time period (SNL 2008b, Table 6-4[a] and Section 6.5.3[a]). This is based on the analysis of the glacial-transition weighted net infiltration and the results of simulations using the Death Valley regional groundwater flow system model (D'Agnese et al. 1999) that showed the same multiplier could be applied for glacial-transition before 10,000 years and for the post-10,000-year case.

The uncertainties associated with the data and all the models presented in this section result in a range of projected advective–dispersive transport times for radionuclides. The saturated zone transport abstraction model produces a range of possible breakthrough curves for the glacial transition climate conditions based on uncertainty in the transport times. Figure 2.3.9-16 shows nonsorbing radionuclides (e.g., ^{14}C, ^{99}Tc, ^{36}Cl, and ^{129}I) with median transport times ranging from about 10 to 10,000 years, although a significant fraction of radionuclide mass has much longer transport times in many realizations due to the effects of matrix diffusion in fractured volcanic units. For moderately sorbing radionuclides, such as ^{237}Np (with K_ds in the range of approximately 1 to 10 mL/g), the median transport times range from about 100 to more than 100,000 years (Figure 2.3.9-45). For highly sorbing radionuclides reversibly attached to colloids (e.g., ^{239}Pu), median transport times generally exceed 10,000 years (Figure 2.3.9-46). For radionuclides irreversibly attached onto colloids, median transport times range from 100 to 100,000 years (Figure 2.3.9-47). These ranges in effective mass breakthrough times reflect the combined effects of the uncertainties associated with the saturated zone flow and transport abstraction model (SNL 2008b, Sections 6.7.1 and 8.2.2). Each figure shows the relative mass arriving at the accessible environment as a function of time, and a histogram of median transport times for a given category of radionuclides. Note that the breakthrough curves and transport times shown in these figures are for a continuous, steady source at the water table below the repository (source region 1) initiated at time equal to zero. The breakthrough curves shown in these figures are simulated for glacial-transition climatic conditions, and do not include the effects of radioactive decay, because the process of radioactive decay was implemented in the convolution integral method (SNL 2008b, Section 6.6).

Variations in the radionuclide transport time among the realizations reflect the aggregate uncertainty in the underlying input parameters to the saturated zone flow and transport abstraction model. Although formal sensitivity analyses have not been applied to these results, sensitivity analyses have been performed on previous saturated zone transport modeling results (Arnold et al. 2003). Those analyses indicate that uncertainties in groundwater specific discharge, sorption coefficients, and retardation of colloids are major factors in the simulated uncertainty in radionuclide transport times. Parameters related to matrix diffusion and geologic uncertainty have significant but secondary importance with regard to the uncertainty in radionuclide transport times. Figure 2.3.9-48 shows a comparison of the no-sorption base case with two cases: (1) matrix sorption allows a small amount of sorption (matrix sorption coefficient of 1.3 mL/g) in the matrix of the volcanic tuffs; and (2) sorption in both the tuff matrix and the alluvium. These results show the saturated zone provides a substantial transport time delay for radionuclides with even limited sorptive capabilities (SNL 2008a, Section 6.8.2). In addition, the results of the sensitivity analysis shown in Figure 2.3.9-48 illustrate some important characteristics of radionuclide transport in the saturated zone. Even without sorption, a significant fraction of radionuclide mass exhibits simulated transport times that are much longer than the median transport time for the base case, as can be seen in the upper tail of the breakthrough curve. For example, the slowest 15% of mass has transport times greater than 10,000 years. This very long "tail" of the breakthrough curve is characteristic of

transport in fractured media with matrix diffusion (Arnold et al. 2003, Section 5), and reflects the slowness of the diffusive process over length scales of 10s of meters into the rock matrix, relative to the rapidity of advective transport in the fractures. Even a modest degree of sorption in the matrix enhances the matrix diffusion process by providing greater effective storage capacity of the radionuclide on sorption sites in the matrix near the fracture (SNL 2008a, Section 6.8.3), as illustrated by the red curve in Figure 2.3.9-48.

2.3.9.3.4.1.2   Abstraction Model and Process Model Comparison

Recognizing that the site-scale saturated zone transport model was used as the basis for the saturated zone flow and transport abstraction model, which was in turn used to perform probabilistic calculations in which parameter uncertainties were evaluated, the intent of validation was to confirm the appropriateness of the radionuclide parameters and processes included in the site-scale saturated zone transport model. Confidence in the results of the model was built by a series of analyses that included comparisons to analogue sites, model–data comparisons, comparison with data published in peer-reviewed scientific literature, and comparison to an independent site-scale groundwater flow model (Winterle et al. 2003, pp. 152 to 153) for the Yucca Mountain saturated zone (SNL 2008a, Section 7).

The data used to build confidence for the relevant transport parameters (e.g., sorption coefficient), submodel processes (e.g., advection, sorption), and site-scale saturated zone flow and transport model processes (e.g., flow pathways, transport times) were based on laboratory testing, field tests, natural analogue sites, and expert elicitation. The site-scale saturated zone transport model was validated by postdevelopment comparison of model transport times with those inferred from ^{14}C data and by qualitative comparison of flow paths simulated by the site-scale saturated zone flow model with those inferred from the hydrochemistry data (SNL 2008a, Section 7).

Validation of the saturated zone flow and transport abstraction model is accomplished through comparison with the underlying process model: the site-scale saturated zone transport model. In making this comparison, three cases for radionuclide transport are defined for implementation: median case, fast case, and slow case. These three cases approximately span the range of uncertainty in results of the saturated zone flow and transport abstraction model with regard to radionuclide transport in the saturated zone, using parameter values from the uncertainty distributions at the 10th, 50th, and 90th percentiles (SNL 2008b, Section 7.1). Comparisons were made for a nonsorbing radionuclide (e.g., ^{14}C, ^{99}Tc, and ^{129}I) and for a sorbing radionuclide (e.g., ^{237}Np) (SNL 2008b, Section 7.3.1[a]).

Comparison of the simulated radionuclide mass breakthrough curves from the saturated zone flow and transport abstraction model and the site-scale saturated zone transport model indicates agreement to within a few percent of relative radionuclide mass (SNL 2008b, Figures 7-1[a] and 7-2[a]). Close agreement between the models was observed for the median, slow, and fast cases for nonsorbing and sorbing radionuclides. In addition, the mass balance of a pulse source of nonsorbing radionuclide (released at 1 g/yr for the first 1,000 years, resulting in a total mass input of 1,000 g) (SNL 2008b, Section 7.3.1[a]) was checked, and between 99.8% and 101.6% of the input mass was output from the model among the three test cases. The small percentage (less than 2%) discrepancy between the input mass and the output mass constitutes an acceptably small error relative to the model validation acceptance criterion (SNL 2008b, Section 7.4.1[a]).

Validation testing of the saturated zone flow and transport abstraction model, including the convolution integral method, indicates good agreement with the site-scale saturated zone transport model (SNL 2008b, Section 8.1[a]). Validation criteria regarding the qualitative comparison of simulated breakthrough curves and the quantitative evaluation of radionuclide mass balance are met. Results of the validation testing indicate that the saturated zone flow and transport abstraction model is valid for the approximate range of uncertainty incorporated into the abstraction model through parameter uncertainty distributions. Results also indicate that the saturated zone flow and transport abstraction model is valid for both nonsorbing and sorbing radionuclide species (SNL 2008b, Section 7.4[a]).

2.3.9.3.4.1.3   Comparison of Site-Scale Saturated Zone Transport Model Results to Empirical Observation

As part of the validation of the site-scale saturated zone transport model, numerical results from the model have been compared to data on ^{14}C concentrations in groundwater to provide confidence that, when combining the components of the transport models with appropriate geologic-, hydrologic-, and boundary-condition information, the overall model is consistent with available data. Specifically, the radionuclide transit times computed from the site-scale saturated zone transport model are compared to ^{14}C data at the site scale, and the flow pathways from the site-scale saturated zone transport model are compared to flow paths determined independently from hydrochemistry data (SNL 2008a, Section 7). The comparison of flow paths was presented in Section 2.3.9.2.4.2 as part of the confidence building of the site-scale saturated zone flow model. The comparison of ^{14}C transit times is presented below.

Evaluation of ^{14}C Transport Times in the Yucca Mountain Region—Although the advective transport properties of specific discharge and effective porosity are acceptably constrained by in situ observations from boreholes, these observations are limited by the temporal and spatial scales over which the tests were conducted. The scales of the C-Wells and Alluvial Testing Complex are tens of meters and days to months; however, transport processes relevant to repository performance occur over scales of kilometers and thousands of years (SNL 2008a, Section 7.2; SNL 2007a, Appendices A and B).

One of the methods used to investigate transport processes over the spatial and temporal scale of interest to repository performance is through investigation of variations in concentrations of naturally occurring radioisotopes, such as ^{14}C. The following discussion summarizes observations of carbon isotopes used in estimating groundwater transport times in the saturated zone (SNL 2007a, Appendices A and B).

The radioactive decay of ^{14}C, with a half-life of 5,730 years, forms the basis for radiocarbon dating. The ^{14}C age of a sample is typically expressed in percent of modern carbon (pmc). In this discussion, the amount of ^{14}C in the water is described by activity that measures the number of decompositions of ^{14}C and is related to the mass of ^{14}C in the water. Thus, activity is also a measure of concentration. A ^{14}C activity of 100 pmc is the ^{14}C activity of the atmosphere in the year 1890, before natural ^{14}C in the atmosphere was diluted by large amounts of ^{14}C-free carbon dioxide gas from the burning of fossil fuels (SNL 2007a, Appendices A and B).

Theoretically, the activity of ^{14}C in a groundwater sample reflects the time when the water was recharged. Unfortunately, precipitation generally has low carbon concentrations and a high affinity for dissolution of solid phases in the soil zone, unsaturated zone, and saturated zone. In particular, in the transition from precipitation compositions to groundwater compositions, the concentration of combined bicarbonate and carbonate in the water commonly increases by orders of magnitude (Langmuir 1997, Table 8-7; Meijer 2002). Because bicarbonate is the principal species that contains ^{14}C in most groundwater, the source of this additional bicarbonate can affect the apparent age calculated from the ^{14}C dating. If the source of carbon is primarily decaying plant material in an active soil zone, the calculated age for the water sample should be close to the true age. By contrast, if the source of bicarbonate is the dissolution of old (i.e., older than 10,000 years) calcite with low ^{14}C activity or the oxidation of old organic material, then the calculated age for the sample will be overestimated (i.e., older than its actual age). Table 2.3.9-17 provides selected examples of corrected and uncorrected ^{14}C ages for water samples collected from 7 wells in the Yucca Mountain region. Discussion of ^{14}C age corrections is provided in the saturated zone flow site-scale model (SNL 2007a, Section A.6.3.6.6.2).

A useful measure of the source of carbon in a water sample is the $\delta^{13}C$ value of the sample, because this value is different for organic materials and calcites (SNL 2007a, Appendices A and B). Carbon isotopes associated with organic materials are referred to as organic carbon, and carbon isotopes associated with calcite and other minerals are referred to as inorganic carbon. The $\delta^{13}C$ values of carbon species typical of the soil waters in arid environments range from $-25‰$ to $-13‰$. At Yucca Mountain, pedogenic carbonate minerals have $\delta^{13}C$ values generally between $-8‰$ and $-4‰$, although early formed calcites are also present that have $\delta^{13}C$ values greater than 0‰. Paleozoic carbonate rocks typically have $\delta^{13}C$ values close to 0‰ (SNL 2007a, Section A6.3.1.2.2).

Under ideal circumstances, the decrease in groundwater ^{14}C activities along a flow path can be used to estimate transport times. The calculation is straightforward when recharge occurs at a single location and the resulting groundwater does not receive additional recharge or mix with other groundwater downgradient from that location. In the Yucca Mountain area, the calculation of transport times of ^{14}C is complicated by the possible presence of multiple distributed recharge areas. If relatively young recharge were added along a flow path, the ^{14}C activity of the mixed groundwater would be higher, and the calculated transport times would be shorter than they would be for the same premixed groundwater without the downgradient recharge. Unfortunately, the chemical and isotopic characteristics of recharge from various areas at Yucca Mountain may not be sufficiently distinct to identify separate sources of local recharge in the groundwater. Conversely, if groundwater from the regional Paleozoic carbonate aquifer were to mix downgradient with Yucca Mountain recharge, the mixture would have a lower ^{14}C activity than the Yucca Mountain recharge component because of the high carbon alkalinity and low ^{14}C activity of the regional Paleozoic carbonate aquifer groundwater. However, the presence of groundwater from the regional Paleozoic carbonate aquifer in the mixture would be recognized because of the distinct chemical and isotopic composition of that groundwater compared with the recharge water, and the effect on the ^{14}C activity of the groundwater mixture could be calculated (SNL 2007a, Appendices A and B).

^{14}C transport times are estimated along various flow path segments using the ^{14}C activities of the groundwater. Measured ^{14}C activities at the upgradient borehole defining the segment were adjusted to account for decreases in the ^{14}C activity resulting from water–rock interactions between boreholes (identified by PHREEQC mixing and chemical reaction models) (SNL 2007a,

Sections A6.3.8 and A7.3.5). This adjustment to the initial ^{14}C activity is necessary to distinguish between the decrease in ^{14}C activity caused by water–rock interaction and the decrease in ^{14}C activity due to transport time between boreholes. After determining the transport time between boreholes, linear groundwater velocities were determined by dividing the distance between the boreholes by the transport time. Groundwater velocities were calculated for several possible flow paths south of the repository (SNL 2007a, Appendix A).

The first comparison of transport times was performed along a flow path connecting boreholes UE-25 WT#3 and NC-EWDP-19. PHREEQC inverse models (SNL 2007a, Section A6.3.8) indicate that groundwater sampled from various zones in borehole NC-EWDP-19D could have evolved from groundwater near borehole UE-25 WT#3 (Figures 2.3.9-4 and 2.3.9-18). The approximate distance between the two wells is 15 km (SNL 2007a, Section A6.3.9.1). The ^{14}C transport times lie in the range of 0 (or negative values) years to 3,110 years over the sampled depths (SNL 2007a, Section A6.3.9.1, Table A6-11). The data are clustered around two ranges corresponding to different sampling intervals: one in the interval of 188 to 535 years and the other in the interval of 1,601 to 3,110 years. For the interwell distance of 15 km, these ranges translate into groundwater velocity ranges of 80 to 28 m/yr and 9.4 to 4.8 m/yr (SNL 2008a, Section 7.2.2). Using a nominal distance of 18 km from the repository footprint to the boundary of the accessible environment at 18 km and taking constant velocities along the flow path, these velocities lead to transit time ranges of 226 to 643 years and 1,915 to 3,750 years. In interpreting these transit time estimates, the possibility of a fraction of younger water mixing with older water leading to the apparent age as determined from the ^{14}C activity cannot be ruled out with complete certainty. Hence, the values obtained from ^{14}C activity data are interpreted as representing the likely range of groundwater transport times, without excluding a small probability of groundwater ages having values outside the indicated range (SNL 2008a, Section 7.2.2).

For comparison, similar analyses in the volcanic rock aquifers in the vicinity of Yucca Mountain have been conducted, resulting in estimated flow velocities between 3 and 30 m/yr (White and Chuma 1987, p. 578).

A second comparison of transport times was performed along a flow path connecting boreholes USW-WT-24 and UE-25WT#3. Transport times were calculated using the dissolved inorganic carbon values of groundwater at borehole USW WT-24 and PHREEQC estimates of the carbon dissolved by this groundwater as it moves toward borehole UE-25 WT#3. The transport time estimate based on the differences in dissolved inorganic carbon of groundwater at these boreholes is 216 years. This estimate of transport time and a linear distance of 10 km between the boreholes in the upper part of the saturated zone results in a linear groundwater velocity of 46 m/yr (SNL 2007a, Appendix A).

Summary of Interpretations of Carbon Isotope Observations—Although uncertainty and variability exist in the ^{14}C and $\delta^{13}C$ observations, they generally indicate advective transport times of unretarded species that range from a few hundred to a few thousand years along likely flow paths within the tuff and alluvium aquifers to a downgradient point (i.e., NC-EWDP-19D) near the accessible environment. This conclusion is consistent with the site-scale saturated zone transport abstraction model, which has a simulated median transport time of about 1,000 years, as shown in Figure 2.3.9-48, and with the saturated zone flow and transport abstraction model, which has a range of simulated median transport times that encompasses the range of a few hundred to a few

thousand years based on ^{14}C observations, as shown in Figure 2.3.9-16. Furthermore, the variability in median transport times among the 200 realizations of the saturated zone flow and transport abstraction model shown in Figure 2.3.9-16 includes many realizations in which the simulated median transport times are less than one hundred years, and only a few realizations in which the median transport time is greater than several thousand years, indicating that the distribution of transport simulation results is skewed toward shorter transport times relative to the range inferred from the ^{14}C data. This comparison of the transport modeling results with the ^{14}C observations indicates that overall the saturated zone flow and transport abstraction model results for nonsorbing radionuclides supplied to the TSPA tends to underestimate the transport times in the saturated zone. The simulated expected transport times from the site-scale saturated zone transport model fall within the range of transport times estimated from the ^{14}C analysis.

2.3.9.3.4.1.4   Analogues to Saturated Zone Radionuclide Transport

The site-scale saturated zone transport model is designed to provide an analytic tool that facilitates understanding of solute transport in the aquifer beneath and downgradient from the repository. It is also a computational tool for performing radionuclide migration predictions in the saturated zone. The study of radionuclide transport parameters, based on observations at analogue sites, leads to increased confidence in the parameters that are used in the transport model presented in this report. The transport parameter values and processes for radionuclides of concern are sensitive to the site-specific geological and geochemical conditions. However, the site-scale saturated zone transport model is intended for use in making TSPA predictions, using a wide range of parameter input values that reflect uncertainty in the input. The analogue studies provide a qualitative comparison of the information with the parameters used here. The analogue studies considered here are the Nevada Test Site and uranium analogue sites. These include the Uranium Mill Tailings Remedial Action sites; El Borrocal, in Spain; Pena Blanca, Mexico; Alligator Rivers, in Australia; Pocos de Caldas, in Brazil; and Cigar Lake, in Canada. The following two sections (Sections 2.3.9.3.4.1.4.1 and 2.3.9.3.4.1.4.2) provide more detailed discussion with respect to these analogue sites. Consistency between the transport parameters from the site-scale saturated zone transport model, and those derived from analogue studies, provides increased confidence in the selection and choice of ranges for the transport parameters.

2.3.9.3.4.1.4.1   Colloidal Transport in the Saturated Zone

Colloids are ubiquitous in groundwaters (McCarthy 1996). However, in deep crystalline rocks with a stable geochemical system, colloid concentrations are typically low. In contrast, shallow aquifer systems generally appear to have the largest colloid concentrations. Enhanced colloid concentrations occur in all rock types where there is some hydrogeochemical perturbation to the system. For example, in fractured granitic systems, colloid concentrations are 20 to 1,000 times higher in groundwaters affected by inputs of surface water, or in hydrothermal zones with large temperature and pressure gradients, as compared to stable hydrogeochemical systems (Degueldre 1994).

In studies at the Nevada Test Site, the radionuclides generally considered to be immobile (such as plutonium, cesium, strontium, and europium) were found to be mobile in the groundwater when associated with colloids (SNL 2008a, Section 7.1.1.1). The uptake and transport of radionuclides by colloids has been investigated in several analogue studies of natural systems with enhanced

radionuclide content: Cigar Lake, Canada (Vilks et al. 1993); Alligator Rivers, Australia (Seo et al. 1994, p. 75); El Berrocal, Spain (Rivas et al. 1998); and Poços de Caldas, Brazil (Miekeley et al. 1992). The proportion of colloid-associated radionuclides was higher for thorium than for uranium because of thorium's lower solubility in most groundwaters. The rare-earth elements (which are analogues for radionuclides) generally show an affinity for colloids intermediate between that of uranium and thorium (Miekeley et al. 1992, pp. 429 and 434).

Several analogue studies suggest that colloid transport of moderately sorbing radionuclides in natural systems is significantly restricted. For instance, at Cigar Lake, the uranium and radium contents of colloids in the ore and the surrounding clay zones are significantly higher than in colloids from the sandstone host rock, indicating that the clay is an effective barrier to colloid migration (Vilks et al. 1993). Similar results at Alligator Rivers and Pocos de Caldas also suggest that colloids have a limited capacity for migration, because the concentrations of colloid-bound radionuclides outside ore bodies are relatively low (Miekeley et al. 1992, pp. 420, 432, and 433).

Nevada Test Site—Studies from the Nevada Test Site involving radionuclides from underground nuclear testing also indicate that colloids can lead to more rapid radionuclide transport. Colloid concentrations of 0.8 through 6.9 mg/L for particles greater than 30 nm were observed in two wells on Pahute Mesa at the Nevada Test Site (Buddemeier and Hunt 1988, p. 537). One well was inside the Cheshire experimental site, and the second (a water well) was 300 m away. Tritium, krypton, strontium, cesium, antimony, cobalt, cerium, and europium were detected in pumped water from the well. All of the cobalt, cesium, and europium were associated with colloids in samples from both wells. Buddemeier and Hunt (1988, p. 535) maintained that the presence of colloidal radionuclides outside the test cavity indicates colloid-facilitated radionuclide transport.

Colloid concentrations have been measured in several groundwater samples from Yucca Mountain and in other areas at the Nevada Test Site. The measured particle concentrations vary between about 1×10^6 and about 3×10^{10} particles per milliliter (SNL 2007f, Figure 6-23). These values are consistent with what has been reported for groundwaters around the world (SNL 2007f, Figure 6-23).

Unambiguous evidence from natural systems indicating colloidal transport over kilometer-scale distances is limited to a few reports. Observations from such places as the Nevada Test Site lend support to the concept that radionuclide transport in the saturated zone can be facilitated by colloids (Kersting et al. 1999), but so far no natural analogue studies have been able to quantify the importance of this process (BSC 2004i, Section 12.4.3).

Isotopic ratios of plutonium used to fingerprint the source of plutonium detected in monitoring wells for a specific underground nuclear test indicate that the plutonium migrated a distance of 1.3 km in a 30-year period between the underground test and groundwater sampling in the monitoring wells (Kersting et al. 1999, p. 56). Plutonium has a tendency to strongly sorb onto tuff minerals, which would retard its transport. Thus, the observed presence of colloids in waters at the Nevada Test Site, and the observed association of plutonium with colloids, indicate that radionuclide transport was facilitated by colloids. Although the plutonium colloid concentration in the monitoring wells was low (BSC 2004i, Section 12.4.3), the relatively large distance (1.3 km) and short transport time (30 years), demonstrated that colloid-facilitated transport is a potentially important process for plutonium migration in groundwater.

Although the Nevada Test Site conditions of plutonium colloid formation (prompt injection of plutonium) and related transport (more recharge) are different from the Yucca Mountain Site, the Nevada Test Site analogue helps understand the concept and effects of colloid-facilitated transport.

Alligator Rivers, Australia—The Koongarra uranium deposit at Alligator Rivers, Australia, is found at a steeply tilted contact between Proterozoic sandstone and schist. The ore body is located in a shallow unsaturated zone that is subject to seasonal infiltration fluctuations due to monsoons. The colloids at this site included clay minerals, particularly kaolinite and chlorite, and fine-grained quartz grains. Iron was present as particle coatings and in a separate colloidal form. The amount of ^{238}U associated with colloids ranged up to 6.5%, and the amount of ^{230}Th associated with colloids ranged from 10% to 85%. However, ^{230}Th was associated to a much greater extent with larger particles, which are likely to be immobile in natural groundwaters. The ^{227}Th/^{230}Th ratio was high in some fractions, indicating that ^{227}Ac could be associated with colloids (^{227}Th is a principal decay product of ^{227}Ac). Overall, however, there was little colloidal material in these groundwaters, with only iron, uranium, thorium, and actinium showing significant association with colloids (BSC 2004i, Section 10.5.2).

Modeling of colloid-facilitated transport with the saturated zone flow and transport abstraction model is conceptually consistent with observations in analogue systems. Radioelements that have been observed in association with colloids such as cesium, plutonium, and thorium are simulated to migrate via colloid-facilitated transport (Table 2.3.9-16; SNL 2008b, Table 6-9[a]). In addition, other radioelements with similar highly sorbing characteristics—such as americium, protactinium, and tin—are assumed to be subject to colloid-facilitated transport (SNL 2008b, Table 6-9[a]). A fraction of plutonium and americium that is permanently or strongly attached to colloids is subject to rapid simulated transport in fractured volcanic rocks without retardation in the saturated zone flow and transport abstraction model (SNL 2008b, Section 6.5.1.1).

2.3.9.3.4.1.4.2   Uranium Studies

Two analogue studies related to the migration of uranium in groundwater are available. The first is the Uranium Mill Tailing Remedial Action Study, where the focus is the transport of uranium (and other constituents) in alluvial aquifers. The second analogue is Peña Blanca, which is a uranium deposit in Mexico situated above the water table in brecciated rhyolitic ash-flow tuff.

Uranium Mill Tailing Remedial Action Study—Pertinent information on the transport of uranium and other constituents of interest in alluvial aquifers at Uranium Mill Tailing Remedial Action sites was analyzed to gain insight into the dispersion characteristics of the contaminant plumes and the retardation behavior of constituents (e.g., uranium) that are found in nuclear waste that is to be emplaced in a repository (BSC 2004i, Section 12.3).

The scope of the work in the Uranium Mill Tailing Remedial Action study was limited to a review of the subsurface transport behavior of uranium and other constituents of interest at Uranium Mill Tailing Remedial Action sites with emphasis on transport behavior in alluvial deposits. This is because the potential transport pathways from Yucca Mountain to the accessible environment pass through alluvium. No Uranium Mill Tailing Remedial Action sites contain bedrock similar to the volcanic rocks at Yucca Mountain (BSC 2004i, Section 12.3).

The approach is to evaluate the Uranium Mill Tailing Remedial Action sites in terms of aquifer materials, hydrologic characteristics, and groundwater chemistry. Those sites that are closest in hydrologic and chemical characteristics to the alluvium downgradient from Yucca Mountain, and for which sufficient data are available for detailed transport analysis, are considered in more detail (BSC 2004i, Section 12.3).

An evaluation of data available for 24 uranium mill tailing remedial action sites determined that only two sites are potentially useful for comparison to transport of radionuclides in the alluvial portion of the Yucca Mountain flow system. Most of the sites are of limited use either because (1) they are situated in a hydrogeologic setting different from Yucca Mountain; or (2) because there is insufficient information available to perform an adequate evaluation of transport behavior. There are enough data available for the Gunnison and New Rifle sites to perform useful analyses. The conclusions derived from an analysis of the Gunnison site are that (1) a fraction of the uranium originating at the site is transported in the alluvial aquifer at a rate similar to the rate at which a nonsorbing constituent is transported; and (2) there is little evidence for transverse dispersion of contaminants downgradient. For the New Rifle site, the main conclusions are that (1) dilution is a significant process in the downgradient direction; and (2) uranium is transported at a slower rate than nonsorbing constituents. The conclusions regarding uranium transport distances relative to nonsorbing constituents must be tempered somewhat by uncertainties regarding the potential presence of complexing agents, such as organic materials, that could enhance uranium transport. Such complexing agents would not be present in the Yucca Mountain repository setting (BSC 2004i, Section 12.3).

Peña Blanca—The Peña Blanca site is similar to the Yucca Mountain site in four ways: (1) both are located in semi-arid to arid regions; (2) both are parts of a basin and range horst structure composed of Tertiary rhyolitic tuffs overlying limestones; (3) both are located in a chemically oxidizing, unsaturated zone 100 m or more above the water table; and (4) the paragenesis of uraninite to secondary uranium minerals at Peña Blanca is similar to the alteration sequence of uranium fuel rods that is expected in a geologic repository such as Yucca Mountain. Data collected for the long-lived uranium-series members indicate limited mobility of uranium and its daughters over 100,000-year time scales. Transport from the uranium deposit to fractures has occurred in the past. However, the main transport activity currently observed is elevated ^{226}Ra in water samples in proximity to the deposit. The large depletions of ^{226}Ra seen in the fractures point to ^{226}Ra mobilization via recoil from fine-grained (submicron) uranium-bearing materials in the fracture coatings. The ^{226}Ra concentrations in waters sampled away from the deposit are quite low, which is typical for surface waters around the world. Hence, the mobilization of radium is a near-field event resulting from recoil of the ^{226}Ra from high-uranium regions into fluids. This mode of radionuclide mobilization would have bearing on transport of uranium and its daughter products from breached canisters at a high-level geologic storage system, but would not have bearing on transport of fission products such as ^{133}Ba, ^{135}Cs, ^{137}Cs, and ^{90}Sr. By analogy to the Peña Blanca observations, one would expect to see any mobilized uranium transported locally to fracture-filling materials. Recoil effects would raise local concentrations of daughter products in the fluids to be redeposited or sorbed at some moderate distance away from the recoil site (BSC 2004i, Section 10.4).

These observations of the mobility of uranium and its daughters are generally consistent with the ranges of parameters and transport models for the saturated zone. The uncertainty distributions for

the uranium sorption coefficient in volcanics and alluvium (Table 2.3.9-4; SNL 2008b, Table 6-8) lead to moderate retardation in the saturated zone (SNL 2008b, Table 6-10[a]), and the values of transverse dispersivities used in the saturated zone flow and transport abstraction model (SNL 2008b, Section 6.5.2.9) are small relative to the values of longitudinal dispersivity. The mobilization of radium via alpha recoil is consistent with the saturated zone one-dimensional transport model, in which decay products are assumed to be in aqueous equilibrium upon ingrowth.

2.3.9.3.4.2   Saturated Zone One-Dimensional Transport Model

2.3.9.3.4.2.1   Saturated Zone One-Dimensional Transport Model Abstraction

The saturated zone one-dimensional transport model is a simplified representation of groundwater flow paths and flow rates constructed for the purpose of simulating radioactive decay and ingrowth of radionuclides in four decay chains. Daughter products in the decay chains may contribute to estimated dose in the TSPA (SNL 2008b, Section 6.5.1.2). In addition, 10 CFR 63.331 requires explicit assessments of ^{226}Ra and ^{228}Ra activity concentrations in groundwater, requiring explicit assessment of their ingrowth and transport. The saturated zone one-dimensional transport model is utilized because the methodology used in the saturated zone flow and transport abstraction model does not simulate ingrowth by radioactive decay (SNL 2008b, Section 6.1). The one-dimensional transport of the four decay chains of interest through the saturated zone is implemented as a series of pipes with the GoldSim software code in the TSPA. The saturated zone one-dimensional transport model is consistent with the site-scale saturated zone flow model in that the lengths and groundwater flow rates in the pipe segments are estimated from the flow model, as described in *Saturated Zone Flow and Transport Model Abstraction* (SNL 2008b, Section 6.5.1.2[a], Tables 6-5[a] and 6-6[a]). The same radionuclide transport processes that are simulated in the site-scale saturated zone transport model (e.g., sorption, matrix diffusion in fractured units, and colloid-facilitated transport) are analyzed in the pipe segment (transverse dispersion is not included). Transverse dispersion is not critical to the modeling results, given the assumption that all radionuclide mass is contained in the representative volume and annual water demand of groundwater (SNL 2008b, Sections 6.3.3 and 6.5). Although strict consistency between the saturated zone one-dimensional transport model and the three-dimensional saturated zone flow and transport abstraction model is not possible, average groundwater flow and transport characteristics of the saturated zone flow and transport abstraction model are used to define flow and transport properties within the pipe segments of the one-dimensional transport abstraction model. Average specific discharges along different segments of the flow path are estimated using the site-scale saturated zone flow model (Section 2.3.9.2.4), and they are applied to the individual pipe segments in the one-dimensional saturated zone transport abstraction model (SNL 2008b, Section 6.5.1.2[a]).

The one-dimensional saturated zone transport abstraction model provides simulation results for the relevant radionuclide chains. There are four decay chains that are considered:

1. Actinium series: ^{243}Am $\rightarrow$ ^{239}Pu $\rightarrow$ ^{235}U $\rightarrow$ ^{231}Pa

2. Neptunium series: ^{241}Am $\rightarrow$ ^{237}Np $\rightarrow$ ^{233}U $\rightarrow$ ^{229}Th

3. Thorium series: $^{240}Pu \rightarrow ^{236}U \rightarrow ^{232}Th$

4. Uranium series: $\left.\begin{array}{c} ^{242}Pu \rightarrow ^{238}U \\ ^{238}Pu \end{array}\right\} \rightarrow ^{234}U \rightarrow ^{230}Th \rightarrow ^{226}Ra$

The radionuclide decay chain analysis is simplified in a manner that overestimates the concentration of daughter product by calculating secular equilibrium between the final decay products and their parents in three of these chains (SNL 2008b, Section 6.5.1.2). ^{227}Ac is in secular equilibrium with ^{231}Pa in the actinium chain at the downstream end of the saturated zone analysis. ^{228}Ra is in secular equilibrium with ^{232}Th in the thorium series. ^{210}Pb is in secular equilibrium with ^{226}Ra in the uranium series. In the saturated zone one-dimensional transport model setup, radionuclides ^{241}Am, ^{243}Am, ^{239}Pu, ^{240}Pu, and ^{242}Pu are subject to transport while irreversibly attached to colloids; and ^{243}Am, ^{238}Pu, ^{239}Pu, ^{240}Pu, ^{242}Pu, ^{231}Pa, ^{229}Th, ^{230}Th, and ^{232}Th are subject to the reversible colloid-facilitated transport model (SNL 2008b). The mass of americium and plutonium irreversibly attached to colloids is defined at the waste form in the TSPA model (Section 2.3.7).

The saturated zone one-dimensional transport model is used to account for the ingrowth of the second- (and subsequent) generation daughters. For each timestep, the inventory of each first-generation daughters is increased or "boosted" by the amount that their respective parent radionuclides would decay during the remaining simulation time. Even though they are accounted for in the saturated zone flow and transport abstraction model, the parents of the second-generation daughters are also transported in the saturated zone one-dimensional transport model. The parents are included in the saturated zone one-dimensional transport model to account for the ingrowth of the second-generation daughters. The radionuclide mass exiting the saturated zone flow and transport abstraction model and the saturated zone one-dimensional model is then screened, such that only the mass for the second- (and subsequent) generation daughter species is taken from the saturated zone one-dimensional model, and all other radionuclide results are taken from the saturated zone flow and transport abstraction model. A more detailed explanation of the implementation described above is provided in *Total System Performance Assessment Model/Analysis for the License Application* (SNL 2008d, Sections 6.3.10.3 and 6.3.10.3[a] and Figure 6.3.10-8[a]).

The saturated zone one-dimensional transport model is directly integrated into the TSPA using pipe elements in the GoldSim software, and is run concurrently with the TSPA simulations. Uncertain parameter values used in the saturated zone flow and transport abstraction model are also used in the saturated zone one-dimensional transport model on a realization-by-realization basis. The timing and the impacts of climate change on groundwater flow in the two abstraction models are also consistent as implemented in the TSPA (SNL 2008b). The mass of americium and plutonium irreversibly attached to colloids is defined at the waste form in the TSPA model.

2.3.9.3.4.2.2 Saturated Zone One-Dimensional Abstraction Model and Process Model Comparison

It is relevant to consider the purpose and use of the saturated zone one-dimensional transport model in evaluating its consistency with the underlying process model. The saturated zone one-dimensional transport model is used for the purpose of simulating radioactive decay and

ingrowth for four decay chains. This simplified model is required because the saturated zone flow and transport abstraction model does not include simulation of ingrowth by radioactive decay. The groundwater protection regulations require assessment of groundwater concentrations for radium and other alpha emitters. The results of the saturated zone one-dimensional transport model are used only for the decay products in these decay chains within the TSPA, as described in *Total System Performance Assessment Model/Analysis for the License Application* (SNL 2008d, Section 6.3.10.3[a]).

It must also be considered that there are fundamental differences between the saturated zone one-dimensional transport model and the saturated zone flow and transport abstraction model that limit the degree of consistency that can be expected on a realization-by-realization basis. Groundwater flow and radionuclide transport simulation in the site-scale saturated zone transport model occur in three dimensions with a relatively complex representation of geologic heterogeneity from the hydrogeologic framework model. Radionuclide transport in the saturated zone one-dimensional transport model is simulated in a significantly simplified representation of the saturated zone system consisting of three pipe segments. Each pipe segment has properties that represent the average characteristics in that area of the site-scale saturated zone transport model. In addition, there are variations in the conditions along flow paths from different source locations within each source zone below the repository in the site-scale saturated zone transport abstraction model. These variations are not captured in the saturated zone one-dimensional transport model, and can lead to additional differences between the saturated zone one-dimensional transport model and the saturated zone flow and transport abstraction model for a given realization (SNL 2008b, Section 7.4.2[a]).

The saturated zone one-dimensional transport model results were compared to the output of the site-scale saturated zone transport model. For the validation test, a constant input of 1 g/yr from the unsaturated zone was applied at the upper boundary of the one-dimensional saturated zone transport model. This is the same radionuclide mass boundary condition used in the site-scale saturated zone transport model. The breakthrough curves from the one-dimensional saturated zone model should approximately match the output from the site-scale saturated zone transport model. This validation test was conducted for both a nonsorbing species (e.g., ^{14}C, ^{99}Tc, and ^{129}I) and for neptunium, and was run for the three validation cases described for the saturated zone flow and transport abstraction model. To facilitate comparison of the results, the transport simulations in both the site-scale saturated zone transport model and the one-dimensional saturated zone transport model were performed without radioactive decay (SNL 2008b, Section 7.1.1).

Groundwater flow rates and flow-path lengths derived from the site-scale saturated zone transport model were used in the development of the saturated zone one-dimensional transport model (SNL 2008b, Section 7.1.2). However, both the approximate nature of the equivalency between the two models (representing the flow path by three homogeneous pipe segments) and the reduction in dimensionality in the saturated zone one-dimensional transport model limit the ability of the saturated zone one-dimensional model to match the results of the site-scale saturated zone transport model (SNL 2008b, Sections 7.1.2[a] and 7.1.2[b]). The results of the validation testing of the saturated zone one-dimensional transport model do not indicate a consistent tendency to overestimate or underestimate radionuclide transport times in the saturated zone relative to the saturated zone flow and transport abstraction model. In contrast, the simplifying assumptions of first-generation parent "boosting" and secular equilibrium for ^{227}Ac, ^{228}Ra, and ^{210}Pb described in

Section 2.3.9.3.4.2.1 both overestimate the release of radionuclide mass from the saturated zone by the saturated zone one-dimensional transport model. The saturated zone one-dimensional transport model is used only for the decay products of the four decay chains in the TSPA model and dissimilarities with the site-scale saturated zone transport model are unbiased or overestimate radionuclide releases. Consequently, differences with the site-scale saturated zone transport model are of minor importance.

Validation testing of the saturated zone one-dimensional transport abstraction model indicates acceptable agreement with the site-scale saturated zone transport model for the three (slow, median, and fast) validation test cases, and for the average transport behavior among 200 realizations of saturated zone transport. Qualitative criteria regarding the comparison of the simulated breakthrough curves with the results of the saturated zone transport model are met (SNL 2008b, Sections 7.4[a] and 7.4[b]). Results of the validation testing indicate that the saturated zone one-dimensional transport model is valid for the approximate range of uncertainty incorporated into the model through parameter uncertainty distributions. Results also indicate that the saturated zone one-dimensional transport model is valid for both nonsorbing and sorbing radionuclide species (SNL 2008b, Sections 7.4[a] and 7.4[b]). The saturated zone one-dimensional transport model provides an acceptable approximation of simulated radionuclide transport in the three-dimensional system of the saturated zone for use in the TSPA.

2.3.9.4   Conclusions

The saturated zone below the repository is a component of the Lower Natural Barrier at Yucca Mountain, which prevents or substantially reduces the flow of water and the movement of radionuclides away from the repository. The saturated zone flow and transport abstraction model simulates the FEPs that contribute to the capability of the barrier to reduce the movement of radionuclides. FEPs that have been determined to be important to the capability of the Lower Natural Barrier (Section 2.1.2.3 and Table 2.1-4) are listed in Section 2.3.9.1, and are presented in the bullets below. The technical bases for the incorporation of these FEPs have been discussed in detail in Sections 2.3.9.2 and 2.3.9.3.

- **Fractures**—Fracture characteristics and their effects on radionuclide transport velocities and filtration of colloids are important in the fractured tuffs where the flow is primarily through the fracture network rather than the matrix. The fracture networks appear to be well-connected over large distances, and are important to the capability of the barrier because of their role as pathways for groundwater flow and the advective transport of radionuclides.Uncertainty in fracture transport characteristics is included in the saturated zone transport analysis model report (SNL 2008a).

- **Faults**—Fault hydrologic characteristics are incorporated into the rock properties, which affect the groundwater flow path to the accessible environment. Some faults, particularly those that are inferred to act as barriers to groundwater flow such as the Solitario Canyon fault, have an important impact on the simulated paths and rates of groundwater flow in the Yucca Mountain area (SNL 2007a). Large-scale heterogeneity is in part incorporated in the site-scale saturated zone flow model through faults (SNL 2007a, p. 6-20). Faults affect groundwater flow patterns because they may act as preferred conduits or barriers to flow (SNL 2007a, p. 6-21).

- **Climate Change**—Climate change alters the volumetric flow through the saturated zone by increasing precipitation, increasing the regional recharge, and causing the water table to rise (SNL 2007a, Section 6.6.4.1). The effect of this increased recharge and associated water table rise is to increase the saturated zone groundwater volumetric flow between the area beneath the repository and the accessible environment. This increased flow tends to decrease the advective transport time from the repository to the accessible environment for both sorbing and nonsorbing radionuclides that may be released from the unsaturated zone below the repository. This increased flow, and potential changes to the groundwater flow paths, are conservatively approximated in the saturated zone transport abstraction by increasing the specific discharge. The approximation is considered conservative because simulations with the site-scale saturated zone transport model with water table rise explicitly included indicate longer transport times in the saturated zone than simulations without water table rise (SNL 2008a, Appendix E). This increase in the specific discharge causes a significant increase in the rate of movement of radionuclides, which degrades the capability of the saturated zone feature of the Lower Natural Barrier (SNL 2007a, Section 6.6.4.1).

- **Climate Modification Increases Recharge**—The increase in recharge associated with future climate states significantly increases the groundwater flow through the tuff and alluvial water-conducting features, which reduces the effectiveness of the barrier capability of these features (SNL 2008a; SNL 2007a, Section 6.6.4.1) by increasing the rate of transport of radionuclides.

- **Stratigraphy**—Stratigraphic heterogeneity affects likely saturated zone flow paths, based on variations in permeability among stratigraphic units. Various parameters that are significant in defining the transport of radionuclides through the saturated zone (e.g., effective diffusion, matrix porosity, and bulk density) are dependent on the stratigraphy and corresponding hydrogeologic units of the model zone. Many of these parameters are treated as constants within a stratigraphic unit, but vary between units (SNL 2008b, Section 6.5.2; SNL 2007a, Section 6.3.1.9). Stratigraphy is included in the performance assessment through the hydrogeologic framework model (saturated zone).

- **Rock Properties of Host Rock and Other Units**—Rock properties have a significant effect on the rate of radionuclide movement through their influence on the transport properties (notably, the flowing interval spacing, matrix diffusion coefficient, fracture porosity, sorption coefficients, matrix porosity of the volcanic units, and effective porosity of the alluvium) (SNL 2008b, Section 6.5.2). Flowing interval spacing is a parameter used to represent the distance between fractures, or sets of fractures, that transmit significant quantities of groundwater.

- **Saturated Groundwater Flow in the Geosphere**—The magnitude and direction of groundwater flow under present and future conditions in the saturated zone are estimated in the performance assessment (SNL 2007a; SNL 2008b). Advection of radionuclides by groundwater flow is one of the primary transport processes in the transport simulations (SNL 2008a, Section 6.4), and thus has a direct impact on the rate of radionuclide migration and the barrier capability of the saturated zone.

• **Water-Conducting Features in the SZ**—Water flow along potential flow paths from beneath the repository to the accessible environment in the saturated zone occurs within the fractured tuff units and the alluvium. The groundwater flow rates, radionuclide transport velocities, and radionuclide retardation characteristics of these different water conducting features are significantly different. In addition to the differences in flow and transport characteristics of the different hydrogeologic units in the saturated zone, the presence of discrete flowing features in the fractured tuff units controls the advective velocities and, therefore, transport times from the base of the unsaturated zone to the alluvium. The flow in the alluvium provides a significant reduction in the movement of radionuclides to the accessible environment due to the nature of the alluvium as a porous medium. These characteristics of the saturated zone have been included in the saturated zone flow and transport abstraction model (SNL 2008b).

• **Advection and Dispersion in the SZ**—Advection is the principal transport mechanism for both dissolved and colloidal radionuclides in the saturated zone. The advective flux is dependent on the hydrogeologic characteristics of the water-conducting features in the saturated zone, as well as the groundwater flow through these features. Dispersive processes tend to spread transient radionuclide pulses that may be released to the saturated zone (e.g., following the water table rise associated with climate changes, which could mobilize a pulse of radionuclide mass from the unsaturated zone above the present-day water table). These processes have been included in *Saturated Zone Flow and Transport Model Abstraction* (SNL 2008b).

• **Matrix Diffusion in the SZ**—Matrix diffusion, like advection and dispersion, is an important component of the saturated zone feature (SNL 2008a, Sections 4.1.2.10 and 6.4.2.4). The process of matrix diffusion enhances the barrier capability of the fractured tuff units in the saturated zone by effectively slowing the migration of radionuclides to the accessible environment. After diffusion into the matrix, radionuclides effectively stop moving until they diffuse out of the matrix at some later time. In addition, matrix diffusion provides access to the sorptive capacity of the tuff matrix, further slowing the migration of sorbing radionuclides.

• **Sorption in the SZ**—Radionuclides released from the repository have varying retardation characteristics. Several radionuclides, including those that contribute the most significant fraction of the inventory (for example, strontium, cesium, plutonium, radium, and americium), are moderately to highly sorbed in the saturated zone. The sorption behavior of these radionuclides prevents or substantially reduces the rate of movement of these radionuclides from beneath the repository to the accessible environment. Other radionuclides, such as neptunium and uranium, are slightly sorbed. For any radionuclide with multiple radioisotopes (such as ^{241}Am, and ^{243}Am), the chemical properties of sorption are assumed to be the same for all radioisotopes. Sorption effects are included in the site-scale saturated zone transport model (SNL 2008a, Section 4.1.2.4).

The site-scale saturated zone flow model, the site-scale saturated zone transport model, and the saturated zone flow and transport abstraction models rely on a technical basis that includes extensive testing at various scales at Yucca Mountain. The site-scale saturated zone flow model has been calibrated to be consistent with available information relevant to flow, including water-level

measurements in wells, recharge, discharge, and hydraulic property data (Section 2.3.9.2.3). The model has also been corroborated with geochemical observations, and tracer test determinations of specific discharge (Section 2.3.9.2.4). Data sources supporting the site-scale saturated zone radionuclide transport model (Section 2.3.9.3.2) include laboratory sorption and matrix diffusion measurements, testing of fracture flow and fracture-matrix interactions, laboratory and field testing of colloid retardation, single well and multi-well tracer tests in volcanic rocks and alluvium, water chemistry analyses, and isotopic studies to address the nature of past saturated zone flow.

The results of the saturated zone radionuclide transport abstraction model (Section 2.3.9.3.4) indicate that the saturated zone portion of the Lower Natural Barrier prevents (or substantially reduces) the rate of movement of radionuclides from beneath the repository to the accessible environment. Because of matrix diffusion, radionuclide sorption and other retardation processes strongly retard the transport of most of the radionuclides in the inventory at Yucca Mountain as discussed in Section 2.1.4. The rate of radionuclide transport is highly dependent on the characteristics of individual radionuclides, the form in which the radionuclide is released (dissolved or colloidal), and the uncertainties associated with transport parameters. Strongly sorbing radionuclides move very slowly, whereas nonsorbing species (such as ^{99}Tc and ^{129}I) travel through fast fracture flow paths, and have modeled median transport times of several hundred years, although some significant fraction of nonsorbing radionuclide mass, on the order of 5% to 15% as shown in Figure 2.3.9-48, may have transport times of 10s to 100s of thousands of years due to matrix diffusion.

Uncertainties Associated with Lower Natural Barrier Capability—The performance of the saturated zone feature of the Lower Natural Barrier is subject to uncertainty that is a function of the applicability of the conceptual and numerical models used to describe flow and transport, and of the degree of knowledge of the characteristics of the Yucca Mountain site. The data uncertainties associated with analyses of the site-scale saturated zone flow and transport models are described in Sections 2.3.9.2.2 and 2.3.9.3.2. The model parameter uncertainties associated with the analysis are described in Sections 2.3.9.2.3 and 2.3.9.3.3. Model uncertainty has been assessed through sensitivity studies and by comparison with results from alternative conceptual models (Sections 2.3.9.2.3.4 and 2.3.9.3.3.3).

To accommodate both variability and uncertainty in the description of the site, many of the input parameters to the saturated zone flow and transport abstraction model have been defined as probability distributions. The uncertainty distributions numerically represent knowledge about a particular parameter on the scale of the model domain (Section 2.3.9.2.3). The distributions incorporate uncertainties associated with field or laboratory data, the use of parameters in the model, and theoretical considerations. Geologic uncertainty is incorporated with regard to the location of the contact between the tuff and alluvium at the water table. Parameters used in the saturated zone flow and transport abstraction model related to groundwater flow or advection are groundwater specific discharge, flowing interval porosity, alluvium effective porosity, and horizontal anisotropy (Section 2.3.9.2.3.6). Parameters related to matrix diffusion include flowing interval spacing, effective diffusion coefficient, and matrix porosity. Dispersion parameters include longitudinal dispersivity, horizontal transverse dispersivity, and vertical transverse dispersivity. Parameters related to sorption include the sorption coefficients for various radionuclides for tuff and alluvium. Parameters used to model colloid-facilitated transport include colloid retardation factor, fast fraction of colloids, groundwater concentration of colloids, and sorption coefficients onto

colloids. Table 2.3.9-4 summarizes the values and uncertainty distributions for all parameters used in the saturated zone transport simulations.

The variability and uncertainty in barrier capability is reflected in the broad range of transport times and radionuclide breakthrough curves resulting from the saturated zone radionuclide transport models and abstractions. Sensitivity studies indicate that uncertainty in the performance of the Lower Natural Barrier, and particularly the saturated zone, is significant with respect to uncertainty in overall TSPA results (Section 2.4.2.3.3). The range of radionuclide breakthrough curves is consistent with the uncertainty in the simulation of the FEPs that affect barrier capability, as represented by the uncertainty distributions for input parameters.

Conservatism in Models Used to Assess the Capability of the Saturated Zone Portion of the Lower Natural Barrier—Several conservative assumptions have been incorporated in models of saturated zone flow and transport. The consequence of these assumptions is a model that generally predicts faster and greater transport of radionuclides through the saturated zone at Yucca Mountain than is indicated by geologic observations and geochemical and experimental data relevant to flow and transport. For example, predicted breakthrough curves for nonsorbing radionuclides (Section 2.3.9.3.4.1.1) range from 10 years to several thousand years, with a median (50%) of several hundred years. This compares to calculated transport times of hundreds to thousands of years (Section 2.3.9.3.4.1.3), based on isotopic analyses of groundwater (^{14}C) in the saturated zone. Alternative models of transport (Section 2.3.9.3.3.3.8) also predict significantly longer transport times for nonsorbing and sorbing radionuclides than does the saturated zone flow and transport abstraction model.

There are also several specific conservative assumptions contained in the saturated zone flow and transport abstraction model. The impact of climate change is incorporated (Section 2.3.9.2.4.1) by assuming an instantaneous increase in specific discharge. This approach is conservative because increases in groundwater flow would occur over some period of time in response to climate change resulting in longer radionuclide transport times during this transition.

Sorption of radionuclides on fracture surfaces is not considered in the saturated zone despite the moderately to strongly sorbing characteristics of many radionuclides, and the presence of sorbing minerals in fractures. This conservatism eliminates retardation of radionuclides in fractures, and reduces radionuclide transport times.

Potential permanent filtration of colloids with irreversibly attached radionuclides has not been included in the saturated zone flow and transport abstraction model, because tracer testing results at Yucca Mountain and other sites are ambiguous with regard to permanent filtration of colloids. Permanent filtration of such colloids would result in less radionuclide mass being released to the accessible environment.

Distributions for transport parameters (e.g., sorption coefficients, sorption onto colloids, colloid concentrations, fracture/matrix interaction) have been set to include conservative values (Section 2.3.9.3.2.3) when significant uncertainties exist in the interpretations of the supporting data. This approach ensures that models do not underestimate the rate of radionuclide transport.

Summary of Consistency Between TSPA Model Abstractions and Process Models—The site-scale saturated zone flow and transport models use the same three-dimensional model domain, flow parameters, and boundary conditions, and the saturated zone flow and transport abstraction model incorporates the results directly into the TSPA (Section 2.4.2.3.2.1). The site-scale saturated zone flow and transport models are also consistent with other component models that comprise the TSPA in the treatment of important features and processes (Section 2.4.2.3.1). For example, climate changes are propagated consistently through the unsaturated zone and saturated zone flow and transport models and abstractions, as well as in other models (such as the thermal-hydrologic-chemical environment) that are affected. Key aspects of the conceptual models of groundwater flow and radionuclide transport are the same in the saturated zone and unsaturated zone component models, including the processes of advective transport, dispersion, matrix diffusion in fractured volcanic rock, sorption, radioactive decay and ingrowth, and colloid-facilitated transport. The saturated zone and unsaturated zone models differ in grid resolution and the detail with which some geologic features are represented, which is appropriate given the differences in spatial scale that are encompassed by these models. Some uncertain parameters, such as sorption coefficients, are sampled independently in the saturated zone and the unsaturated zone, based on potential differences in chemistry and mineralogy in the two regimes and on differences in the density of supporting data. Time-dependent variations in infiltration and percolation fluxes are propagated consistently through the thermal-hydrologic-chemical environment, seepage, and transport abstraction models. Consistent definitions of flow and transport properties and characteristics are used throughout the TSPA model, except in cases where model simplifications (e.g., the one-dimensional saturated zone transport abstraction) requires the definition of alternative, but comparable, parameters.

Summary of Key Output Parameters Provided to the TSPA—The TSPA uses two models, developed in Section 2.3.9, to represent saturated zone flow and transport. The three-dimensional saturated zone flow and transport abstraction model calculates the flow fields and transport of individual radionuclides important to dose. The model considers a range of spatial locations and times of radionuclide releases from the unsaturated zone to produce radionuclide mass breakthrough curves at the accessible environment that are directly used in the TSPA. The saturated zone one-dimensional transport model simulates the transport of radionuclides associated with four decay chains, incorporating the processes of radioactive decay and ingrowth. In the TSPA, the biosphere model converts the mass release rate from the saturated zone to radionuclide concentrations distributed in the 3,000 acre-ft/yr of groundwater specified in 10 CFR 63.312(c) and 63.332(a)(3). These outputs to the TSPA embody key conceptual understanding of FEPs relevant to groundwater flow and radionuclide transport in the saturated zone. In addition, the outputs use reasonable and valid models that incorporate available data and evaluate the impacts of uncertainty in important input parameters.

2.3.9.5 General References

Altman, W.D.; Donnelly, J.P.; and Kennedy, J.E. 1988. *Qualification of Existing Data for High-Level Nuclear Waste Repositories: Generic Technical Position*. NUREG-1298. Washington, D.C.: U.S. Nuclear Regulatory Commission. TIC: 200652.

Anghel, I. 2001. *Comparison of Polystyrene and Silica Colloids Transport in Saturated Rock Fractures.* Master's thesis. Albuquerque, New Mexico: University of New Mexico. TIC: 253148.

Arnold, B.W.; Kuzio, S.P.; and Robinson, B.A. 2003. "Radionuclide Transport Simulation and Uncertainty Analyses with the Saturated-Zone Site-Scale Model at Yucca Mountain, Nevada." *Journal of Contaminant Hydrology*, *62–63*, 401–419. New York, New York: Elsevier. TIC: 254205.

Belcher, W.R. 2004. *Death Valley Regional Ground-Water Flow System, Nevada and California - Hydrogeologic Framework and Transient Ground-Water Flow Model*. Scientific Investigations Report 2004-5205. Reston, Virginia: U.S. Geological Survey. ACC: MOL.20050323.0070.

Bower, K.M.; Gable, C.W.; and Zyvoloski, G.A. 2000. *Effect of Grid Resolution on Control Volume Finite Element Groundwater Modeling of Realistic Geology*. LA-UR-001870. Los Alamos, New Mexico: Los Alamos National Laboratory. TIC: 248256.

BSC (Bechtel SAIC Company) 2004a. *Water-Level Data Analysis for the Saturated Zone Site-Scale Flow and Transport Model*. ANL-NBS-HS-000034 REV 02. Las Vegas, Nevada: Bechtel SAIC Company. ACC: DOC.20041012.0002.

BSC 2004b. *Geologic Framework Model (GFM2000)*. MDL-NBS-GS-000002 REV 02. Las Vegas, Nevada: Bechtel SAIC Company. ACC: DOC.20040827.0008.

BSC 2004c. *Yucca Mountain Site Description*. TDR-CRW-GS-000001 REV 02 ICN 01. Two volumes. Las Vegas, Nevada: Bechtel SAIC Company. ACC: DOC.20040504.0008.

BSC 2004d. *Recharge and Lateral Groundwater Flow Boundary Conditions for the Saturated Zone Site-Scale Flow and Transport Model*. ANL-NBS-MD-000010 REV 01. Las Vegas, Nevada: Bechtel SAIC Company. ACC: DOC.20041008.0004.

BSC 2004e. *Saturated Zone Colloid Transport*. ANL-NBS-HS-000031 REV 02. Las Vegas, Nevada: Bechtel SAIC Company. ACC: DOC.20041008.0007.

BSC 2004f. *Probability Distribution for Flowing Interval Spacing*. ANL-NBS-MD-000003 REV 01. Las Vegas, Nevada: Bechtel SAIC Company. ACC: DOC.20040923.0003.

BSC 2004g. *Future Climate Analysis*. ANL-NBS-GS-000008 REV 01. Las Vegas, Nevada: Bechtel SAIC Company. ACC: DOC.20040908.0005.

BSC 2004h. *Analysis of Hydrologic Properties Data*. ANL-NBS-HS-000042 REV 00. Las Vegas, Nevada: Bechtel SAIC Company. ACC: DOC.20041005.0004.

BSC 2004i. *Natural Analogue Synthesis Report.* TDR-NBS-GS-000027 REV 01. Las Vegas, Nevada: Bechtel SAIC Company. ACC: DOC.20040524.0008.

Buddemeier, R.W. and Hunt, J.R. 1988. "Transport of Colloidal Contaminants in Groundwater: Radionuclide Migration at the Nevada Test Site." *Applied Geochemistry, 3*, 535–548. Oxford, England: Pergamon Press. TIC: 224116.

Burbey, T.J. and Wheatcraft, S.W. 1986. *Tritium and Chlorine-36 Migration from a Nuclear Explosion Cavity.* DOE/NV/10384-09. Reno, Nevada: University of Nevada, Desert Research Institute, Water Resources Center. TIC: 201927.

Claassen, H.C. 1985. *Sources and Mechanisms of Recharge for Ground Water in the West-Central Amargosa Desert, Nevada—A Geochemical Interpretation.* U.S. Geological Survey Professional Paper 712-F. Washington, D.C.: United States Government Printing Office. TIC: 204574.

CRWMS M&O (Civilian Radioactive Waste Management System Management and Operating Contractor) 1998. *Saturated Zone Flow and Transport Expert Elicitation Project*. Deliverable SL5X4AM3. Las Vegas, Nevada: CRWMS M&O. ACC: MOL.19980825.0008.

Czarnecki, J.B. 1985. *Simulated Effects of Increased Recharge on the Ground-Water Flow System of Yucca Mountain and Vicinity, Nevada–California.* Water-Resources Investigations Report 84-4344. Denver, Colorado: U.S. Geological Survey. TIC: 203222.

Czarnecki, J.B. and Waddell, R.K. 1984. *Finite-Element Simulation of Ground-Water Flow in the Vicinity of Yucca Mountain, Nevada–California*. Water-Resources Investigations Report 84-4349. Denver, Colorado: U.S. Geological Survey. ACC: NNA.19870407.0173.

D'Agnese, F.A.; O'Brien, G.M.; Faunt, C.C.; and San Juan, C.A. 1999. *Simulated Effects of Climate Change on the Death Valley Regional Ground-Water Flow System, Nevada and California.* Water-Resources Investigations Report 98-4041. Denver, Colorado: U.S. Geological Survey. TIC: 243555.

Degueldre, C.A. 1994. *Colloid Properties in Groundwaters from Crystalline Formations.* PSI Bericht Nr. 94-21. Villigen, Switzerland: Paul Scherrer Institut. TIC: 224100.

Degueldre, C.; Triay, I.; Kim, J.I; Vilks, P.; Laaksoharju, M.; and Miekeley, N. 2000. "Groundwater Colloid Properties: A Global Approach." *Applied Geochemistry, 15* (7), 1043–1051. New York, New York: Pergamon Press. TIC: 249340.

de Marsily, G. 1986. *Quantitative Hydrogeology: Groundwater Hydrology for Engineers.* San Diego, California: Academic Press. TIC: 208450.

DOE (U.S. Department of Energy) 1997. *Regional Groundwater Flow and Tritium Transport Modeling and Risk Assessment of the Underground Test Area, Nevada Test Site, Nevada*. DOE/NV-477. Las Vegas, Nevada: U.S. Department of Energy. ACC: MOL.20010731.0303.

EPA (U.S. Environmental Protection Agency) 1999. *Understanding Variation in Partition Coefficient, K_d, Values*. EPA 402-R-99-004A&B Two volumes. Washington, D.C.: U.S. Environmental Protection Agency. TIC: 249201.

Erickson, J.R. and Waddell, R.K. 1985. *Identification and Characterization of Hydrologic Properties of Fractured Tuff Using Hydraulic and Tracer Tests—Test Well USW H-4, Yucca Mountain, Nye County, Nevada*. Water-Resources Investigations Report 85-4066. Denver, Colorado: U.S. Geological Survey. ACC: NNA.19890713.0211.

Ervin, E.M.; Luckey, R.R.; and Burkhardt, D.J. 1994. *Revised Potentiometric-Surface Map, Yucca Mountain and Vicinity, Nevada*. Water-Resources Investigations Report 93-4000. Denver, Colorado: U.S. Geological Survey. ACC: NNA.19930212.0018.

Ferrill, D.A.; Winterle, J.; Wittmeyer, G.; Sims, D.; Colton, S.; Armstrong, A.; and Morris, A.P. 1999. "Stressed Rock Strains Groundwater at Yucca Mountain, Nevada." *GSA Today*, *9* (5), 1–8. Boulder, Colorado: Geological Society of America. TIC: 246229.

Forester, R.M.; Bradbury, J.P.; Carter, C.; Elvidge-Tuma, A.B.; Hemphill, M.L.; Lundstrom, S.C.; Mahan, S.A.; Marshall, B.D.; Neymark, L.A.; Paces, J.B.; Sharpe, S.E.; Whelan, J.F.; and Wigand, P.E. 1999. *The Climatic and Hydrologic History of Southern Nevada During the Late Quaternary*. Open-File Report 98-635. Denver, Colorado: U.S. Geological Survey. TIC: 245717.

Freifeld, B.; Doughty, C.; and Finsterle, S. 2006. *Preliminary Estimates of Specific Discharge and Transport Velocities Near Borehole NC-EWDP-24PB*. LBNL-60740. Berkeley, California: Lawrence Berkeley National Laboratory. ACC: MOL.20070111.0001.

Geldon, A.L.; Umari, A.M.A.; Fahy, M.F.; Earle, J.D.; Gemmell, J.M.; and Darnell, J. 1997. *Results of Hydraulic and Conservative Tracer Tests in Miocene Tuffaceous Rocks at the C-Hole Complex, 1995 to 1997, Yucca Mountain, Nye County, Nevada*. Milestone SP23PM3. Las Vegas, Nevada: U.S. Geological Survey. ACC: MOL.19980122.0412.

Gelhar, L.W.; Welty, C.; and Rehfeldt, K.R. 1992. "A Critical Review of Data on Field-Scale Dispersion in Aquifers." *Water Resources Research*, *28* (7), 1955–1974. Washington, D.C.: American Geophysical Union. TIC: 235780.

Gelman, A.; Carlin, J.B.; Stern, H.S.; and Rubin, D.B. 2004. *Bayesian Data Analysis. Texts in Statistical Science*. 2nd Edition. New York, New York: Chapman & Hall. TIC: 259516.

Harter, T. and Hopmans, J.W. 2004. "Role of Vadose-Zone Flow Processes in Regional-Scale Hydrology: Review, Opportunities and Challenges." Chapter 6 of *Unsaturated-Zone Modeling*. Feddes, R.A.; de Rooij, G.H.; and van Dam, J.C., eds. Wageningen UR Frontis Series Volume 6. Boston, Massachusetts: Kluwer Academic Publishers. TIC: 258894.

Honeyman, B.D. and Ranville, J.F. 2002. "Colloid Properties and their Effects on Radionuclide Transport through Soils and Groundwaters." Chapter 7 of *Geochemistry of Soil Radionuclides*. Zhang, P.C. and Brady, P.V., eds. SSSA Special Publication Number 59. Madison, Wisconsin: Soil Science Society of America. TIC: 253952.

Jury, W.A.; Sposito, G.; and White, R.E. 1986. "A Transfer Function Model of Solute Transport Through Soil. 1. Fundamental Concepts." *Water Resources Research*, *22* (2), 243–247. Washington, D.C.: American Geophysical Union. TIC: 254552.

Kersting, A.B.; Efurd, D.W.; Finnegan, D.L.; Rokop, D.J.; Smith, D.K.; and Thompson, J.L. 1999. "Migration of Plutonium in Ground Water at the Nevada Test Site." *Nature*, *397* (6714), 56–59. London, England: Macmillan Journals. TIC: 243597.

Kingston, W.L. and Whitbeck, M. 1991. *Characterization of Colloids Found in Various Groundwater Environments in Central and Southern Nevada.* DOE/NV/10384-36. Las Vegas, Nevada: Desert Research Institute, Water Resources Center. ACC: NNA.19930607.0073.

Kotra, J.P.; Lee, M.P.; Eisenberg, N.A.; and DeWispelare, A.R. 1996. *Branch Technical Position on the Use of Expert Elicitation in the High-Level Radioactive Waste Program.* NUREG-1563. Washington, D.C.: U.S. Nuclear Regulatory Commission. TIC: 226832.

Langmuir, D. 1997. *Aqueous Environmental Geochemistry.* Upper Saddle River, New Jersey: Prentice Hall. TIC: 237107.

LANL (Los Alamos National Laboratory) 2003a. *Validation Test Plan (VTP) for the FEHM Application Version 2.21.* 10086-VTP-2.21-00. Los Alamos, New Mexico: Los Alamos National Laboratory. ACC: MOL.20031031.0264; MOL.20031031.0265.

LANL 2003b. *Validation Test Report (VTR) for the FEHM Application Version 2.21.* Document ID: 10086-VTR-2.21-00. Los Alamos, New Mexico: Los Alamos National Laboratory. ACC: MOL.20031031.0267.

Levy, S.S. 1991. "Mineralogic Alteration History and Paleohydrology at Yucca Mountain, Nevada." *High Level Radioactive Waste Management, Proceedings of the Second Annual International Conference, Las Vegas, Nevada, April 28-May 3, 1991. 1,* 477-485. La Grange Park, Illinois: American Nuclear Society. TIC:204272.

Lu, N.; Conca, J.; Parker, G.R.; Leonard, P.A.; Moore, B.; Strietelmeier, B.; and Triay, I.R. 2000. *Adsorption of Actinides onto Colloids as a Function of Time, Temperature, Ionic Strength, and Colloid Concentration, Waste Form Colloids Report for Yucca Mountain Program (Colloid Data Summary from 1999 to 2000 Research).* LA-UR-00-5121. Los Alamos, New Mexico: Los Alamos National Laboratory. ACC: MOL.20031204.0108.

Lu, N.; Triay, I.R.; Cotter, C.R.; Kitten, H.D.; and Bentley, J. 1998. *Reversibility of Sorption of Plutonium-239 onto Colloids of Hematite, Goethite, Smectite, and Silica.* LA-UR-98-3057. Los Alamos, New Mexico: Los Alamos National Laboratory. ACC: MOL.19981030.0202.

Luckey, R.R.; Tucci, P.; Faunt, C.C.; Ervin, E.M.; Steinkampf, W.C.; D'Agnese, F.A.; and Patterson, G.L. 1996. *Status of Understanding of the Saturated-Zone Ground-Water Flow System at Yucca Mountain, Nevada, as of 1995.* Water-Resources Investigations Report 96-4077. Denver, Colorado: U.S. Geological Survey. ACC: MOL.19970513.0209.

Marshall, B.D.; Peterman, Z.E.; and Stuckless, J.S. 1993. "Strontium Isotopic Evidence for a Higher Water Table at Yucca Mountain." *High-Level Radioactive Waste Management, Proceedings of the Fourth Annual International Conference, Las Vegas, Nevada, April 26–30, 1993, 2,* 1948–1952. La Grange Park, Illinois: American Nuclear Society. TIC: 208542.

McCarthy, J.F. 1996. "Natural Analogue Studies of the Role of Colloids, Natural Organics and Microorganisms on Radionuclide Transport." *Sixth EC Natural Analogue Working Group Meeting, Proceedings of an International Workshop Held in Santa Fe, New Mexico, USA on September 12–16, 1994*, von Maravic, H. and Smellie, J., eds. EUR 16761 EN. Page 195–210. Luxembourg, Luxembourg: Commission of the European Communities. TIC: 225227.

Meijer, A. 2002. "Conceptual Model of the Controls on Natural Water Chemistry at Yucca Mountain, Nevada." *Applied Geochemistry, 17* (6), 793–805. New York, New York: Elsevier. TIC: 252808.

Miekeley, N.; Couthinho de Jesus, H.; Porto da Silveira, C.L.; and Degueldre, C. 1992. "Chemical and Physical Characterization of Suspended Particles and Colloids in Waters from the Osamu Utsumi Mine and Morro do Ferro Analogue Study Sites, Poços-de-Caldas, Brazil." *Journal of Geochemical Exploration*, *45*, 409–437. Amsterdam, The Netherlands: Elsevier. TIC: 245687.

MO0712DELNPCCA.001. Delineation of Postclosure Controlled Area. Submittal date: 12/03/2007.

Neuman, S.P. 1990. "Universal Scaling of Hydraulic Conductivities and Dispersivities in Geologic Media." *Water Resources Research, 26,* (8), 1749-1758. Washington, D.C.: American Geophysical Union. TIC: 237977.

Paces, J.B. and Whelan, J.F. 2001. "Water-Table Fluctuations in the Amargosa Desert, Nye County, Nevada." *"Back to the Future—Managing the Back End of the Nuclear Fuel Cycle to Create a More Secure Energy Future," Proceedings of the 9th International High-Level Radioactive Waste Management Conference (IHLRWM), Las Vegas, Nevada, April 29–May 3, 2001.* La Grange Park, Illinois: American Nuclear Society. TIC: 247873.

Penrose, W.R.; Polzer, W.L.; Essington, E.H.; Nelson, D.M.; and Orlandini, K.A. 1990. "Mobility of Plutonium and Americium Through a Shallow Aquifer in a Semiarid Region." *Environmental Science & Technology, 24*, 228–234. Washington, D.C.: American Chemical Society. TIC: 224113.

Press, W.H.; Teukolsky, S.A.; Vetterling, W.T.; and Flannery, B.P. 1992. *Numerical Recipes in Fortran 77, The Art of Scientific Computing. Volume 1 of Fortran Numerical Recipes.* 2nd Edition. Cambridge, United Kingdom: Cambridge University Press. TIC: 243606.

Reimus, P.W.; Haga, M.J.; Humphrey, A.R.; Counce, D.A.; Callahan, T.J.; and Ware, S.D. 2002. *Diffusion Cell and Fracture Transport Experiments to Support Interpretations of the BULLION Forced-Gradient Experiment.* LA-UR-02-6884. Los Alamos, New Mexico: Los Alamos National Laboratory. TIC: 253859.

Reimus, P.W.; Ware, S.D.; Benedict, F.C.; Warren, R.G.; Humphrey, A.; Adams, A.; Wilson, B.; and Gonzales, D. 2002. *Diffusive and Advective Transport of ^3H, ^{14}C, and ^{99}Tc in Saturated, Fractured Volcanic Rocks from Pahute Mesa, Nevada.* LA-13891-MS. Los Alamos, New Mexico: Los Alamos National Laboratory. TIC: 253905.

Renard, Ph. and de Marsily, G. 1997. "Calculating Equivalent Permeability: A Review." *Advances in Water Resources, 20* (5–6), 253–278. New York, New York: Elsevier. TIC: 256209.

Rivas, P.; Hernan, P.; Astudillo, J.; Bruno, J.; Carrerra, J.; De la Cruz, B.; Guimera, J.; Gomez, P.; Ivanovich, M.; Marin, C.; Miller, W.; and Perez del Villar, L. 1998. *Nuclear Science and Technology, El Berrocal Project.* EUR 17830 EN. Luxembourg, Luxembourg: Commission of European Communities. TIC: 247318.

Rousseau, J.P.; Kwicklis, E.M.; and Gillies, D.C., eds. 1999. *Hydrogeology of the Unsaturated Zone, North Ramp Area of the Exploratory Studies Facility, Yucca Mountain, Nevada.* Water-Resources Investigations Report 98-4050. Denver, Colorado: U.S. Geological Survey. ACC: MOL.19990419.0335.

Savard, C.S. 1998. *Estimated Ground-Water Recharge from Streamflow in Fortymile Wash Near Yucca Mountain, Nevada.* Water-Resources Investigations Report 97-4273. Denver, Colorado: U.S. Geological Survey. TIC: 236848.

Schijven, J.F.; Hoogenboezem, W.; Hassanizadeh, S.M.; and Peters, J.H. 1999. "Modeling Removal of Bacteriophages MS2 and PRD1 by Dune Recharge at Castricum, Netherlands." *Water Resources Research*, *35* (4), 1101–1111. Washington, D.C.: American Geophysical Union. TIC: 252295.

Seo, T.; Edis, R.; and Payne, T.E. 1994. "A Study of Colloids in Groundwaters at the Koongarra Uranium Deposit." *Fifth CEC Natural Analogue Working Group Meeting and Alligator Rivers Analogue Project (ARAP) Final Workshop, Proceedings of an International Workshop, held in Toledo, Spain, from 5 to 9 October 1992*, von Maravic, H. and Smellie, J., eds. EUR 15176 EN. Pages 71–76. Luxembourg, Luxembourg: Commission of the European Communities. TIC: 247923.

Sharpe, S. 2003. *Future Climate Analysis—10,000 Years to 1,000,000 Years After Present.* MOD-01-001 REV 01. Reno, Nevada: Desert Research Institute. ACC: MOL.20030407.0055.

SNL (Sandia National Laboratories) 2007a. *Saturated Zone Site-Scale Flow Model.* MDL-NBS-HS-000011 REV 03. Las Vegas, Nevada: Sandia National Laboratories. ACC: DOC.20070626.0004.

SNL 2007b. *Saturated Zone In-Situ Testing.* ANL-NBS-HS-000039 REV 02. Las Vegas, Nevada: Sandia National Laboratories. ACC: DOC.20070608.0004.

SNL 2007c. *Hydrogeologic Framework Model for the Saturated Zone Site-Scale Flow and Transport Model.* MDL-NBS-HS-000024 REV 01. Las Vegas, Nevada: Sandia National Laboratories. ACC: DOC.20070411.0003;.

SNL 2007d. *UZ Flow Models and Submodels.* MDL-NBS-HS-000006 REV 03 ADD 01. Las Vegas, Nevada: Sandia National Laboratories. ACC: DOC.20080108.0003; DOC.20080114.0001.

SNL 2007e. *Radionuclide Transport Models Under Ambient Conditions.* MDL-NBS-HS-000008 REV 02 ADD 01. Las Vegas, Nevada: Sandia National Laboratories. ACC: DOC.20070718.0003.

SNL 2007f. *Waste Form and In-Drift Colloids-Associated Radionuclide Concentrations: Abstraction and Summary.* MDL-EBS-PA-000004 REV 03. Las Vegas, Nevada: Sandia National Laboratories. ACC: DOC.20071018.0019.

SNL 2008a. *Site-Scale Saturated Zone Transport.* MDL-NBS-HS-000010 REV 03 ADD 01. Las Vegas, Nevada: Sandia National Laboratories. ACC: DOC.20080121.0003.

SNL 2008b. *Saturated Zone Flow and Transport Model Abstraction.* MDL-NBS-HS-000021 REV 03 ADD 02. Las Vegas, Nevada: Sandia National Laboratories. ACC: DOC.20080107.0006.

SNL 2008c. *Simulation of Net Infiltration for Present-Day and Potential Future Climates.* MDL-NBS-HS-000023 REV 01 ADD 01. Las Vegas, Nevada: Sandia National Laboratories. ACC: DOC.20080201.0002.

SNL 2008d. *Total System Performance Assessment Model/Analysis for the License Application.* MDL-WIS-PA-000005 REV 00 ADD 01. Las Vegas, Nevada: Sandia National Laboratories. ACC: DOC.20080312.0001;.

SNL 2008e. *Particle Tracking Model and Abstraction of Transport Processes.* MDL-NBS-HS-000020 REV 02 ADD 02. Las Vegas, Nevada: Sandia National Laboratories. ACC: DOC.20080129.0008.

Stenhouse, M.J. 1995. *Sorption Databases for Crystalline, Marl and Bentonite for Performance Assessment.* NAGRA Technical Report 93-06. Wettingen, Switzerland: National Cooperative for the Disposal of Radioactive Waste. TIC: 247885.

Turin, H.J.; Groffman, A.R.; Wolfsberg, L.E.; Roach, J.L.; and Strietelmeier, B.A. 2002. "Tracer and Radionuclide Sorption to Vitric Tuffs of Busted Butte, Nevada." *Applied Geochemistry, 17,* (6), 825–836. New York, New York: Pergamon. TIC: 254046.

Valocchi, A.J. 1985. "Validity of the Local Equilibrium Assumption for Modeling Sorbing Solute Transport Through Homogeneous Soils." *Water Resources Research, 21* (6), 808–820. Washington, D.C.: American Geophysical Union. TIC: 223203.

Vanmarcke, E. 1983. *Random Fields: Analysis and Synthesis.* Cambridge, Massachusetts: Massachusetts Institute of Technology. TIC: 249691.

Vilks, P.; Cramer, J.J.; Bachinski, D.B.; Doern, D.C.; and Miller, H.G. 1993. "Studies of Colloids and Suspended Particles, Cigar Lake Uranium Deposit, Saskatchewan, Canada." *Applied Geochemistry, 8* (6), 605–616. London, England: Pergamon Press. TIC: 237449.

Viswanathan, H. 2003. Contaminant Transport Modeling of the Saturated Zone at Yucca Mountain, NV. Scientific Notebook SN-LANL-SCI-297-V1. ACC: MOL.20030609.0493; MOL.20030821.0052.

White, A.F. and Chuma, N.J. 1987. "Carbon and Isotopic Mass Balance Models of Oasis Valley—Fortymile Canyon Groundwater Basin, Southern Nevada." *Water Resources Research*, *23* (4), 571–582. Washington, D.C.: American Geophysical Union. TIC: 237579.

Winograd, I.J. and Thordarson, W. 1975. *Hydrogeologic and Hydrochemical Framework, South–Central Great Basin, Nevada–California, with Special Reference to the Nevada Test Site.* Geological Survey Professional Paper 712-C. Washington, D.C.: United States Government Printing Office. ACC: NNA.19870406.0201.

Winterle, J. 2005. *Simulation of Spring Flows South of Yucca Mountain, Nevada, Following a Potential Future Water Table Rise.* San Antonio, Texas: Center for Nuclear Waste Regulatory Analyses. ACC: MOL.20061120.0234.

Winterle, J.R. 2003. *Evaluation of Alternative Concepts for Saturated Zone Flow: Effects of Recharge and Water Table Rise on Flow Paths and Travel Times at Yucca Mountain*. San Antonio, Texas: Center for Nuclear Waste Regulatory Analyses. ACC: MOL.20061120.0233.

Winterle, J.R.; Claisse, A.; and Arlt, H.D. 2003. "An Independent Site-Scale Groundwater Flow Model for Yucca Mountain." *Proceedings of the 10th International High-Level Radioactive Waste Management Conference (IHLRWM), March 30–April 2, 2003, Las Vegas, Nevada*, 151–158. La Grange Park, Illinois: American Nuclear Society. TIC: 254559.

Zyvoloski, G.A.; Robinson, B.A.; Dash, Z.V.; and Trease, L.L. 1997. *User's Manual for the FEHM Application—A Finite-Element Heat- and Mass-Transfer Code*. LA-13306-M. Los Alamos, New Mexico: Los Alamos National Laboratory. TIC: 235999.

Table 2.3.9-1. Included Saturated Zone Features, Events, and Processes

FEP Number and FEP Name	FEP Description	Summary of Technical Basis/Approach for FEP Inclusion
1.2.02.01.0A Fractures	Groundwater flow in the Yucca Mountain region and transport of any released radionuclides may take place along fractures. The rate of flow and the extent of transport in fractures are influenced by characteristics such as orientation, aperture, asperity, fracture length, connectivity, and the nature of any linings or infills.	The effective continuum approach is adopted to simulate groundwater flow through the fractured rock within the domain of the site-scale saturated zone flow model (Section 2.3.9.2.3). The saturated zone transport conceptual models of fluid flow within fractures of the saturated zone are represented through the uncertain parameters of flowing interval spacing, flowing interval porosity, and horizontal anisotropy (Section 2.3.9.3.2.1).
1.2.02.02.0A Faults	Numerous faults of various sizes have been noted in the Yucca Mountain region, and specifically in the repository area. Faults may represent an alteration of the rock permeability and continuity of the rock mass, an alteration or short-circuiting of the flow paths and flow distributions close to the repository, and/or unexpected pathways through the repository.	In general, large-scale hydraulic features (e.g., major faults, fault zones, zones of chemical alteration) have been incorporated into the site-scale saturated zone flow model as zones of enhanced or reduced permeability. The faults were generally modeled as anisotropic features with high conductivity along the fault (strike) and low conductivity in the direction across the fault (Section 2.3.9.2.3.1).
1.3.01.00.0A Climate Change	Climate change may affect the long-term performance of the repository. This includes the effects of long-term change in global climate (e.g., glacial-interglacial cycles) and shorter-term change in the regional and local climate. Climate is typically characterized by temporal variations in precipitation and temperature.	Climate change is included in the saturated zone by incorporating changes in the groundwater specific discharge using the groundwater flow scaling factors for monsoonal and glacial-transition climatic states (Section 2.3.9.3.4.1.1).
1.3.07.02.0A Water table rise affects SZ	Climate change could produce increased infiltration, leading to a rise in the regional water table, possibly affecting radionuclide release from the repository by altering flow and transport pathways in the saturated zone. A regionally higher water table and change in saturated zone flow patterns might move discharge points closer to the repository.	Water table rise and the effect of increased flow (due to wetter future climate conditions) on the saturated zone breakthrough curves are modeled using scaling factors representing the future climate states. The scaling factors used in this approach are the ratio of average saturated zone groundwater flow under the future climatic conditions to the flow under present conditions (Section 2.3.9.3.3.3.4). The scaling factors are a direct input to TSPA. Alterations of flow and transport pathways in the saturated zone due to water table rise are not explicitly included in the saturated zone flow and transport abstraction model simulations. However, transport simulations with the site-scale saturated zone transport model adapted for an estimated higher water table indicate that the simplified approach with the abstraction model results in faster simulated transport of radionuclides. For glacial transition climatic conditions, natural discharge points for groundwater from beneath the repository would not be closer to the repository than US 95.

Table 2.3.9-1. Included Saturated Zone Features, Events, and Processes (Continued)

FEP Number and FEP Name	FEP Description	Summary of Technical Basis/Approach for FEP Inclusion
1.4.01.01.0A Climate modification increases recharge	Climate modification causes an increase in recharge in the Yucca Mountain region. Increased recharge might lead to increased flux through the repository, perched water, or water table rise.	Climate modification is expected to lead to an increase in precipitation and net infiltration (Section 2.3.1). The increased net infiltration will become increased recharge to the saturated zone. As more recharge enters the saturated zone, the water table may rise (see FEP 1.3.07.02.0A) and the volumetric flow of groundwater will increase. The larger flow in the saturated zone is simulated by a groundwater specific discharge scaling factor that increases the flow of water in the saturated zone corresponding to future climate conditions without changing the position of the water table (Sections 2.3.9.2.3.4, 2.3.9.3.3.3.4, and 2.3.9.3.4.1.1). The scaling factors are a direct input to the TSPA.
1.4.07.02.0A Wells	One or more wells drilled for human use (e.g., drinking water, bathing) or agricultural use (e.g., irrigation, animal watering) may intersect the contaminant plume.	Dilution of radionuclide concentrations in groundwater used by the RMEI occurs both during transport in the saturated zone because of dispersion and in the representative volume from which groundwater is extracted by wells to meet the annual demand (Section 2.3.9). The site-scale saturated zone flow model domain was made sufficiently large to include wells in the Amargosa Desert at the southern end of the modeled area (Section 2.3.9.2.1). At the accessible environment, located about 18 km south of Yucca Mountain, the RMEI is postulated to use well water that is extracted from the aquifer (Section 2.3.9). All radionuclide mass reaching the downgradient accessible environment is captured by the wells of the receptor group (Section 2.3.9).
2.2.03.01.0A Stratigraphy	Stratigraphic information is necessary information for the performance assessment. This information should include identification of the relevant rock units, soils and alluvium, and their thickness, lateral extents, and relationships to each other. Major discontinuities should be identified.	The site-scale HFM is a representation of the hydrogeologic units and major structural features within the saturated zone flow system, encompassed by the domain of the site-scale saturated zone flow model (Section 2.3.9.2.2.2). To represent the geologic heterogeneity introduced by stratigraphy in a groundwater model, geologic units were simplified into hydrogeologic units on the basis of similar hydrogeologic properties. The rocks and surficial deposits in the vicinity of Yucca Mountain were classified into 23 hydrogeologic units (Section 2.3.9.2.2.2).

Table 2.3.9-1. Included Saturated Zone Features, Events, and Processes (Continued)

FEP Number and FEP Name	FEP Description	Summary of Technical Basis/Approach for FEP Inclusion
2.2.03.02.0A Rock properties of host rock and other units	Physical properties, such as porosity and permeability of the relevant rock units, soils, and alluvium, are necessary for the performance assessment. Possible heterogeneities in these properties should be considered. Questions concerning events and processes that may cause these physical properties to change over time are considered in other FEPs.	Physical rock and other unit properties are included in the site-scale saturated zone flow and transport models through information regarding the geology, hydrogeology, recharge–discharge relationships, and hydrochemistry of the saturated zone flow system near Yucca Mountain (Section 2.3.9.3). The site-scale saturated zone flow model assigns representative properties for permeability and porosity to each node in the computation grid (Section 2.3.9.2.3.1). Uncertainty in rock properties of host rock and other units are included in the saturated zone flow and transport abstraction model for the following parameters: dispersivity, flowing interval spacing, flowing interval porosity, effective diffusion coefficients, sorption coefficients in volcanic and alluvium units, and bulk density in alluvium units (Section 2.3.9.3.3.4).
2.2.07.12.0A Saturated groundwater flow in the geosphere	Groundwater flow in the saturated zone below the water table may affect long-term performance of the repository. The location, magnitude, and direction of flow under present and future conditions and the hydraulic properties of the rock are all relevant.	Steady-state, saturated, three-dimensional groundwater flow within the Yucca Mountain vicinity is modeled through the site-scale saturated zone flow model. Flow through fractures is modeled through an effective continuum flow model. The continuum approach allows the use of widely accepted mathematical equations describing groundwater flow through porous medium as the mathematical basis for the site-scale saturated zone flow model (Section 2.3.9.2.3.1). In the future, wetter monsoon and glacial-transition climatic conditions will increase the amount of recharge to the regional groundwater flow system. The effect of increased flow on the saturated zone breakthrough curves is modeled using a scaling factor representing the alternative climate state (Section 2.3.9.3.3.3.4).
2.2.07.13.0A Water-conducting features in the SZ	Geologic features in the saturated zone may affect groundwater flow by providing preferred pathways for flow.	To represent discrete features and regions having distinct hydrologic properties within the site-scale saturated zone flow model domain, a set of 10 hydrogeologic features complementary to the HFM were identified and incorporated into the site-scale saturated zone flow model (Section 2.3.9.2.3.1). In the volcanic tuffs, fractures and faults often have common orientations, and it is likely that preferential flow paths exist along these features. Anisotropy in horizontal permeability of the volcanic tuffs affects uncertainty in flow paths (Section 2.3.9.2.3.4)

Table 2.3.9-1. Included Saturated Zone Features, Events, and Processes (Continued)

FEP Number and FEP Name	FEP Description	Summary of Technical Basis/Approach for FEP Inclusion
2.2.07.15.0A Advection and dispersion in the SZ	Advection and dispersion processes may affect radionuclide transport in the saturated zone.	The processes of advection and dispersion are modeled in the saturated zone transport models using the advective–dispersive transport equations. The equations are implemented using the FEHM code (Section 2.3.9.3.3.1). Uncertainty in advection and dispersion process-related parameters are included in Section 2.3.9.3.2.1. Parameters used in the models related to dispersion are longitudinal dispersivity, horizontal transverse dispersivity, and vertical transverse dispersivity (Section 2.3.9.3.3.4).
2.2.07.16.0A Dilution of radionuclides in groundwater	Dilution due to mixing of contaminated and uncontaminated water may affect radionuclide concentrations in groundwater during transport in the saturated zone and during pumping at withdrawal wells.	Dilution of radionuclide concentrations in groundwater used by the RMEI occurs both during transport in the saturated zone because of dispersion and in the representative volume from which groundwater is extracted by wells to meet the annual demand (Section 2.3.9).
2.2.07.17.0A Diffusion in the SZ	Molecular diffusion processes may affect radionuclide transport in the saturated zone.	The molecular diffusion coefficient is included as a component of the dispersion coefficient in radionuclide transport simulations in the saturated zone (Section 2.3.9.3.3.1). The dispersion coefficient is dominated by the hydrodynamic dispersion component for most groundwater flow rates.
2.2.08.01.0A Chemical characteristics of groundwater in the SZ	Chemistry and other characteristics of groundwater in the saturated zone may affect groundwater flow and radionuclide transport of dissolved and colloidal species. Groundwater chemistry and other characteristics, including temperature, pH, Eh, ionic strength, and major ionic concentrations, may vary spatially throughout the system as a result of different rock mineralogy.	Hydrochemical data and chemical data on rock types in the flow system are used to corroborate groundwater flow patterns and flow rates, and to provide input to determine the sorption coefficient distributions (Section 2.3.9.2.2.5). The effect of chemical characteristics of groundwater in the saturated zone on sorption coefficients is reflected in the uncertainty distributions used in the saturated zone transport abstraction model. The effects of potentially reducing conditions in the saturated zone on sorption of redox-sensitive species are not included because zones of low Eh have not been clearly identified and such conditions would result in higher sorption coefficients for technetium and neptunium (Section 2.3.9.3.2.2).
2.2.08.06.0A Complexation in the SZ	Complexing agents, such as carbonate, fluoride, humic, and fulvic acids, present in natural groundwaters could affect radionuclide transport in the saturated zone.	Variations in groundwater chemistry may influence complexation of radionuclides with other aqueous species. Complexation can impact the sorption of radionuclides onto the aquifer material. In particular, the sorption behavior of uranium, neptunium, and plutonium is sensitive to bicarbonate and carbonate concentrations in groundwater. The influence of these variations is incorporated into the uncertainty distributions developed for sorption coefficients (Section 2.3.9.3.2.2)

Table 2.3.9-1. Included Saturated Zone Features, Events, and Processes (Continued)

FEP Number and FEP Name	FEP Description	Summary of Technical Basis/Approach for FEP Inclusion
2.2.08.08.0A Matrix diffusion in the SZ	Matrix diffusion is the process by which radionuclides and other species transported in the saturated zone by advective flow in fractures or other pathways move into the matrix of the porous rock by diffusion. Matrix diffusion can be a very efficient retarding mechanism, especially for strongly sorbed radionuclides due to the increase in rock surface accessible to sorption.	Diffusion in the saturated zone is implemented through a dual porosity effective continuum approach (Section 2.3.9.2.3.1). The saturated zone transport model includes matrix diffusion in the volcanic rock matrix and is parameterized by the effective diffusion coefficient to distinguish it from the free water diffusion coefficient. (Section 2.3.9.3.3.4). Parameters used in the transport models related to matrix diffusion are flowing interval spacing, flowing interval porosity, effective diffusion coefficient, and matrix porosity (Sections 2.3.9.3.3.4 and 2.3.9.3.2.1).
2.2.08.09.0A Sorption in the SZ	Sorption of dissolved and colloidal radionuclides in the saturated zone can occur on the surfaces of both fractures and matrix in rock or soil along the transport path. Sorption may be reversible or irreversible, and it may occur as a linear or nonlinear process. Sorption kinetics and the availability of sites for sorption should be considered. Sorption is a function of the radioelement type, mineral type, and groundwater composition.	Sorption is modeled in the saturated zone transport models using the linear sorption isotherm with sorption coefficient parameters that appear in the equations being treated as effective variables appropriate for the model scale (Section 2.3.9.3.3.3.5). Sorption is modeled to occur in the matrix of fractured volcanic rocks and in the porous medium of the alluvium. Sorption coefficients are primarily based on laboratory measurements using samples from the Yucca Mountain site. These data are combined with information on the variability and uncertainty in hydrochemical and mineralogical composition to assess the uncertainty in sorption coefficients (Section 2.3.9.3.3.4).
2.2.08.10.0A Colloidal transport in the SZ	Radionuclides may be transported in groundwater in the saturated zone as colloidal species. Types of colloids include true colloids, pseudo colloids, and microbial colloids.	The impact of colloid filtration in the saturated zone is incorporated in transport simulations of radionuclides irreversibly attached to colloids with the colloid retardation factor parameter (Section 2.3.9.3.3.4). Radionuclides that are reversibly sorbed onto colloids are modeled as temporarily attached to the surface of colloids. Colloid-facilitated transport of radionuclides reversibly attached to colloids is a function of two parameters: the concentration of colloids in the groundwater and the sorption coefficient for that radionuclide onto colloids (Section 2.3.9.3.3.4). The saturated zone transport models use a semianalytical method to include retardation due to matrix diffusion and sorption and colloid-facilitated transport in a random-walk model (Section 2.3.9.3.3.1).
2.2.10.03.0A Natural geothermal effects on flow in the SZ	The existing geothermal gradient and spatial or temporal variability in that gradient may affect groundwater flow in the saturated zones.	Representative hydrologic properties were assigned to each node in the computational grid. For flow modeling, these properties include permeability, porosity, and viscosity. Because the viscosity of groundwater depends on temperature, the nodal values for viscosity were assigned based on the estimated natural temperature distribution in the subsurface (Sections 2.3.9.2.3.1 and 2.3.9.2.4.2).

Table 2.3.9-1. Included Saturated Zone Features, Events, and Processes (Continued)

FEP Number and FEP Name	FEP Description	Summary of Technical Basis/Approach for FEP Inclusion
2.2.12.00.0B Undetected features in the SZ	Undetected features in the saturated zone portion of the geosphere can affect long-term performance of the disposal system. Undetected but important features may be present, and may have significant impacts. These features include unknown active fracture zones, inhomogeneities, faults and features connecting different zones of rock, and different geometries for fracture zones.	The HFM contains an inherent level of uncertainty that is a function of data distribution and geologic complexity. Uncertainty in the HFM is addressed in the site-scale flow model and is presented in Section 2.3.9.2.3.4. Through the definition and assemblage of the hydrogeologic units integral to its construction, the HFM provides an internally consistent, volume-filling representation of the spatial distribution of block-averaged hydrologic properties within the site-scale saturated zone flow model domain (Section 2.3.9.2.2.2). In general, large-scale hydraulic features (e.g., major faults, fault zones, zones of chemical alteration) have been incorporated into the site-scale model as zones of enhanced or reduced permeability (Section 2.3.9.2.3.1). Undetected features in the saturated zone may impart anisotropy in permeability. Uncertainty in anisotropy of horizontal permeability in fractured volcanic units is included in the saturated zone flow and transport abstraction model (Section 2.3.9.3.3.4). The effects of features, such as the previously undetected zone of high groundwater flow in well 24PB, are included within the range of transport model results from the saturated zone flow and transport abstraction model (Section 2.3.9.3.3.3).
3.1.01.01.0A Radioactive decay and ingrowth	Radioactivity is the spontaneous disintegration of an unstable atomic nucleus that results in the emission of subatomic particles. Radioactive species (isotopes) of a given element are known as radionuclides. Radioactive decay of the fuel in the repository changes the radionuclide content in the fuel with time and generates heat. Radionuclide quantities in the system at any time are the result of the radioactive decay and the ingrowth of decay products as a consequence of that decay. Over a 10,000-year performance period, these processes will produce decay products that need to be considered in order to adequately evaluate the release and transport of radionuclides to the accessible environment.	The one-dimensional saturated zone transport model is used to calculate the mass of daughter products from the radioactive decay of several radionuclides (Section 2.3.9.3.4.2.1). The one-dimensional model, which is implemented directly in the TSPA simulations, simulates the radioactive decay and in-growth of radionuclides in four decay chains (Section 2.3.9.3.4.2). Radioactive decay is also applied to radionuclide mass flux calculated with the convolution integral method in the saturated zone flow and transport abstraction model (Section 2.3.9.3.4.1.1).

NOTE: HFM = hydrogeologic framework model.

Table 2.3.9-2.   Specific Discharges and Groundwater Velocities Estimated from the Different Ambient Flow Velocity Analysis Methods as a Function of Assumed Flow Porosity at 19D

Assumed Flow Porosity[a]	Specific Discharge (m/yr) / Groundwater Velocity (m/yr)		
	0.05	0.18	0.3
Peak Arrival Analysis	1.2 / 24.5	2.4 / 13.1	3.0 / 9.9
Late Arrival Analysis[b]	3.9 / 77.1	7.3 / 40.4	9.4 / 31.3
Mean Arrival Analysis[c]	2.0 / 40.3	3.8 / 20.9	4.9 / 16.4
Mean Arrival Analysis[d]	2.5 / 49.1	4.6 / 25.8	6.0 / 20.2
Linked Analytical Solutions	1.5 / 15 with a flow porosity of 0.10 and a longitudinal dispersivity of 5 m.		

NOTE: [a]The three values are approximately the lowest, expected, and highest values of the alluvium flow porosity used in Yucca Mountain performance assessments (SNL 2008b, Figure 6-10).
[b]Time/Volume associated with approximately 86.4% recovery in each test (the final recovery in the 0.5-hr rest period test, which had the lowest final recovery of any test).
[c]Mean arrival time calculated by truncating all tracer response curves at approximately 86.4% recovery in each test.
[d]Alternative mean arrival time calculated by extrapolating the tracer response curves in the 0.5-hr rest period test to 91.3% and truncating the response curves in the 2-day rest-period test to 91.3% recovery (the final recovery in the 30-day rest-period test).

Source: SNL 2007b, Table 6.5-5.

Table 2.3.9-3.   Specific Discharges and Groundwater Velocities at 22S Estimated from Different Drift Analysis Methods as a Function of Assumed Flow Porosity

Assumed Flow Porosity[a]	Specific Discharge (m/yr) / Groundwater Velocity (m/yr)		
	0.05	0.18	0.3
Single-Well Peak Arrival Analysis	0.47 / 9.5	0.89 / 5.0	1.2 / 3.9
Single-Well Late Arrival Analysis[b]	2.2 / 43.8	4.2 / 23.1	5.4 / 17.9
Single-Well Mean Arrival Analysis[c]	0.82 / 16.4	1.6 / 8.6	2.0 / 6.7
Analysis of Cross-Hole Tracer Responses after 159-day Flow Interruption	0.46 / 9.25	1.7 / 9.25	2.8 / 9.25

NOTE: [a]The three values are approximately the lowest, expected, and highest values of the alluvium flow porosity used in Yucca Mountain performance assessments (SNL 2008b, Figure 6-10).
[b]Time/Volume associated with approximately 96.7% recovery in each test.
[c]Mean arrival time calculated by truncating the two tracer response curves at 96.7% recovery in each test.

Source: SNL 2007b, Table 6.5-6.

Table 2.3.9-4.   Model/Analyses Inputs Used in the Saturated Zone Flow and Transport Abstraction Model and the Saturated Zone One-Dimensional Transport Model

Input Name	Input Description	Value or Distribution	Units	Type of Uncertainty
GWSPD	Groundwater specific discharge multiplier (updated uncertainty distribution)	CDF (cumulative distribution function): (Log_{10}-transformed) Probability Value 0.0 −0.951 0.05 −0.506 0.10 −0.394 0.25 −0.208 0.5 0.000 0.75 0.208 0.90 0.394 0.95 0.506 1.0 0.951	NA	Epistemic
FISVO	Flowing interval spacing in volcanic units (updated uncertainty distribution)	CDF: Probability Value 0.0 1.860 0.01 2.925 0.20 12.036 0.50 25.773 0.80 39.965 0.90 45.797 0.92 47.207 0.94 49.115 0.96 51.710 0.98 55.249 0.99 58.439 1.0 80.0	m	Epistemic
Kd_Pu_Col	Plutonium sorption coefficient onto smectite colloids (updated uncertainty distribution)	CDF: Probability Value 0.0 10^2 0.45 5×10^3 0.80 10^4 0.95 5×10^4 1.0 10^5	mL/g	Epistemic
Kd_Cs_Col	Cesium sorption coefficient onto smectite colloids (updated uncertainty distribution)	CDF: Probability Value 0.0 50 0.05 10^2 0.40 5×10^2 0.70 10^3 1.0 5×10^3	mL/g	Epistemic
FPLANW	Northwestern boundary of the alluvial uncertainty zone (new parameter)	Uniform: Minimum 0.0 Maximum 1.0	NA	Epistemic

Table 2.3.9-4.   Model/Analyses Inputs Used in the Saturated Zone Flow and Transport Abstraction Model and the Saturated Zone One-Dimensional Transport Model (Continued)

Input Name	Input Description	Value or Distribution	Units	Type of Uncertainty
Kd_Se_Vo	Selenium sorption coefficient for devitrified tuff in volcanic units (new parameter)	Truncated Log-Normal: Mean 14.0. Standard Deviation 11.2 Minimum 1.0 Maximum 50.0	mL/g	Epistemic
Kd_Se_Al	Selenium sorption coefficient for devitrified tuff in alluvium (new parameter)	Truncated Log-Normal: Mean 14.0. Standard Deviation 11.2 Minimum 1.0 Maximum 50.0	mL/g	Epistemic
Kd_Sn_Col	Tin sorption coefficient onto smectite colloids (new parameter)	Log-Uniform: Minimum 10^5 Maximum 10^6	mL/g	Epistemic
Kd_Sn_Vo	Tin sorption coefficient for devitrified tuff in volcanic units (new parameter)	Log-Uniform: Minimum 10^2 Maximum 10^5	mL/g	Epistemic
Kd_Sn_Al	Tin sorption coefficient for devitrified in alluvium (new parameter)	Log-Uniform: Minimum 10^2 Maximum 10^5	mL/g	Epistemic
Correlation matrix for K_d sampling in the saturated zone	Correlation coefficient values among radionuclides and between volcanic units and alluvium	See SNL 2008b, Tables 6-8 and 6-7[a]	NA	NA
sw_x_min_up	UTM easting minimum, upper SW corner of alluvial uncertainty zone	549110	m	NA
sw_x_max_up	UTM easting maximum, upper SW corner of alluvial uncertainty zone	547600	m	NA
ne_x_min_up	UTM easting minimum, upper NE corner of alluvial uncertainty zone	553280	m	NA
ne_x_max_up	UTM easting maximum, upper NE corner of alluvial uncertainty zone	552800	m	NA
sw_x_min_low	UTM easting minimum, lower SW corner of alluvial uncertainty zone	550000	m	NA
sw_x_max_low	UTM easting maximum, lower SW corner of alluvial uncertainty zone	547600	m	NA
ne_x_min_low	UTM easting minimum, lower NE corner of alluvial uncertainty zone	552500	m	NA
ne_x_max_low	UTM easting maximum, lower NE corner of alluvial uncertainty zone	552800	m	NA

Table 2.3.9-4. Model/Analyses Inputs Used in the Saturated Zone Flow and Transport Abstraction Model and the Saturated Zone One-Dimensional Transport Model (Continued)

Input Name	Input Description	Value or Distribution	Units	Type of Uncertainty
sw_y_min_up	UTM northing minimum, upper SW corner of alluvial uncertainty zone	4062470	m	NA
sw_y_max_up	UTM northing maximum, upper SW corner of alluvial uncertainty zone	4063400	m	NA
ne_y_min_up	UTM northing minimum, upper NE corner of alluvial uncertainty zone	4065900	m	NA
ne_y_max_up	UTM northing maximum, upper NE corner of alluvial uncertainty zone	4066000	m	NA
sw_y_min_low	UTM northing minimum, lower SW corner of alluvial uncertainty zone	4062470	m	NA
sw_y_max_low	UTM northing maximum, lower SW corner of alluvial uncertainty zone	4063400	m	NA
ne_y_min_low	UTM northing minimum, lower NE corner of alluvial uncertainty zone	4064590	m	NA
ne_y_max_low	UTM easting maximum, lower NE corner of alluvial uncertainty zone	4066000	m	NA
sw_z_min_low	Elevation minimum, lower SW corner of alluvial uncertainty zone	686	m	NA
sw_z_max_low	Elevation maximum, lower SW corner of alluvial uncertainty zone	727	m	NA
ne_z_min_low	Elevation minimum, lower NE corner of alluvial uncertainty zone	616	m	NA
ne_z_max_low	Elevation maximum, lower NE corner of alluvial uncertainty zone	726	m	NA
KDNPVO	Neptunium sorption coefficient in volcanic units	CDF: Probability / Value 0.0 / 0.0 0.05 / 0.99 0.90 / 1.83 1.0 / 6.0	mL/g	Epistemic
KDNPAL	Neptunium sorption coefficient in alluvium	CDF: Probability / Value 0.0 / 1.8 0.05 / 4.0 0.95 / 8.7 1.0 / 13.0	mL/g	Epistemic

Table 2.3.9-4.   Model/Analyses Inputs Used in the Saturated Zone Flow and Transport Abstraction Model and the Saturated Zone One-Dimensional Transport Model (Continued)

Input Name	Input Description	Value or Distribution	Units	Type of Uncertainty
KDSRVO	Strontium sorption coefficient in volcanic units	Uniform: Minimum 20 Maximum 400	mL/g	Epistemic
KDSRAL	Strontium sorption coefficient in alluvium	Uniform: Minimum 20 Maximum 400	mL/g	Epistemic
KDUVO	Uranium sorption coefficient in volcanic units	CDF: <u>Probability</u> <u>Value</u> 0.0 0.0 0.05 5.39 0.95 8.16 1.0 20.0	mL/g	Epistemic
KDUAL	Uranium sorption coefficient in alluvium	CDF: <u>Probability</u> <u>Value</u> 0.0 1.7 0.05 2.9 0.95 6.3 1.0 8.9	mL/g	Epistemic
KDRAVO	Radium sorption coefficient in volcanic units	Uniform: Minimum 100 Maximum 1,000	mL/g	Epistemic
KDRAAL	Radium sorption coefficient in alluvium	Uniform: Minimum 100 Maximum 1,000	mL/g	Epistemic
KD_Pu_Vo	Plutonium sorption coefficient in volcanic units	CDF: <u>Probability</u> <u>Value</u> 0 10 0.25 89.9 0.95 129.87 1.0 300	mL/g	Epistemic
KD_Pu_Al	Plutonium sorption coefficient in alluvium	Beta: Mean 100 Standard Deviation 15 Minimum 50 Maximum 300	mL/g	Epistemic

Table 2.3.9-4.   Model/Analyses Inputs Used in the Saturated Zone Flow and Transport Abstraction Model and the Saturated Zone One-Dimensional Transport Model (Continued)

Input Name	Input Description	Value or Distribution	Units	Type of Uncertainty
KD_Am_Vo	Americium sorption coefficient in volcanic units	Truncated Normal: Mean 5,500 Standard Deviation 1,500 Minimum 1,000 Maximum 10,000	mL/g	Epistemic
KD_Am_Al	Americium sorption coefficient in alluvium	Truncated Normal: Mean 5,500 Standard Deviation 1,500 Minimum 1,000 Maximum 10,000	mL/g	Epistemic
KD_Cs_Vo	Cesium sorption coefficient in volcanic units	CDF: Probability Value 0.0 100 0.05 3,000.59 1.0 6,782.92	mL/g	Epistemic
KD_Cs_Al	Cesium sorption coefficient in alluvium	Truncated Normal: Mean 728 Standard Deviation 464 Minimum 100 Maximum 1,000	mL/g	Epistemic
CORAL	Colloid retardation factor in alluvium	CDF: (Log$_{10}$-transformed) Probability Value 0.0 0.903 0.331 0.904 0.50 1.531 1.0 3.715	NA	Epistemic
CORVO	Colloid retardation factor in volcanic units	CDF: (Log$_{10}$-transformed) Probability Value 0.0 0.778 0.15 0.779 0.25 1.010 0.50 1.415 0.80 1.778 1.0 2.903	NA	Epistemic

Table 2.3.9-4.   Model/Analyses Inputs Used in the Saturated Zone Flow and Transport Abstraction Model and the Saturated Zone One-Dimensional Transport Model (Continued)

Input Name	Input Description	Value or Distribution	Units	Type of Uncertainty
HAVO	Ratio of horizontal anisotropy in permeability	CDF: Probability Value 0.0 0.05 0.0042 0.2 0.0168 0.4 0.0379 0.6 0.0674 0.8 0.10 1.0 0.60 5. 0.744 8. 0.856 11. 0.936 14. 0.984 17. 1.0 20.	NA	Epistemic
LDISP[a]	Longitudinal dispersivity	Normal: (Log_{10}-transformed) Mean 2.0 Standard Deviation 0.75	m	Epistemic
Kd_Am_Col	Americium sorption coefficient onto colloids	CDF: Probability Value 0.0 10^4 0.07 5×10^4 0.17 10^5 0.40 5×10^5 0.60 10^6 0.92 10^6 1.0 10^7	mL/g	Epistemic
Conc_Col	Groundwater concentration of colloids	CDF: (Log_{10}-transformed) Probability Value 0.0 −9.0 0.50 −7.0 0.75 −6.0 0.90 −5.0 0.98 −4.3 1.0 −3.7	g/mL	Epistemic
NVF26	Effective porosity in shallow alluvium	Truncated Normal: Mean 0.18 Standard Deviation 0.051 Minimum 0.00 Maximum 0.30	NA	Epistemic

Table 2.3.9-4.   Model/Analyses Inputs Used in the Saturated Zone Flow and Transport Abstraction Model and the Saturated Zone One-Dimensional Transport Model (Continued)

Input Name	Input Description	Value or Distribution	Units	Type of Uncertainty
NVF11	Effective porosity in undifferentiated valley fill	Truncated Normal: Mean 0.18 Standard Deviation 0.051 Minimum 0.00 Maximum 0.30	NA	Epistemic
FPVO	Fracture porosity in volcanic units	CDF: (Log_{10}-transformed) Probability Value 0.0 −5.0 0.05 −4.0 0.50 −3.0 0.80 −2.0 1.0 −1.0	NA	Epistemic
DCVO	Effective diffusion coefficient in volcanic units	CDF: (Log_{10}-transformed) Probability Value 0.0 −11.3 0.08 −10.7 0.50 −10.3 0.83 −9.9 1.0 −9.3	m^2/s	Epistemic
bulkdensity	Bulk density of alluvium	Normal: Mean 1910 Standard Deviation 78	kg/m^3	Epistemic
SRC1X SRC1Y SRC2X SRC2Y SRC3X SRC3Y SRC4X SRC4Y	Source regions beneath the repository	Uniform: Minimum 0.0 Maximum 1.0	NA	Epistemic and Aleatory
A1_1_x	UTM easting, SW corner source zone 1	547,570	m	NA
A1_1_y	UTM northing, SW corner source zone 1	4,078,630	m	NA
A1_2_x	UTM easting, SE corner source zone 1	548,500	m	NA
A1_2_y	UTM northing, SE corner source zone 1	4,078,630	m	NA
A1_3_x	UTM easting, NE corner source zone 1	548,500	m	NA

Table 2.3.9-4. Model/Analyses Inputs Used in the Saturated Zone Flow and Transport Abstraction Model and the Saturated Zone One-Dimensional Transport Model (Continued)

Input Name	Input Description	Value or Distribution	Units	Type of Uncertainty
A1_3_y	UTM northing, NE corner source zone 1	4,081,090	m	NA
A1_4_x	UTM easting, NW corner source zone 1	547,570	m	NA
A1_4_y	UTM northing, NW corner source zone 1	4,081,090	m	NA
A2_1_x	UTM easting, SW corner source zone 2	548,500	m	NA
A2_1_y	UTM northing, SW corner source zone 2	4,078,630	m	NA
A2_2_x	UTM easting, SE corner source zone 2	549,320	m	NA
A2_2_y	UTM northing, SE corner source zone 2	4,078,630	m	NA
A2_3_x	UTM easting, NE corner source zone 2	549,320	m	NA
A2_3_y	UTM northing, NE corner source zone 2	4,081,210	m	NA
A2_4_x	UTM easting, NW corner source zone 2	548,500	m	NA
A2_4_y	UTM northing, NW corner source zone 2	4,081,210	m	NA
A3_1_x	UTM easting, SW corner source zone 3	547,720	m	NA
A3_1_y	UTM northing, SW corner source zone 3	4,076,170	m	NA
A3_2_x	UTM easting, SE corner source zone 3	548,500	m	NA
A3_2_y	UTM northing, SE corner source zone 3	4,076,170	m	NA
A3_3_x	UTM easting, NE corner source zone 3	548,500	m	NA
A3_3_y	UTM northing, NE corner source zone 3	4,078,630	m	NA
A3_4_x	UTM easting, NW corner source zone 3	547,720	m	NA
A3_4_y	UTM northing, NW corner source zone 3	4,078,630	m	NA

Table 2.3.9-4. Model/Analyses Inputs Used in the Saturated Zone Flow and Transport Abstraction Model and the Saturated Zone One-Dimensional Transport Model (Continued)

Input Name	Input Description	Value or Distribution	Units	Type of Uncertainty
A4_1_x	UTM easting, SW corner source zone 4	548,500	m	NA
A4_1_y	UTM northing, SW corner source zone 4	4,076,170	m	NA
A4_2_x	UTM easting, SE corner source zone 4	548,890	m	NA
A4_2_y	UTM northing, SE corner source zone 4	4,076,170	m	NA
A4_3_x	UTM easting, NE corner source zone 4	548,890	m	NA
A4_3_y	UTM northing, NE corner source zone 4	4,078,630	m	NA
A4_4_x	UTM easting, NW corner source zone 4	548,500	m	NA
A4_4_y	UTM northing, NW corner source zone 4	4,078,630	m	NA
Max_al_por	Total alluvium porosity	0.30	NA	NA
Fpor	Average fracture porosity in volcanic units	0.001	NA	NA
Mpor	Average matrix porosity in volcanic units	0.22	NA	NA
Bdens	Average bulk density in volcanic units	1.88	g/mL	NA
Matrix porosity	Expected values for matrix porosity per volcanic unit	Unit 15: 0.15 Units 14, 10, and 8: 0.25 Unit 13: 0.23 Unit 12: 0.18 Unit 11: 0.21 Unit 9: 0.21	NA	NA
Bulk Density	Expected bulk density values per volcanic unit	Unit 18: 2.50 Units 17, 6, 5, and 3: 2.77 Unit 16: 2.44 Unit 15: 2.08 Units 14, 10 and 8: 1.77 Unit 13: 1.84 Unit 12: 2.19 Unit 11: 2.11 Unit 9: 2.05 Units 4 and 2: 2.55 Unit 1: 2.65	g/cm^3	NA

Table 2.3.9-4.   Model/Analyses Inputs Used in the Saturated Zone Flow and Transport Abstraction Model and the Saturated Zone One-Dimensional Transport Model (Continued)

Input Name	Input Description	Value or Distribution	Units	Type of Uncertainty
Effective Porosity	Expected effective porosity values for other units (SNL 2008b, Section 6.5.2.20)	Unit 18: 0.32 Unit 17: 0.01 Unit 16: 0.08 Units 6, 5 and 3: 0.01 Unit 4: 0.18 Unit 2: 0.18 Unit 1: 0.0001	NA	NA

NOTE: [a]The sampled values and the uncertainty distribution of the parameter LDISP have been modified for implementation in the saturated zone flow and transport abstraction model, and the saturated zone one-dimensional transport model, as documented in Section 2.3.9.3.3.4.
The unit numbers refer to the HFM unit definitions in SNL 2008b, Table 6-9.
CDF = cumulative distribution function; HFM = hydrogeologic framework model; NA = not applicable.

Source: SNL 2008b, Tables 6-8 and 6-7[a].

Table 2.3.9-5. Comparison of Target and Site-Scale Volumetric/Mass Flow Rates

Boundary Zone Range	Target Flow		Site-Scale Flow		Calibration Weight
	Flow (kg/s)	Flow (m³/yr)	Flow (kg/s)	Flow (m³/yr)	
North (533,000–563,000)	−158.9	-5.0×10^{6}	−57.1	-1.8×10^{6}	5
West (4,046,500–4,091,500)	−120.3	-3.9×10^{6}	−101.0	-3.2×10^{6}	5
East1 (4,046,500–4,052,500)	−273.1	-8.6×10^{6}	−232.1	-7.3×10^{6}	1
East2 (4,052,501–4,058,500)	33.3	1.0×10^{6}	−97.4	-3.1×10^{6}	1
East3 (4,058,501–4,069,000)	−127.8	-4.0×10^{6}	260.9	8.2×10^{6}	1
East4 (4,069,001–4,079,500)	30.2	9.5×10^{5}	−206.6	6.5×10^{6}	1
East5 (4,079,501–4,091,500)	−0.4	-1.2×10^{4}	−30.7	-9.7×10^{5}	1
South (533,000–563,000)	681.9	2.2×10^{7}	528.1	1.7×10^{7}	NA

NOTE: The weights for the north, west, and east boundaries are each given a value of 5, but the east boundary is the sum of 5 segments, each with a weight of 1. Negative values indicate flow into the model. South boundary volumetric/mass flow rates were not used as targets for the calibration of the site-scale saturated zone flow model; rather, in both models they were calculated from the balance of infiltration and the volumetric/mass flow rates across north, west, and east boundaries.

Conversion factor: $m^{3}/yr = \dfrac{m^{3}}{1,000kg} \cdot \dfrac{86,400s}{day} \cdot \dfrac{365.25day}{yr} \cdot \dfrac{kg}{s}$

Source: SNL 2007a, Table 6-11.

Table 2.3.9-6.   Summary of Vertical Head Differences Observed at Boreholes in the Vicinity of Yucca Mountain

Borehole	Open Interval (m below land surface)	Potentiometric Level (m above sea level)	Head Difference, Deepest to Shallowest Intervals (m)
USW H-1 tube 4	573 to 673	730.94	54.7
USW H-1 tube 3	716 to 765	730.75	
USW H-1 tube 2	1,097 to 1,123	736.06	
USW H-1 tube 1	1,783 to 1,814	785.58	
USW H-3 upper	762 to 1,114	731.19	28.9
USW H-3 lower	1,114 to 1,219	760.07	
USW H-4 upper	525 to 1,188	730.49	0.1
USW H-4 lower	1,188 to 1,219	730.56	
USW H-5 upper	708 to 1,091	775.43	0.2
USW H-5 lower	1,091 to 1,219	775.65	
USW H-6 upper	533 to 752	775.99	2.2
USW H-6 lower	752 to 1,220	775.91	
USW H-6	1,193 to 1,220	778.18	
UE-25 b#1 upper	488 to 1,199	730.71	−1.0
UE-25 b#1 lower	1,199 to 1,220	729.69	
UE-25 p#1 (volcanic)	384 to 500	729.90	21.4
UE-25 p#1 (carbonate)	1,297 to 1,805	751.26	
UE-25 c#3	692 to 753	730.22	0.4
UE-25 c#3	753 to 914	730.64	
USW G-4	615 to 747	730.3	−0.5
USW G-4	747 to 915	729.8	
UE-25 J#13 upper	282 to 451	728.8	−0.8
UE-25 J#13	471 to 502	728.9	
UE-25 J#13	585 to 646	728.9	
UE-25 J#13	820 to 1,063	728.0	
NC-EWDP-1DX (shallow)	Water table to 419	786.8	−38.0
NC-EWDP-1DX (deep)	658 to 683	748.8	

Table 2.3.9-6.   Summary of Vertical Head Differences Observed at Boreholes in the Vicinity of Yucca Mountain (Continued)

Borehole	Open Interval (m below land surface)	Potentiometric Level (m above sea level)	Head Difference, Deepest to Shallowest Intervals (m)
NC-EWDP-2D (volcanic)	Water table to 493	706.1	7.2
NC-EWDP-2DB (carbonate)	820 to 937	713.3	
NC-EWDP-3S probe 2	103 to 129	719.8	−1.5
NC-EWDP-3S probe 3	145 to 168	719.4	
NC-EWDP-3D	Water table to 762	718.3	
NC-EWDP-4PA	124 to 148	717.9	5.7
NC-EWDP-4PB	225 to 256	723.6	
NC-EWDP-9SX probe 1	27 to 37	766.7	0.1
NC-EWDP-9SX probe 2	43 to 49	767.3	
NC-EWDP-9SX probe 4	101 to 104	766.8	
NC-EWDP-12PA	99 to 117	722.9	2.2
NC-EWDP-12PB	99 to 117	723.0	
NC-EWDP-12PC	52 to 70	720.7	
NC-EWDP-19P	109 to 140	707.5	5.3
NC-EWDP-19D	106 to 433	712.8	

NOTE: Negative values indicate downward gradient.

Source: BSC 2004a, Table 6-4.

Table 2.3.9-7. Compositions of Waters Used in Sorption Experiments

Chemical Constituent	UE-25 J-13 Well Water	Range of Concentrations in Downgradient Wells in Volcanics (mg/L)	Range of Concentrations in Downgradient Wells in Alluvium (mg/L)	UE-25 p#1 (Carbonate) Water (mg/L)	Synthetic p#1 Water (mg/L)
Ca^{2+}	11.5	0.8 to 37	0.8 to 20.3	87.8	—
Mg^{2+}	1.76	<0.1 to 10	0.0 to 7.7	31.9	—
Na^+	45	38 to 120	57.9 to 180.5	171	261
K^+	5.3	1.1 to 8.9	1.8 to 5.5	13.4	—
SiO_2	64.2	36 to 57	40.5 to 61	37.3	—
Cl^-	6.4	6.0 to 13	5.6 to 18	37	—
F^-	2.1	1.0 to 6.7	1.6 to 4.2	3.5	—
SO_4^{2-}	18.1	14 to 38	18.7 to 61.7	129	—
HCO_3^-	143	107 to 344	110 to 255.5	698	691
CO_3^{2-}	0.0	0.0	0.0 to 23.5	0.0	—
pH	6.9	6.8 to 8.4	7.5 to 8.9	6.7	—
Eh	—	—	128 to 197 mV	—	—

Source: SNL 2008a, Tables A-2a and A-2b.

Table 2.3.9-8. Hydrologic Features in the Site-Scale Saturated Zone Flow Model

Feature Name and Description	Number of Nodes	Hydrogeologic Characteristics	Impact on Model
1. Fortymile Wash Fault (#401 and #402) This is a north-south trending feature east of Yucca Mountain. Vertically, it extends from top to bottom of the model.	3,317 and 2,028	Possible control of fluid pathways near Yucca Mountain. Because this fault is likely a conducting feature, it is defined isotropically.	The fault is a possible preferential flow path.
2. Bare Mountain Fault (#41) This is a northwest- to southeast-trending feature in the southwestern corner of the model. Vertically, it extends from top to bottom of the model.	7,939	This fault has a vertical permeability anisotropy factor of 10.	The fault directs flow from Crater Flat to the Amargosa Desert.
3. Crater Flat Fault (#42) This is a north-south trending feature in the western half of the model, starting south of the Claim Canyon and terminating near U.S. Highway 95, almost halfway between the western boundary of the model and the Solitario Canyon Fault. Vertically, it extends from top to bottom of the model.	7,095	This fault has plane parallel permeability anisotropy factor of 10.	The fault generates a higher head in the western half of the model thereby limiting the inflow from the western boundary (it restricts the flow to the east).
4. U.S. Highway 95 Fault (#43) This is an east-west trending feature in the lower half of the western portion of the model. Vertically, it extends from top to bottom of the model, but it does not continue through the alluvial units defining the Lower Fortymile Wash zone.	3,633	This fault has plane parallel permeability anisotropy factor of 10.	This fault restricts flow in the north-south direction and supports high heads to its north.
5. Sever Wash Fault (#46) This is a northwest-southeast trending feature. Vertically, it extends from top to bottom of the model.	2,437	This fault has a vertical permeability anisotropy factor of 10.	This fault may serve to divert southerly flow around the repository to the east thereby facilitating southeast flow paths from the repository.
6. Solitario Canyon Fault (#44) This is a north-south trending feature just to the west of Yucca Mountain. Vertically, it extends from top to bottom of the model.	7,041	This fault has plane parallel permeability anisotropy factor of 10.	This fault generates a higher head to the west of Yucca Mountain and impedes flow from Crater Flat to Yucca Mountain.

Table 2.3.9-8. Hydrologic Features in the Site-Scale Saturated Zone Flow Model (Continued)

Feature Name and Description	Number of Nodes	Hydrogeologic Characteristics	Impact on Model
7. Stage Coach Fault (#45) This fault forms the eastern splay starting at the southerly end of the Solitario Canyon Fault. Vertically, it extends from top to bottom of the model.	1,182	This fault has plane parallel permeability anisotropy factor of 10.	This fault generates a higher head to the west and impedes flow from the east.
8. Windy Wash Fault (#47) This fault forms the eastern splay starting at the southerly end of the Solitario Canyon Fault. Vertically, it extends from top to bottom of the model. Only that portion of the fault south of its connection to the Solitario Canyon Fault is used in the model.	2,437	This fault has plane parallel permeability anisotropy factor of 10.	This fault generates a higher head to the west and impedes flow from the east.
9. Lower Fortymile Wash Alluvial Zone (#50)[a] This is a region of alluvium to the south of Yucca Mountain in the southern half of the model that connects to the southern end of Fortymile Wash Fault.	See footnote [a]	This zone represents the possible increased permeability due to the deposition of alluvium by flowing water in Fortymile Wash.	This zone influences the site-scale saturated zone flow model and it is expected to be important to TSPA due to its effect on solute transport.

Table 2.3.9-8. Hydrologic Features in the Site-Scale Saturated Zone Flow Model (Continued)

Feature Name and Description	Number of Nodes	Hydrogeologic Characteristics	Impact on Model
10. Anisotropic/Crater Flat Zone (#39/#60)[b] This is a region east of the Solitario Canyon Fault and west of Fortymile Wash Fault. It is included in the model to facilitate representation of the low-gradient area southeast of the repository and also to allow the model to better represent the heads in wells USW H-5, G-1, and UZ-14. Furthermore, pumping at the C-holes was in the Lower Bullfrog Unit (within the Crater Flat tuff) and the responses analyzed in ONC-1, H-4, WT-3, and WT-14 are in the combined Miocene tuffaceous rocks, including the Crater Flat tuff. This would also speak to the existence of an area bounded by H-4 on the west, WT-14 on the east, and WT-3 on the south within which there is anisotropy of horizontal hydraulic conductivity in the saturated volcanic rocks. Vertically, it extends from top to bottom of the model, but it is compose only of the three Crater Flat tuffs. This zone also defines the horizontally anisotropic region, but in this instance, it includes all volcanic units within this quadrilateral. (units 12, 14, 15, 16, 17, 18, 19, 20, and 25)	See footnote b	This zone represents a possible permeability increase in the Yucca Mountain region for the Crater Flat units. Also, this zone defines the horizontally anisotropic volcanic units.	This zone may affect the gradient near the repository and also the specific discharge.

NOTE: [a]Zone defined by a bounding quadrilateral (UTM): (x_1, y_1) = 540,000; 4,046,500, (x_2, y_2) = 550,000; 4,046,500, (x_3, y_3) = 552,100; 4,062,400, (x_4, y_4) = 550,840; 4,062,400.

[b]Zone defined by a bounding quadrilateral (UTM): (x_1, y_1) = 548,500; 4,081,288, (x_1, y_1) = 554,100; 4,078,462, (x_1, y_1) = 553,445; 4,067,200, (x_1, y_1) = 546,800; 4,070,549.

Linear interpolation was used to specify fault location coordinates to ensure that spacing between data points defining the fault was never more than 125 m from its neighbors. This guarantees that the fault will be defined with a stair-stepping appearance when viewed from above (each fault node is connected to at least two other fault nodes in the horizontal. Fortymile Wash fault was defined as all nodes within 250 m of the specified fault coordinates. Anisotropy in the horizontal hydraulic conductivity was based on responses of USW H-4, UE-25 C#1, UE-25 WT#14, and UE-25 WT#3 to pumping at the C-holes from May 1996 to November 1997. The range of anisotropies and their directions calculated were included by SNL 2007b, Appendix C6.2. The calculated directions of anisotropy from this effort (derived from the shape of the cone of depression from the C-Wells test) support the principally north-south anisotropy direction between the C-holes and USW H-4 along Antler Wash. The outer perimeter limits of the area of applicability of the results would be USW H-4 on the west, UE-25 WT#14 on the east, and UE-25 WT#3 in the south. Overall, the zone of anisotropy is defined to include all volcanics that fall within a generalized region east of the Solitario Canyon Fault and west of Fortymile Wash Fault.

UTM = Universal Transverse Mercator.

Source: SNL 2007a, Table 6-7.

Table 2.3.9-9.   Wells Used in Validation of the Site Scale Saturated Zone Model with Observed and
Simulated Water Levels

Well ID	Easting (UTM) (m)	Northing (UTM) (m)	z(elevation) (m)	Observed Head (m)	Modeled Head (m)	Water Level Residual (m)
NC-EWDP Phase V wells used for validation						
NC-EWDP-13P	543471	4066433	758.9	764.4	760.0	–4.4
NC-EWDP-22PC upper	552036.	4062019	702.3	724.9	724.5	–0.4
NC-EWDP-24PB	549387	4062025	621.6	727.2	725.9	–1.3
NC-EWDP-32P upper	546183	4054789	696.4	701.7	711.6	9.9
NC-EWDP-33P upper	545117	4057146	713.1	720.8	716.1	–4.8
Non NC-EWDP wells used in gradient validation						
USW H-6 upper	546188	4077816	662.9	776.0	786.2	10.6
USW WT-2	548595	4077028	702.0	730.6	734.6	4.0
USW WT-1	549152	4074967	708.4	730.4	734.5	4.1
UE-25 WT#3	552090	4072550	705.8	729.6	734.2	4.6
NC-EWDP calibration wells used in gradient calculation						
NC-EWDP 19P	549329	4058292	694.7	707.3	717.7	10.4
NC-EWDP 2D	547823	4057170	507.1	706.1	716.6	10.5

NOTE: Datum is mean sea level. z (elevation) is center of screened interval.
            UTM = Universal Transverse Mercator.

Source: SNL 2007a, Table 7-2.

Table 2.3.9-10. Simulated and Observed Hydraulic Gradient for Identified Wells

Flow Segment	$\Delta H/\Delta L$ (Measured)	$\Delta H/\Delta L$ (Simulated)	Relative Difference
USW H-6 to USW-25 WT#2	1.79×10^{-2}	2.04×10^{-2}	0.14
USW-25 WT#2 to USW-25 WT#1	9.37×10^{-5}	4.68×10^{-5}	−0.50
USW-25 WT#1 to UE-25 WT#3	2.10×10^{-4}	7.89×10^{-5}	−0.63
UE-25 WT#3 to NC-EWDP-22PC/24PB	3.37×10^{-4}	8.48×10^{-4}	1.52
NC-EWDP-22PC/24PB to NC-EWDP-19P/2D	4.03×10^{-3}	1.69×10^{-3}	−0.58
NC-EWDP-19P/2D to NC-EWDP-32P	1.59×10^{-3}	1.62×10^{-3}	0.02

NOTE: Data results computed from Table 2.3.9-9.
        NC-EWDP-22PC/24PB uses the average location and head values for wells NC-EWDP-22PC and
        NC-EWDP-24PB.
        NC-EWDP-19P/2D uses the average location and head values for wells NC-EWDP-19P and NC-EWDP-2D.

Source: SNL 2007a, Table 7-1.

Table 2.3.9-11. Summary of Bases for Regional Flow Paths and Mixing Zones Derived from Geochemistry Observations

Flow Path or Mixing Zone (Figure 2.3.9-18)	Geochemical Flow Path or Mixing Zone Description	Geochemical Evidence of Flow Path or Mixing Zone
1	Oasis Valley through the Amargosa Desert along the axis of the Amargosa River to the confluence with Fortymile Wash	Areal plots of chloride and scatterplots of SO_4^{2-} versus Cl^-. Groundwater along this flow path becomes more dilute to the south as it becomes increasingly mixed with groundwater near Fortymile Wash. Upstream of this mixing zone, high groundwater ^{14}C activities and variable δD and $\delta^{18}O$ compositions indicate the presence of relatively young recharge in the groundwater due to runoff or irrigation in the area.
2	Fortymile Canyon area southward along the axis of Fortymile Wash into the Amargosa Desert	Similar anion and cation concentrations along the flow line and dissimilarities compared to regions to the east and west. Groundwater along the northern part of this flow path is distinguished from groundwater at Yucca Mountain by δD and $\delta^{18}O$ compositions that are heavier or more offset from the Yucca Mountain meteoric water line than the groundwater found under Yucca Mountain. Based on the observation that ^{14}C activities do not decrease systematically southward in the northern or southern segments of the wash, some part of the groundwater along Fortymile Wash may also be derived from recharge due to runoff or irrigation in the area.
3	Jackass Flats in the vicinity of well UE-25 J-11 southward along the western edge of the Lathrop Wells area and southward through boreholes in the Fortymile Wash–East area	High SO_4^{2-} and low $\delta^{34}S$ characteristics of groundwater from well UE-25 J-11 distinguish it from the high SO_4^{2-} and high $\delta^{34}S$ groundwater characteristic of the Gravity Fault and the low SO_4^{2-} and low $\delta^{34}S$ groundwater of Fortymile Wash. A scatter plot of $\delta^{34}S$ versus $1/SO_4^{2-}$ indicates a mixing trend involving well UE-25 J-11 as an end member, with wells in the Lathrop Wells and Fortymile Wash–East groups having up to 20% of a UE-25 J-11–like groundwater. These mixing relations were confirmed with PHREEQC inverse models involving selected boreholes in these groups.
4	Lower Beatty Wash area into northwestern Crater Flat. This groundwater flows predominantly southward in Crater Flat past boreholes USW VH-1 and NC-EWDP-3D.	Scatterplots and PHREEQC inverse models show that a mixture of groundwater is required to account for the Cl^-, δD, and $\delta^{18}O$ compositions characteristic of this flow path. East of Flow Path 4, the extremely light $\delta^{13}C$ and high $\delta^{87}Sr$ of groundwater in northern Yucca Mountain compared to Timber Mountain groundwater indicates that groundwater from the Timber Mountain and Beatty Wash areas is not the dominant component of groundwater at Yucca Mountain north of Drill Hole Wash. This path includes the possibility that groundwater from the Crater Flat region, or from the direction of well VH-1, or possibly a mix of these waters, flows southeast to the region of the Nye County wells 27P, 16P, and 28P.

Table 2.3.9-11. Summary of Bases for Regional Flow Paths and Mixing Zones Derived from Geochemistry Observations (Continued)

Flow Path or Mixing Zone (Figure 2.3.9-18)	Geochemical Flow Path or Mixing Zone Description	Geochemical Evidence of Flow Path or Mixing Zone
5	Southwest Crater Flat Group	Chemically and isotopically distinct from groundwater that characterizes flow path 4, with higher concentrations of most major ions (but lower concentrations of fluoride and SiO_2), and relatively high $\delta^{18}O$ and δD. Groundwater in Oasis Valley has some of the lightest oxygen and hydrogen isotopic compositions in the Yucca Mountain area, eliminating flow from Oasis Valley under Bare Mountain as a possible source of groundwater in southwest Crater Flat. A more likely source for groundwater along this flow path is local recharge at Bare Mountain, a source indicated by the similarly heavy δD and $\delta^{18}O$ compositions of perched water emanating from a spring at Bare Mountain (Specie Spring) and groundwater in southwest Crater Flat. This similarity indicates that local recharge and runoff from Bare Mountain may be the source of groundwater along this flow path, as schematically indicated by the dashed nature of the beginning of this flow path in Figure 2.3.9-18.
6	From borehole USW WT-10 southward toward borehole NC-EWDP-15P	This flow path is identified from PHREEQC models that indicate that groundwater from borehole NC-EWDP-15P is formed from subequal amounts of groundwater from boreholes USW WT-10 and USW VH-1, and less than 5% of groundwater from the regional Paleozoic carbonate aquifer. Although the predominant direction of flow from the Solitario Canyon area is southward along the Solitario Canyon Fault, evidence for the leakage of small amounts of groundwater eastward across the fault is provided by similarities in the concentrations of many ions and isotopes between boreholes in the Solitario Canyon Wash and Yucca Mountain Crest areas. This chemical and isotopic similarity indicates that groundwater as far east as borehole USW H-4 may have some component of groundwater from the Solitario Canyon Wash area and possibly NC-EWDP-19D. The short southeast-oriented dashed lines from boreholes in the Solitario Canyon Group schematically illustrate this leakage. New geochemical data from Nye County wells 27P, 16P and 28P confirm a southerly flow from the Solitario Canyon Wash area along this flow path. Slightly elevated sulfate and chloride values in two samples suggest that groundwater from regions to the northwest and /or west are added along this flow path. The exact source of these groundwaters is not well constrained by the data.
7	From northern Yucca Mountain southeastward toward Yucca Mountain–southeast boreholes in the Dune Wash area, then southwestward along the western edge of Fortymile Wash	The upper segment of this flow path is motivated by the high groundwater $^{234}U/^{238}U$ activity ratios found in the northern Yucca Mountain and Dune Wash areas. High $^{234}U/^{238}U$ activity ratios (greater than 7) typify perched water and groundwater along and north of Drill Hole Wash but not groundwater along Yucca Crest at borehole USW SD-6 or perched water at borehole USW SD-7. Based on the conceptual model for the evolution of $^{234}U/^{238}U$ activity ratios, congruent dissolution of thick vitric tuffs that underlie the Topopah Spring welded tuff along Yucca Crest south of Drill Hole Wash would be expected to decrease the $^{234}U/^{238}U$ activity ratios of deep unsaturated zone percolation south of the wash. High $^{234}U/^{238}U$ activity ratios are expected only where these vitric tuffs are absent, as in northern Yucca Mountain.

Table 2.3.9-11. Summary of Bases for Regional Flow Paths and Mixing Zones Derived from Geochemistry Observations (Continued)

Flow Path or Mixing Zone (Figure 2.3.9-18)	Geochemical Flow Path or Mixing Zone Description	Geochemical Evidence of Flow Path or Mixing Zone
8	Leakage of groundwater from the regional Paleozoic carbonate aquifer across the Gravity Fault	Hydrogeologists and geochemists have recognized leakage across the fault (Winograd and Thordarson 1975, p. 85; Claassen 1985, p. F3). The carbonate aquifer component in this groundwater is recognized by many of the same chemical and isotopic characteristics that typify groundwater discharging from the regional Paleozoic carbonate aquifer at Ash Meadows. These characteristics include high concentrations of Ca and Mg, low SiO_2, heavy $\delta^{13}C$ values, low $\delta^{14}C$ activity, and $\delta^{18}O$ and δD values comparable to Ash Meadows groundwater. Based on new data from Nye County well 23P, an additional arrow indicating eastward flow was added.
9	Deep underflow of groundwater from the carbonate beneath the Amargosa Desert and Funeral Mountains to discharge points in Death Valley	The similarity in the chemical and isotopic characteristics of groundwater found in the Gravity Fault area and groundwater that discharges from Nevares and Travertine springs support this interpretation. The dissimilarity in chlorine, magnesium, and SiO_2 concentrations in these springs compared to the groundwater from the alluvial aquifer along the Amargosa River indicates that this alluvial groundwater is not the predominant source of the spring discharge in Death Valley.
Mix A	Samples from the Nye County and Southwest Crater Flat boreholes along U.S. Highway 95	The zone is demonstrated by groundwater compositions of samples that are intermediate between the compositionally distinct groundwater of the regional Paleozoic carbonate aquifer and dilute groundwater of the volcanic aquifer that is interpreted to have originated in the Yucca Mountain area (see discussion of flow paths 6 and 7).
Mix B	Samples from the Fortymile Wash–west and Amargosa River–Fortymile Wash groups, plus a few samples from the Fortymile Wash–south group	The zone highlights groundwater with compositions that are intermediate between the distinct and consistent groundwater compositions of the Amargosa River Group and the dilute groundwater of the Fortymile Wash–south group.
Mix C	All samples from the Lathrop Wells and Fortymile Wash–east groups, a few of the more westerly samples form the Gravity Fault group, and at least one sample (#141) from the Fortymile Wash–south group	Characterized by small percentages of the distinctively high SO_4 groundwater from Well UE-25 J-11. Groundwater with this distinctive signature is mixed to variable degrees with dilute water from the Fortymile Wash–south group to the west or with groundwater from the regional Paleozoic carbonate aquifer (Gravity Fault Group) to the east. New data from Nye County well 23P has led to the extension of mixing zone C slightly to the north.

Source: Adapted from SNL 2007a, Appendix A and Section B6.6.

Table 2.3.9-12. Flowing Interval Porosity from Conservative Tracer Tests

Tracer Test	Unit	Boreholes (UE-25)	Flowing Interval Porosity
Single-Porosity, Partial-Recirculating Solution: 2,4,5 TFBA	Prow Pass	c#3 to c#2	0.05%
Dual-Porosity, Partial-Recirculating Solution: 2,4,5 TFBA	Prow Pass	c#3 to c#2	0.05%
Iodide	Bullfrog-Tram	c#2 to c#3	8.60%
Difluorobenzoic acid	Lower Bullfrog	c#2 to c#3	7.2% to 9.9%
Pyridone	Lower Bullfrog	c#1 to c#3	NA

NOTE: This parameter (flowing interval porosity) may be called effective flow porosity in the analysis model report.
        TFBA = trifluorobenzoic acid.

Source: SNL 2007b, Tables D-2 and D-3.

Table 2.3.9-13. Flowing Interval Porosity Values from Multiple Tracer Tests

Tracer Test	Lower Bound Flowing Interval Porosity	Upper Bound Flowing Interval Porosity
Prow Pass	0.3%	0.6%
Lower Bullfrog	0.3%	3.1%

Source: SNL 2007b, Table D-10.

Table 2.3.9-14. Recommended Composite Distribution for K_ds In Volcanics and Alluvium

Species	Unit/Analysis	Distribution	Coefficents Describing Distribution (mL/g)
Uranium	Composite (Volcanics)	Cumulative	(K_d, prob) (0, 0.) (5.39, 0.05) (8.16, 0.95) (20, 1.0)
	Alluvium	Cumulative	(K_d, prob) (1.7, 0.) (2.9, 0.05) (6.3, 0.95) (8.9,1.0)
Neptunium	Composite (Volcanics)	Cumulative	(K_d, prob) (0, 0) (0.99, 0.05) (1.83, 0.90) (6, 1.0)
	Alluvium	Cumulative	(K_d, prob) (1.8, 0.) (4.0, 0.05) (8.7, 0.95) (13, 1.0)
Plutonium	Composite (Volcanics)	Cumulative	(K_d, prob) (10, 0.) (89.9, 0.25) (129.87, 0.95) (300, 1.0)
	Alluvium (Devitrified)	Beta	μ = 100, Range = 50 to 300, σ = 15
Cesium	Composite (Volcanics)	Cumulative	(K_d, prob) (100, 0.) (3,000.59, 0.05) (6,782.92, 1.0)
	Alluvium (Devitrified)	Truncated Norm	Range = 100 to 1,000 μ = 728, σ = 464
Americium/ Thorium/ Protactiniu m	Volcanics and Alluvium	Truncated Norm	Range = 1,000 to 10,000 μ = 5,500, σ = 1,500
Strontium	Volcanics and Alluvium	Uniform	Range = 20 to 400
Radium	Volcanics and Alluvium	Uniform	Range = 100 to 1,000
Selenium	Volcanics	Truncated Log Normal	Range = 1 to 50; m = 14.0; s = 11.2
	Alluvium	Truncated Log Normal	Range = 1 to 50; m = 14.0; s = 11.2
Tin	Volcanics	Truncated Log Uniform	Range = 100 to 36,700
	Alluvium	Truncated Log Uniform	Range = 100 to 36,700
Carbon/ Technetium / Iodine	Volcanics and Alluvium	Constant	Zero

NOTE: μ = mean; σ = standard deviation.

Source: Development of the distributions is based on SNL 2008a, Tables A-4 and C-14[a].

Table 2.3.9-15. Carboxylate-Modified Latex Microsphere Filtration Parameters for Multi-pathway Fits to the Microsphere Response using the Nonreactive Transport Parameters Deduced from the Fits to the Trifluorobenzoic Acid and Bromide Breakthrough Curves Assuming the Minimum and Maximum Possible Amounts of Matrix Diffusion

	Parameter	Pathway 1	Pathway 2	Pathway 3
Minimum Diffusion Case	Mass fraction, f (minimum diffusion)	0.05	0.58	0.33
	k_{filt} (1/hr)	0.16	0.048	>0.04
	k_{res} (1/hr)	0.0011	0.00034	—
Maximum Diffusion Case	Mass fraction, f (maximum diffusion)	0.05	0.68	0.27
	k_{filt} (1/hr)	0.16	0.048	>0.045
	k_{res} (1/hr)	0.0011	0.00034	—

NOTE: Other transport parameters used to obtain the fits are given in SNL 2007b, Tables G-14 (minimum diffusion case) and G-15 (maximum diffusion case).

Source: SNL 2007b, Table 6.5-7.

Table 2.3.9-16. Radioelements Transported in the Saturated Zone Flow and Transport Abstraction Model

Radionuclide Number	Transport Mode	Radioelements
1	Solute	Carbon, technetium, iodine, chlorine
2	Colloid-facilitated (reversible)	Americium, thorium, protactinium
3	Colloid-facilitated (reversible)	Cesium
4	Colloid-facilitated (reversible)	Plutonium
5	Solute	Neptunium
6	Colloid-facilitated (irreversible)	Plutonium, americium
7	Solute	Radium
8	Solute	Strontium
9	Solute	Uranium
10	Colloid-facilitated (fast fraction of irreversible)	Plutonium, americium
11	Solute	Selenium
12	Colloid-Facilitated (Reversible)	Tin

Source: SNL 2008b, Table 6-9[a].

Table 2.3.9-17. Chemistry and Ages of Groundwater from Seven Boreholes at Yucca Mountain

Borehole	$^{234}U/^{238}U$ Activity Ratio	^{14}C Activity (pmc)	DIC, as HCO_3^- (mg/L)	Corrected ^{14}C Age (years)	Uncorrected ^{14}C Age (years)
USW G-2	7.6	20.5	127.6	13,100	13,100
UE-25 WT#17	7.6	16.2	150.0	13,750 to 14,710	15,040
UE-25 WT#3	7.2	22.3	144.3	11,430 to 12,380	12,400
UE-25 WT#12	7.2	11.4	173.9	15,430 to 16,390	17,950
UE-25 c#3	8.1	15.7	140.2	14,570 to 15,300	15,300
UE-25 b#1 (Tcb)	—	18.9	152.3	12,350 to 13,300	13,770
USW G-4	—	22.0	142.8	11,630 to 12,510	12,500

NOTE: DIC = dissolved inorganic carbon; pmc = percent modern carbon.

Source: SNL 2007a, Table A6-7.

INTENTIONALLY LEFT BLANK
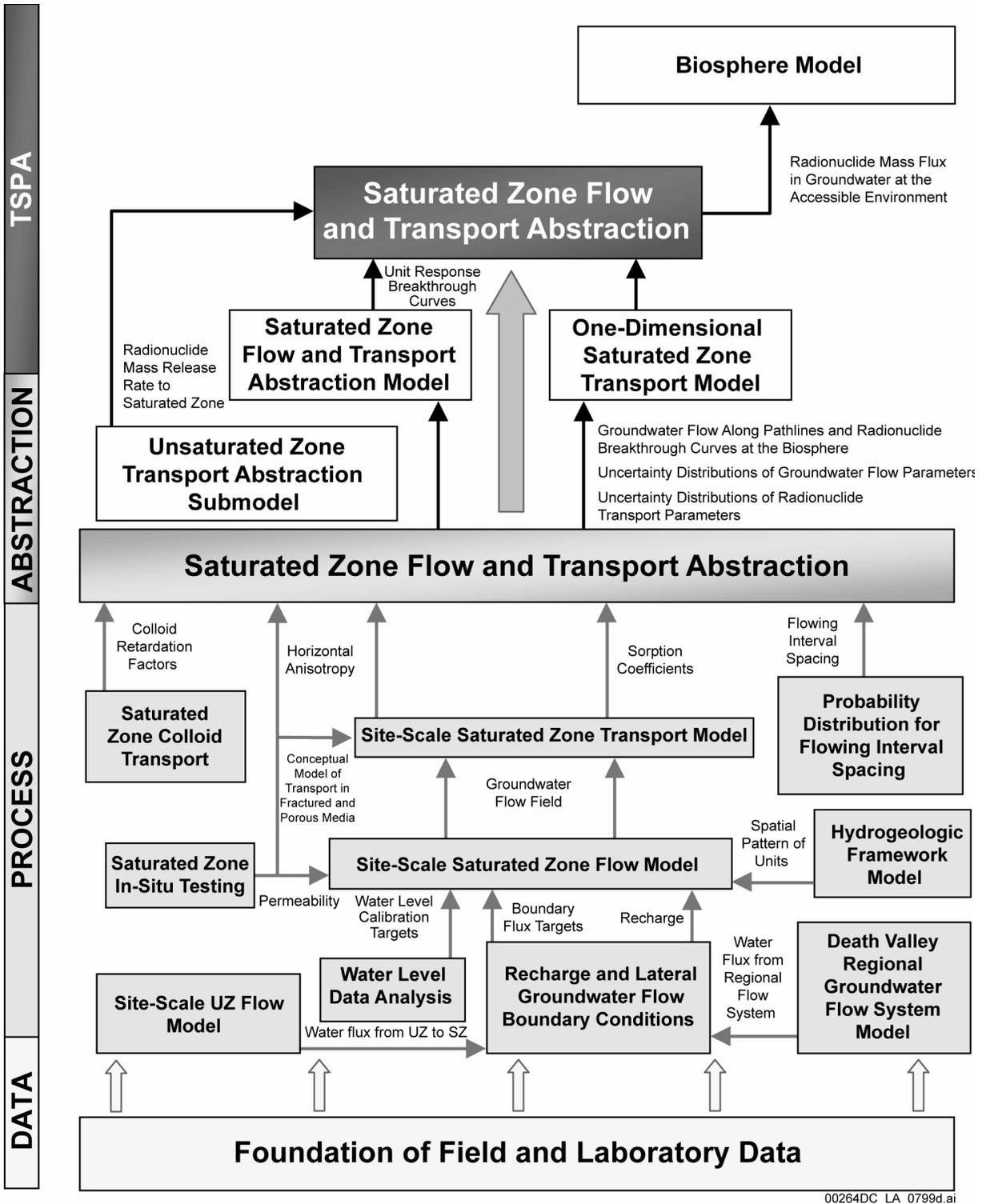
Figure 2.3.9-1.   Information Flow Supporting TSPA Saturated Zone Calculations at the Data, Process, Abstraction, and TSPA Levels

NOTE: SZ = saturated zone; UZ = unsaturated zone.

Source: Adapted from SNL 2008b, Figure 1-1.
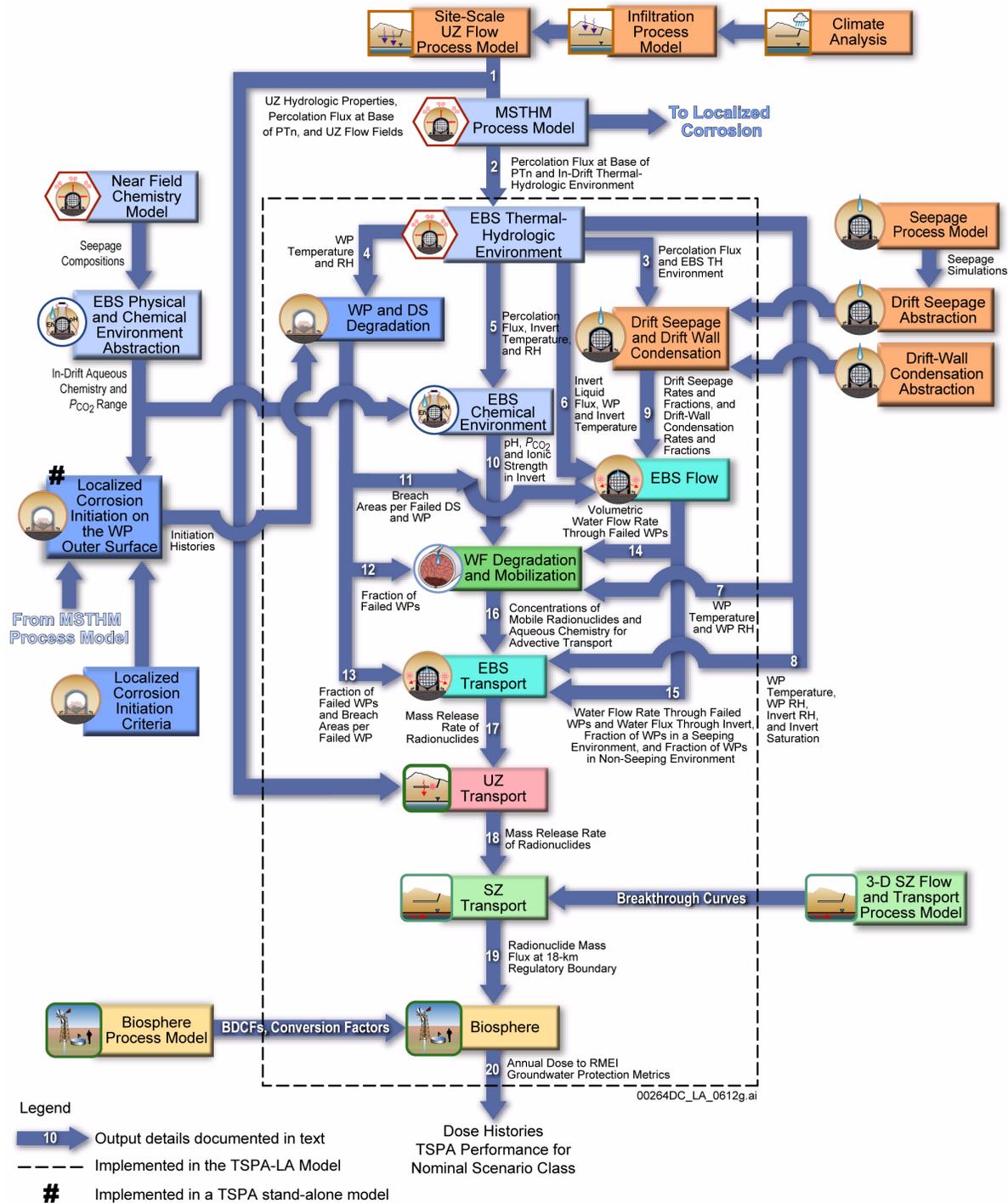
Figure 2.3.9-2.   Information Transfer among the Principal Model Components of the TSPA Nominal Scenario Class Model

NOTE: Three-dimensional saturated zone flow and transport process model is the same as the saturated zone flow and transport abstraction model described in Section 2.3.9.3.4.1.1.
BDCFs = biosphere dose conversion factors; DS = drip shield; EBS = Engineered Barrier System;
LC = localized corrosion; PA = performance assessment; RH = relative humidity; SZ = saturated zone;
TH = thermal-hydrologic; UZ = unsaturated zone; WF = waste form; WP = waste package. For details about outputs and information transfer shown on this figure, see Section 2.4.2.3.2.1.
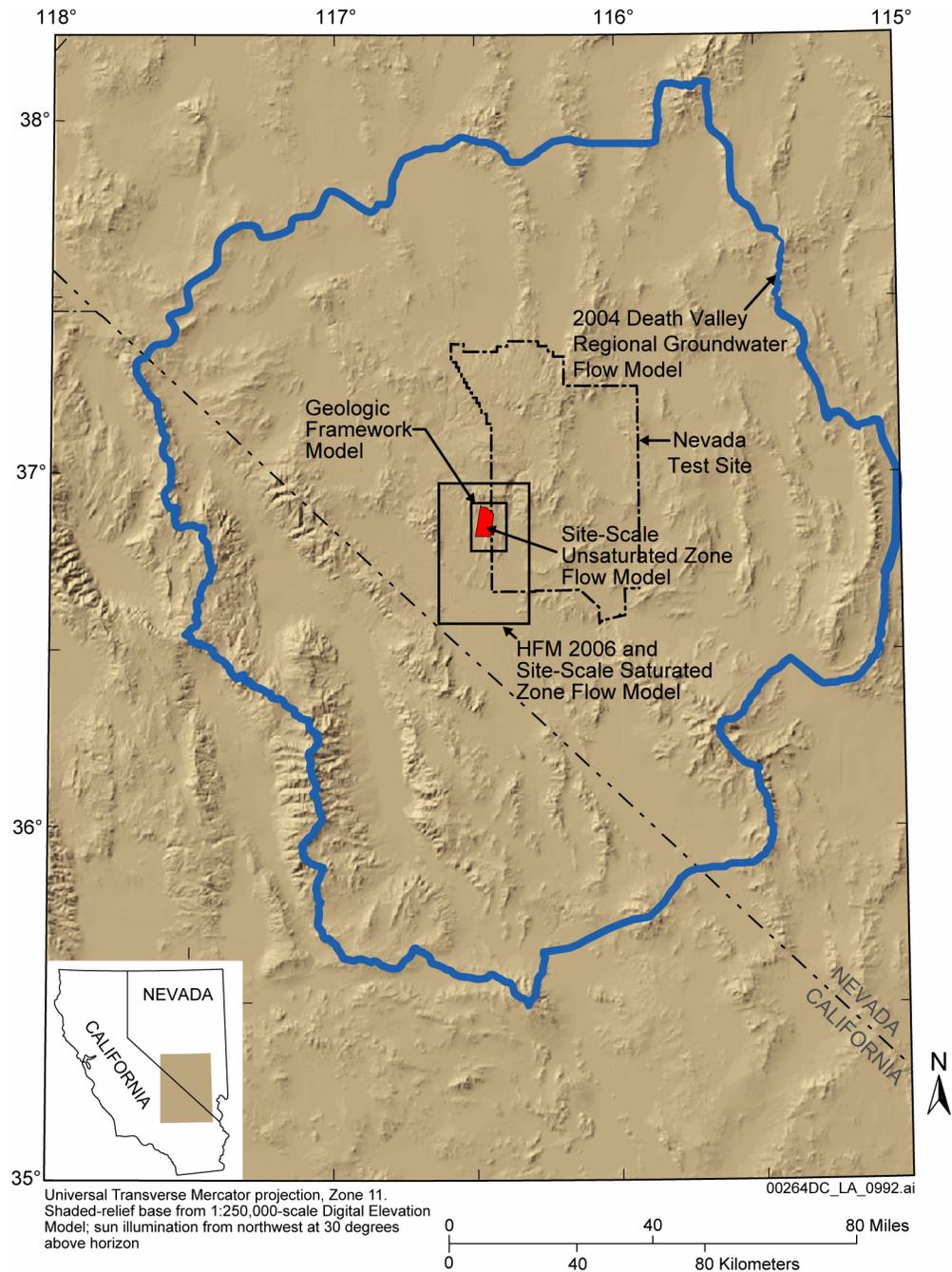
Figure 2.3.9-3. Map Showing the Boundaries of Regional and Site-Scale Models

NOTE: HFM = hydrogeologic framework model.

Source: Adapted from SNL 2007c, Figure 6-1.
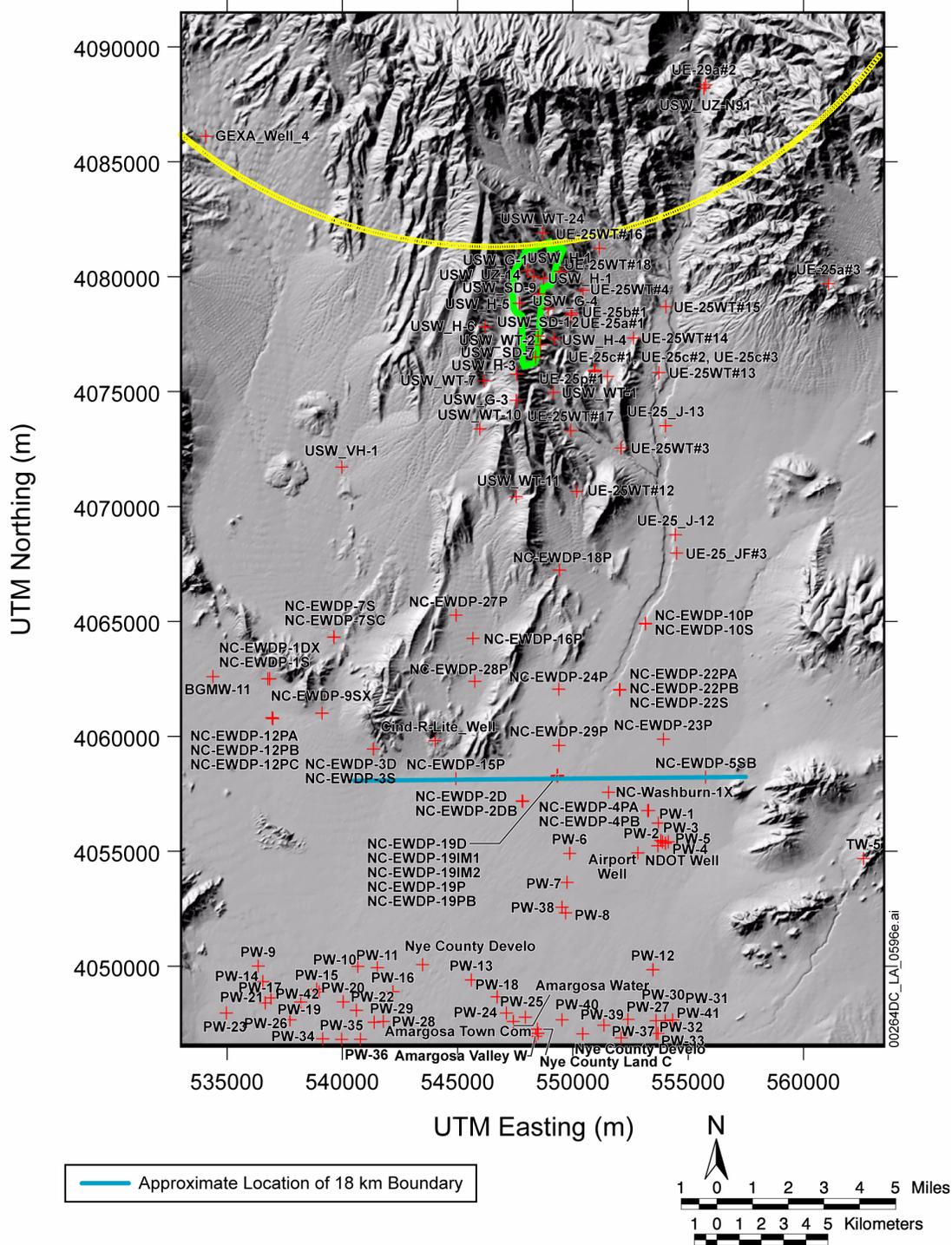
Figure 2.3.9-4.   Map Showing the Locations of Boreholes Used to Characterize Groundwater Flow and
                    Boundary of the Site-Scale Saturated Zone Flow Model

NOTE: The yellow arc at the top of the figure is the thermally altered zone and also represents the area of high
        hydraulic gradient. The straight blue line is the southern edge of the postclosure controlled area boundary
        consistent with 10 CFR 63.302.

Source: Adapted from SNL 2007a, Table 6-8 and Figure 6-13.
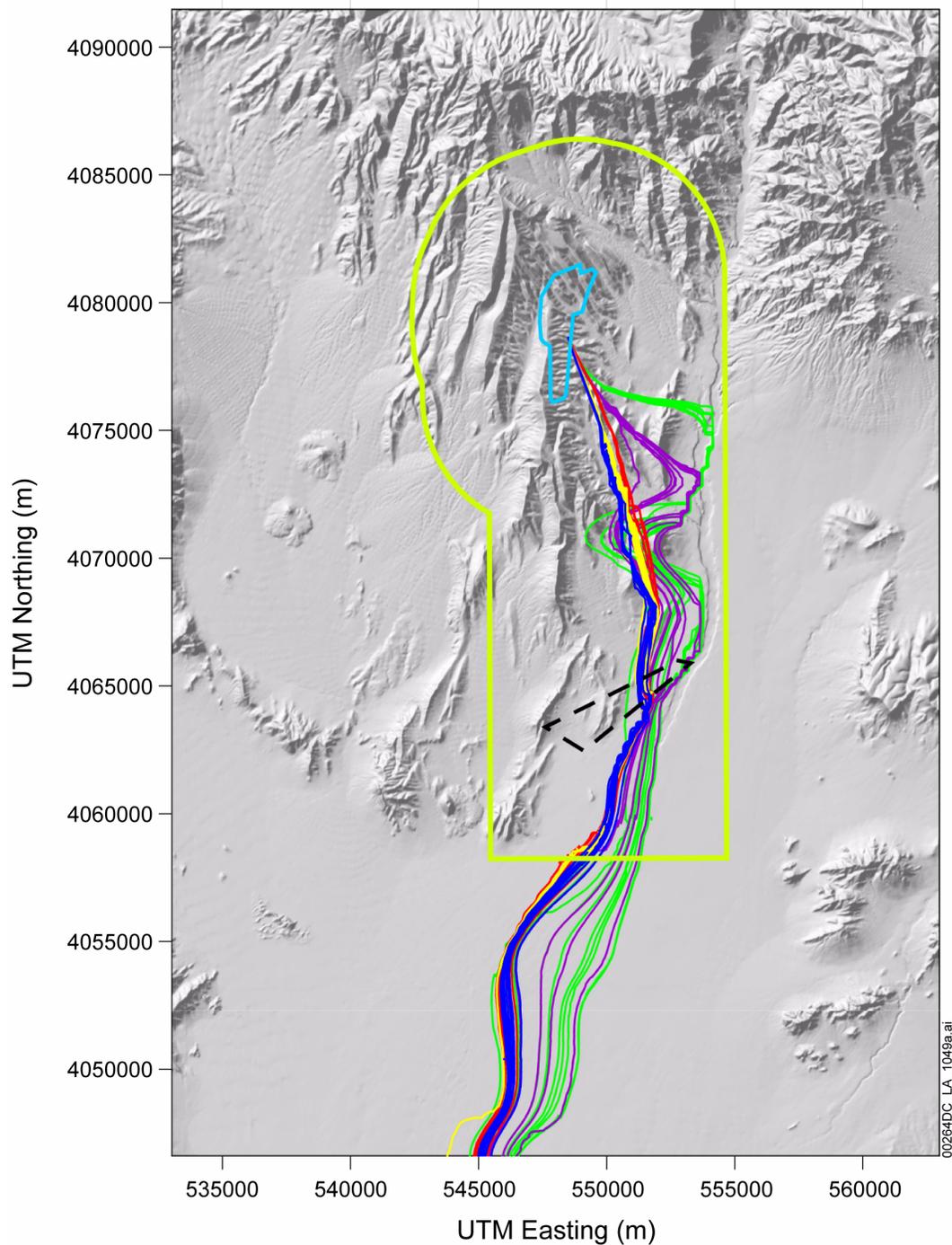
Figure 2.3.9-5. Simulated Particle Paths for Different Values of Horizontal Anisotropy in Permeability

NOTE: Repository boundary is the outside edge of the repository footprint. Black dashed line is the outline of the
Alluvial Uncertainty Zone. Green, purple, blue, yellow, and red lines show simulated particle paths for
horizontal anisotropy values of 0.05, 0.20, 1.0, 5.0, and 20.0, respectively. Postclosure controlled area
boundary is shown with the chartreuse line.
UTM = Universal Transverse Mercator.

Source: SNL 2008b, Figures 6-1[a] and 6-4[a]. Postclosure controlled area boundary from DTN:
MO0712DELNPCCA.001.
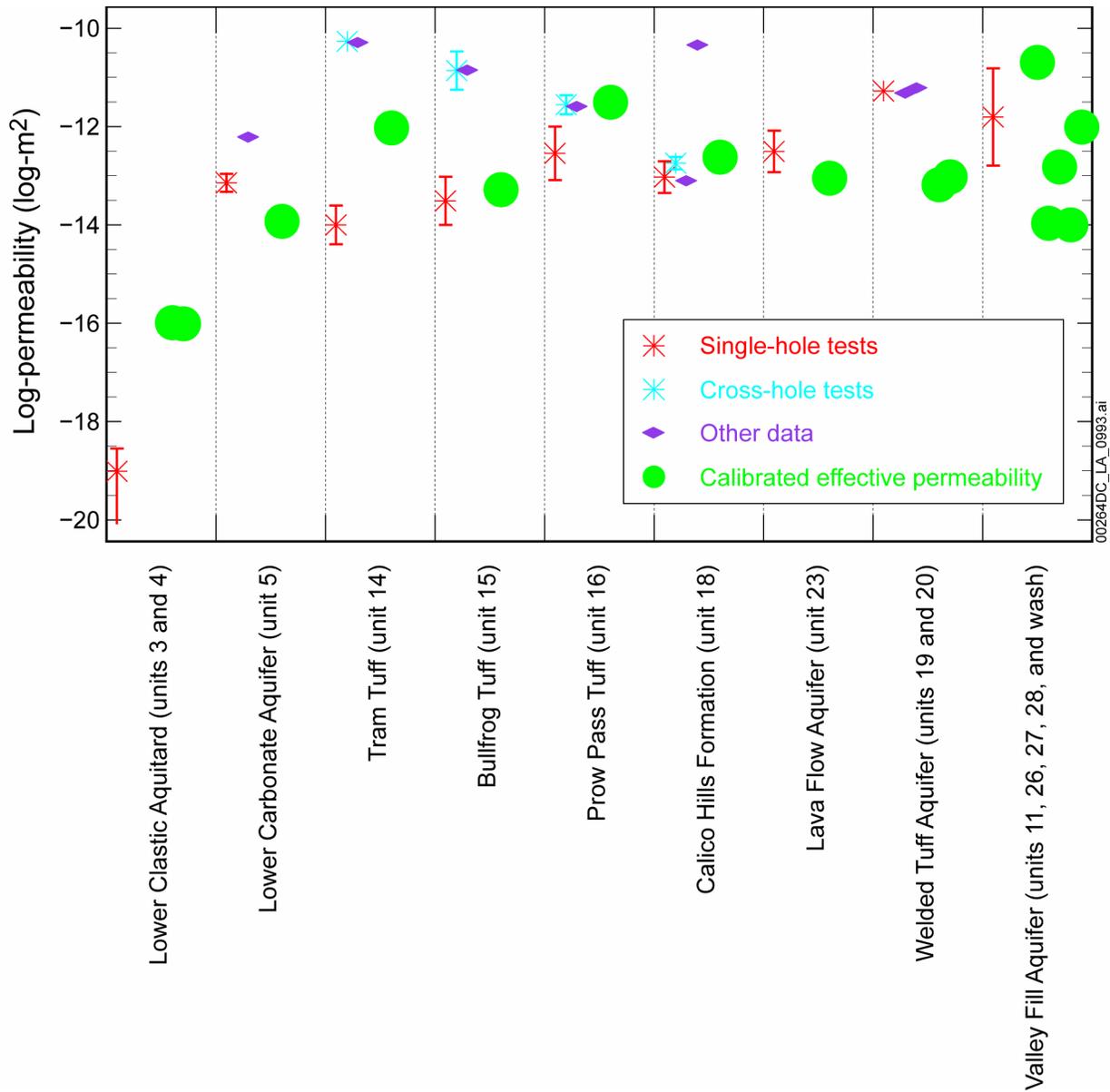
Figure 2.3.9-6.   Logarithms of Permeabilities Estimated During Model Calibration Compared to Mean Logarithms of Permeability Determined from Pump-Test Data from Yucca Mountain

Source: SNL 2007a, Figure 7-4.
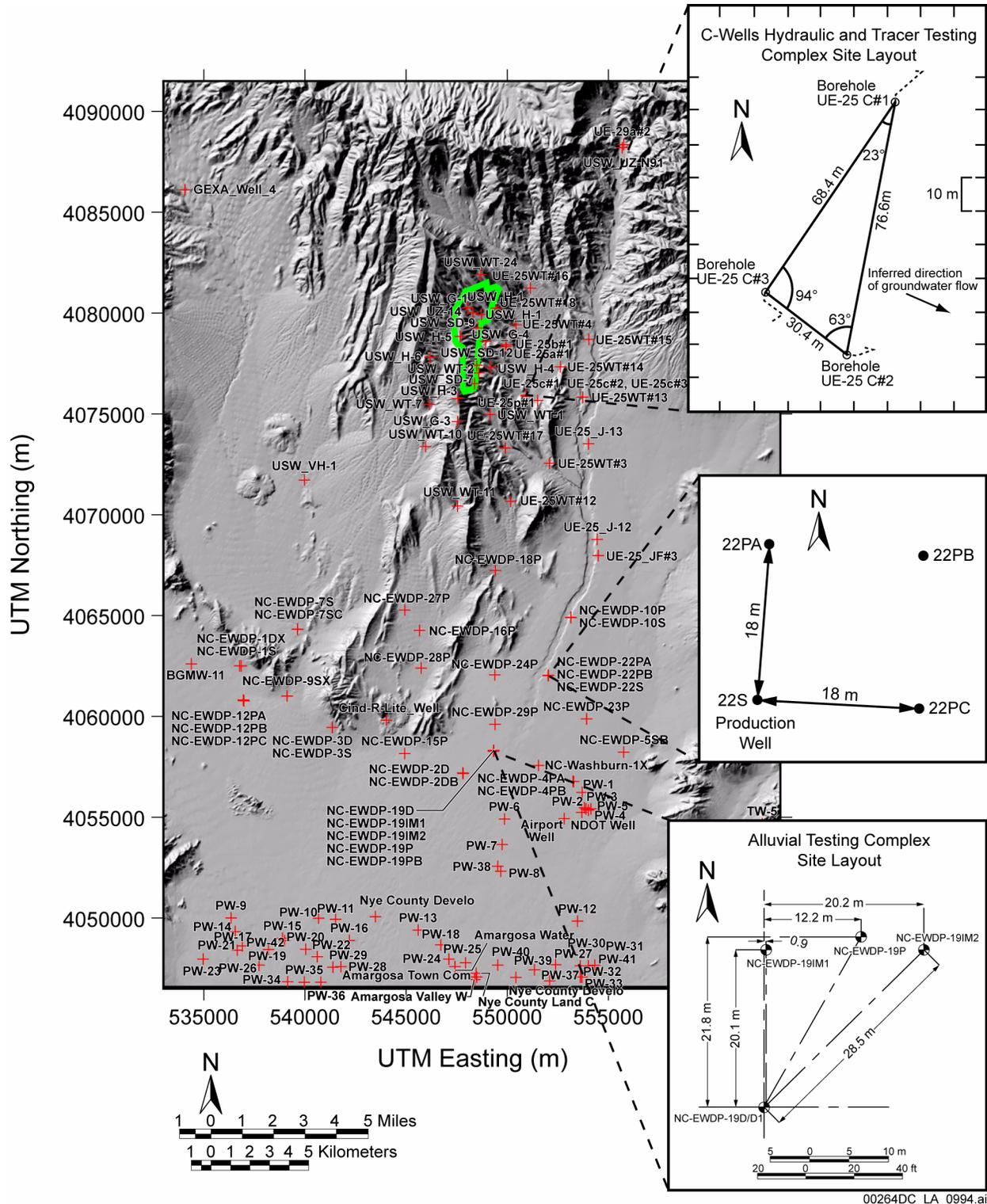
Figure 2.3.9-7.   Location of the C-Wells, NC-EWDP-22 Wells, and the Alluvial Testing Complex with Designators on all Boreholes

Source: SNL 2007b, Figures 6.1-1, 6.1-6, 6.1-7 and 6.1-8; BSC 2004a, Figure 1-2.
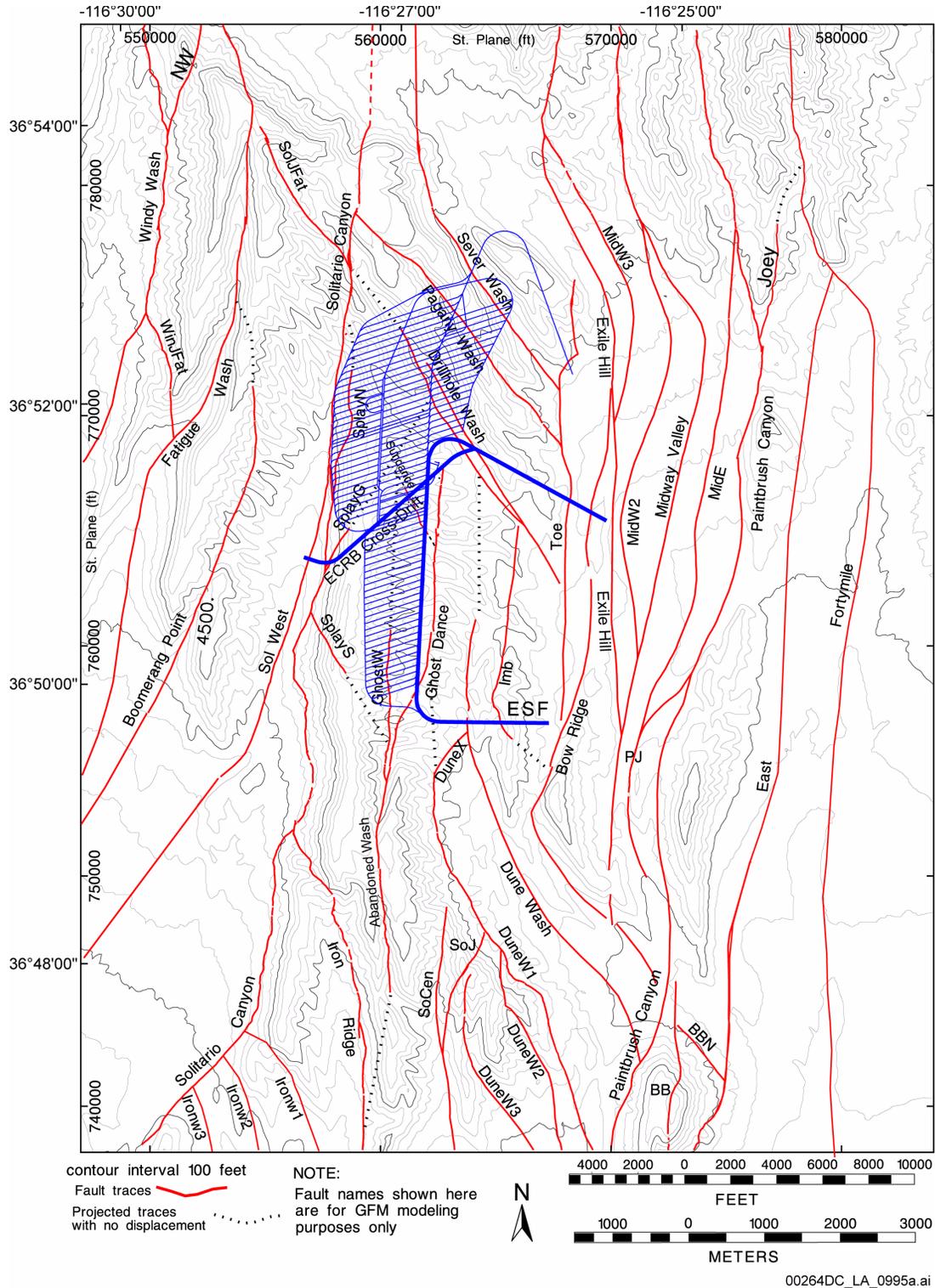
Figure 2.3.9-8. Surface Trace of Faults in the Yucca Mountain Repository Area

NOTE: The dotted lines correspond to cross sections used in the analysis of the site-scale hydrogeologic framework model.

Source: BSC 2004b, Figure 6-2.

00264DC_LA_0976.ai

Legend

Plot 0   Model Fit
Plot 1   Data Curve
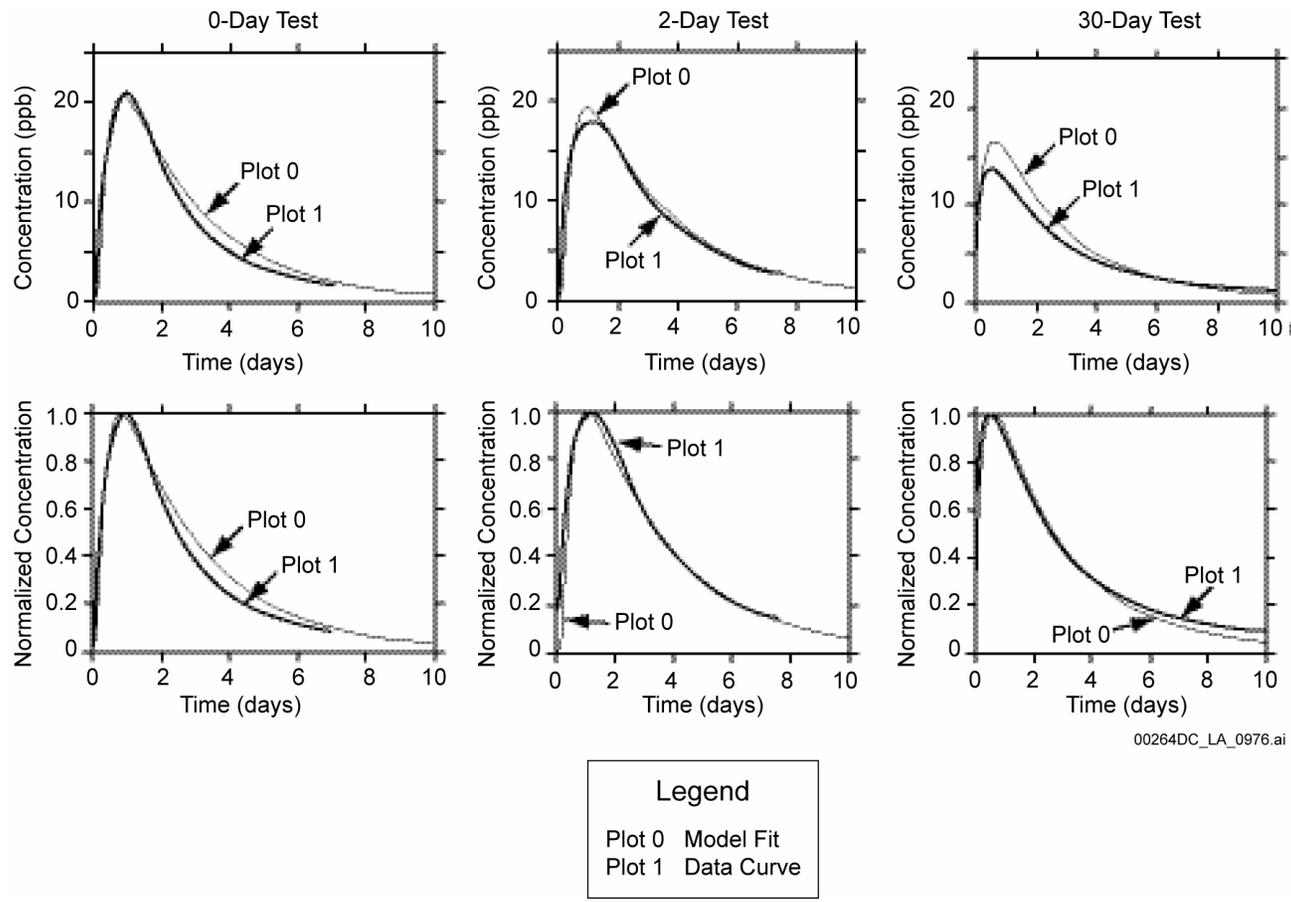
Figure 2.3.9-9. Fitting the Injection–Pumpback Tracer Tests in Screen 1 of Borehole NC-EWDP-19D1 Using the Linked-Analytical Solutions Method

NOTE: The plots are fits of three injection–pumpback tracer tests with theoretical curves resulting from three solutions to the advection–dispersion equation for the three phases of injection, drift, and pumpback. "Plot 0" is the model fit, and "Plot 1" is the data curve. The parameters used in the calculations are: flow porosity = 0.1; matrix porosity = 0.0; longitudinal dispersivity = 5.05 m; transverse dispersivity = 1.00 m; test interval thickness = 32.0 ft; tracer volume injected = 2,800 gal; chase volume injected = 22,000 gal; injection rate = 15.0 gpm; mass injected = 5.0 kg; natural gradient = 0.002 m/m; *T* for gradient = 20.0 m^2/day; specific discharge = 1.5 m/yr. The *Q* values for the 0-, 2-, and 30-day tests are 13.41, 11.00, and 13.50, respectively.

Source: SNL 2007b, Figure G-29.
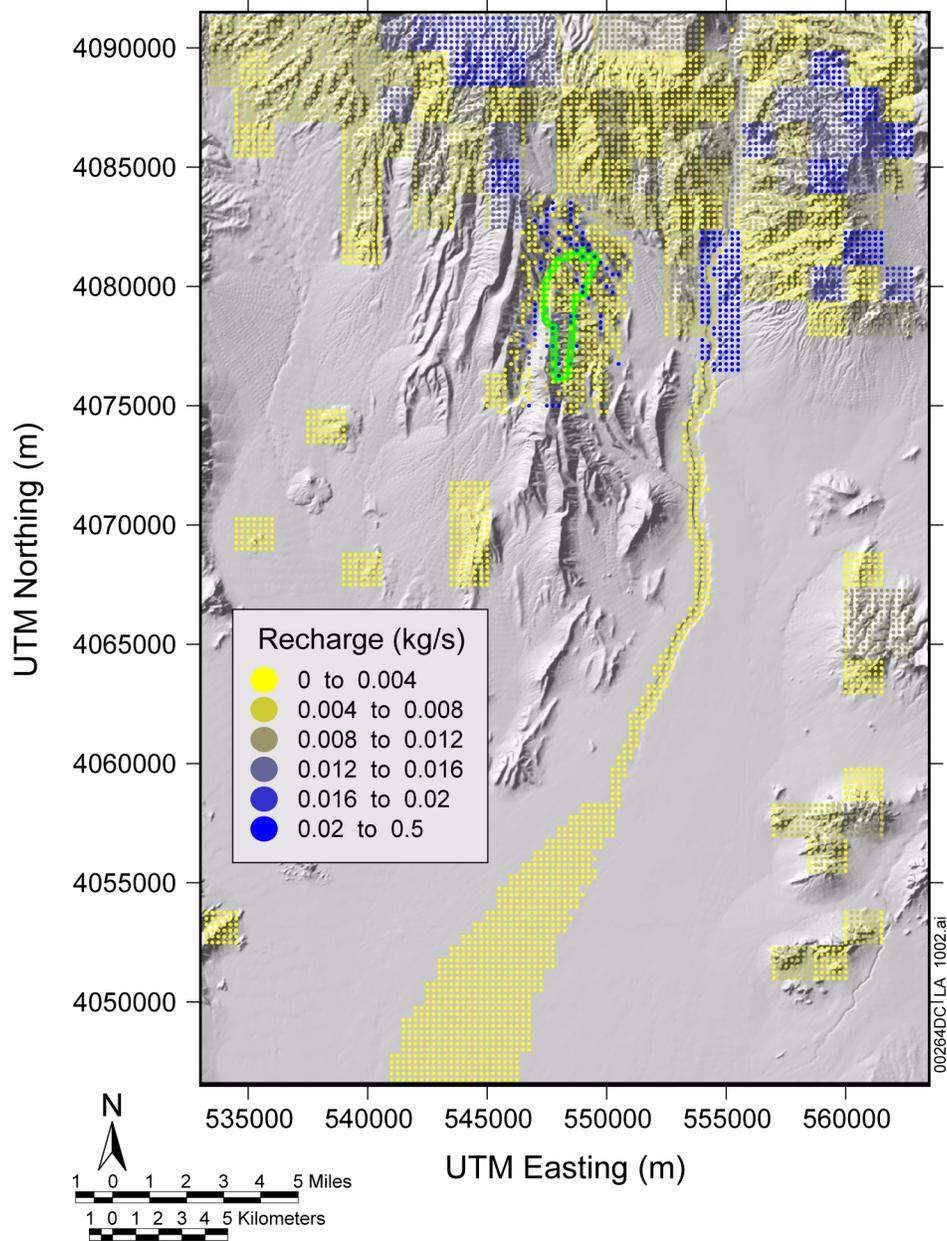
Figure 2.3.9-10. Recharge to the Site-Scale Saturated Zone Flow Model

Source: SNL 2007a, FIgure 6-14.
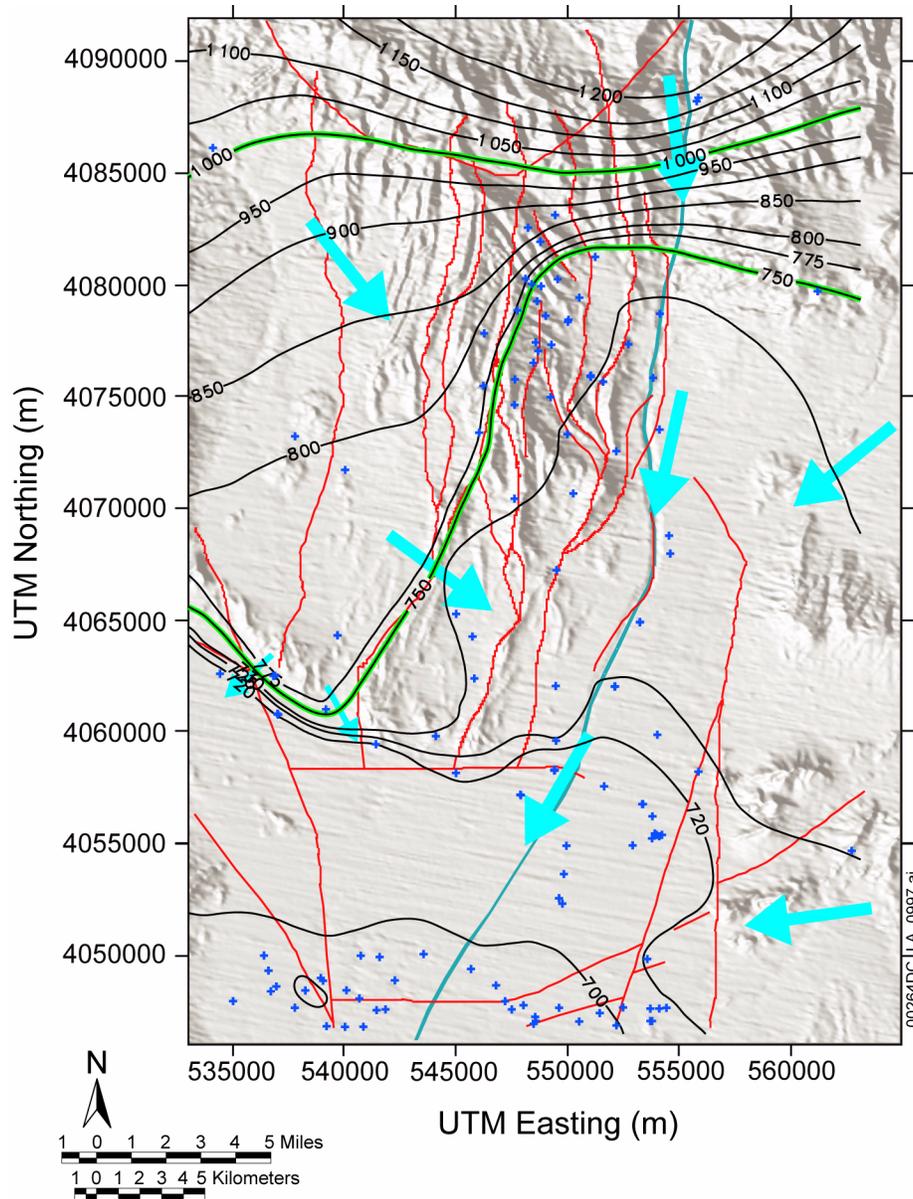
Figure 2.3.9-11.   Site-Scale Potentiometric Surface Assuming Perched Conditions North of Yucca Mountain in the Site-Scale Saturated Zone Model Area

NOTE: Contours are elevation above mean sea level in meters, red lines are surface traces of major faults, blue crosses are well locations, and blue arrows indicate the general directions of groundwater flow in the upper saturated zone.

Source: SNL 2007a, Figure 6-4.
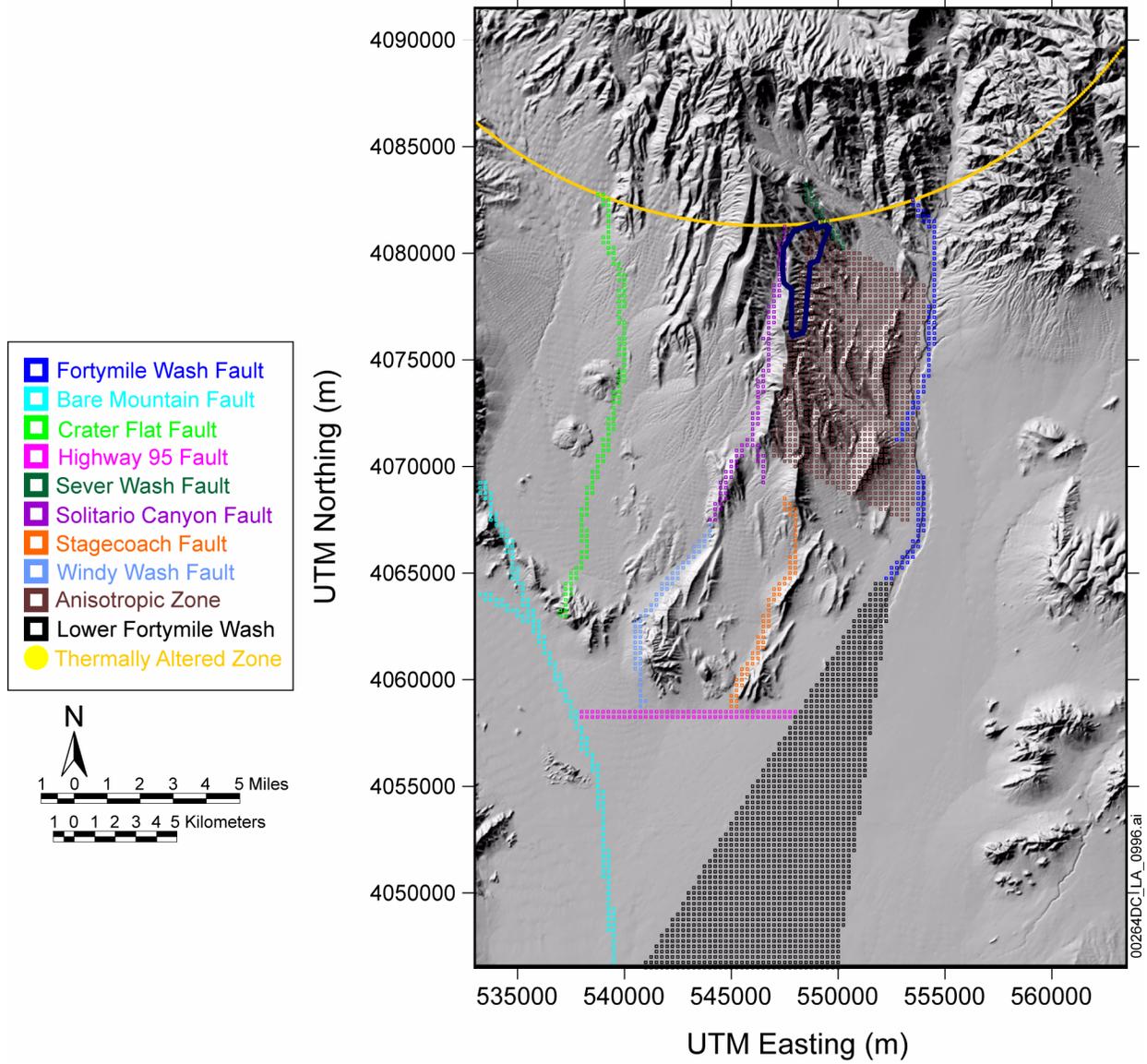
Figure 2.3.9-12. Saturated Zone Flow Zones

Source: SNL 2007a, Figure 6-12.
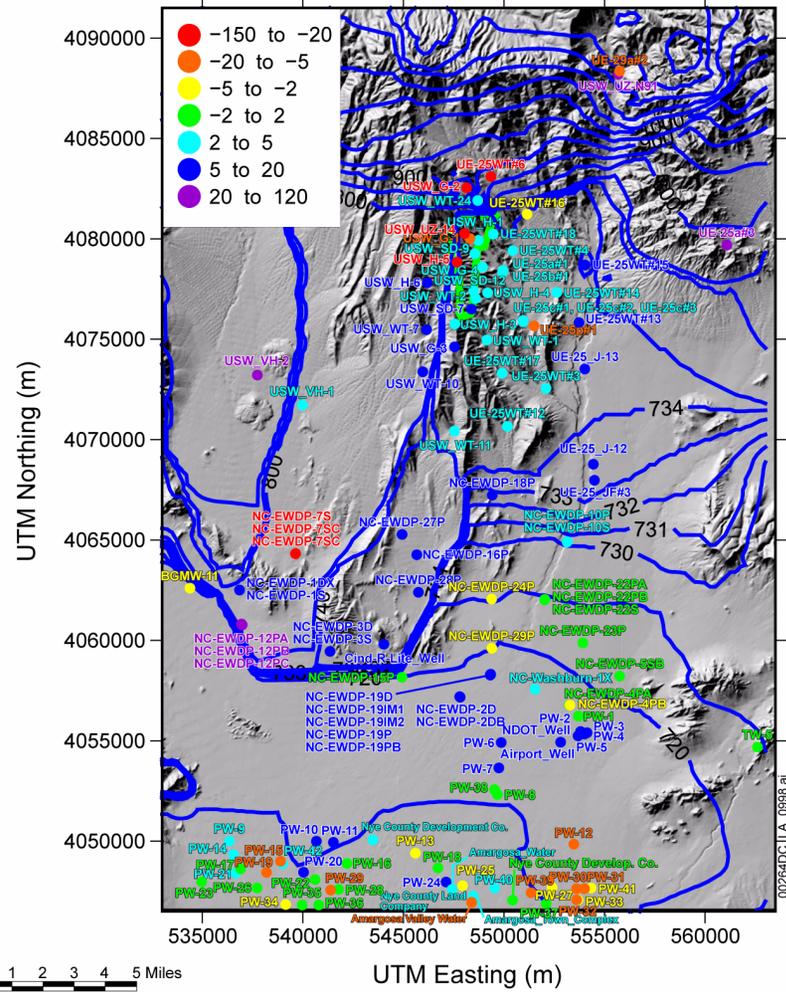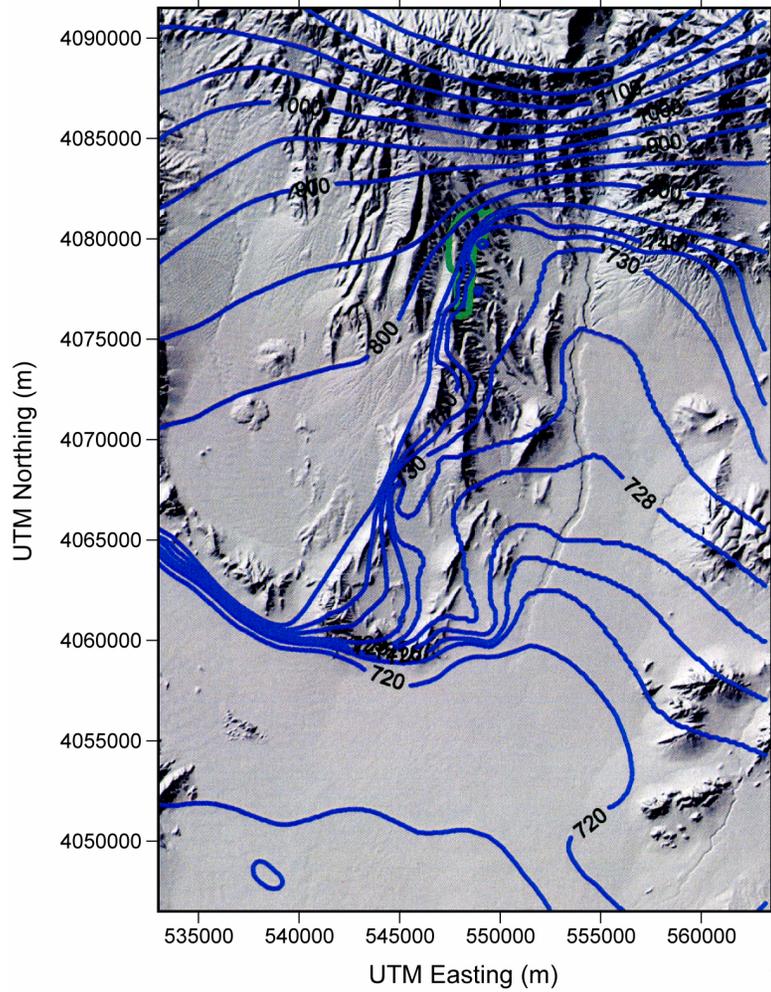
Figure 2.3.9-13.   Contour Plot of Potentiometric Surface (Left Panel) and Hydraulic Heads Simulated by the Site-Scale Saturated Zone Flow Model with Hydraulic Head Residuals at Observation Locations (Right Panel)

Source: SNL 2007a, Figure 6-15.
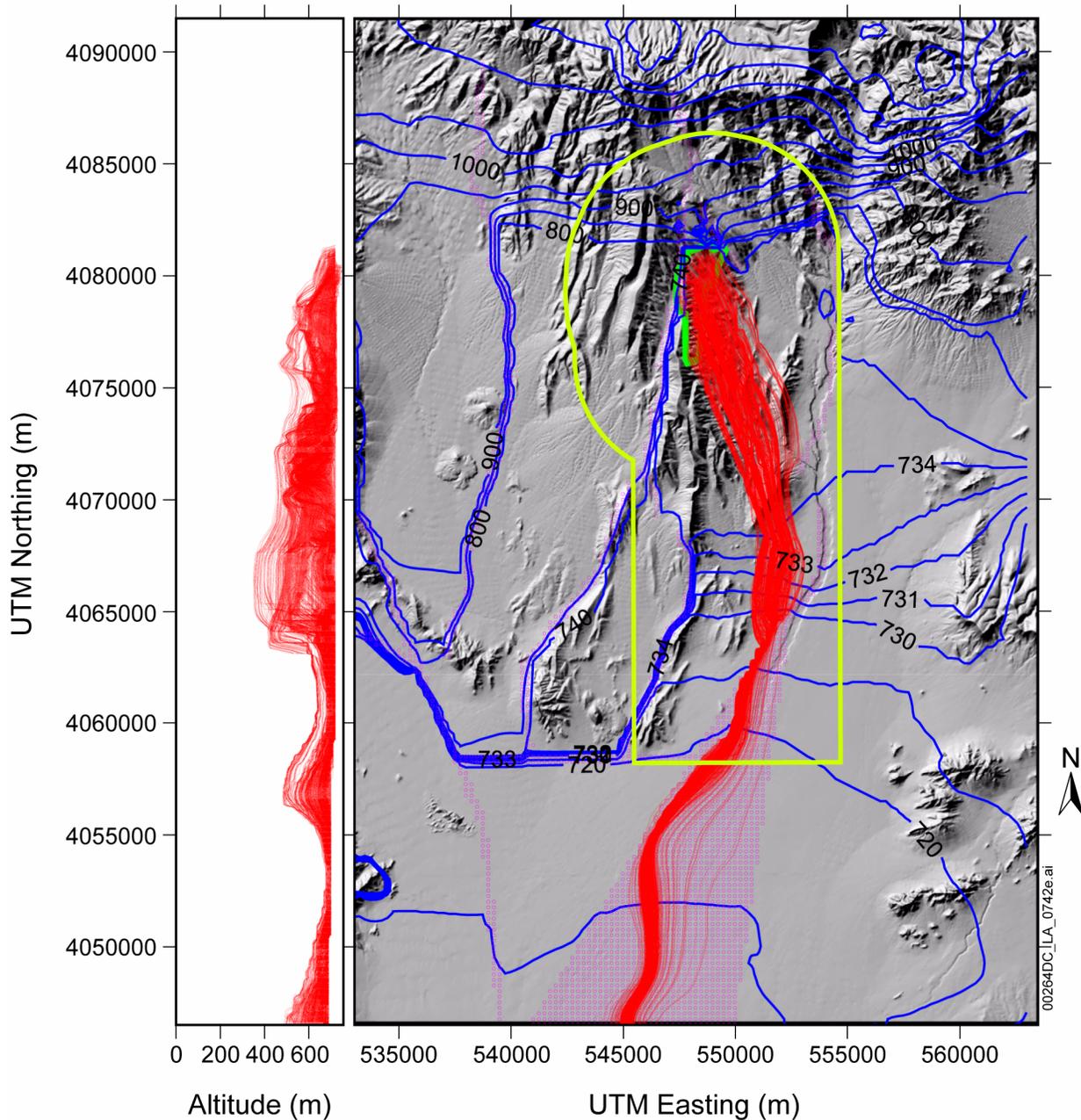
Figure 2.3.9-14.   Simulated Groundwater Paths from Beneath the Repository with Hydraulic Heads
                   Simulated with the Site-Scale Saturated Zone Flow Model

NOTE: Blue lines refer to head contours; red lines refer to particles. The left panel plots all flow paths projected onto a
       north–south vertical plane; the right panel plots the flow paths in plan view. The 0 in the left panel corresponds
       to sea level elevation. Particle paths are simulated using a value of 5.0 for horizontal anisotropy in
       permeability. Postclosure controlled area boundary is shown with the chartreuse line.

Source: SNL 2007a, Figure 6-17. Postclosure controlled area boundary from DTN: MO0712DELNPCCA.001.
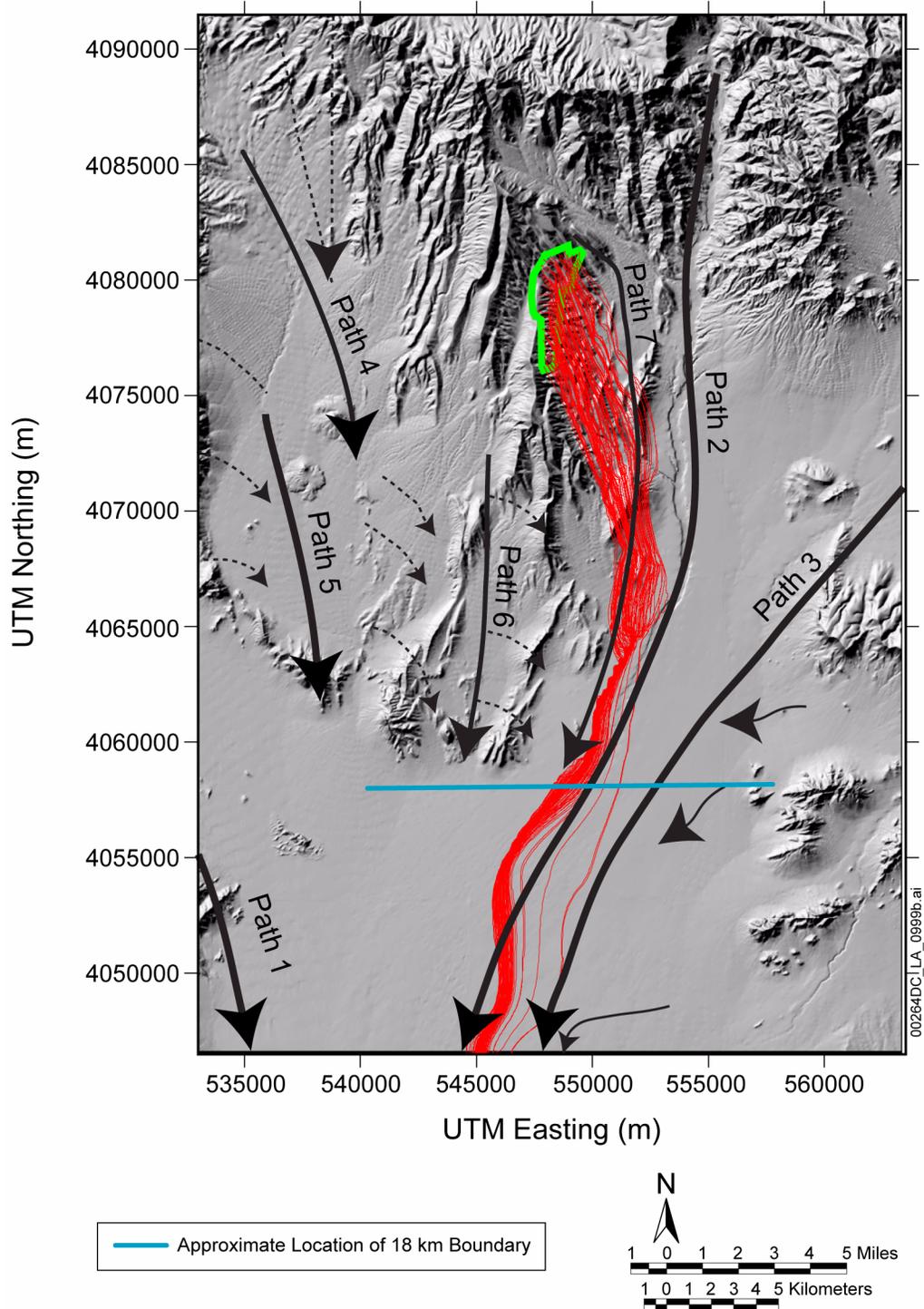
Figure 2.3.9-15.   Simulated Groundwater Flow Path Trajectories and Flow Paths Inferred from Geochemistry

NOTE: Red lines are simulated flow paths; black lines with arrowheads are flow paths inferred from geochemical data (Figure 2.3.9-18). The southern extent of the postclosure controlled area boundary, consistent with 10 CFR 63.302, is also shown as the straight blue line.
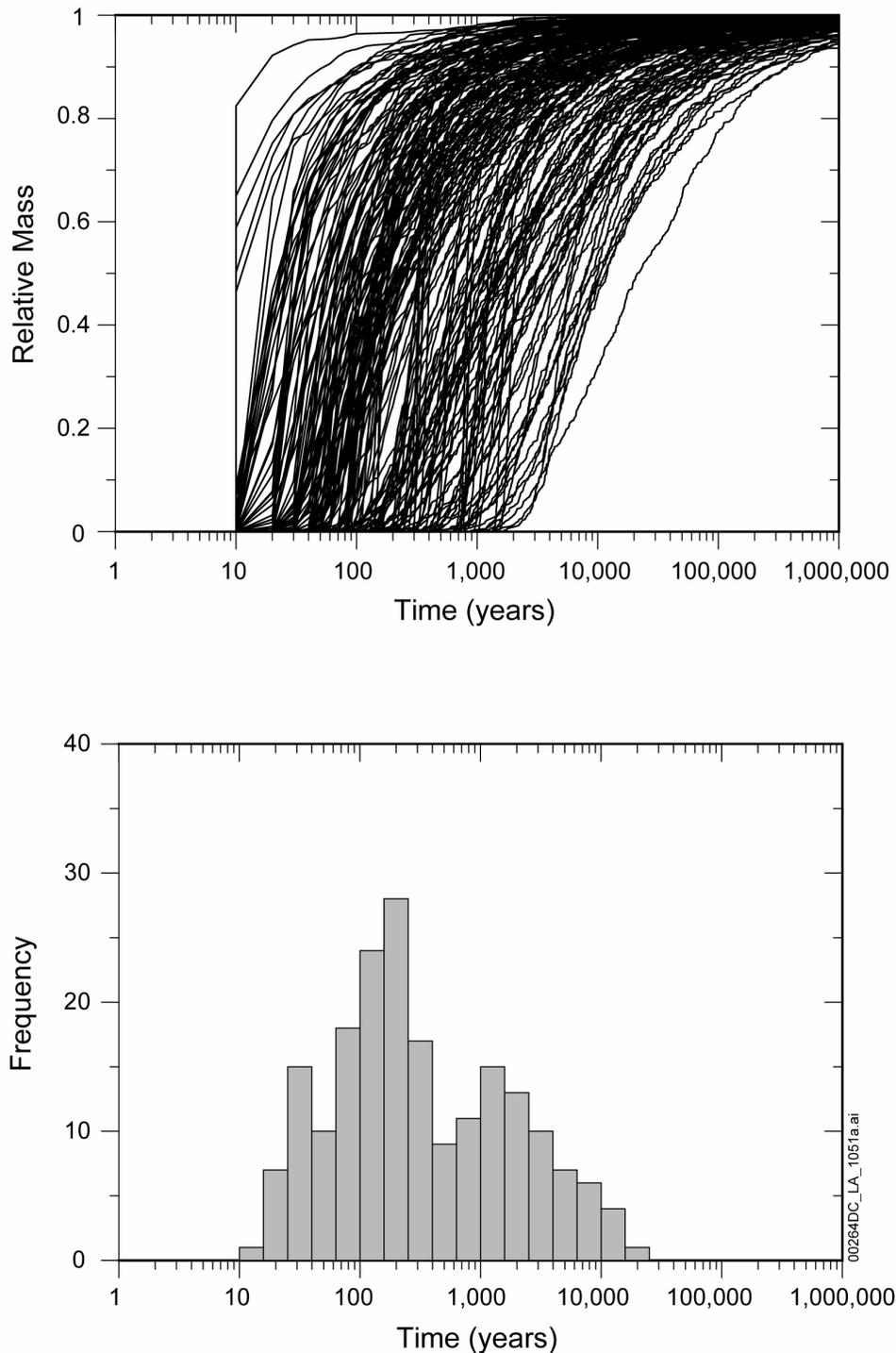
Source: SNL 2007a, Figure 7-5.

Figure 2.3.9-16.   Mass Breakthrough Curves (Upper) and Median Transport Times (Lower) for Carbon, Technetium, Chlorine, and Iodine at the Accessible Environment for the Glacial-Transition Climate

NOTE: Mass breakthrough curves and median transport times are scaled for glacial-transition climate, and do not include radionuclide decay. Results shown for 200 realizations from source region 1.

Source: SNL 2008b, Figure 6-6[a].
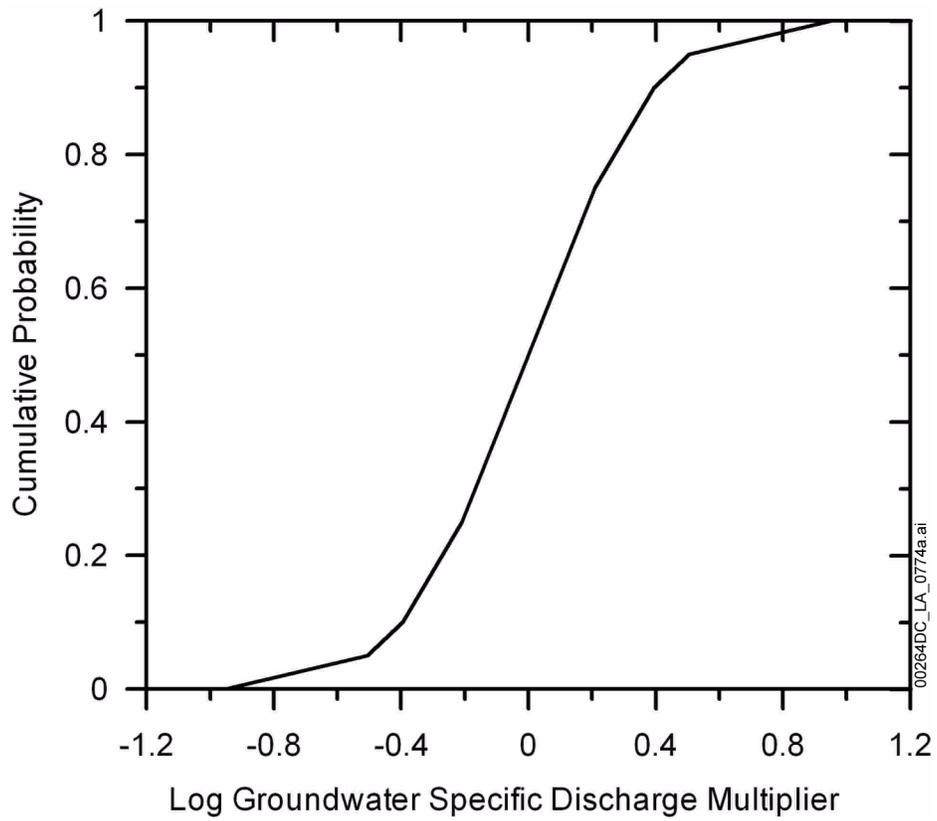
Figure 2.3.9-17.   Cumulative Distribution Function of Uncertainty in Groundwater Specific Discharge Multiplier

Source: SNL 2008b, Figure 6-2[a].
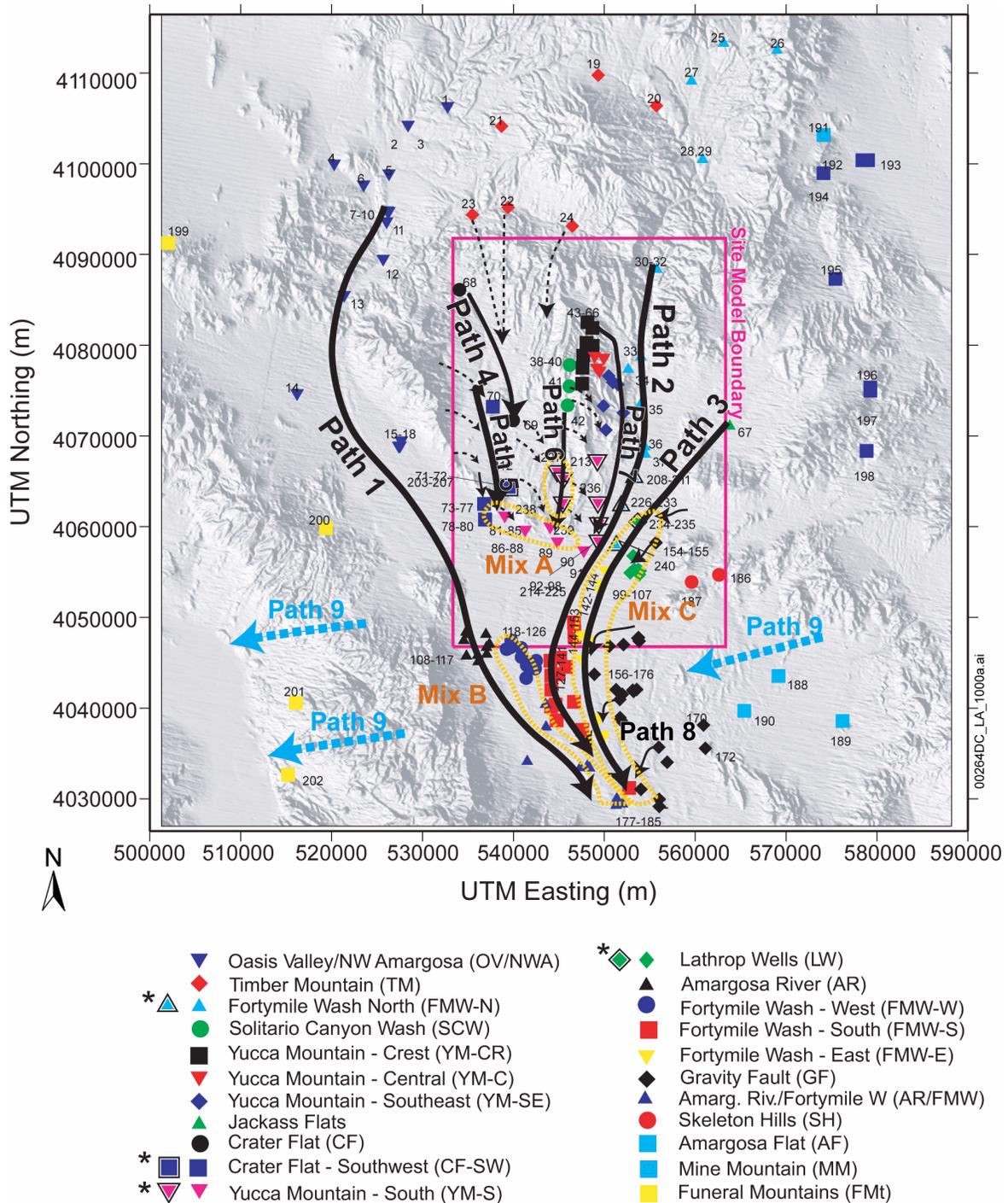
Figure 2.3.9-18.   Location of Geochemical Groundwater Types and Regional Flow Paths Inferred from Hydrochemical and Isotopic Data

NOTE: The termination of flow paths implies that the flow paths could not be traced from geochemical information downgradient from these areas because of mixing or dilution by more actively flowing groundwater; flow path terminations do not imply that groundwater flow has stopped. Table 2.3.9-11 summarizes the bases for the illustrated flow paths.

Source: SNL 2007a, Figure B6-15.
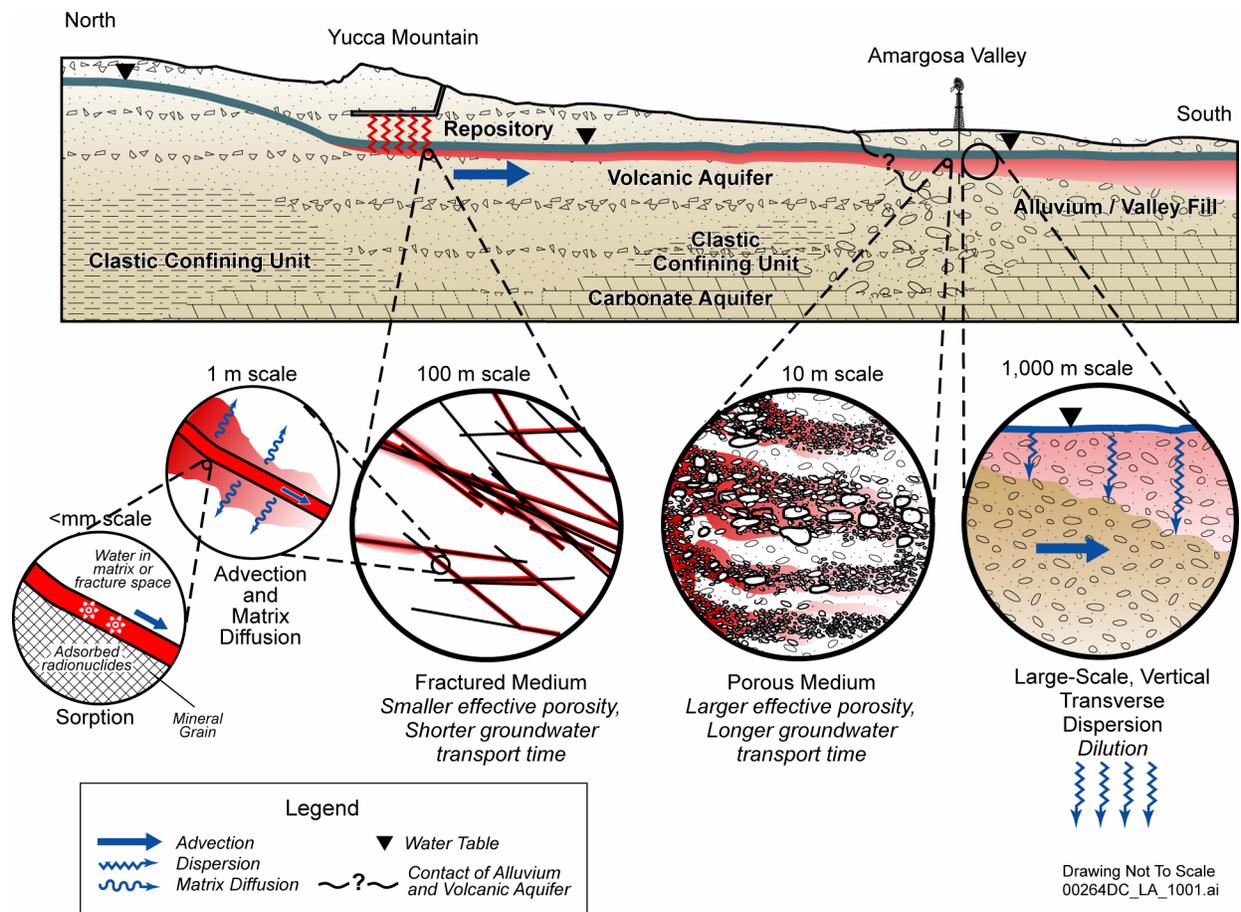
Figure 2.3.9-19. Conceptual Model of Radionuclide Transport Processes in the Saturated Zone

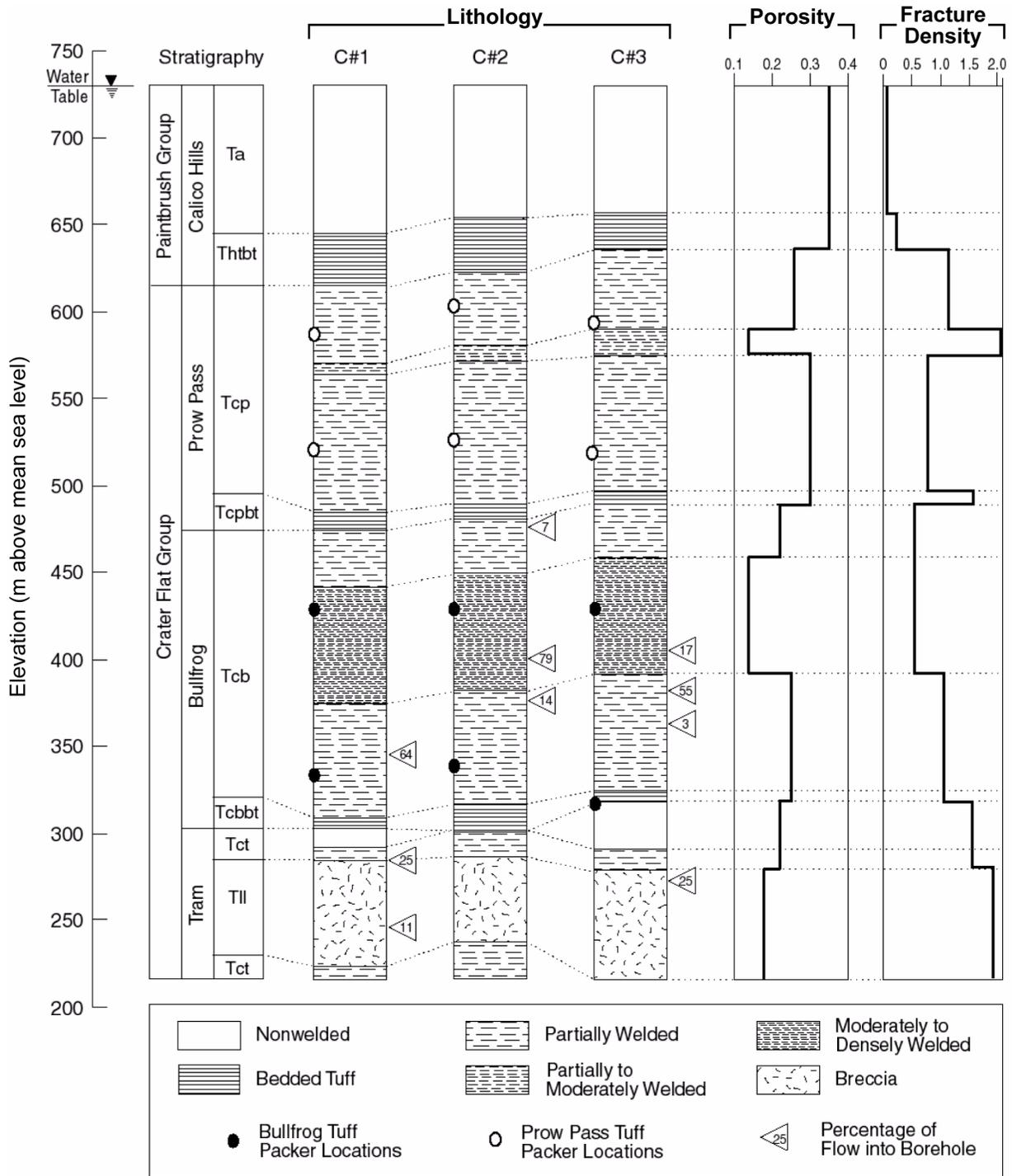Source: Adapted from SNL 2008b, Figure 6-1.

Figure 2.3.9-20.   Stratigraphy, Lithology, Matrix Porosity, Fracture Density, and Inflow from Open-Hole Surveys at the C-Wells

NOTE: Packer locations indicate intervals in which tracer tests were conducted (tracer tests conducted between UE-25 c#2 and UE-25 c#3). The two borehole logs represent matrix porosity and fracture density (number of fractures per meter), from left to right, respectively.

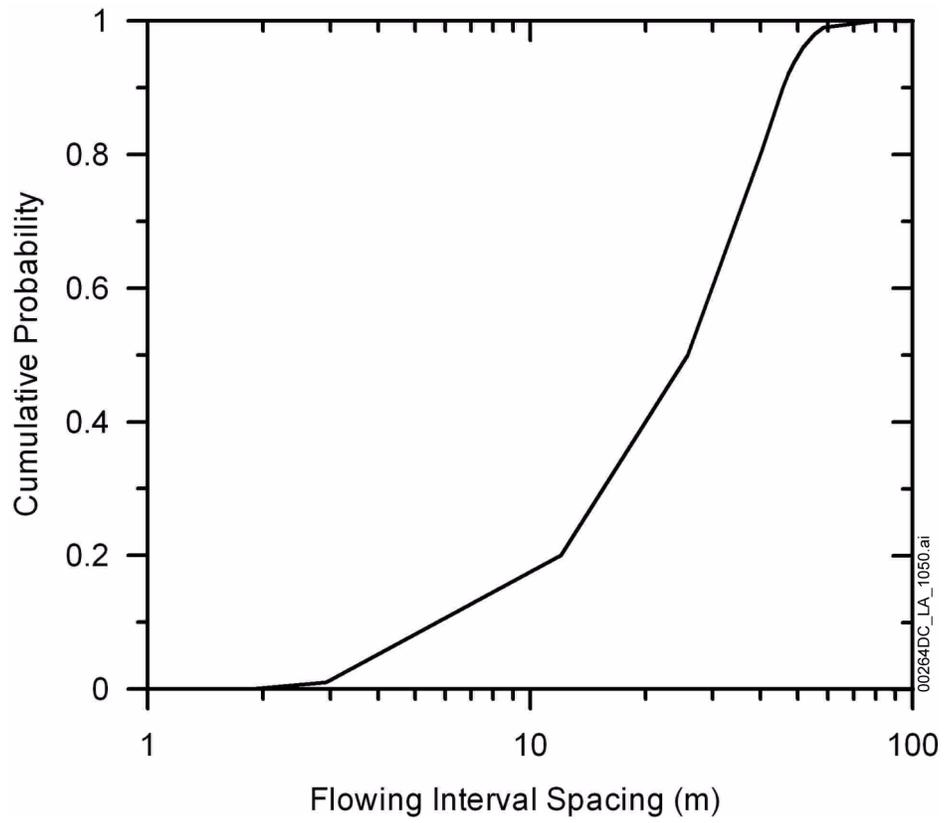Source: SNL 2007b, Figure 6.1-2.

Figure 2.3.9-21. Cumulative Probability Density Function of Flowing Interval Spacing

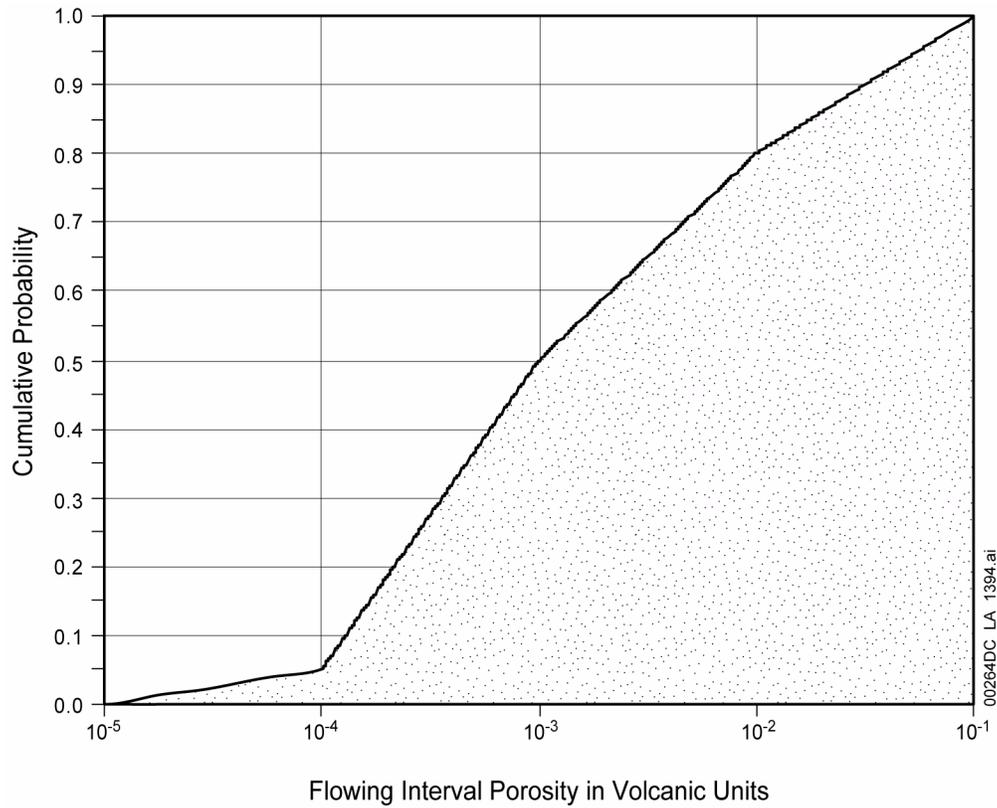Source: SNL 2008b, Figure 6-5[a].

Figure 2.3.9-22.   Cumulative Probability Density Function of Effective Flow Porosity in Fractured Tuffs at Yucca Mountain

Source: SNL 2008b, Figure 6-13.